N-Carboxyanhydride Polymerization of Immunomodulatory Glycopolypeptides for Cancer Immunotherapy

By

Matthew N. Zhou

A dissertation submitted in partial satisfaction of the

requirements for the degree of

Doctor of Philosophy

in

Chemistry

in the

Graduate Division

of the

University of California, Berkeley

Committee in charge:

Professor Carolyn R. Bertozzi, Co-chair
Professor David E. Wemmer, Co-chair
Professor Michelle C. Chang
Professor Sarah A. Stanley

Spring 2018

N-Carboxyanhydride Polymerization of Immunomodulatory Glycopolypeptides for Cancer Immunotherapy

by Matthew N. Zhou

Abstract

N-Carboxyanhydride Polymerization of Immunomodulatory Glycopolypeptides for Cancer Immunotherapy

by

Matthew N. Zhou

Doctor of Philosophy in Chemistry

University of California, Berkeley

Professor Carolyn R. Bertozzi, Co-Chair
Professor David E. Wemmer, Co-Chair

Glycopolymers have served as useful tools for studying glycobiology for over two decades. A significant body of literature has demonstrated that these macromolecules are capable of predictably stimulating lectin receptors, suggesting a potential for clinical applications ranging from adjuvants to immunosuppressants. However, commonly-used scaffolds exhibit notable limitations, including unnatural backbones and glycosidic linkages, which limit their therapeutic potential. In a recent publication, we demonstrated that N-carboxyanhydride (NCA) polymerization is amenable to glycosylated monomers, allowing for the synthesis of true glycopolypeptides. In this dissertation, I demonstrate the applicability of the platform to a variety of glycan structures. In particular, I focus on potentially immunogenic carbohydrate motifs with the ultimate goal of developing synthetic C-type lectin receptor (CLR) agonists designed to activate antigen-presenting cells (APCs) for cancer immunotherapy.

Designing such immunostimulatory glycopeptides requires a general understanding of the cells and pathways important to generating an anticancer immune response. In Chapter 1, I provide an overview of APCs and their associated immune receptors, including CLRs. I include in this section a brief summary of reported pattern recognition receptor agonists, including clinically-approved synthetic ligands, and note the lack of well-defined CLR agonists. I then discuss the relationship between cancer and the immune system with the goal of rationalizing our strategy of activating APCs to induce a robust anticancer response. To provide further context, I conclude with a summary of modern and historical approaches to cancer immunotherapy.

Our initial NCA polymerization publication focused on an *N*-acetylgalactosamine-serine monomer; synthesis of the desired immune-activating glycopolypeptides required that I first establish the generalizability of the platform to other carbohydrates. In Chapter 2, I present work showing that di- and trisaccharide-serine NCAs can be polymerized using transition metal initiators to give glycopolypeptides of controllable length and glycosylation density. In particular, I focus on mannosylated and glucosylated structures that could potentially bind and activate CLRs on antigen-presenting cells, setting the stage for my intended therapeutic application.

In Chapter 3, I demonstrate for the first time that NCA-derived glycopolypeptides can be rationally designed to activate desired CLRs. Specifically, glucosylated and mannobiosylated structures stimulate murine monocyte-derived cells and dendritic cells *in vitro* through the CLRs Dectin-1 and Dectin-2, respectively. Activation was dependent on the carbohydrate structures used and consistent with previous literature describing glycan preferences of these receptors. Chapter 4 expands on these promising results by taking the mannobiosylated glycopolypeptides, which activate the dendritic cell receptor Dectin-2, into murine models of pancreatic cancer. I first show that these materials are able to inhibit tumor growth *in vivo*. Furthermore, conjugation of these Dectin-2 agonists to a costimulatory Toll-like receptor agonist greatly enhances cytokine release in cell culture and tumor growth inhibition *in vivo*. Alternatively, attachment of these glycopolypeptides to tumor-targeting antibodies similarly enhances their immunostimulatory effects. These observations provide promising evidence that activation of APCs via NCA-derived glycopolypeptides may indeed be a viable strategy for cancer immunotherapy.

Finally, in Chapter 5 I describe some ongoing challenges with the NCA polymerization technology. As a platform, it would be desirable to have access to glycopolypeptides with multiple functional handles to maximize the available conjugation possibilities. Here, I describe my efforts to improve on our previously-reported dual-end-labeling technology. Through additional characterization and optimization of functionalized NCA initiators, I uncover some flaws with our initial strategy and propose potential solutions. This work points to the need for new initiators for the NCA polymerization of glycopolypeptides. Advancements in this area will allow us to better access multicomponent glycopolypeptide-based conjugates in the future.

To my wife, my parents, and my brothers.

Table of Contents

List of Tables

List of Figures

List of Schemes

Acknowledgements

First and foremost, I thank you for taking the time to open this dissertation, even if just as a reference for your own acknowledgments page. If you are looking for alternative formats, I would recommend Peter Robinson's and Paresh Agarwal's dissertations as solid examples of the list approach. As with any reputable acknowledgements section, I would like to begin by thanking my advisor, Professor Carolyn Bertozzi. Your vision and enthusiasm are inspirational, and the research environment you have fostered has made the lab a special place to work. The collective intellect of my colleagues has been astounding, and their collegiality and openness have shaped my own approach as a scientist.

Along those lines, I would like to thank all of the graduate students, postdocs, undergraduates, and assorted other labmates I have worked with for being an outstanding group of scientists, mentors, and friends. In particular, my podmates, formerly of Latimer 817 and now Keck 260B, Gaby, Peter, Frances, Sam, Corleone, and Steven, have been a constant source of inspiration and amusement. Thanks also to Elliot, Neil, and Mireille, my fellow classmates, as well as the countless other colleagues who have helped and mentored me through graduate school. Good luck to you all! I would also be remiss not to thank all of the support staff who have made my research possible: Asia, Olga, Sia, Cheryl, Karen, Meridee, and Maryann. Thank you so much for all of your hard work keeping the lab running!

Much of the work described over the following pages would not have been feasible without technical support from and collaboration with talented individuals outside of the Bertozzi lab. Many thanks to Ed Engleman, Justin Kenkel, and Shelley Ackerman, who proposed the idea of applying glycopolypeptides for cancer immunotherapy and with whom I have worked closely over the past three years. I would also like to thank all of the facilities staff and technicians, both at Stanford and Berkeley, who helped to generate much of the data I present here.

I would also like to acknowledge my friends and family. To all of my friends, thank you for being awesome people and keeping me sane. My brothers, Alex and Kevin, constantly impress me with their wit and intellect and are infinitely cooler than I am. Seriously, you should hang out with them some time. To my mother and father: I will never be able to repay you for all you have done to raise and support me. Thank you so much for everything, I'll try to call more often!

Finally, thank you to my wife, Talia. Your humor, intelligence, and caring have helped to keep me going through all of the tough times. I hope I have been even half as supportive of you as you have been of me. We can get a cat now!

Chapter 1

Modern approaches to immune activation and cancer immunotherapy

1.1 Antigen-presenting cells bridge the adaptive and innate branches of the immune system

The immune system is a highly complex network of cells and signaling pathways designed to protect an organism from a diverse set of threats, from pathogenic microbes to cancerous cells.[1] In order to accomplish this task, protective mechanisms must be able to respond rapidly but specifically to foreign or precancerous material. This poses a significant challenge. A finely-tuned response to a specific pathogen allows for more effective and efficient clearance; however, development of such a response against an infection that the organism has not yet been exposed to may not be rapid enough to protect in the short term. In vertebrates, the evolutionary solution to this problem features two interconnected arms: adaptive and innate immunity.

Even prior to the general acceptance of germ theory, people recognized that those who had recovered from certain diseases were thereafter resistant to further infection. Written records of this phenomenon, known now as immune memory, date back to the writings of Thucydides in 430 BCE, though it was almost certainly known prior to that.[1] Attempts to harness this effect intentionally were perhaps most famously conducted in the late 18th century by Edward Jenner, who developed a smallpox vaccination strategy based on inoculation with cowpox, a related virus.[2] Two centuries of immunological research since then have helped to uncover the pathways and cells responsible for pathogen-specific immune responses. Referred to now as adaptive immunity, this branch of the immune system is broadly mediated by T cells and B cells, which perform a diverse set of tasks including direct destruction of target cells, secretion of antigen-specific antibodies, and expression of immunomodulatory cytokines.[3]

Once primed, adaptive immune machinery is highly effective at detecting and combating a 'known' infection. However, adaptive immune responses operate on the order of weeks, and development of robust immune memory may even require multiple exposures over the course of months or years.[4] A complementary system must exist to handle infections on a shorter time scale. This is one of the key roles of the innate immune system. On a passive level, innate immunity includes physical impediments such as mucus and skin that protect against invading organisms.[1] Humoral components, such as complement proteins, bind to potential pathogens that evade these barriers and induce a variety of downstream effects, including direct cellular damage via pore formation and recruitment of phagocytes.[5] On the cellular side, leukocytes of the innate immune branch often possess the ability to release potent cytotoxic and proinflammatory molecules, as with natural killer (NK) cells and mast cells.[6-7] Alternatively, phagocytes may neutralize pathogens by endocytosis into lysosomal compartments, which degrade internalized cellular material via acidification, oxidative stress, and hydrolytic enzymes.[8] Unlike adaptive immune cells, innate immune cells generally sense threats through receptors that bind generic pathogen-associated molecular patterns (PAMPs) or damage-associated molecular patterns (DAMPs).

Bridging the two arms of the immune system are the professional antigen-presenting cells (APCs).[9] Phagocytic APCs such as dendritic cells and macrophages operate on the front lines of infection and routinely encounter and process foreign material.[10-11] Upon sensing PAMPs or DAMPs, APCs endocytose the associated cells or foreign material, degrade internalized proteins to peptide fragments, and display them on cell-surface major histocompatibility complex class I (MHC I) or class II (MHC II) proteins.[10] Interaction with an activated APC bearing an MHC-bound antigen is required for T cell activation via the T-cell receptor. In particular, dendritic cells appear to be the

primary class of cells responsible for activating naïve T cells in the secondary lymphoid organs.[12] As such, despite their general categorization as innate immune cells, dendritic cells and macrophages are necessary components of an effective adaptive immune response.

1.2 Pattern recognition receptors are a key feature of a competent immune system

Recognition of PAMPs or DAMPs by APCs and other immune cells involves a myriad of pattern recognition receptors (PRRs) that bind molecular structures not found on healthy host tissues.[13] The downstream result of binding varies based on the receptor, immune cell class, and surrounding cytokine context, ranging from phagocytosis and antigen processing by APCs to lysis of target cells via NK cell degranulation.[13-14] The first discovered and best studied class of PRRs are the Toll-like receptors (TLRs). Named after their homology to the *Drosophila* membrane protein Toll, in humans they represent 11 known receptors that all feature leucine-rich repeats in their ligand binding domains.[1] However, their signaling pathways, ligand specificities, and cellular localizations vary significantly. PAMPs recognized by various TLRs include bacterial lipids, viral RNA, bacterial DNA, and microbe-associated cell surface carbohydrates.[1,15] TLRs that recognize cell-surface patterns, such as peptidoglycan or flagellin, tend to reside on the cell surface, while those that bind nucleic acids tend to be active only in endosomal compartments. As with many PRRs, TLRs are most prominently featured on dendritic cells and macrophages, although NK cells, mast cells, and even B and T cells express some TLR classes.[15]

The C-type lectin receptors (CLRs) represent another key set of PRRs. Originally named for their ability to bind carbohydrates in a calcium-dependent manner, is has since been established that not all CLRs require calcium for binding.[16] The first discovered CLR in animals, the hepatic asialoglycoprotein receptor (ASGPR) was described by Ashwell et al. in the 1960s.[17] ASGPR binds to sialic acid-deficient serum glycoproteins via terminal *N*-acetylgalactosamine residues, a potential DAMP, and mediates their removal from the blood.[18] Since then, 17 different classes of CLRs have been described to date with a highly diverse set of roles.[19] Carbohydrate receptors are particularly useful for identifying pathogens or diseased tissues because all living cells express a variety of cell-surface glycans which vary from organism to organism and can be highly specific. For instance, sialic acids represent a common terminal carbohydrate on animal tissues but are not synthesized by fungi and bacteria; conversely, many microbes display terminal mannan structures that are not found on healthy human tissues.[20] Among the best studied PAMP-binding CLRs are DC-SIGN, Dectin-1, and the Dectin-2 class of receptors, which include Dectin-2, Mincle, and the macrophage mannose receptor.[21]

Although TLRs and CLRs represent the largest and most studied classes of innate immune receptors, it is worth noting that there are a variety of important receptors that do not belong in either class. These include the intracellular NOD-like receptors, best-known for detecting bacterial peptidoglycan, the RIG-I-like receptors, which sense viral dsRNA, and stimulator of interferon genes (STING), which detects cytosolic DNA. A subset of the discussed PRR classes and selected receptors is summarized in Table 1.1.

Table 1.1. Selected Pattern-Recognizing Immune Receptors.[1, 22-24]

Receptor Class	Receptor	Ligand	Notes
Toll-like receptors	TLR1	Triacyl lipopeptides	Dimerizes with TLR2
	TLR2	Lipidated peptidoglycan components	Dimerizes with TLR1 and TLR6
	TLR3	Viral dsRNA	Endosomal
	TLR4	Bacterial lipopolysaccharide	Moves to endosome upon ligand binding
	TLR5	Flagellin	
	TLR6	Diacyl lipoplypeptides	
	TLR7	Viral ssRNA	Endosomal
	TLR8	Viral ssRNA	Endosomal
	TLR9	Bacterial DNA	Endosomal, high affinity for CpG unmethylated dinucleotides
	TLR10	Unknown	Pseudogene in mice
	TLR11	Profilin	
C-type lectin receptors	ASGPR	terminal *N*-acetylgalactosamine	First discovered CLR in animals
	Dectin-1	β-glucans	Preference for β-1,3 linkage
	Dectin-2	α-mannans	Preference for α-1,2 linkage, dimerizes with self or Dectin-3
	Dectin-3	α-mannans	Also known as MCL, dimerizes with Dectin-2
	Mincle	Glycolipids, glucans, mannans	Best known as receptor for mycobacterial trehalose mycolates
	DC-SIGN	mannans	Binds HIV gp120 glycoprotein, promoting viral infection
	hDCIR	mannans	Immunosuppressive signaling via ITIM domain
NOD-like receptors	NOD1	D-glutamyl-meso-diaminopimelic acid	Cytosolic
	NOD2	Muramyl dipeptide	Cytosolic
RIG-I-like receptors	RIG-I	Short viral RNA	Cytosolic, antiviral response
	MDA5	Long viral RNA	Cytosolic, antiviral response
	LGP2	Viral RNA	Modulates activity of RIG-I and MDA5
Stimulator of interferon genes (STING)	STING	DNA	Cytosolic DNA sensor

1.3 Synthetic and semisynthetic platforms for immune activation

Modulation of the immune system has been a therapeutic goal since the earliest attempts at vaccination. Immunostimulatory applications naturally include vaccines against infectious agents, and have been more recently applied to cancer as well with promising results.[25-27] Conversely, immunosuppression is often desirable in the case of autoimmune disorders, hypersensitivities such as allergies, and cytokine release syndrome.[28] For the purposes of this work, I will focus here on strategies for immune activation.

Although the natural ligands for immune receptors are often macromolecules or molecular patterns that are displayed on cell surfaces in a multivalent fashion, much work has gone into the development of small molecule PRR agonists. This has likely been driven in part by the well-established precedent of small molecule medicinal chemistry techniques relative to our comparatively poor understanding of desirable structural and compositional characteristics for effective macromolecular therapeutics. The resulting molecules tend to fall into two categories: analogs or derivatives of natural agonists, and ligands developed through traditional medicinal chemistry techniques (Figure 1.1). Of the latter category, the best characterized and most clinically successful have been the TLR7 and TLR8 agonists based on the imidazoquinoline scaffold first disclosed in 1985 by Gerster.[29] Of these, the most prominent has been the TLR7 ligand imiquimod, which is FDA approved as a topical treatment for actinic keratosis, basal cell carcinoma, and warts.[25] STING ligands have similarly generated significant interest in the pharmaceutical industry for cancer therapy, with Aduro Biotech and Novartis initiating clinical testing of the compound MIW815/ADU-S100 against solid tumors and lymphomas in 2017.[30] Previous work by Antisoma and Novartis similarly produced the potent murine STING agonist DMXAA, which remains a useful tool compound despite being unable to activate the human receptor.[31]

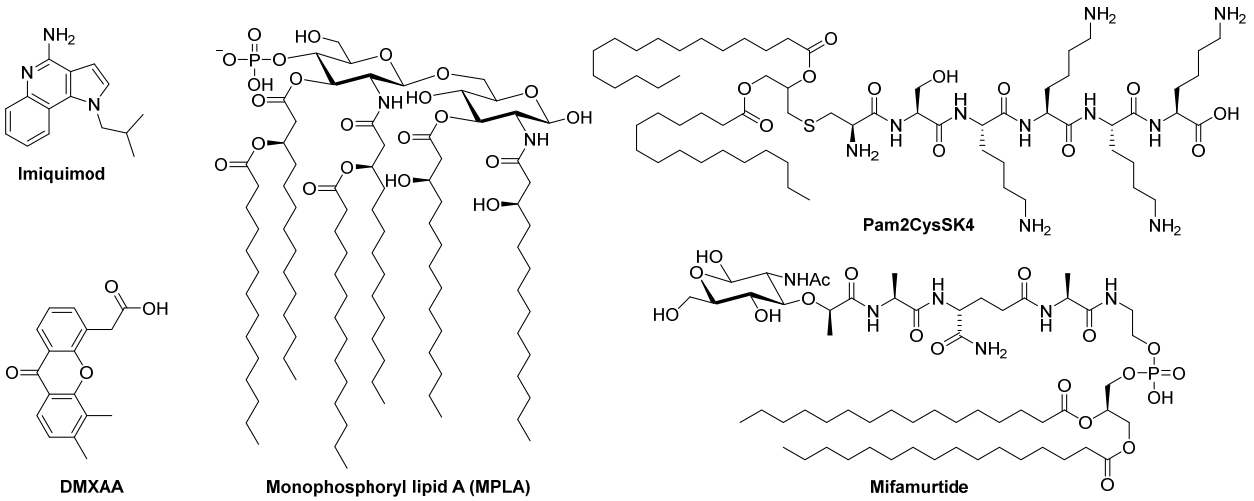

Figure 1.1. Representative small molecule and peptide PRR agonists. Imiquimod and DMXAA are TLR7 and murine STING agonists, respectively. Monophosphoryl lipid A is a fragment of the bacterial lipopolysaccharide structure and a TLR4 agonist. Pam2CysSK4 is one of several optimized acylated lipopeptides found to potently stimulate TLR2. Mifamurtide is an analog of the muramyl dipeptide fragment of bacterial cell wall peptidoglycan, a known Nod2 ligand, which was optimized for decreased toxicity.

Identification of relatively small (< 2000 Da) PRR agonists based on natural ligands has proven somewhat more fruitful, although many of the resulting compounds feature problematic pharmacokinetic or toxicity profiles that limit their clinical utility. One of the more widely used has been monophosphoryl lipid A (MPLA), a TLR4 agonist and fragment of the highly immunogenic bacterial lipopolysaccharides (LPS). Whereas LPS itself is too potent of an immunostimulant to be safely used in humans, MPLA has been investigated as a vaccine adjuvant with some success.[32] Mifamurtide, an analog of the bacterial cell wall muramyl dipeptide fragment and Nod2 agonist, has similarly seen success in the clinic and is currently approved in Europe against osteosarcoma.[26] As an additional example of naturally-derived PRR agonists, di- and tripalmitoylcysteine-containing peptides are known to be potent TLR2 agonists and are commonly used to study TLR biology.[27]

Notably, to the best of our knowledge no small molecule immunostimulatory CLR ligands have been developed to date. CLRs have some problematic characteristics from a traditional medicinal chemistry perspective. Conventional small molecule receptor ligands, which are generally relatively hydrophobic, derive a degree of entropic benefit from desolvation upon binding.[33] Lectins tend to possess relatively hydrophilic binding domains due to their need to accept heavily hydroxylated glycans, making it more difficult to design agonists that prefer the binding pocket over bulk solvation.[34] In fact, dissociation constants for even favorable monosaccharide-lectin interactions can be in the mM range, and strong interactions are generally achieved through multivalency.[35] Furthermore, clustering of receptors through binding of multiple CLRs to a multivalent structure is necessary for effective signaling for some CLRs. This has been explicitly shown with a few receptors, including Dectin-1, Mincle and the macrophage mannose receptor, and is likely the case for other related CLRs.[36-39] Notably, other immune receptors such as TLR2 and the T cell receptor are also known to cluster.[39-40] This likely serves as a form of signaling control that reduces spurious immune cell activation. Given these factors, established CLR ligands to date have been limited to natural extracts for use as biological tools and are generally not suitable for therapeutic applications.

With this in mind, many research groups have focused on platforms for immune stimulation using multivalent macromolecular or nanoparticle scaffolds. In addition to accounting for receptor clustering effects, multivalent scaffolding provides the opportunity to combine different immune receptor ligands into a single structure to afford a synergistic effect.[41-44] First described in the late 1970s, dendrimers represent a classic platform for multivalent display in the academic literature, and a variety of glycosylated dendrimers have been reported as CLR and TLR agonists.[45-47] Similarly, nanoparticles and functionalized liposomes have been used to target STING, CLRs, TLRs, and various other combinations of immune receptors.[48-51] Glycopolymers have also been widely used to probe CLR biology; further discussion of modern glycopolymer approaches is presented in Chapter 2. Although macromolecular technologies, both in the context of immune activation as well as for other applications, have generated a wealth of publications, for the most part they have not translated readily into the clinic. Other than protein conjugates, which suffer from limited control over glycosylation site/density and potential undesired immunogenicity, liposomal strategies for drug delivery represent perhaps the most successful class of macromolecular therapeutics to date.[52] Unfavorable biodistribution profiles and pharmacokinetics, generally characterized by accumulation in the liver, are a common problem for macromolecular therapeutics.[53-54] Poor choice of scaffold chemistry can also result in unanticipated toxicity,

especially if nonbiological structures are used. These concerns, as well as consideration of scale-up practicality and related technical issues, must be addressed if macromolecular immune receptor agonists are to be therapeutically relevant.

1.4 Cancers manipulate host immunity to suppress anti-tumor activity

All cancers must evade detection and/or destruction by the host immune system in order to multiply and spread. It has been conjectured at least since the early 1900s that cancers might occur much more frequently without a competent immune system, a hypothesis coined cancer immunsurveillance by Burnet in 1970.[55] More recently, an updated model, deemed the cancer immunoediting hypothesis, was proposed by Schreiber et al. and is summarized in Figure 1.2.[56] Briefly, cells that develop potentially cancerous mutations are generally recognized and eliminated by cytotoxic immune cells. This creates a selective pressure to accumulate mutations that promote immune evasion, leading to an intermediate 'equilibrium' phase in which mutant cells are prevented from propagating significantly but are not efficiently eliminated. Sufficient mutation under selective pressure can ultimately lead to a population of cells escaping from effective immune control, leading to disease.

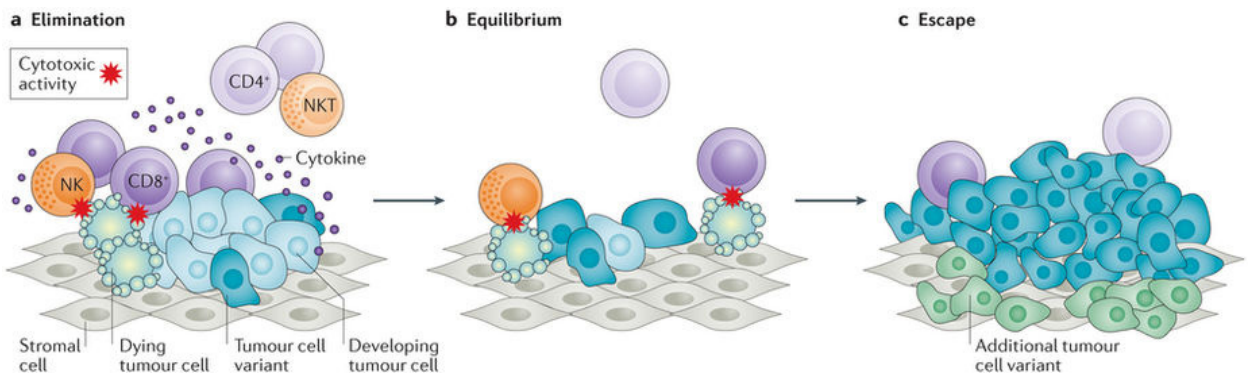

Figure 1.2. Microevolutionary model of cancer progression. The majority of cells that exhibit potentially cancerous characteristics are rapidly eliminated by the immune system. This creates selective pressure that favors mutations that suppress or avoid recognition and destruction by the immune system. Over time, accumulation of oncogenic mutations results in successful escape of the cancer from immune control. Figure adapted with permission.[56]

Understanding the mechanisms by which cancers can escape immune control is of utmost importance to rationally designing therapeutic strategies. Some early arguments against the cancer immunosurveillance model proposed that cancers, which are derived from healthy host cells, are inherently nonimmunogenic due to central tolerance.[55] These claims were driven by numerous experiments in nude mice with severely compromised T cell populations, which showed no notable increases in tumor occurrence. Although these experiments largely discounted the potential compensatory role of innate immunity, as well as the fact that nude mice are not completely devoid of T cell activity, central tolerance certainly plays a role in hindering tumor immunogenicity. For example, highly upregulated cancer-associated biomarkers, such as the well-characterized oncogene Her2, are often inefficient antigens for cancer vaccines.[57-58] This necessitates strategies that bypass central tolerance either by inducing responses to cancer neoantigens that are not present

on healthy tissues, or by introducing exogenous immunogenicity through approaches like cancer cell-specific opsonization.

Cancers also extensively manipulate peripheral tolerance to not only avoid detection by immune cells but also to create generally immunosuppressive cell signaling environments that prevent effective activation of T cells and myeloid cells (Figure 1.3).[59] All immune cells that respond to antigens and potential pathogens display an array of both stimulatory and inhibitory receptors. Immune evasion can therefore occur through downregulation of potentially immunostimulatory ligands or through upregulation of immunosuppressive signals. For example, T cell activation requires binding of the T cell receptor to an antigen bound to MHC I on the cell surface. Reduced expression of MHC I is therefore a common feature of immune escape.[60] At the same time, T cells also express programmed cell death protein 1 (PD-1), which binds the cell surface ligand PD-L1 as part of a mechanism for preventing autoimmunity. Binding of an effector T cell to PD-L1 induces T cell apoptosis, whereas the same interaction activates regulatory T (Treg) cells. Stimulated Tregs then inhibit further immune activation through secretion of anti-inflammatory cytokines such as IL-10 and TGF-β, creating a favorable microenvironment for cancer cell growth.[59] PD-L1 is therefore overexpressed on some tumors as an immunosuppressive signal.[61] Similar interactions are also exploited to alter innate immune cell behavior: overexpression of cell-surface sialic acids, a common cancer-associated mutation, appears to inhibit natural killer cell antibody-dependent cell-mediated cytotoxicity through engagement of inhibitory Siglec receptors and blocking of the activating NKG2D receptor.[62]

The counterintuitive result of this web of interactions is that cancers often evade destruction by recruiting both innate and adaptive immune cells; notably, solid tumors are generally highly infiltrated with antigen-presenting cells that would normally be key to developing an anticancer immune response (Figure 1.3).[59] By hijacking pathways designed to avoid autoimmunity and manage inflammatory responses, cancers actively inhibit induction of an effective immune response and promote development of a favorable tumor microenvironment. Successful cancer therapies must therefore either bypass or counteract central and peripheral tolerance pathways.

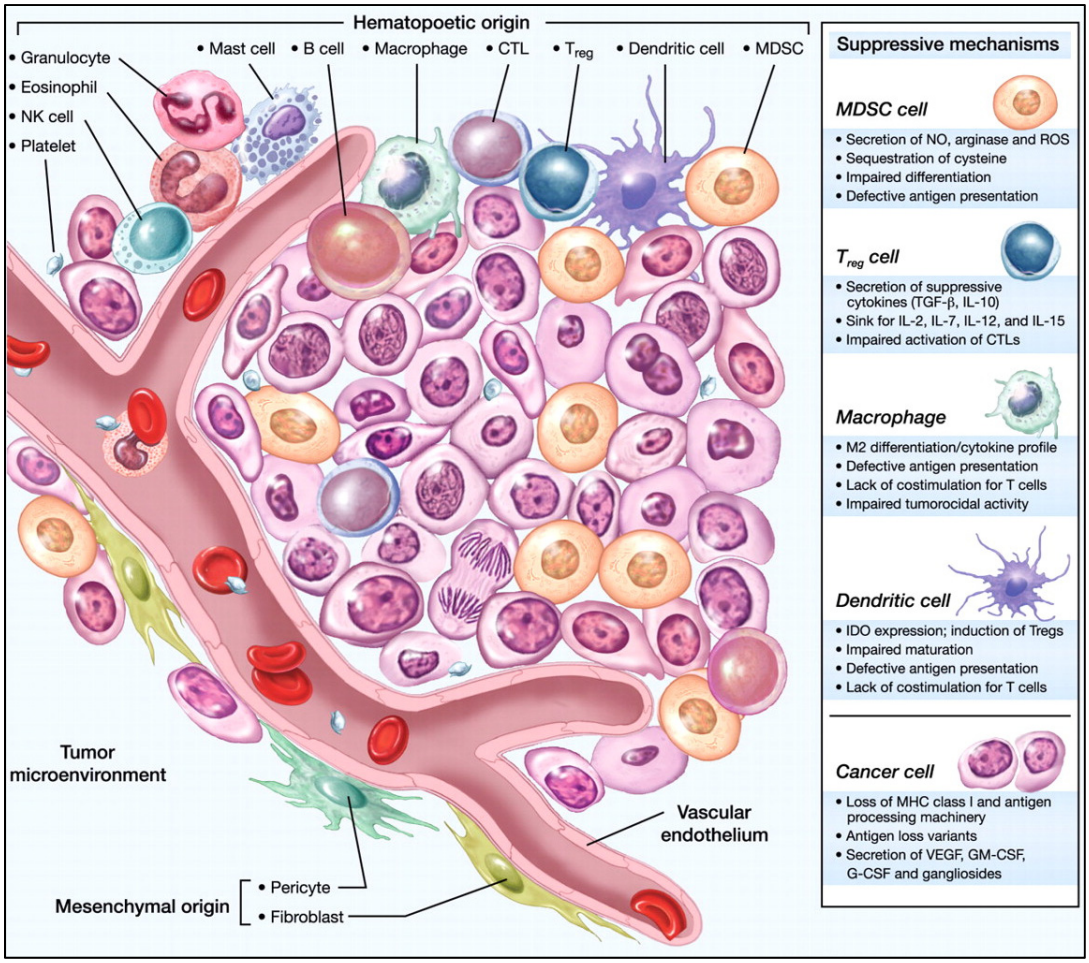

Figure 1.3. The tumor microenvironment is highly infiltrated by immune cells. However, recruitment of suppressive immune cell types, such as myeloid-derived suppressor cells (MDSCs) and regulatory T (Treg) cells, and upregulation of immunosuppressive cytokines and cell surface ligands prevent induction of an effective antitumor response. Figure adapted with permission.[59]

1.5 Activating the immune system to combat cancer

Although several breakthrough cancer immunotherapies have been brought to bear over the past two decades, the premise of employing immune system machinery to combat cancer is not a recent concept. As far back as 1891, surgeon William Coley, having observed a correlation between acute streptococcal infection and tumor remission, performed intratumoral injections of streptococcal cultures in an attempt to replicate this effect.[63] Remarkably, even this crude approach was effective at shrinking tumors in some patients, although severe side effects post-inoculation were unsurprisingly observed. In fact, the strategy of administering adjuvants such as granulocyte macrophage colony-stimulating factor (GM-CSF), IL-2, IFN-α, and TLR agonists, often in combination with other therapies, remains a treatment option for some cancers.[64-67] Although side effects are much more manageable than those observed with live culture injections, toxicity from inflammation and cytokine release syndrome remain a concern.[68-69]

Modern immunotherapies often aim to derive cancer-specific activity by targeting known antigens that are either highly upregulated in cancers or neoantigens that arise due to the genetic instability inherent to cancers. Although the existence of such tumor-associated antigens (TAAs) has long been inferred from experimental observations, systematic characterization of TAAs became possible with the development of autologous typing by Lloyd Old and coworkers in the 1970s.[70] Later technologies, most notably serological analysis of autologous tumor antigens by recombinant cDNA expression cloning (SEREX), made it possible to readily identify specific antibody/TAA pairs.[71] Along with the development of the Nobel prize-winning hybridoma technology that greatly facilitated monoclonal antibody expression, these developments paved the way for the first antibody-based cancer therapeutics, arguably the first class of "modern" cancer immunotherapies. Approved by the FDA in 1997, rituximab represented the first monoclonal anti-cancer monoclonal antibody therapy and remains in use today as a treatment for B cell lymphomas.[72]

Antibody-based therapeutics can operate through a variety of mechanisms of action. By binding to tumor proteins, antibodies can directly interfere with processes necessary for tumor survival. For instance, Rituximab displays antitumor properties independently of host immune cells, suggesting that antibody binding itself induces cell death.[73] The anti-PD-1/PD-L1 and anti-CTLA-4 checkpoint inhibitors physically prevent receptor engagement and subsequent immunosuppressive signaling via PD-1 or CTLA-4, respectively, allowing for activation of anti-cancer T cells.[74] Binding of antibodies on a tumor cell surface can also induce complement dependent cytotoxicity (CMC) via the complement system or antibody-dependent cell-mediated cytotoxicity (ADCC) through binding of NK cells to the antibody Fc domain. ADCC is thought to be a primary mechanism of action of trastuzumab, a prominent therapeutic for HER2-positive breast cancers, although binding of antibody to HER2 also appears to interfere with downstream signaling pathways to inhibit cancer growth.[75]

Over the past decade, adoptive cell transfer technologies have risen to the forefront of cutting edge cancer therapy. As discussed above, immunosuppressive signaling in the context of cancer tends to prevent proper development of cancer-specific immune cells by preventing appropriate cell differentiation and activation. Adoptive cell transfer techniques seek to bypass this problem by engineering anti-cancer immune cells *ex vivo* and then transplanting these primed cells into the patient.[76] As early as 1964, Delorme and Alexander demonstrated in a pilot study that tumor cells could be used to generate cancer-specific lymphocytes in donor rats.[77] Introduction of these lymphocytes back into tumor-bearing rats resulted in tumor regression that could not be accounted for by a general graft-versus-host response. While encouraging, technical challenges associated with expanding and handling primary cells *ex vivo* without extensive cell death or loss of effector function stymied clinical applications for several decades.

The first FDA approved adoptive cell transfer therapy, sipuleucel-T, was developed by Engleman and Strober in the 1990s and approved in 2010 as a treatment for prostate cancer.[78-79] Sipuleucel-T represented a methodology by which patient dendritic cells were isolated and loaded with the prostate cancer antigen prostatic acid phosphatase (PAP) before administration as a cell-based therapeutic. More recently, adoptive cell transfer has been combined with genetic techniques in the form of T cells engineered to express tumor specific T-cell receptors or chimeric antigen receptors (CAR-T).[80] The first approvals of CAR-T therapies in 2017 of tisagenleucel (Kymriah™) and axicabtagene ciloleucel (Yescarta™) highlighted their sometimes extraordinary

remission rates.[81-82] Notably, CAR-T therapies to date have proven less successful for solid tumors, and both approved therapies target B cell lymphomas. Perhaps most concerning for any adoptive cell transfer therapy are the current cost and scale-up issues associated with manufacturing.[76] Because each treatment course requires isolation and engineering of a patient's cells, costs range from at least $93,000 for Sipuleucel-T to over $300,000 for CAR-T therapies.[83-84] The individualized nature of each treatment course introduces operational and manufacturing complexity that will need to be addressed in order to support widespread adoption.

1.6 Summary and Outlook

Pattern-recognition receptors on innate immune cells are a key component of the human immune system. In binding common microbial molecular signatures, they allow for pathogen-directed immune responses in the absence of fully-established adaptive immunity against an invading threat. Furthermore, antigen-presenting cells that make heavy use of TLRs, CLRs, and other PRRs serve as key mediators between the adaptive and innate immune systems. Understanding the roles of these diverse receptors and the kinds of immune responses they can elicit in different contexts is an ongoing challenge in the immunology field. Towards that end, a variety of synthetic ligands have been developed to probe these receptors, and have provided useful insight into immune signaling pathways.

Synthetic immunomodulatory compounds also have significant clinical potential. In fact, innate immune receptor agonists are already used in the clinic to treat some cancers, where the majority of research has focused on TLRs and STING.[67] Given the complexity of immune signaling pathways and the known synergy afforded by stimulating multiple immune receptor types simultaneously, it would be useful to identify synthetic ligands for other PRRs. In the following chapters, I describe my efforts to develop an N-carboxyanhydride (NCA) polymerization platform for synthesizing immunomodulatory glycopolypeptides, with a particular focus on cancer immunotherapy. I first present the successful synthesis and polymerization of a panel of glycosylated NCA monomers, establishing that the technique is generalizable to a variety of carbohydrate motifs and setting the stage for a wide variety of biological applications. I will then focus on the specific use of glucosylated and mannosylated glycopolypeptides as activators of innate immune cells via the C-type lectin receptors Dectin-1 and Dectin-2, and explore Dectin-2 targeting as a strategy for cancer immunotherapy. The closing chapter covers my efforts to improve on the polymerization technology through attempts to better characterize the transition metal initiators, and exploration of alternative initiation strategies.

1.7 References

1. Owen, J. A. P., J.; Stranford, Sharon A., *Kuby Immunology*. 7th ed.; W. H. Freeman: 2013.

2. Baxby, D., Edward Jenner's Inquiry; a bicentenary analysis. *Vaccine* **1999,** *17* (4), 301-307.

3. Pancer, Z.; Cooper, M. D., The evolution of adaptive immunity. *Annu Rev Immunol* **2006,** *24*, 497-518.

4. Antia, R.; Ganusov, V. V.; Ahmed, R., The role of models in understanding CD8+ T-cell memory. *Nat Rev Immunol* **2005,** *5* (2), 101-11.

5. Dunkelberger, J. R.; Song, W. C., Complement and its role in innate and adaptive immune responses. *Cell Res* **2010,** *20* (1), 34-50.

6. Hamerman, J. A.; Ogasawara, K.; Lanier, L. L., NK cells in innate immunity. *Curr Opin Immunol* **2005,** *17* (1), 29-35.

7. Mekori, Y. A.; Metcalfe, D. D., Mast cells in innate immunity. *Immunological Reviews* **2000,** *173* (1), 131-140.

8. Davidson, S. M.; Vander Heiden, M. G., Critical Functions of the Lysosome in Cancer Biology. *Annu Rev Pharmacol Toxicol* **2017,** *57*, 481-507.

9. Iwasaki, A.; Medzhitov, R., Control of adaptive immunity by the innate immune system. *Nat Immunol* **2015,** *16* (4), 343-53.

10. Guermonprez, P.; Valladeau, J.; Zitvogel, L.; Thery, C.; Amigorena, S., Antigen presentation and T cell stimulation by dendritic cells. *Annu Rev Immunol* **2002,** *20*, 621-67.

11. Merad, M.; Sathe, P.; Helft, J.; Miller, J.; Mortha, A., The dendritic cell lineage: ontogeny and function of dendritic cells and their subsets in the steady state and the inflamed setting. *Annu Rev Immunol* **2013,** *31*, 563-604.

12. Théry, C.; Amigorena, S., The cell biology of antigen presentation in dendritic cells. *Current Opinion in Immunology* **2001,** *13* (1), 45-51.

13. Brubaker, S. W.; Bonham, K. S.; Zanoni, I.; Kagan, J. C., Innate immune pattern recognition: a cell biological perspective. *Annu Rev Immunol* **2015,** *33*, 257-90.

14. Souza-Fonseca-Guimaraes, F.; Adib-Conquy, M.; Cavaillon, J. M., Natural killer (NK) cells in antibacterial innate immunity: angels or devils? *Mol Med* **2012,** *18*, 270-85.

15. Zarember, K. A.; Godowski, P. J., Tissue Expression of Human Toll-Like Receptors and Differential Regulation of Toll-Like Receptor mRNAs in Leukocytes in Response to Microbes, Their Products, and Cytokines. *The Journal of Immunology* **2002,** *168* (2), 554-561.

16. Osorio, F.; Reis e Sousa, C., Myeloid C-type lectin receptors in pathogen recognition and host defense. *Immunity* **2011,** *34* (5), 651-64.

17. Ashwell, G.; Harford, J., Carbohydrate-specific receptors of the liver. *Annu Rev Biochem* **1982,** *51*, 531-54.

18. Spiess, M., The asialoglycoprotein receptor: a model for endocytic transport receptors. *Biochemistry* **2002,** *29* (43), 10009-10018.

19. Mayer, S.; Raulf, M. K.; Lepenies, B., C-type lectins: their network and roles in pathogen recognition and immunity. *Histochem Cell Biol* **2017,** *147* (2), 223-237.

20. *Essentials of Glycobiology*. 3rd ed.; Cold Spring Harbor: Cold Spring Harbor (NY), 2015-2017.

21. Dambuza, I. M.; Brown, G. D., C-type lectins in immunity: recent developments. *Curr Opin Immunol* **2015,** *32*, 21-7.

22. Kerscher, B.; Willment, J. A.; Brown, G. D., The Dectin-2 family of C-type lectin-like receptors: an update. *Int Immunol* **2013,** *25* (5), 271-7.

23. Li, K.; Qu, S.; Chen, X.; Wu, Q.; Shi, M., Promising Targets for Cancer Immunotherapy: TLRs, RLRs, and STING-Mediated Innate Immune Pathways. *Int J Mol Sci* **2017,** *18* (2).

24. Zhu, L. L.; Zhao, X. Q.; Jiang, C.; You, Y.; Chen, X. P.; Jiang, Y. Y.; Jia, X. M.; Lin, X., C-type lectin receptors Dectin-3 and Dectin-2 form a heterodimeric pattern-recognition receptor for host defense against fungal infection. *Immunity* **2013,** *39* (2), 324-34.

25. Aldara (imiquimod) Cream. Package insert. 3M Health Care Limited: Loughborough, England, 2010. **1997**.

26. Frampton, J. E., Mifamurtide: a review of its use in the treatment of osteosarcoma. *Paediatr Drugs* **2010,** *12* (3), 141-53.

27. Steinhagen, F.; Kinjo, T.; Bode, C.; Klinman, D. M., TLR-based immune adjuvants. *Vaccine* **2011,** *29* (17), 3341-55.

28. Northrup, L.; Christopher, M. A.; Sullivan, B. P.; Berkland, C., Combining antigen and immunomodulators: Emerging trends in antigen-specific immunotherapy for autoimmunity. *Adv Drug Deliv Rev* **2016,** *98*, 86-98.

29. Gerster, J. F. 1H-Imidazo[4,5-c]quinolines and 1H-imidazo[4,5-c]quinolin-4-amines. EP 0145340, 1985.

30. Pharmaceuticals, N., Study of the Safety and Efficacy of MIW815 With PDR001 to Patients With Advanced/Metastatic Solid Tumors or Lymphomas.

31. Conlon, J.; Burdette, D. L.; Sharma, S.; Bhat, N.; Thompson, M.; Jiang, Z.; Rathinam, V. A.; Monks, B.; Jin, T.; Xiao, T. S.; Vogel, S. N.; Vance, R. E.; Fitzgerald, K. A., Mouse, but not human STING, binds and signals in response to the vascular disrupting agent 5,6-dimethylxanthenone-4-acetic acid. *J Immunol* **2013,** *190* (10), 5216-25.

32. Cluff, C. W., Monophosphoryl Lipid A (MPL) as an Adjuvant for Anti-Cancer Vaccines: Clinical Results.

33. Homans, S. W., Dynamics and Thermodynamics of Ligand–Protein Interactions. **2007,** *272*, 51-82.

34. Weis, W. I.; Drickamer, K., Structural basis of lectin-carbohydrate recognition. *Annu Rev Biochem* **1996,** *65*, 441-73.

35. Gestwicki, J. E.; Cairo, C. W.; Strong, L. E.; Oetjen, K. A.; Kiessling, L. L., Influencing Receptor−Ligand Binding Mechanisms with Multivalent Ligand Architecture. *Journal of the American Chemical Society* **2002,** *124* (50), 14922-14933.

36. Honjoh, C.; Chihara, K.; Yoshiki, H.; Yamauchi, S.; Takeuchi, K.; Kato, Y.; Hida, Y.; Ishizuka, T.; Sada, K., Association of C-Type Lectin Mincle with FcepsilonRIbetagamma Subunits Leads to Functional Activation of RBL-2H3 Cells through Syk. *Sci Rep* **2017,** *7*, 46064.

37. Walachowski, S.; Tabouret, G.; Foucras, G., Triggering Dectin-1-Pathway Alone Is Not Sufficient to Induce Cytokine Production by Murine Macrophages. *PLoS One* **2016,** *11* (2), e0148464.

38. Goodridge, H. S.; Reyes, C. N.; Becker, C. A.; Katsumoto, T. R.; Ma, J.; Wolf, A. J.; Bose, N.; Chan, A. S.; Magee, A. S.; Danielson, M. E.; Weiss, A.; Vasilakos, J. P.; Underhill, D. M., Activation of the innate immune receptor Dectin-1 upon formation of a 'phagocytic synapse'. *Nature* **2011,** *472* (7344), 471-5.

39. Inoue, M.; Moriwaki, Y.; Arikawa, T.; Chen, Y. H.; Oh, Y. J.; Oliver, T.; Shinohara, M. L., Cutting edge: critical role of intracellular osteopontin in antifungal innate immune responses. *J Immunol* **2011,** *186* (1), 19-23.

40. Werlen, G.; Palmer, E., The T-cell receptor signalosome: a dynamic structure with expanding complexity. *Current Opinion in Immunology* **2002,** *14* (3), 299-305.

41. van Haren, S. D.; Dowling, D. J.; Foppen, W.; Christensen, D.; Andersen, P.; Reed, S. G.; Hershberg, R. M.; Baden, L. R.; Levy, O., Age-Specific Adjuvant Synergy: Dual TLR7/8 and Mincle Activation of Human Newborn Dendritic Cells Enables Th1 Polarization. *J Immunol* **2016,** *197* (11), 4413-4424.

42. Tom, J. K.; Dotsey, E. Y.; Wong, H. Y.; Stutts, L.; Moore, T.; Davies, D. H.; Felgner, P. L.; Esser-Kahn, A. P., Modulation of Innate Immune Responses via Covalently Linked TLR Agonists. *ACS Cent Sci* **2015,** *1* (8), 439-448.

43. Ryu, K. A.; Slowinska, K.; Moore, T.; Esser-Kahn, A., Immune Response Modulation of Conjugated Agonists with Changing Linker Length. *ACS Chem Biol* **2016,** *11* (12), 3347-3352.

44. Trinchieri, G.; Sher, A., Cooperation of Toll-like receptor signals in innate immune defence. *Nat Rev Immunol* **2007,** *7* (3), 179-90.

45. Lepenies, B.; Lee, J.; Sonkaria, S., Targeting C-type lectin receptors with multivalent carbohydrate ligands. *Adv Drug Deliv Rev* **2013,** *65* (9), 1271-81.

46. Ganneau, C.; Simenel, C.; Emptas, E.; Courtiol, T.; Coic, Y. M.; Artaud, C.; Deriaud, E.; Bonhomme, F.; Delepierre, M.; Leclerc, C.; Lo-Man, R.; Bay, S., Large-scale synthesis and structural analysis of a synthetic glycopeptide dendrimer as an anti-cancer vaccine candidate. *Org Biomol Chem* **2016,** *15* (1), 114-123.

47. Shukla, N. M.; Salunke, D. B.; Balakrishna, R.; Mutz, C. A.; Malladi, S. S.; David, S. A., Potent adjuvanticity of a pure TLR7-agonistic imidazoquinoline dendrimer. *PLoS One* **2012,** *7* (8), e43612.

48. Koshy, S. T.; Cheung, A. S.; Gu, L.; Graveline, A. R.; Mooney, D. J., Liposomal Delivery Enhances Immune Activation by STING Agonists for Cancer Immunotherapy. *Advanced Biosystems* **2017,** *1* (1-2), 1600013.

49. Kim, W. G.; Choi, B.; Yang, H. J.; Han, J. A.; Jung, H.; Cho, H.; Kang, S.; Hong, S. Y., Covalent Conjugation of Small-Molecule Adjuvants to Nanoparticles Induces Robust Cytotoxic T Cell Responses via DC Activation. *Bioconjug Chem* **2016,** *27* (9), 2007-13.

50. Reichardt, N. C.; Martin-Lomas, M.; Penades, S., Opportunities for glyconanomaterials in personalized medicine. *Chem Commun (Camb)* **2016,** *52* (92), 13430-13439.

51. Barbeau, J.; Lemiegre, L.; Quelen, A.; Malard, V.; Gao, H.; Goncalves, C.; Berchel, M.; Jaffres, P. A.; Pichon, C.; Midoux, P.; Benvegnu, T., Synthesis of a trimannosylated-equipped archaeal diether lipid for the development of novel glycoliposomes. *Carbohydr Res* **2016,** *435*, 142-148.

52. Anselmo, A. C.; Mitragotri, S., Nanoparticles in the clinic. *Bioengineering & Translational Medicine* **2016,** *1* (1), 10-29.

53. Wu, L. P.; Ficker, M.; Christensen, J. B.; Trohopoulos, P. N.; Moghimi, S. M., Dendrimers in Medicine: Therapeutic Concepts and Pharmaceutical Challenges. *Bioconjug Chem* **2015,** *26* (7), 1198-211.

54. Xin, Y.; Yin, M.; Zhao, L.; Meng, F.; Luo, L., Recent progress on nanoparticle-based drug delivery systems for cancer therapy. *Cancer Biol Med* **2017,** *14* (3), 228-241.

55. Burnet, F. M., The Concept of Immunological Surveillance. **1970,** *13*, 1-27.

56. van der Burg, S. H.; Arens, R.; Ossendorp, F.; van Hall, T.; Melief, C. J., Vaccines for established cancer: overcoming the challenges posed by immune evasion. *Nat Rev Cancer* **2016,** *16* (4), 219-33.

57. Correa, I.; Plunkett, T., Update on HER-2 as a target for cancer therapy: HER2/neu peptides as tumour vaccines for T cell recognition. *Breast Cancer Research* **2001,** *3* (6).

58. Kobayashi, H.; Wood, M.; Song, Y.; Appella, E.; Celis, E., Defining promiscuous MHC class II helper T-cell epitopes for the HER2/neu tumor antigen. *Cancer Res* **2000,** *60* (18), 5228-36.

59. Kerkar, S. P.; Restifo, N. P., Cellular constituents of immune escape within the tumor microenvironment. *Cancer Res* **2012,** *72* (13), 3125-30.

60. Garrido, F.; Aptsiauri, N.; Doorduijn, E. M.; Garcia Lora, A. M.; van Hall, T., The urgent need to recover MHC class I in cancers for effective immunotherapy. *Curr Opin Immunol* **2016,** *39*, 44-51.

61. Patel, S. P.; Kurzrock, R., PD-L1 Expression as a Predictive Biomarker in Cancer Immunotherapy. *Mol Cancer Ther* **2015,** *14* (4), 847-56.

62. Xiao, H.; Woods, E. C.; Vukojicic, P.; Bertozzi, C. R., Precision glycocalyx editing as a strategy for cancer immunotherapy. *Proc Natl Acad Sci U S A* **2016,** *113* (37), 10304-9.

63. Coley, W. B., II. Contribution to the Knowledge of Sarcoma. *Ann Surg* **1891,** *14* (3), 199-220.

64. Lee, S.; Margolin, K., Cytokines in cancer immunotherapy. *Cancers (Basel)* **2011,** *3* (4), 3856-93.

65. Marabelle, A.; Kohrt, H.; Caux, C.; Levy, R., Intratumoral immunization: a new paradigm for cancer therapy. *Clin Cancer Res* **2014,** *20* (7), 1747-56.

66. Kaufman, H. L.; Ruby, C. E.; Hughes, T.; Slingluff, C. L., Jr., Current status of granulocyte-macrophage colony-stimulating factor in the immunotherapy of melanoma. *J Immunother Cancer* **2014,** *2*, 11.

67. Tang, J.; Shalabi, A.; Hubbard-Lucey, V. M., Comprehensive analysis of the clinical immuno-oncology landscape. *Ann Oncol* **2018,** *29* (1), 84-91.

68. Stern, A. C.; Jones, T. C., The side-effect profile of GM-CSF. *Infection* **1992,** *20* (2), S124-S127.

69. Petrovsky, N.; Aguilar, J. C., Vaccine adjuvants: current state and future trends. *Immunol Cell Biol* **2004,** *82* (5), 488-96.

70. Shiku, H. T., T., Autologous typing: a tedious but orthodox approach for defining human tumor antigens with clarity. *Cancer Immunity* **2012,** *12*.

71. Schietinger, A.; Philip, M.; Schreiber, H., Specificity in cancer immunotherapy. *Semin Immunol* **2008,** *20* (5), 276-85.

72. Oldham, R. K.; Dillman, R. O., Monoclonal antibodies in cancer therapy: 25 years of progress. *J Clin Oncol* **2008,** *26* (11), 1774-7.

73. Weiner, G. J., Rituximab: mechanism of action. *Semin Hematol* **2010,** *47* (2), 115-23.

74. Pardoll, D. M., The blockade of immune checkpoints in cancer immunotherapy. *Nat Rev Cancer* **2012,** *12* (4), 252-64.

75. Hudis, C. A., Trastuzumab--mechanism of action and use in clinical practice. *N Engl J Med* **2007,** *357* (1), 39-51.

76. June, C. H.; Riddell, S. R.; Schumacher, T. N., Adoptive cellular therapy: a race to the finish line. *Sci Transl Med* **2015,** *7* (280), 280ps7.

77. Delorme, E. A. P., Treatment of Primary Fibrosarcoma in the Rat with Immune Lymphocytes. *The Lancet* **1964,** *284* (7351), 117-120.

78. Kantoff, P. W.; Higano, C. S.; Shore, N. D.; Berger, E. R.; Small, E. J.; Penson, D. F.; Redfern, C. H.; Ferrari, A. C.; Dreicer, R.; Sims, R. B.; Xu, Y.; Frohlich, M. W.; Schellhammer, P. F.; Investigators, I. S., Sipuleucel-T immunotherapy for castration-resistant prostate cancer. *N Engl J Med* **2010,** *363* (5), 411-22.

79. Engleman, E., Dendritic cell-based cancer immunotherapy. *Seminars in Oncology* **2003,** *30*, 23-29.

80. Rosenberg, S. A.; Restifo, N. P., Adoptive cell transfer as personalized immunotherapy for human cancer. *Science* **2015,** *348* (6230), 62-8.

81. FDA approval brings first gene therapy to the United States. In *CAR T-cell therapy approved to treat certain children and young adults with B-cell acute lymphoblastic leukemia*, U.S. Food & Drug Administration.

82. FDA approves CAR-T cell therapy to treat adults with certain types of large B-cell lymphoma. In *Yescarta is the second gene therapy product approved in the U.S.*, U.S. Food & Drug Administration.

83. Chambers, J. D.; Neumann, P. J., Listening to Provenge--what a costly cancer treatment says about future Medicare policy. *N Engl J Med* **2011,** *364* (18), 1687-9.

84. Clarke, T. B., B. FDA approves Gilead cancer gene therapy; price set at $373,000 *Reuters* [Online], 2017. https://www.reuters.com/article/us-gilead-sciences-fda/fda-approves-gilead-cancer-gene-therapy-price-set-at-373000-idUSKBN1CN35H (accessed Feb 1, 2018).

Chapter 2

Expanding the N-carboxyanhydride glycopolypeptide platform through the synthesis and polymerization of a panel of O-glycosylated monomers

This work was adapted in part from Zhou, M. N.; Delaveris, C. S.; Kramer, J. R.; Kenkel, J. A.; Engleman, E. G.; Bertozzi, C. R. N-carboxyanhydride polymerization of glycopolypeptides that activate antigen presenting cells through Dectin-1 and -2. *Angew. Chemie Int. Ed.* **2018**.

2.1 Glycopolymers as tools for glycobiology research

The central dogma of molecular biology—describing the relationship between DNA, RNA, and protein—has motivated our understanding and study of biology on the cellular and molecular levels for over half a century.[1] Lost in this framework are the vital roles of other biomolecules such glycans, which play essential roles in diverse biological processes from fertilization and adhesion to cancer and immunity.[2] Despite a burgeoning interest in glycobiology, systematic characterization of specific glycosylation patterns in signaling processes remains a challenge. Unlike proteins, glycans are often only indirectly controlled by genetic factors, and are therefore difficult to probe by the wealth of increasingly powerful genetic tools.[3] Furthermore, glycosylation patterns can be difficult to analyze by mass spectrometry techniques due to their poor ionization characteristics and complexity.[4-5] Combined with a historical lack of focus on glycobiology, such experimental challenges mean that the study of and therapeutic targeting of glycan signaling has lagged behind that of proteins, DNA, and RNA.

Advancing our understanding of how glycans impact biological processes will certainly require a multipronged approach. Along these lines, ongoing fields of research include improving glycoproteomics and glycan mass spectrometry, as well as genetic studies that attempt to deconvolute the complex pathways responsible for synthesizing, processing, and recognizing biological glycans. An alternative approach is to synthesize mimics of natural glycosylated biopolymers as probes for studying how perturbing factors such as glycan density and composition impact cellular processes. Given the appropriate biological systems and robust enough ligands, such structures could even serve as therapeutic molecules analogous to conventional small molecule ligands for enzymes. Unfortunately, due to their size and chemical complexity, synthesis of truly native glycosylated biopolymers remains laborious and challenging.[6-8]

As a workaround to de novo synthesizing native glycoproteins, researchers have often made use of synthetic glycopolymers to probe glycan-receptor interactions. Free radical polymerization of polyacrylamide-based glycopolymers has been reported as far back as the 1970s.[9] Since then, ring-opening metathesis polymerization (ROMP) and reversible addition-fragmentation chain transfer (RAFT) polymerization have emerged as the dominant technologies represented in the chemical biology literature (Scheme 2.1). Starting in the mid-1990s, Kiessling et al. reported studies on the dependence of Concanavalin A binding to ROMP polymers of varying lengths and glycosylations, establishing the technology as a viable glycobiology tool.[10-11] Since then, the scaffold has been used to investigate a variety of glycan-dependent signal transduction pathways and to synthesize chondroitin sulfate proteoglycan mimics.[12-14] ROMP glycopolymers are generally synthesized using glycosylated monomers, which reliably react with ruthenium carbene catalysts to give well-defined polymers of controlled length. End groups can in principle be controlled via catalyst structure, and glycan density can be controlled either through copolymerization with nonglycosylated monomers or by varying the number of glycans displayed on each monomer unit. Notably, because the polymerization can be performed using glycosylated monomers, ROMP avoids concerns about glycosylation efficiency inherent to post-polymerization functionalization.

Concurrently, our lab and others have employed RAFT and other controlled radical polymerizations to great effect in a variety of systems including viral binding of host cell glycans, selectin selectivity and signaling, and cell-surface mucin biology.[12, 15-18] As with conventional free

radical polymerizations, RAFT induces radical formation in conjugated vinyl monomers to initiate and propagate polymerization. However, by using a chain-transfer agent, most often a trithiocarbonate or dithioester, RAFT polymerization limits the activity of propagating chains by trapping a portion of the growing chain ends in an inactive form at any given time.[19-20] Increasing the ratio of initiation rate to propagation rate significantly improves polymer dispersity, making RAFT one of the most widely used radical polymerization techniques. Because glycans are not readily compatible with the elevated temperatures and radical species involved in RAFT polymerization, glycopolymers made by this route generally require post-polymerization functionalization. This can be easily done using poly(methyl vinyl ketone) (PMVK) polymers, which react readily with aminooxy glycans to give oxime linkages.[21] Glycosylation density can be tuned relatively simply by varying reagent ratios, and isolated polymers can be designed to feature functional chain ends for conjugation to a variety of substrates.[22] However, as with ROMP polymers, RAFT polymers lack native backbone structures or glycosidic linkages.

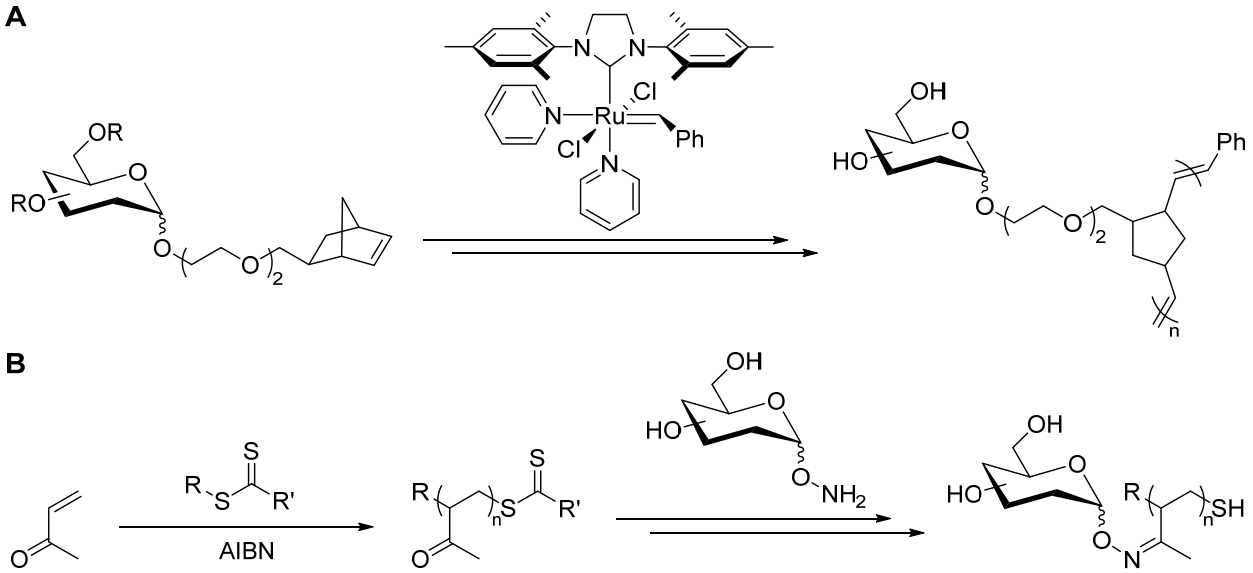

Scheme 2.1. Generalized synthetic routes to ROMP and RAFT polymers. A) Ring-opening olefin metathesis using ruthenium catalysts gives glycopolymers of controllable length and good dispersities. B) RAFT polymerization of vinyl monomers using azobisisobutyronitrile (AIBN) or other radical initiators similarly allows for good polymer length control and dispersity due to the use of a trithiocarbonate or dithioester chain transfer agent (CTA).

Given roughly two decades of glycobiology research using synthetic glycopolymers, hydrocarbon scaffolds have certainly progressed our understanding of carbohydrate-receptor interactions and their downstream signaling pathways. Yet, to the best of our knowledge, such materials have largely been confined to academic settings despite a wealth of publications demonstrating their biological activity and proposing their utility in therapeutic applications.[6, 23-24] While the reasons for this gap are certainly varied and differ between applications and scaffolds, development of a more biomimetic platform would certainly address concerns such as unclear biodegradation products or off-target effects resulting from unnatural chemical structures. Notably, polyvalent carbohydrate-based therapeutics generally feature glycans conjugated to carrier proteins, viral particles, or other biological macromolecules, resulting in less control over glycosylation but more favorable pharmacokinetics and pharmacodynamics than a polyalkyl chain.[25-27]

2.2 N-carboxyanhydride polymerization: a promising and underexplored glycopolymer platform

As a glycopolymer platform, true polypeptides would represent the most biomimetic scaffold possible for mimicking native glycoproteins. Along these lines, a variety of labs have reported the synthesis of glycopolypeptides by solid-phase peptide synthesis. Derivatives of mucin tandem repeat glycopeptides have been particularly popular as potential platforms for cancer vaccines, as aberrantly glycosylated mucins are highly expressed on the surfaces of many cancers.[28-30] These tumor associated carbohydrate antigens (TACAs) are a common focus in the glycopolymer and glycopeptide literature, despite evidence that cancer immunoediting selects for TACAs that suppress immune activation.[28, 31-32] Other applications vary from synthetic glycopeptide opioids to more conventional antifungal and antibacterial vaccines.[33-34] As an alternative, conjugation of immunomodulatory glycans to either inert or biologically active carrier proteins represents another major strategy for generating glycosylated peptide-based materials.[35-36] Carrier proteins provide the ability to generate large, sequence-defined structures and introduce additional functionality via the choice of protein scaffold. However, the ability to tune factors such as glycosylation density is often limited. A complementary glycopolypeptide-based system that can combine the high tunability of solid-phase synthetic peptides with the size of protein scaffolds might therefore prove to be a useful platform.

Fortunately, a robust technique for the synthesis of high molecular weight polypeptides has been known to the polymer chemistry and materials science fields for decades. In 1906, Hermann Leuchs first reported the synthesis of α-amino acid N-carboxyanhydrides (NCAs) (Scheme 2.2).[37] Although these unusual ring structures were recognized to form oligomers, serious study of NCAs as monomers for polypeptide synthesis began in the 1920s with the work of Curtius and Wessely and has remained an active field since.[38-40] Polymerization of a blend of NCA monomers affords random copolymers, with achievable lengths into the hundreds of amino acid residues in a single polymerization reaction, a significant improvement over the ~50 amino acid average practical limit for solid-phase peptide synthesis.[41] Moreover, length can be controlled fairly trivially through varying monomer:initiator ratios rather than requiring a separate set of deprotection/coupling reactions for the addition of each monomer. The technique does sacrifice control over amino acid sequence and generates a distribution of polymer lengths rather than a homogeneous polypeptide, making it best suited for applications that do not depend on a specific polypeptide primary sequence.

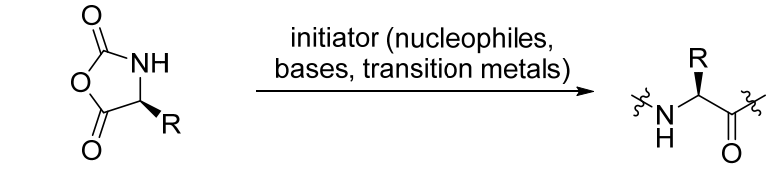

Scheme 2.2. N-carboxyanhydride (NCA) monomers readily undergo polymerization in the presence of a variety of initiators to give polypeptides.

Much of the focus in the NCA polymerization field has been on improving initiation technologies to yield tighter polymer dispersities. Water and alcohols served as the first reported initiators for

NCA polymerization, followed shortly after by stronger nucleophiles such as amines, which remain in use to date.[42] As an alternative to classic nucleophilic initiation, Deming et al. reported in 1997 a transition metal-based strategy for NCA polymerization.[43] Ni(0) and Co(0) initiators bearing sigma-donating ligands rapidly initiated polymerization; IR spectroscopy and isotope-labeling experiments suggested a mechanism involving oxidative addition of the metal across the NCA anhydride bond, followed by loss of CO to give an initial metallocycle intermediate (Scheme 2.3).[44] Subsequent monomer addition/ring contraction steps could then generate a putative amido-amidate propagating species, although formal characterization of this intermediate has been limited. At the time of the initial publications in the late 90s, the low dispersities and rapid reaction rates observed with these initiators represented a significant advance over conventional initiation with primary amines. Subsequent publications demonstrated the ability to add functionality to the polypeptide C-terminus using Ni(II) amido-amidates.[45] We therefore anticipated that these transition metal initiators might be a promising approach to synthesizing NCA-derived glycopolypeptides.

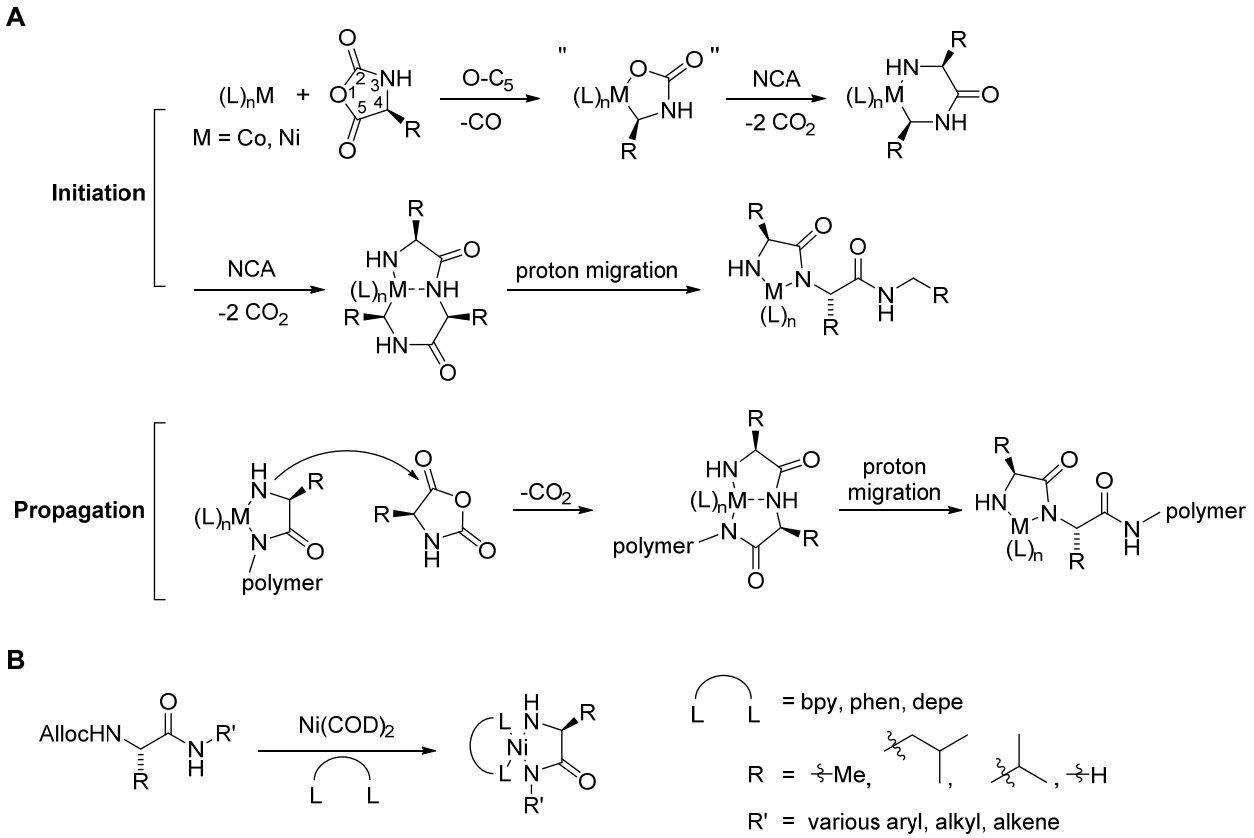

Scheme 2.3. Overview of transition metal initiated NCA polymerization. A) Proposed mechanisms of initiation and propagation for NCA polymerization using Co(0) and Ni(0) complexes.[44] B) Synthetic overview and summary of Ni(II) initiators synthesized by Deming et al. for generating end-functionalized polypeptides.[45] Bpy = 2,2′-bipyridine; phen = 1,10-phenanthroline; depe = 1,2-bis(diethylphosphino)ethane.

Notably, upon studying the NCA polymerization literature we found that there had been very little successful crossover to date between the NCA polymerization and glycopolymer fields. A number of groups have reported successful polymerization of glycosylated lysine NCAs, while the

majority of approaches rely on post-polymerization glycosylation.[46] None of these structures faithfully reproduce native N- or O-type glycosylation, negating one of the key advantages of NCA polymerization. Interestingly, it has been reported that O-glycosylated NCA monomers cannot be polymerized to give high molecular weight glycopolypeptides.[47-49] Given the generalizability of NCA polymerization to a diverse variety of amino acids, we suspected that low monomer purity may have undermined these previous attempts at glycopolypeptide synthesis. In a recent publication, we confirmed that purification of N-acetylgalactosamine-serine (GalNAc-Ser) NCAs by anhydrous column chromatography allowed for polymerization to give high molecular weight O-glycosylated polypeptides.[50] This opened the door for the synthesis of glycopolypeptides with precise control over glycosylation density and polymer lengths and dispersities at least on par with previous synthetic glycopolymer scaffolds. Meanwhile, the use of a native proteinaceous backbone and glycosidic linkages avoided introducing structural artifacts that could alter biophysical properties and receptor binding. From a translational perspective, we were heartened to find that NCA-based polypeptides have been successfully employed as active pharmaceutical ingredients: the NCA-derived polypeptide glatiramer acetate was approved by the FDA in 1996 as a multiple sclerosis therapy (Fig. 2.1).[51] With these factors in mind, the natural next step, and one of the early goals of my work, was to investigate the generalizability of the glyco-NCA platform by synthesizing and polymerizing a panel of glycosylated monomers with potential translational applications.

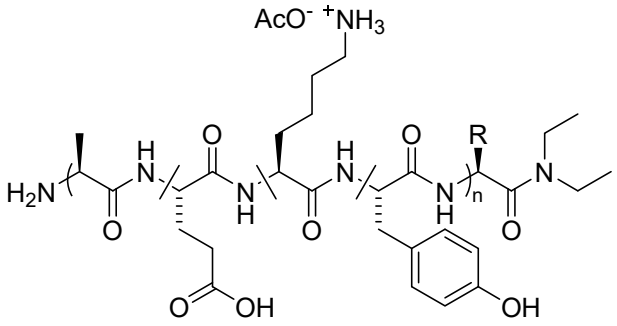

Figure 2.1. Structure of glatiramer acetate, an FDA approved NCA-derived polypeptide therapeutic for multiple sclerosis.

Because we envision the glyco-NCA technology as a platform for probing and perturbing biological processes, my panel of glyco-NCA monomers featured carbohydrates with plausible biological relevance. High-mannose and high-glucose structures are commonly associated with microbial cell walls and are often recognized by C-type lectins on host immune cells. We therefore synthesized serine-derived NCA monomers bearing mannose (Man), D-α-1,2-mannobiose (Man2), β-1,6-glucobiose (gentiobiose), β-1,3-glucobiose (laminaribiose, Glc2), and β-1,3-glucotriose (laminaritriose, Glc3) as potentially immunogenic lectin agonists (Scheme 2.4). Anticipating a need for control glycans, I also synthesized monomers featuring L-α-1,2-mannobiose and lactose (Lac). To build on our GalNAc-Ser work, I focused my efforts on O-glycosylated monomers, although polymerization of N-glycosylated structures is an ongoing area of research in the Bertozzi lab.

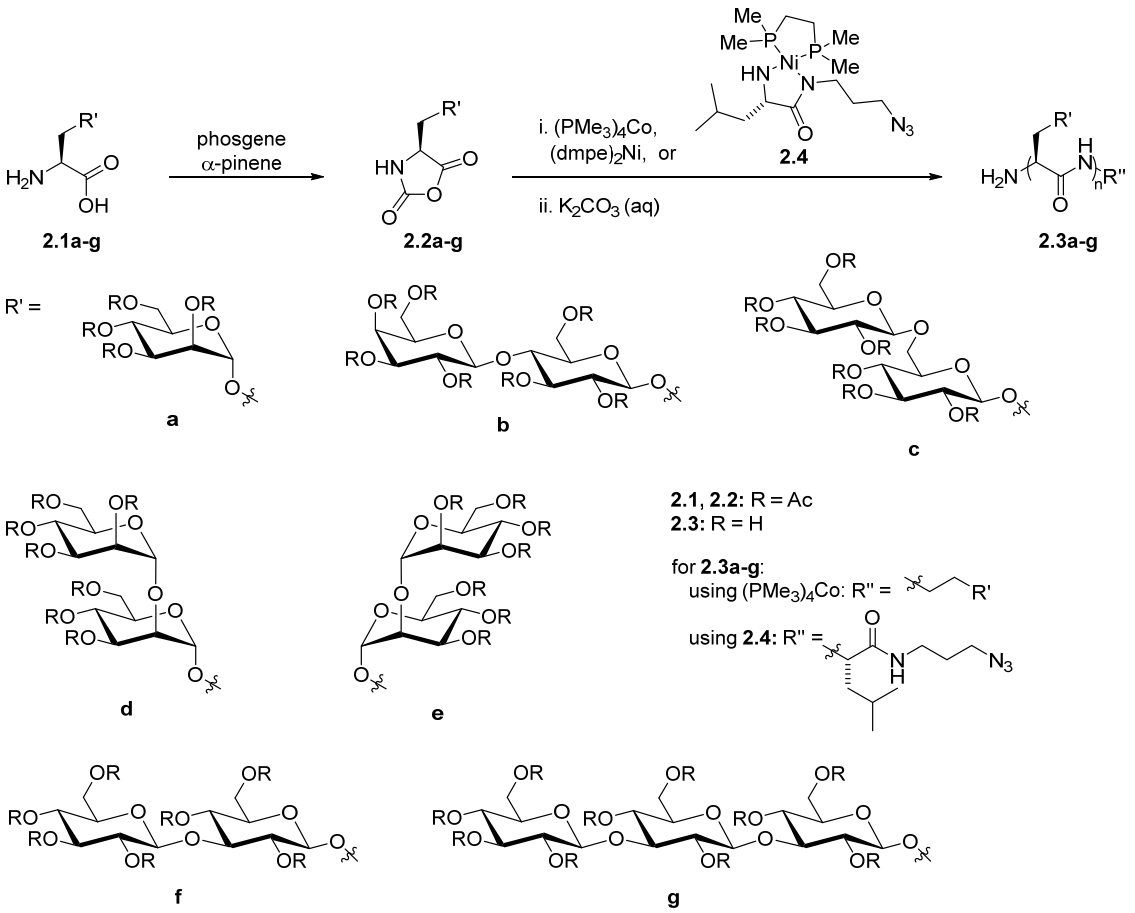

Scheme 2.4. Synthesis and polymerization of a panel of O-glycosylated serine NCA monomers using transition metal catalysts. Glycans of various sizes and stereochemistries were tested to probe the compatibility of the polymerization with different carbohydrate structures. Co(0) and Ni(0) initiators were used to give glycopolypeptides with functionalizable N-termini. C-terminal functionality was installed using Ni(II) catalyst **2.4**, which adds an alkyl azide for conjugation. Dmpe = 1,2-bis(dimethylphosphino)ethane.

2.3 General route to O-acetylated glycosylated serine NCA monomers and the synthesis of mannose-, lactose-, and gentiobiose-serine monomers from commercially available carbohydrates.

Given our successful synthesis and polymerization of peracetylated GalNAc-Ser NCA monomers, I designed the panel of O-glycosylated NCA monomers with a similar strategy in mind. Although a variety of hydroxyl protecting groups are used in the synthesis of complex carbohydrates, I chose peracetylation as a simple and versatile protection strategy with well-established and reliable post-polymerization deprotection protocols.[50] Along these lines, commercially available carbohydrates such as mannose, lactose, and gentiobiose were acetylated using acetic anhydride in the presence of either pyridine or iodine to access the corresponding protected sugars in good yields. Treatment of peracetylated sugars with HBr in acetic acid afforded the corresponding glycosyl bromides in generally good yields, which could be immediately used for Koenigs-Knorr type glycosylation using silver salts. While generally reliable, the bromides exhibited some inconvenient properties,

including a tendency to decompose upon storage. Furthermore, rigorous purification of the 1-bromo sugars to completely remove residual acetic acid and HBr sometimes proved difficult on larger scales. Repeated aqueous washes and/or column chromatography to improve purity occasionally led to decreased yields. To address these concerns, in some cases I instead made use of the popular trichloroacetimidate (TCA) donor approach. Briefly, anomeric acetates were deprotected reliably and specifically using stoichiometric hydrazine acetate in THF. The resulting 1-hydroxy sugars were reacted with trichloroacetonitrile in the presence of DBU to give the relatively-stable trichloroacetimidates in reasonable yields. Notably, during acid-promoted glycosylations, trichloroacetimidates bearing glucose-type 2-OH stereochemistry failed to react efficiently to give glycosylated products due to the ease of orthoester formation and subsequent rearrangements and side reactions upon activation of the TCA leaving group, a known problem with these classes of carbohydrates.[52] In these cases, the Koenigs-Knorr approach empirically gave better results.

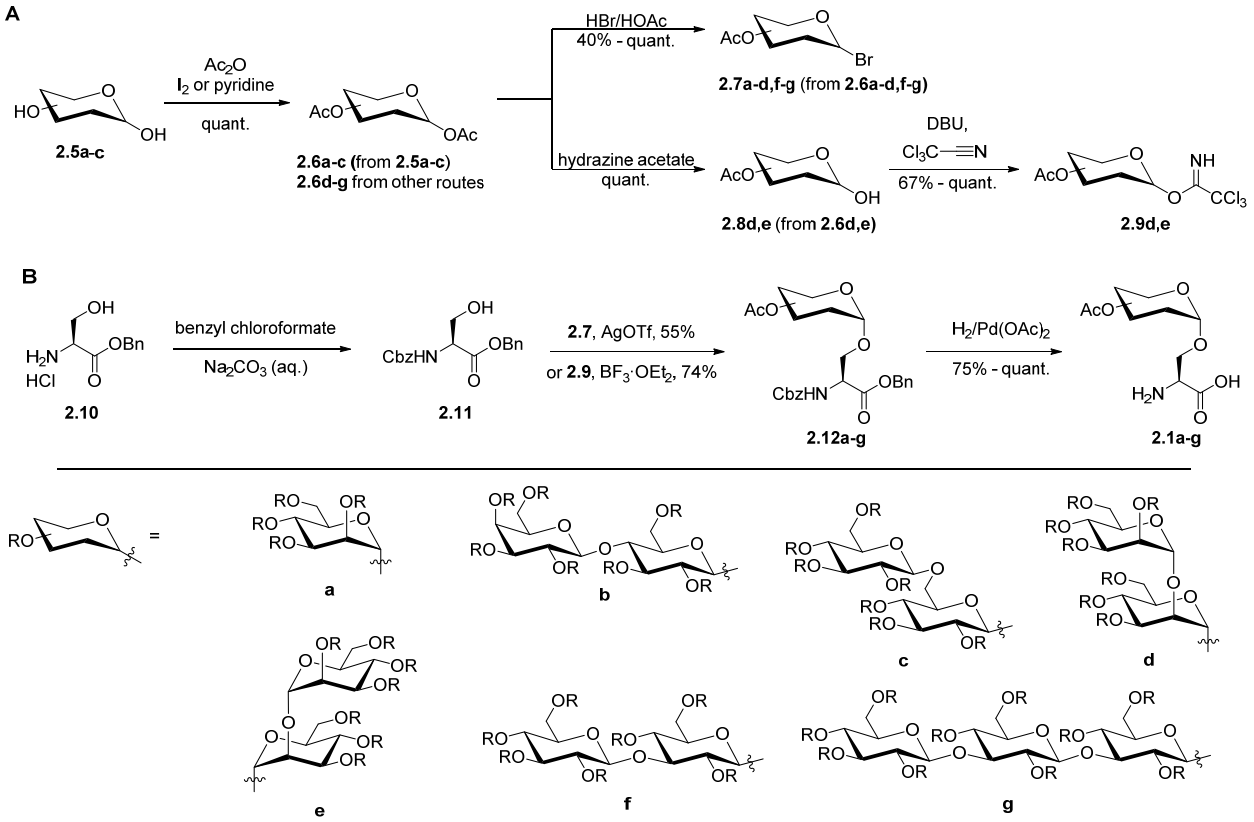

Scheme 2.5. General route to O-glycosylated NCA monomers. A) Synthesis of activated, protected glycan donors. B) Serine benzyl ester hydrochloride **2.10** was converted to the Z-Ser-OBn **2.11** under Schotten-Baumann conditions, glycosylated as appropriate for the sugar donor, and deprotected to give **2.1a-g**.

With the general glycosylation strategy established, I investigated a variety of protection strategies for the Ser acceptor. Due to the popular use of Fmoc/*t*Bu-protected amino acids in solid phase peptide synthesis, I initially tested the readily available acceptor Fmoc-Ser(OH)-O*t*Bu. I immediately encountered a variety of problems with this strategy. Purification of the glycosylated product by column chromatography was complicated by deprotection of the tBu ester on silica gel.

Although pooling of protected and deprotected material afforded workable yields, isolation of pure material after subsequent Fmoc deprotection proved difficult. Optimization of deprotection conditions and workup via preparative HPLC may have allowed for appropriately pure material; however, I decided the simpler solution would be to alter the protection strategy.

An optimal Ser scheme would allow for a single step, pH-neutral deprotection in anticipation of the NCA cyclization reaction, which in our experience can be sensitive to both acids and bases. This was readily achieved through Cbz-protection of the serine benzyl ester HCl salt using benzyl chloroformate in aqueous sodium carbonate. As a side note, glycosylation of carbamate- and ester-protected Ser is known to be impeded by reduced nucleophilic character of the Ser hydroxyl group compared to conventional aliphatic alcohol.[53] This is believed to be due to a hydrogen-bonding interaction between the proton of the protected amine and the hydroxyl group oxygen (Fig. 2.2). Various alternative protection schemes have been described that exploit hydrogen bonding properties to instead activate the hydroxyl group. I therefore tested the viability of a benzophenone imine protection strategy as well. However, in my hands the ease of synthesis and post-glycosylation deprotection of Z-Ser(OH)-OBn made it a more efficient acceptor overall. In particular, partial imine deprotection was observed during column chromatography, complicating purification and handling.

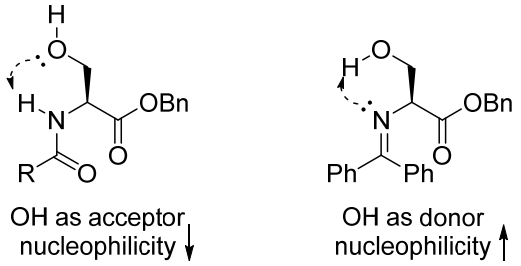

Figure 2.2. The serine hydroxyl group exhibits reduced nucleophilicity, likely due to intramolecular hydrogen bonding. The choice of amine protecting group influences the nature of these interactions and has been reported to impact reactivity of the hydroxyl group.[53]

2.4 Syntheses of per-*O*-acetyl-D- and L-α-1,2-mannobiose

Synthesis of the D- and L-α-1,2-mannobiose disaccharides was achieved through coupling of a 2-hydroxy-1,3,4,6-*O*-acetylmannose acceptor with a thioether donor (Scheme 2.6). In the case of the D-sugar enantiomer, the acceptor was commercially available on a scale of hundreds of milligrams. The L-sugar enantiomer or larger quantities of the D-sugar were prepared through 1,2-orthoester protection of 3,4,6-acetylated mannose via the 1-bromosugar (Scheme 2.6a). Exposure of the orthoester to dilute aqueous acid afforded a mixture of products, from which the desired material could be cleanly precipitated using a 1:1 ethyl acetate:hexanes mixture. The relatively low yields, likely due to competitive formation of 1-hydroxy-2,3,4,6-acetylmannose and other byproducts, were in agreement with literature observations and considered acceptable due to the easy and relatively inexpensive large-scale synthesis of the 1-bromo sugar from mannose.[54] Interestingly, due to the stereochemical requirements of orthoester formation, the isolated product adopts a beta-configuration at the anomeric position, which is unusual among mannose derivatives. Thioether donors were prepared via Lewis acid-promoted substitution of 1-acetylated sugars (Scheme 2.6b). Reaction of mannose derivatives **2.6a** and **2.6h** with ethanethiol afforded the

corresponding thioether, which could be crystallized from cold methanol to give the purified product without column chromatography. In the presence of *N*-iodosuccinimide and a Lewis acid, the thioether donor and 2-hydroxy acceptor coupled rapidly to give the desired peracetylated D- or L-mannobiose.

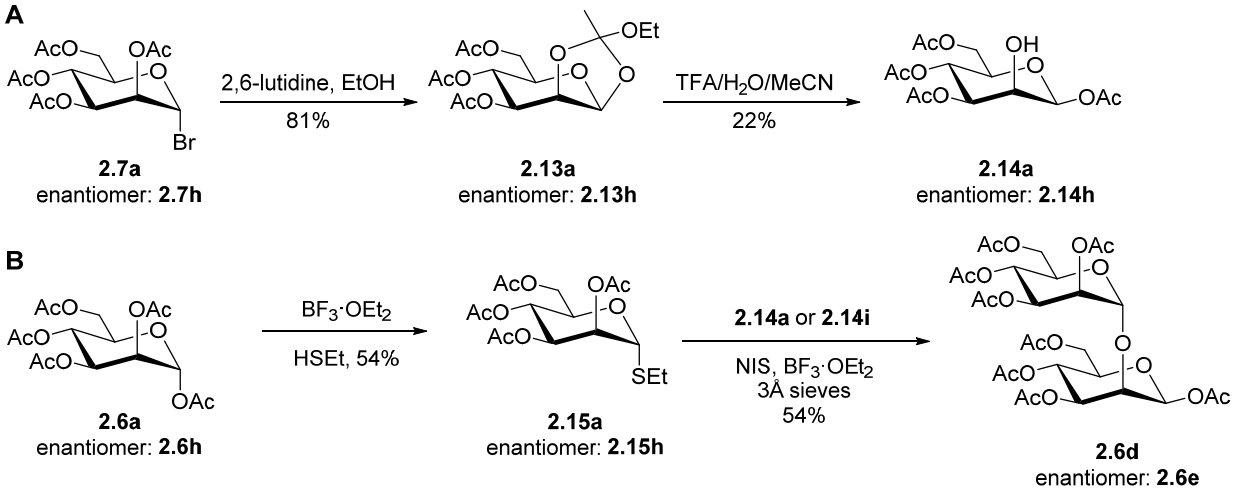

Scheme 2.6. Route to peracetylated D-mannobiose **2.6d** and L-mannobiose **2.6e**. A) 1-Bromo-2,3,4,6-O-acetylmannose **2.7a** was converted to orthoester **2.13d** in ethanol under basic conditions. Acidic deprotection afforded a variety of products, including the desired glycosyl acceptor **2.14d**. B) Conversion of peracetylated mannose to a thioether donor was achieved using ethanethiol in the presence of boron trifluoride. The resulting acetylated donor and acceptor were coupled in the presence of *N*-iodosuccinimide and boron trifluoride to give the desired disaccharide products.

2.5 Syntheses of per-*O*-acetyl-β-1,3-glucobiose and –glucotriose from bacterially-derived mannans

Synthesis of oligomannans heavily favors the alpha configuration under most conditions, simplifying purification of the peracetylated mannobiose products. A similar approach to oligoglucans is complicated somewhat by competition between the anomeric effect, which stabilizes alpha conformers, and steric influence from the equatorial 2-OR neighboring group, which favors nucleophilic attack to give the beta conformer. Although a variety of strategies have been employed to bias glucosylation towards one epimer over the other, we determined that a semisynthetic approach would allow for a high degree of stereochemical control over the glycosidic bond with fewer protecting group manipulations. Fortunately, β-1,3-glucans can be isolated readily from fungal cell walls and are therefore commercially available on gram scale. Acetolysis of the material afforded a complex mixture of oligomers and side products; however, we were able to isolate and purify protected laminaribiose and laminaritriose on workable scale in one step from commercially-available material (Scheme 2.7).[55] The peracetylated glucans were conjugated to serine as described above.

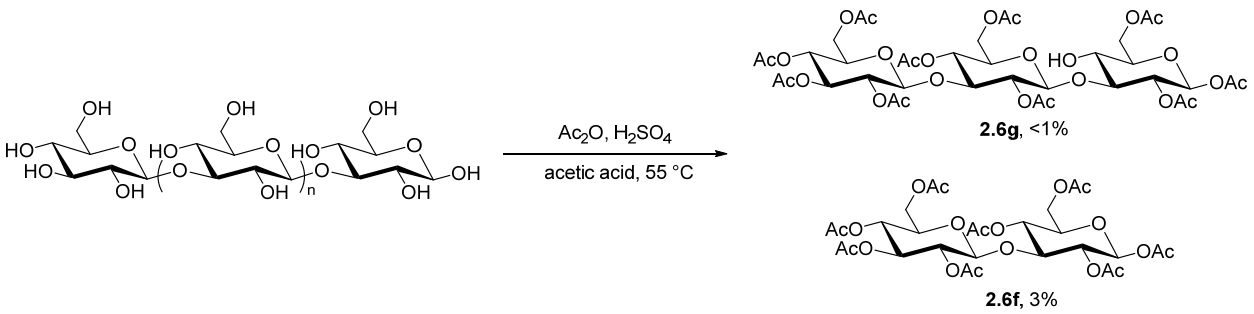

Scheme 2.7. Acetolysis of the commercially-available bacterial cell wall extract curdlan, a β-glucan, to give peracetylated glucans **2.6f** and **2.6g** in low but workable yields.

2.6 Glycosylated NCAs are competent monomers for glycopolypeptide synthesis.

With glycosylated monomers in hand, we then sought to investigate their polymerization properties. Initial experiments were conducted using $(PMe_3)_4Co$, which is known to induce controlled polymerization of other NCAs. In a nitrogen-filled glovebox, monomers were dissolved in the appropriate solvent. To these solutions, a solution of initiator was rapidly added via syringe. After workup, the resulting polymers were analyzed by ^{1}H-NMR and/or GPC to determine size and dispersity. Polymer length appeared to vary approximately linearly with monomer:initiator ratio at least up to 100:1 for a variety of monomers, with dispersities generally under 1.3 (Tables 2.1-2.4). As a practical note, monomer purity was observed to be extremely important, as repeated column purification was sometimes required before isolated glycosylated NCAs could be successfully polymerized. However, rigorous identification of problematic impurities and characterization of the mechanism of inhibition by these impurities has proven somewhat elusive. ^{1}H- and ^{13}C-NMR have given no clear indications of detectible organic contaminants that correlate with inefficient polymerization. Qualitative analysis for halides by exposure of aliquots of NCA to aqueous $AgNO_3$ has suggested a correlation between observed precipitation, indicating the presence of halide ions, and inhibition of polymerization. Further characterization may be called for to aid in improving monomer purification strategies.

Table 2.1. Polymerization data for Ser(Man) NCA 2.2a at various monomer to initiator ratios using $(PMe_3)_4Co$ initiator in THF at 20 °C.

[M]/[I]	M_n[a]	DP[b]	$Đ_M$[c]
10	13,063	31	1.24
25	32,868	78	1.10
50	66,578	158	1.13
100	130,628	310	1.08

[a] Molecular weight after polymerization as determined by ^{1}H NMR and GPC. [b] DP = number average degree of polymerization. [c] Dispersity (M_w/M_n) after polymerization as determined by GPC.

Table 2.2. Polymerization data for Ser(Man2) NCA 2.2a at various monomer to initiator ratios using $(PMe_3)_4Co$ initiator in THF at 20 °C.

[M]/[I]	M_n[a]	DP[b]	$Đ_M$[c]
10	24,127	34	1.26
25	61,738	87	1.14
50	119,218	168	1.10
100	237,726	335	1.11

[a] Molecular weight after polymerization as determined by ^{1}H NMR and GPC. [b] DP = number average degree of polymerization. [c] Dispersity (M_w/M_n) after polymerization as determined by GPC.

Table 2.3. Polymerization data for Ser(Lac) NCA 2.2b at various monomer to initiator ratios using $(PMe_3)_4Co$ initiator in THF at 20 °C.

[M]/[I]	M_n[a]	DP[b]	$Đ_M$[c]
10	22,708	32	1.18
25	57,480	81	1.11
50	111,412	157	1.12
100	223,533	315	1.06

[a] Molecular weight after polymerization as determined by ^{1}H NMR and GPC. [b] DP = number average degree of polymerization. [c] Dispersity (M_w/M_n) after polymerization as determined by GPC.

Table 2.4. Polymerization data for Ser(Glc2) NCA 2.2f at various monomer to initiator ratios using $(PMe_3)_4Co$ initiator in THF at 20 °C.

[M]/[I]	M_n[a]	DP[b]	$Đ_M$[c]
10	25,547	36	1.25
25	62,447	88	1.19
50	125,605	177	1.09
100	247,661	349	1.14

[a] Molecular weight after polymerization as determined by ^{1}H NMR and GPC. [b] DP = number average degree of polymerization. [c] Dispersity (M_w/M_n) after polymerization as determined by GPC.

For comparison, data was also obtained for Ser(Man) NCA **2.2a** using azidopropyl-Leu-Ni initiator **2.4**, as Ni initiators are generally observed to initiate polymerization more slowly than Co initiators, which can result in higher dispersities.[44] Fortunately, we still observed good dispersities under 1.2, along with a linear relationship between M:I and dispersity (Table 2.5). Interestingly, calculated degrees of polymerization for the Co initiator were significantly higher than would be predicted from the M:I ratio. Although our particular experiments were not designed to probe the role of initiator vs. solvent in causing this effect, literature reports have consistently observed an inflation of polymer length using transition metal initiators in THF.[56] To the best of our knowledge there is no experimentally-supported chemical rationale to explain this effect, which has been attributed by Deming et al. to inactivation of some portion of the initiator via an unknown mechanism. Until further characterization is obtained, this remains an empirical observation to account for.

Table 2.5. Polymerization data for Ser(Man) NCA 2.2a at various monomer to initiator ratios using azidopropyl-Leu-Ni initiator in DMF at 20 °C.

[M]/[I]	M_n[a]	DP[b]	$Đ_M$[c]
25	14,748	35	1.15
50	29,075	69	1.13
100	57,729	137	1.10
200	113,773	270	1.07

[a] Molecular weight after polymerization as determined by ^{1}H NMR and GPC. [b] DP = number average degree of polymerization. [c] Dispersity (M_w/M_n) after polymerization as determined by GPC.

Interestingly, Ser(Glc3) NCA **2.2g** could only be fully polymerized at M:I ratios lower than ~30:1, possibly due to difficulty removing trace impurities that impeded polymerization at higher ratios (Table 2.6). Polymerization with $(PMe_3)_4Co$ in THF at an M:I ratio of 20:1 gave fully glycosylated chains over 100 residues in length, suggesting that steric hindrance is not a limitation in this reaction. Promisingly, **2.2g** could still be efficiently copolymerized at higher M:I ratios as a mixture of 20% Ser(Glc3) NCA with 80% Glu(O*t*Bu) NCA, yielding copolypeptides up to ca. 360 residues (Table 2.7).

Table 2.6. Polymerization data for Ser(Glc3) NCA 2.2g at various monomer to initiator ratios using $(PMe_3)_4Co$ initiator in THF at 20 °C.

[M]/[I]	M_n[a]	DP[b]	$Đ_M$[c]
10	36,901	52	1.19
20	76,640	108	1.15
40	na	na	na
60	na	na	na

[a] Molecular weight after polymerization as determined by ^{1}H NMR and GPC. [b] DP = number average degree of polymerization. [c] Dispersity (M_w/M_n) after polymerization as determined by GPC.

Table 2.7. Polymerization data for statistical copolymerization of 20% Ser(Glc3) NCA 2.2g with 80% *t*Bu-L-Glu NCA at various monomer to initiator ratios using $(PMe_3)_4Co$ initiator in THF at 20 °C.

[M]/[I]	M_n[a]	DP[b]	$Đ_M$[c]
10	10,429	36	1.15
25	26,652	92	1.12
50	52,436	181	1.11
100	105,741	365	1.07

[a] Molecular weight after polymerization as determined by ^{1}H NMR and GPC. [b] DP = number average degree of polymerization. [c] Dispersity (M_w/M_n) after polymerization as determined by GPC.

In order to tune glycopolypeptide glycosylation density, the glyco-NCAs must polymerize at a rate comparable to non-glycosylated comonomers, a nontrivial assumption given the bulkiness of the glycans and potential interference of the large number of acetate groups with the polymerization. We therefore compared polymerization rates for Ser(Man) and Ser(Man2) monomers to TFA-lysine NCA, which has been extensively studied using transition metal catalysis. In our hands, it indeed appeared that the three monomers polymerized at approximately the same rate (Fig. 2.3). Although indirect, this result suggested to us that random copolymers should indeed be accessible

through simply blending monomers at the desired final ratio. As an attempt to directly characterize copolymers, I attempted N-terminal sequencing of a Lac-Ser-*stat*-Ala-*stat*-Glu polymer by Edman degradation. Unfortunately, I was unable to observe and quantify the glycosylated residues. As even unmodified Ser is known to be difficult to accurately quantify by Edman sequencing, I decided against further analysis by this technique.

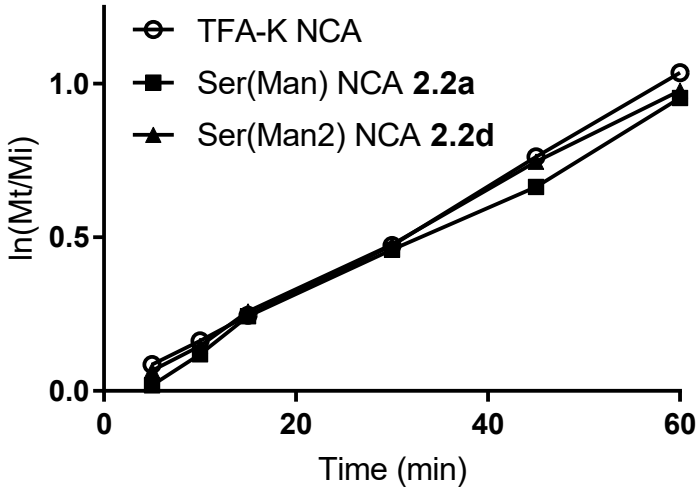

Figure 2.3. Polymerization rates of NCAs **2.2a**, **2.2d**, and TFA-Lys using $(PMe_3)_4Co$ in THF. Kinetic analysis demonstrates that monosaccharide-Ser NCA **2.2a** and disaccharide-Ser NCA **2.2d** polymerize at comparable rates to the previously reported TFA-Lys NCA, indicating that incorporation of glyco-NCAs will be stochastic, rather than tapered or block-like. Data are representative of duplicate independent experiments.

We previously reported a rigid extended conformation for α-GalNAc-O-Ser glycopolypeptides, which we and others proposed is due to hydrogen bonding between the peptide backbone and the glycosyl acetamide.[57] This was supported by the unusual circular dichroism (CD) absorbances we observed. Because secondary structure could plausibly influence receptor-glcyopolypeptide interactions, we decided it would be prudent to see if other glycopolypeptides similarly form ordered structures. Interestingly, 2-hydroxylated glycosylation patterns appear to result in much more flexible polymers. Glc2- and Man2-functionalized polypeptides **2.3f** and **2.3d** gave aqueous CD absorption spectra corresponding to disordered, random coil conformations, while Man-bearing **2.3a** showed absorptions consistent with some helical character (Fig. 2.4).[58] The larger steric bulk and hydration sphere of the disaccharide sidechains may inhibit the formation of organized structures.

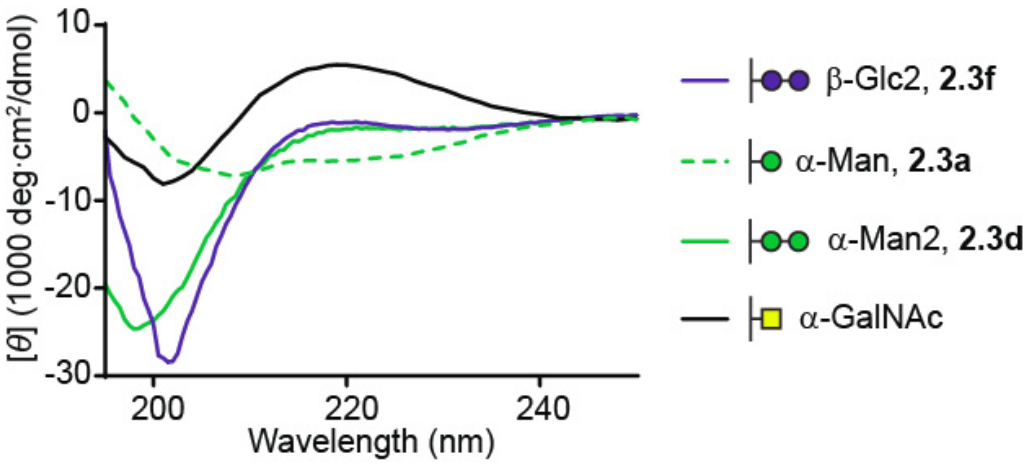

Figure 2.4. Circular dichroism spectra for various glycopolypeptides. As previously reported, α-GalNAc-serine homopolymers appear to take on an unusual structural conformation.[50] In contrast, Ser(Man2) and Ser(Glc2) homopolymers give CD spectra consistent with random coils, whereas Ser(Man) appears to adopt some helical character.

2.7 Summary and outlook

Previous work provided an initial proof of concept that O-glycosylated NCAs could be efficiently polymerized to give glycopolypeptides.[50] Here, we synthesized and polymerized a variety of mono-, di-, and trisaccharide-serine NCAs, demonstrating that the polymerization tolerates even relatively bulky glycan substituents. Given the number of permutations of glycans accessible even with disaccharides, this represents an important step towards developing the NCA glycopolypeptide platform as a generalizable tool for probing glycobiology. In the following chapters, I present data showing that these structures can be designed to bind and activate C-type lectin receptors in a predictable manner, and may even be useful as immune adjuvants for cancer immunotherapy. Work is ongoing in the lab to investigate other monomers, including fucosylated and sialylated polymers, N-glycans, and post-polymerization enzymatic elaboration of glycopolypeptides. Successful polymerization of such structurally-diverse glycopolypeptides will unlock even greater opportunities and applications.

2.8 Materials, methods, and syntheses of new compounds

General Materials and Methods

Unless stated otherwise, reactions were conducted in oven-dried glassware under an atmosphere of nitrogen using anhydrous solvents. Tetrahydrofuran (THF) and dichloromethane (DCM) were purified by first purging with dry nitrogen, followed by passage through columns of activated alumina. Anhydrous *N*,*N*-dimethylformamide (DMF) was purchased and stored over activated 4 Å molecular sieves. Deionized water was purified to 18 MΩ-cm using a Millipore Milli-Q Biocel A10 purification unit. All commercially obtained reagents were used as received without further purification unless otherwise stated. Flash chromatography was performed using Silicycle SiliaFlash P60 silica gel. Analytical thin layer chromatography was performed using glass-backed Analtech Uniplate silica gel plates containing a fluorescent indicator, and visualized using a combination of UV, anisaldehyde, $KMnO_4$, H_2SO_4, ninhydrin, and phosphomolybdic acid

staining. NMR spectra were obtained on Varian spectrometers at room temperature at the Stanford Department of Chemistry NMR Facility. NMR spectra are reported relative to residual solvent signals. Data for ^{1}H NMR spectra are reported as follows: chemical shift (δ ppm), multiplicity, coupling constant (Hz) and integration. Splitting patterns are designated as follows: s, singlet; d, doublet; t, triplet; q, quartet; m, multiplet; br, broad. Data for ^{13}C NMR spectra are reported in terms of chemical shift. High-resolution mass spectrometry was performed at the Stanford University Mass Spectrometry core facility. All attenuated total reflectance (ATR) Fourier Transform infrared (FTIR) samples were recorded on a Bruker Alpha spectrometer. Gel permeation chromatography (GPC) was performed using a Viscotek TDA 302 fitted with serial Phenomenex Phenogel 00H-0442-K0, 00H-0444-K0, and 00H-0445-K0 columns running 0.10 M LiBr in DMF as the eluent at 60 °C with differential refractive index detection.

The following compounds were prepared according to a previous publication.[50] *O*-(2-acetamido-2-deoxy-3,4,6-tri-*O*-acetyl-α-D-galactopyranosyl)-L-serine *N*-carboxyanhydride (α-GalNAc-Ser NCA **2e**), L-Alanine *N*-carboxyanhydride (Ala NCA), γ-*tert*-Butyl-L-glutamate *N*-carboxyanhydride (*t*Bu-Glu NCA), *N*ε-Trifluoroacetyl-L-Lysine *N*-carboxyanhydride (TFA-Lys NCA), azidopropyl-Leu-Ni initiator. $(PMe_3)_4Co$ initiator was prepared according to the literature using magnesium as the reductant under glovebox conditions where possible.[59]

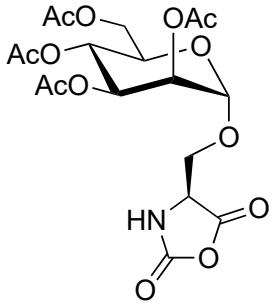

_O_-α-Tetraacetylmannopyranosyl L-Serine _N_-Carboxyanhydride (Man-Ser NCA), 2.2a

Mannosyl-serine **2.1a**[33] (200 mg, 0.46 mmol) was suspended in anhydrous THF (20 mL, 23 mM) under N_2. To this stirred suspension was added α-pinene (290 µl, 1.83 mmol, 4.0 equiv.), followed by a solution of 15% (w/w) phosgene in toluene (654 µl, 0.92 mmol, 2.0 equiv.). **Caution: Phosgene is extremely hazardous and all manipulations must be performed in a well-ventilated chemical fume hood with proper personal protection and necessary precautions taken to avoid exposure.** The reaction mixture was stirred at room temperature under a positive pressure of N_2. After 12 h, the reaction mixture was determined to have gone to completion by FTIR. The mixture was concentrated under high vacuum for 1 h using two sequential liquid nitrogen-cooled traps to condense solvent, byproducts, and phosgene. The collected condensate was quenched with ammonium hydroxide to consume residual phosgene prior to disposal. The crude NCA was purified by anhydrous silica chromatography (0–20% anhydrous THF in anhydrous DCM). Fractions were visualized by $KMnO_4$ and H_2SO_4 stains. Fractions containing NCA were combined and concentrated in vacuo to give αMan2-Ser NCA **2.2a** (216 mg, 73%) as a white solid. ^{1}H NMR (400 MHz, $CDCl_3$) δ 5.16-26 (m, 3H), 4.85 (d, J = 1.8 Hz, 1H), 4.58 (dd, J = 6.4, 3.0 Hz, 1H), 4.23 (dd, J = 12.3, 5.2 Hz, 1H), 4.10 (dd, J = 12.2, 2.8 Hz, 1H), 4.05 (dd, J = 10.5, 3.2 Hz, 1H), 3.96 (ddd, J = 9.8, 5.1, 2.7 Hz, 1H), 3.79 (dd, J = 10.5, 6.6 Hz, 1H), 2.10 (s, 3H), 2.06 (s, 3H), 2.01 (s, 3H), 1.93 (s, 3H). ^{13}C NMR (101 MHz, $CDCl_3$) δ 171.00, 170.26, 170.12,

169.81, 167.59, 152.26, 98.21, 69.09, 68.96, 68.92, 66.97, 65.91, 62.53, 58.02, 20.82, 20.78, 20.69, 20.68. FTIR-ATR ν_{max}/cm^{-1} 1861, 1787, 1744, 1370, 1223, 1140, 1085, 1048, 981, 918. ESI HRMS: Calcd. for $C_{18}H_{23}NO_{13}$ $[M+H]^+$ 484.1067; obs. $[M+H]^+$ 484.1052

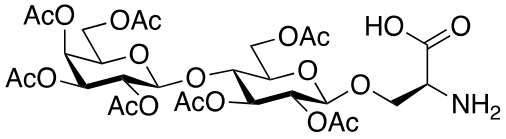

***O*-β-Heptaacetyllactosyl L-Serine, 2.1b**

A solution of peracetylbromolactose[33] (7.70 g, 11.0 mmol, 1.0 equiv,) and *N*-carboxybenzyl L-serine benzyl ester (3.98 g, 12.1 mmol, 1.1 equiv.) in anhydrous DCM (55 mL, 0.2 M) was stirred over powdered 4 Å molecular sieves (8.0 g) under N_2 for 30 minutes at room temperature. The reaction vessel was covered in foil and silver triflate (3.10 g, 12.1 mmol, 1.1 equiv.) was quickly added. The reaction mixture was stirred at room temperature under nitrogen for 24 h. The reaction mixture was quenched by the addition *N*,*N*-diisopropylethylamine (1.91 mL, 11.0 mmol, 1.0 equiv.) and stirred at room temperature for an hour. The suspension was then filtered and then concentrated in vacuo to afford a yellow foam. The residue was purified by flash chromatography on silica to afford the intermediate protected serine as a white foam (4.06 g), which was dissolved in MeOH (35 mL) and 20% (w/w on carbon, dry basis) palladium hydroxide (350 mg, 10% w/w) was added. The atmosphere of the reaction vessel was then flushed thrice with hydrogen and stirred under a H_2 balloon at ambient temperature for 2 h. The reaction mixture was filtered through celite, washed with MeOH, and then concentrated in vacuo overnight to afford **1f** as a white solid (2.90 g, 37%). Spectral data was in agreement with the literature.[33] The product was determined to be anomerically pure by NMR analysis.

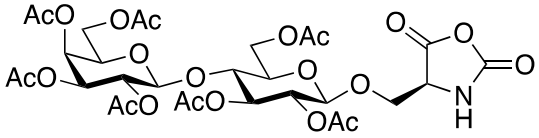

***O*-β-Heptaacetyllactosyl L-Serine *N*-Carboxyanhydride (βLac-Ser NCA), 2.2b**

Compound **2.1b** (500 mg, 0.69 mmol) was suspended in anhydrous tetrahydrofuran (15.3 mL, 45 mM) under N_2 in an oven-dried 50 mL round-bottom flask with a stir bar. To this stirred suspension was added α-pinene (438 μL, 2.76 mmol, 4.0 equiv.), followed by a solution of 15% (w/w) phosgene in toluene (980 μL, 1.38 mmol, 2.0 equiv.). **Caution: Phosgene is extremely hazardous and all manipulations must be performed in a well-ventilated chemical fume hood with proper personal protection and necessary precautions taken to avoid exposure.** The reaction mixture was stirred at room temperature under static N_2 and the flask was sealed with Parafilm. After 48 h, the reaction mixture was determined to have gone to completion by FTIR. The mixture was concentrated under high vacuum for 1 h using two sequential liquid nitrogen-cooled traps to condense solvent, byproducts, and phosgene. The collected condensate was quenched with ammonium hydroxide to consume residual phosgene prior to disposal. The crude NCA was dissolved in cold ethyl acetate (50 mL) and rapidly washed with ice-cold 5% (w/w) $NaHCO_3$ (50 mL) and water (150 mL). The organic phase was dried on a large excess of Na_2SO_4, filtered over glass wool, and concentrated in vacuo. The residue was dissolved in minimal anhydrous DCM and purified via anhydrous flash chromatography (0–40% anhydrous THF in anhydrous DCM).

Fractions were monitored by TLC, eluting with 20% THF in DCM and visualizing with ninhydrin. Product-containing fractions starting just after the 15% THF hold were collected and concentrated in vacuo to afford **2.2b** as a white foam (320 mg, 62%). ^{1}H NMR (500 MHz, $CDCl_3$): δ 6.63 (s, 1H), 5.35 (d, *J* = 3.3 Hz, 1H), 5.18 (t, *J* = 9.1 Hz, 1H), 5.12 (dd, *J* = 10.1, 8.2 Hz, 1H), 5.03 – 4.94 (m, 1H), 4.92 – 4.84 (m, 1H), 4.75 (d, *J* = 12.1 Hz, 1H), 4.58 – 4.50 (m, 2H), 4.45 (d, *J* = 6.6 Hz, 1H), 4.33 – 4.21 (m, 1H), 4.18 – 4.04 (m, 2H), 4.02 (dd, *J* = 12.2, 5.2 Hz, 1H), 3.89 (t, *J* = 6.9 Hz, 1H), 3.83 (dd, *J* = 12.1, 6.9 Hz, 1H), 3.75 (d, *J* = 8.3 Hz, 2H), 3.69 (d, *J* = 5.4 Hz, 1H), 2.21 (s, 3H), 2.15 (s, 3H), 2.09 – 2.02 (m, 12H), 1.97 (s, 3H). ^{13}C NMR (126 MHz, $CDCl_3$): δ 171.25, 170.62, 170.33, 169.90, 169.85, 169.33, 167.19, 151.56, 101.48, 101.34, 75.95, 73.69, 72.46, 71.16, 71.11, 71.00, 70.81, 69.30, 66.79, 61.95, 60.96, 59.17, 20.79-21.19 (7C). FTIR-ATR ν_{max}/cm^{-1} 1860, 1791, 1749, 1433, 1371, 1226, 1172, 1129, 1056, 918. ESI HRMS: Calcd. for $C_{30}H_{39}NO_{21}$ $[M+Na]^+$ 772.1907; obs. $[M+Na]^+$ 772.1892

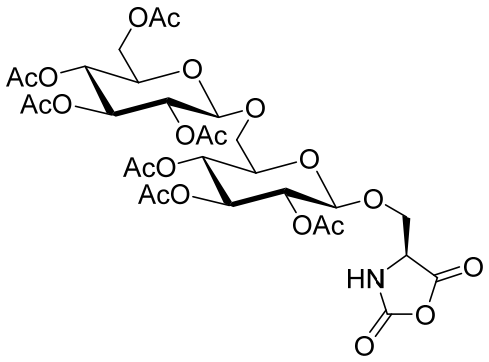

***O*-β-Heptaacetylgentiobiosyl L-Serine *N*-Carboxyanhydride, 2.2c**

Compound **2.1c** (196 mg, 0.271 mmol) was suspended in anhydrous tetrahydrofuran under N_2 in an oven-dried 50 mL round-bottom flask with a stir bar. To this stirred suspension was added α-pinene (171 μL, 1.08 mmol, 4.0 equiv.), followed by a solution of 15% (w/w) phosgene in toluene (385 μL, 0.542 mmol, 2.0 equiv.). **Caution: Phosgene is extremely hazardous and all manipulations must be performed in a well-ventilated chemical fume hood with proper personal protection and necessary precautions taken to avoid exposure.** The reaction mixture was stirred at room temperature under static N_2 and the flask was sealed with Parafilm. After 48 h, the reaction mixture was determined to have gone to completion by FTIR. The mixture was concentrated under high vacuum for 1 h using two sequential liquid nitrogen-cooled traps to condense solvent, byproducts, and phosgene. The collected condensate was quenched with ammonium hydroxide to consume residual phosgene prior to disposal. The residue was dissolved in minimal anhydrous DCM and purified via anhydrous flash chromatography (0–40% anhydrous THF in anhydrous DCM). Fractions were monitored by TLC, eluting with 20% THF in DCM and visualizing with ninhydrin. Product-containing fractions were collected and concentrated in vacuo to afford **2.2c** as a white foam (89 mg, 44%, 7.7:1 β:α ratio by NMR). ^{1}H NMR (400 MHz, $CDCl_3$) δ 7.09 (s, 1H), 5.24 – 5.09 (m, 2H), 5.05 (t, *J* = 9.3 Hz, 2H), 4.90 (t, *J* = 8.9 Hz, 1H), 4.83 (t, *J* = 9.6 Hz, 1H), 4.68 (d, *J* = 7.9 Hz, 1H), 4.54 (d, *J* = 7.9 Hz, 1H), 4.48 (d, *J* = 6.0 Hz, 1H), 4.17 (dd, *J* = 11.3, 4.4 Hz, 3H), 3.91 (dd, *J* = 12.2, 6.0 Hz, 1H), 3.73 (dq, *J* = 16.1, 8.5, 6.6 Hz, 4H), 2.05 (s, 3H), 2.01 (s, 9H), 1.98 (s, 3H), 1.95 (d, *J* = 3.1 Hz, 6H). ^{13}C NMR (101 MHz, $CDCl_3$) δ 170.76, 170.22, 170.11, 169.62, 169.51 (2C), 169.44, 167.62, 151.82, 101.22, 100.63, 73.08, 72.55, 72.35,

72.25, 70.79, 70.44, 70.34, 68.80, 68.14, 67.73, 61.86, 59.40, 20.60-20.82 (7C). ESI LRMS: $[M+Na]^+$ calcd. 772.2; obs. 771.8.

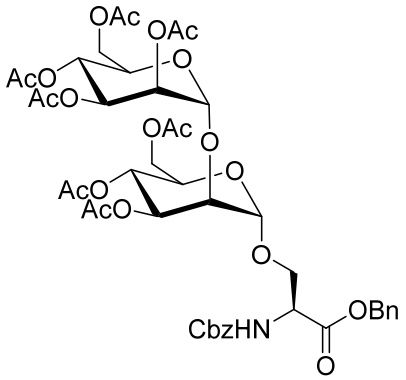

_O_-α-Heptaacetylmannobiosyl _N_-Carboxybenzyl L-Serine Benzyl Ester, 2.12d

A solution of _O_-α-heptaacetyl-1-bromo-mannobiose[60-61] (200 mg, 0.286 mmol) and _N_-carboxybenzyl L-serine benzyl ester (104 mg, 0.315 mmol, 1.1 equiv.) in anhydrous DCM (50 mL, 5.7 mM) was stirred over activated 4 Å molecular sieves under N_2 for 15 minutes at room temperature. The reaction vessel was covered in foil and silver triflate (81 mg, 0.315 mmol, 1.1 equiv.) was quickly added. The reaction mixture was stirred under nitrogen at room temperature for 11 h. The reaction mixture was quenched by the addition of _N_,_N_-diisopropylethylamine (54 μL, 0.310 mmol, 1.1 equiv). The suspension was then filtered through a 0.2 μm PTFE syringe filter to remove silver salts and concentrated in vacuo to afford a brown residue. The crude product was purified by flash chromatography on silica to afford **2.12d** as a white foam (150 mg, 55%). ^{1}H NMR (400 MHz, $CDCl_3$) δ 7.26 (m, 10H), 5.81 (d, J = 8.1 Hz, 1H), 5.30 (dd, J = 10.0, 3.4 Hz, 1H), 5.23 – 5.02 (m, 9H), 4.79 (dd, J = 26.6, 2.0 Hz, 2H), 4.53 (dt, J = 7.8, 3.3 Hz, 1H), 4.19 – 3.96 (m, 5H), 3.94 – 3.87 (m, 2H), 3.81 – 3.74 (m, 2H), 2.07 (s, 3H), 2.01 (s, 3H), 2.00 (s, 3H), 1.95 (s, 3H), 1.94 (s, 3H), 1.92 (s, 6H). ^{13}C NMR (75 MHz, $CDCl_3$) δ 170.57, 170.26, 169.97, 169.63, 169.52, 169.30, 169.25, 169.16, 155.66, 135.89, 134.94, 128.47 (2C), 128.36 (3C), 128.24 (2C), 128.08, 127.97 (2C), 98.80, 98.57, 76.54, 69.64, 69.47, 68.99, 68.87, 68.82, 68.15, 67.35, 66.95, 66.15, 65.68, 62.40, 61.70, 54.17, 26.68, 20.66, 20.39-20.50 (6C). ESI HRMS: $[M+Na]^+$ calcd. 970.2957; obs. 970.2988

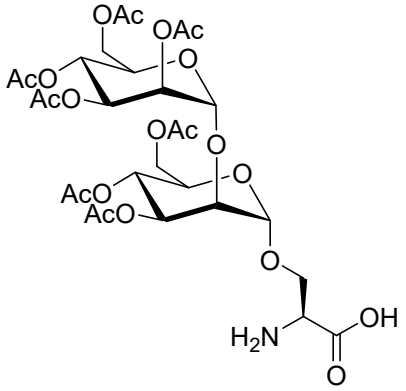

***O*-α-Heptaacetylmannobiosyl L-Serine, 2.1d**

Compound **2.12d** (500 mg, 0.527 mmol, 1.0 equiv.) and 20% (w/w on carbon, dry basis) palladium hydroxide (50 mg, 10% w/w) were added to a 100 ml round-bottom flask, followed by anhydrous MeOH (25 ml). The flask was purged with argon, charged with H_2, and allowed to stir under a H_2 balloon for 3 h. The reaction mixture was filtered through a 0.2 μm PTFE syringe filter, concentrated in vacuo, and precipitated from diethyl ether to afford **2.1d** (287 mg, 76%) as a white solid. ^{1}H-NMR (400 MHz, CD_3OD) δ 5.49 – 5.20 (m, 5H), 5.15 (d, J = 2.0 Hz, 1H), 5.04 (d, J = 1.9 Hz, 1H), 4.92 (s, 1H), 4.34 – 4.12 (m, 9H), 4.07 (dt, J = 10.0, 2.7 Hz, 1H), 3.99 (dd, J = 11.9, 6.1 Hz, 1H), 2.15 (s, 3H), 2.13 (s, 3H), 2.08 (s, 3H), 2.07 (s, 3H), 2.05 (s, 3H), 2.03 (s, 3H), 1.99 (s, 3H). ^{13}C-NMR (101 MHz, CD_3OD) δ 172.62, 172.29, 172.07, 171.46, 171.41, 171.29, 171.24, 100.42, 100.06, 78.04, 71.45, 70.75, 70.67, 70.27, 70.04, 67.37, 67.10, 66.94, 63.63, 62.82, 54.29, 20.88, 20.86, 20.77, 20.69 (2C), 20.66, 20.59. ESI HRMS: $[M+H]^+$ calcd. 724.2300; obs. 724.2312

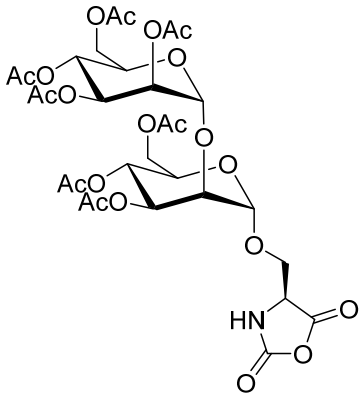

***O*-α-Heptaacetylmannobiosyl L-Serine *N*-Carboxyanhydride (αMan2-Ser NCA), 2.2d**

Compound **2.1d** (0.287 g, 0.3966 mmol, 1.0 equiv.) was suspended in anhydrous THF (25 ml, 16 mM) under N_2. α-Pinene was added (0.250 μl, 1.58 mmol, 4.0 equiv., 0.858 g/ml) followed by a solution of 15% (w/w) phosgene in toluene (0.564 μl, 0.7932 mmol, 2.0 equiv.). **Caution: Phosgene is extremely hazardous and all manipulations must be performed in a well-ventilated chemical fume hood with proper personal protection and necessary precautions taken to avoid exposure.** The reaction mixture was stirred at room temperature under a positive pressure of N_2. After 12 h, the reaction mixture was determined to have gone to completion by FTIR. The mixture was concentrated under high vacuum for 1 h using two sequential liquid nitrogen-cooled traps to condense solvent, byproducts, and phosgene. The collected condensate

was quenched with ammonium hydroxide to consume residual phosgene prior to disposal. The crude NCA was purified by anhydrous silica chromatography (0–20% anhydrous THF in anhydrous DCM). Fractions were visualized by potassium permanganate and sulfuric acid dip stains. Fractions containing NCA were combined and concentrated *in vacuo* to give **2.2d** (0.216 g, 73%) as a white solid. ^{1}H-NMR (400 MHz, Chloroform-d) δ 7.10 (s, 1H), 5.43 – 5.10 (m, 5H), 4.98 (d, J = 2.2 Hz, 1H), 4.96 – 4.92 (m, 1H), 4.56 (dd, J = 5.9, 2.8 Hz, 1H), 4.27 – 4.20 (m, 2H), 4.20 – 4.01 (m, 5H), 3.95 – 3.85 (m, 2H), 2.14 (s, 3H), 2.14 (s, 3H), 2.10 (s, 3H), 2.07 (s, 3H), 2.05 (s, 3H), 2.04 (s, 3H), 2.00 (s, 3H). ^{13}C-NMR (101 MHz, cdcl3) δ 171.14, 171.10, 170.30, 169.77, 169.73, 169.55, 169.42, 167.23, 151.87, 98.90, 98.57, 75.09, 69.69, 69.40, 69.13, 68.76, 68.20, 67.89, 66.71, 66.31, 62.92, 62.34, 58.02, 20.79, 20.73, 20.66, 20.63-20.60 (3C). FTIR-ATR ν_{max}/cm^{-1} 1862, 1790, 1741, 1369, 1222, 1135, 1078, 1044, 979, 918. ESI HRMS: $[M+Na]^+$ calcd. 772.1912; obs. 772.1908.

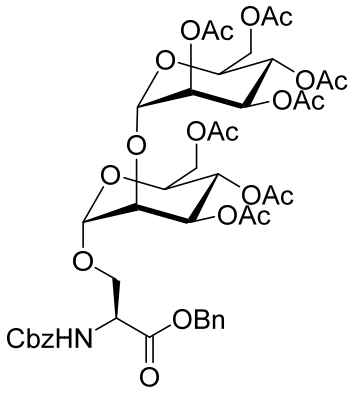

***O*-L-α-Heptaacetylmannobiosyl *N*-Carboxybenzyl L-Serine Benzyl Ester, 2.12e**

A solution of **2.9e** (311 mg, 0.398 mmol, 1 equiv.) and *N*-carboxybenzyl L-serine benzyl ester (131 mg, 0.398 mmol, 1 equiv.) in 50 ml anhydrous DCM was stirred over activated 4 Å molecular sieves under N_2 for 30 minutes at room temperature. Boron trifluoride diethyl etherate (9.82 µl, 0.08 mmol, 1.15 g/ml, 0.2 equiv.) was added by syringe. The reaction mixture was stirred under nitrogen at ambient temperature for 3 h and monitored by TLC. The suspension was washed with three portions of saturated $NaHCO_3$ and the organic fraction dried over $MgSO_4$, filtered, and concentrated under reduced pressure. The crude product was purified by silica column chromatography afford **2.12e** (230 mg, 61%) as a white foam that was carried forward without additional analysis. ESI LRMS: $[M+Na]^+$ calcd. 970.3; obs. 969.7.

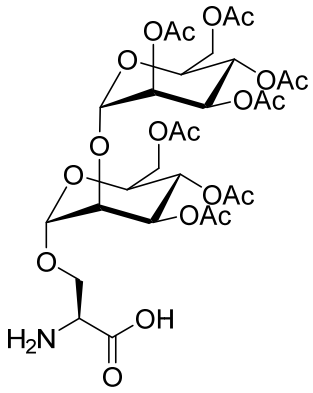

***O*-α-Heptaacetylmannobiosyl L-Serine, 2.1e**

Compound **2.12e** (230 mg, 0.243 mmol, 1.0 equiv.) and 20% (w/w on carbon, dry basis) palladium hydroxide (23 mg, 10% w/w) were added to a 100 ml round-bottom flask, followed by anhydrous MeOH (25 ml). The flask was purged with argon, charged with H_2, and allowed to stir under a H_2 balloon for 3 h. The reaction mixture was filtered through a 0.2 μm PTFE syringe filter, concentrated in vacuo, and precipitated from diethyl ether to afford **2.1e** (113 mg, 65%) as a white solid that was carried forward without additional analysis.

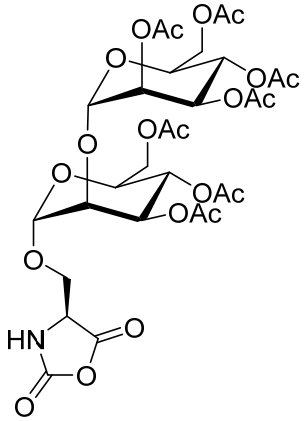

***O*-L-α-Heptaacetylmannobiosyl L-Serine *N*-Carboxyanhydride, 2.2e**

Compound **2.1e** (113 mg, 0.156 mmol, 1.0 equiv.) was suspended in 25 ml anhydrous THF under N_2. α-Pinene was added (99 μl, 0.624 mmol, 4.0 equiv., 0.858 g/ml) followed by a solution of 15% (w/w) phosgene in toluene (221 μl, 0.3122 mmol, 2.0 equiv., 0.924 g/ml). **Caution: Phosgene is extremely hazardous and all manipulations must be performed in a well-ventilated chemical fume hood with proper personal protection and necessary precautions taken to avoid exposure.** The reaction mixture was stirred at room temperature under a positive pressure of N_2. After 12 h, the reaction mixture was determined to have gone to completion by FTIR. The mixture was concentrated under high vacuum for 1 h using two sequential liquid nitrogen-cooled traps to condense solvent, byproducts, and phosgene. The collected condensate was quenched with ammonium hydroxide to consume residual phosgene prior to disposal. The crude NCA was purified by anhydrous silica chromatography (0–20% anhydrous THF in anhydrous DCM). Fractions were visualized by potassium permanganate and sulfuric acid dip stains. Fractions containing NCA were combined and concentrated *in vacuo* to give **2.2e** (55.4 mg, 47%) as a white

solid. ^{1}H NMR (400 MHz, $CDCl_3$) δ 7.13 (s, 1H), 5.36 – 5.06 (m, 6H), 4.97 (s, 1H), 4.88 (d, *J* = 2.4 Hz, 1H), 4.65 – 4.47 (m, 1H), 4.38 – 3.93 (m, 7H), 3.86 (ddd, *J* = 8.4, 5.3, 2.6 Hz, 2H), 2.15 – 2.07 (m, 6H), 2.05 (d, *J* = 2.0 Hz, 3H), 2.01 (td, *J* = 4.8, 3.8, 1.8 Hz, 9H), 1.96 (d, *J* = 2.0 Hz, 3H). ^{13}C NMR (101 MHz, $CDCl_3$) δ 171.20, 170.97, 170.48, 169.89, 169.83, 169.66, 169.60, 167.97, 152.19, 98.96, 75.90, 69.88, 69.57, 69.37, 68.89, 68.26, 67.02, 66.44, 65.93, 63.11, 62.02, 58.21, 20.69-20.87 (7C). FTIR-ATR ν_{max}/cm^{-1} 2938.43, 1862.54, 1791.60, 1746.04, 1370.86, 1226.37, 1046.22. ESI LRMS: $[M+Na]^+$ calcd. 772.2; obs. 771.8.

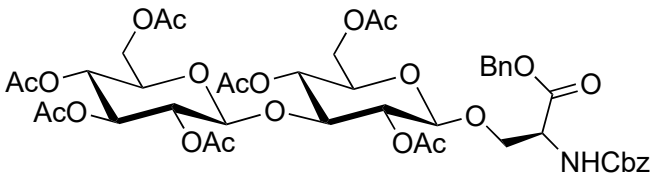

***O*-β-Heptaacetyl -D-laminaribiosyl *N*-Carboxybenzyl L-Serine Benzyl Ester, 2.12f**

A solution of heptaacetyl-1-bromo-D-laminaribiose[1] (450 mg, 0.64 mmol) and *N*-carboxybenzyl L-serine benzyl ester (233 mg, 0.70 mmol, 1.1 equiv.) in anhydrous DCM (32 mL, 0.02 M) was stirred over activated 4 Å molecular sieves under N_2 for 1 h at room temperature. The reaction vessel was covered in foil and silver triflate (181 mg, 0.70 mmol, 1.1 equiv.) was quickly added. The reaction mixture was stirred at room temperature under N_2 for 48 h. The reaction mixture was quenched by the addition of *N*,*N*-diisopropylethylamine (111 μL, 0.64 mmol, 1.0 equiv) and stirred for 30 min. The suspension was then filtered through a 0.2 μm PTFE syringe filter to remove silver salts and concentrated in vacuo to afford a brown residue. The residue was purified by flash chromatography on silica to yield a white foam (202 mg, 33%). The products were afforded in a 1:2 α:β anomeric ratio by ^{1}H NMR analysis. ^{1}H NMR (500 MHz, $CDCl_3$): δ 7.33 (m, 5H), 7.31 (m, 5H), 6.22 (d, 0.2H, J = 3.7 Hz, aH), 5.61 (d, 0.8H, J = 7.8 Hz, bH), 5.15(d, J = 3.3 Hz, 2H), 5.10 (m, 3H), 5.00 (m, 2H), 4.88 (m, 3H), 4.54 (d, J = 8.1 Hz, 1H), 4.48 (m, 1H), 4.36 (dd, J = 4.1, 12.6 Hz, 1H), 4.32 (d, J = 8.3 Hz, 1H), 4.21 (dd, *J* = 10.5, 3.3 Hz, 1H), 4.14 (dd, *J* = 12.4, 4.7 Hz, 1H), 4.08 (m, 1H), 4.04 4.04 (dd, *J* = 14.0, 2.3 Hz, 1H), 3.84-3.78 (m, 2H), 3.65 (m, 1H), 3.54 (m, 1H), 2.04 (s, 3H), 2.03 (s, 3H), 2.00 (s, 3H), 1.98 (s, 3H), 1.97 (s, 3H), 1.95 (s, 3H). ^{13}C NMR (126 MHz, $CDCl_3$): δ 170.96, 170.72, 170.59, 169.59, 169.53, 169.40, 169.15, 156.03, 136.36, 135.33, 128.81, 128.71, 128.62, 128.56, 128.50, 128.44, 101.15, 100.98, 73.14, 72.66, 72.09, 71.91, 71.21, 69.13, 68.17, 67.86, 67.33, 62.21, 61.89, 54.63, 20.96, 20.91, 20.81, 20.80, 20.71, 20.59. ESI HRMS: Calcd. for $C_{44}H_{53}NO_{22}$ $[M+Na]^+$ 970.2998; obs. $[M+Na]^+$ 970.2975

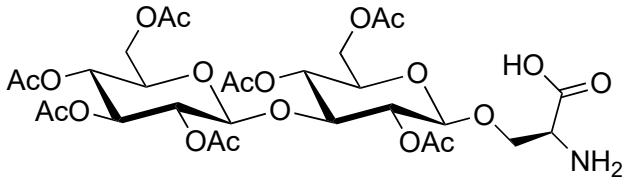

***O*-β-Heptaacetyl -D-laminaribiosyl L-Serine, 2.1f**

To a solution of **2.12f** (134 mg, 0.13 mmol) in methanol (MeOH) (5 mL) was added 20% (w/w on carbon, dry basis) palladium hydroxide (13 mg, 10% w/w). The atmosphere of the reaction vessel was then flushed thrice with hydrogen and stirred under a H_2 balloon at room temperature for 3 h.

The reaction mixture was filtered through a 0.2 μm PTFE syringe filter and concentrated in vacuo. The resulting white residue was triturated with 3 × 5 mL diethyl ether and dried under high vacuum, affording **2.1f** as a white solid (100 mg, 98%). ^{1}H NMR (500 MHz, CD_3OD): δ 8.0 (br, 3H), 6.21 (d, J = 3.7 Hz, 0.2H), 5.16-5.01 (m, 3H), 4.99-4.93 (m, 1H), 4.93-4.82 (m, 1H), 4.68-4.52 (m, 2H), 4.44-4.36 (m, 1H), 4.33 (t, *J* = 7.1 Hz, 1H), 4.27 (m, 1H) 4.17 (dd, *J* = 12.7, 4.3 Hz, 2H), 4.12-3.98 (m, 2H), 3.87 (m, 1H), 3.78 (m, 1H), 3.71 (m, 1H), 2.15 (s, 3H), 2.08 (s, 3H), 2.05 (s, 3H), 2.02 (s, 3H), 1.98 (s, 3H), 1.97 (s, 3H), 1.95 (s, 3H). ^{13}C NMR (126 MHz, CD_3OD): δ 171.77, 170.73, 170.62, 170.51, 170.17, 169.63, 169.58, 169.53, 101.14, 101.00, 89.41, 79.09, 76.36, 73.20, 73.09, 72.49, 71.88, 71.78, 71.50, 71.38, 70.12, 68.21, 68.08, 67.57, 61.84, 21.41, 21.23, 21.01, 20.93, 20.81, 20.73, 20.65. ESI HRMS: Calcd. for $C_{29}H_{42}NO_{20}$ $[M+H]^+$ 724.2295; obs. $[M+H]^+$ 724.2281

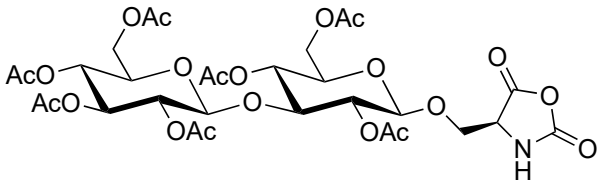

***O*-β-Heptaacetyl -D-Laminaribiosyl L-Serine *N*-Carboxyanhydride (βGlc2-Ser NCA), 2.2f**

Compound **2.1f** (115 mg, 0.16 mmol) was suspended in anhydrous tetrahydrofuran (3.5 mL, 45 mM) under N_2 in an oven-dried 50 mL round-bottom flask with a stir bar. To this stirred suspension was added α-pinene (100 μL, 0.64 mmol, 4.0 equiv.), followed by a solution of 15% (w/w) phosgene in toluene (226 μL, 0.32 mmol, 2.0 equiv.). **Caution: Phosgene is extremely hazardous and all manipulations must be performed in a well-ventilated chemical fume hood with proper personal protection and necessary precautions taken to avoid exposure.** The reaction mixture was stirred at room temperature under static N_2 and the flask was sealed with Parafilm. After 36 h, the reaction mixture was determined to have gone to completion by FTIR. The mixture was concentrated under high vacuum for 1 h using two sequential liquid nitrogen-cooled traps to condense solvent, byproducts, and phosgene. The collected condensate was quenched with ammonium hydroxide to consume residual phosgene prior to disposal. The crude NCA was dissolved in minimal anhydrous dichloromethane and purified by flash chromatography on anhydrous silica gel (5–20% anhydrous THF in anhydrous DCM). Fractions were monitored by TLC (visualized with $KMnO_4$ stain) and FTIR. Product-containing fractions were concentrated in vacuo to afford **2.2f** as a white solid (69 mg, 58%). The products were afforded in a 1:3 α:β anomeric ratio by ^{1}H NMR analysis. ^{1}H NMR (500 MHz, $CDCl_3$): δ 7.31 (s, 1H), 6.79 (s, 1H), 5.18 (t, *J* = 10.7 Hz, 1H), 5.12 (t, *J* = 9.4 Hz, 1H), 5.01-4.93 (m, 1H), 4.91-4.86 (m, 2H), 4.67 (d, *J* = 11.9 Hz, 1H), 4.57 (d, *J* = 8.1 Hz, 1H), 4.45 (m, 2H), 4.36 (m 1H), 4.21-4.12 (m, 2H), 4.08 (dd, *J* = 12.6, 5.6 Hz, 1H), 4.05-4.00 (m, 1H), 3.91-3.85 (m, 2H), 3.73-3.68 (m, 2H), 3.62-3.53 (m, 2H), 2.16 (s, 3H), 2.08 (s, 3H), 2.06 (s, 3H), 2.04 (s, 3H), 1.99 (s, 6H), 1.97 (s, 3H). ^{13}C NMR (126 MHz, $CDCl_3$): δ 171.61, 170.76, 170.59, 169.71, 169.56, 169.42, 167.63, 151.99, 101.15, 100.98, 84.45, 78.67, 74.62, 73.06, 72.75, 72.09, 71.94, 71.25, 70.91, 68.72, 68.46, 68.15, 63.21, 62.31, 61.87, 59.25, 58.99, 21.14, 20.93, 20.82, 20.74, 20.61. FTIR-ATR ν_{max}/cm^{-1} 1858, 1788, 1744, 1370, 1223, 1038. ESI HRMS: Calcd. for $C_{40}H_{39}NO_{21}$ $[M+Na]^+$ 772.1898; obs. $[M+Na]^+$ 772.1928

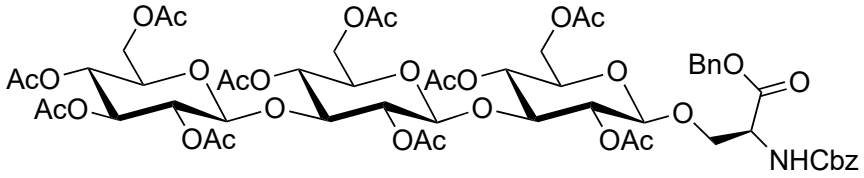

***O*-β-Decacetyl -D-laminaritriosyl *N*-Carboxybenzyl L-Serine Benzyl Ester, 2.12g**

A solution of decaacetyl-1-bromo-D-laminaritriose[62] (165 mg, 0.17 mmol) and *N*-carboxybenzyl L-serine benzyl ester (60 mg, 0.18 mmol, 1.1 equiv.) in anhydrous DCM (8 mL, 0.02 M) was stirred over activated 4 Å molecular sieves under N_2 for 15 min at room temperature. The reaction vessel was covered in foil and silver triflate (69 mg, 0.27 mmol, 1.1 equiv.) was quickly added. The reaction mixture was stirred at room temperature under nitrogen for 48 h. The reaction mixture was quenched by the addition of *N*,*N*-diisopropylethylamine (29 μL, 0.17 mmol, 1.0 equiv) and stirred for 15 min. The suspension was then filtered through a 0.2 μm PTFE syringe filter to remove silver salts and concentrated in vacuo to afford a brown residue. The residue was purified by flash chromatography on silica to afford product as a white foam (91 mg, 44%). ^{1}H NMR (500 MHz, $CDCl_3$): δ 7.35 (m, 5H, Ar), 7.34 (m, 5H, Ar), 6.23 (d, *J* = 3.7 Hz, 0.3H), 5.63 (d, *J* = 7.8 Hz, 0.7H), 5.18 (s, 2H), 5.13-5.05 (m, 4H), 4.93-4.84 (m, 4H), 4.52-4.47 (m, 2H), 4.42-4.37 (m, 2H), 4.34 (d, *J* = 7.9 Hz, 1H), 4.30 (dd, *J* = 4.4, 12.4 Hz, 1H), 4.23 (dd, *J* = 10.4, 3.2 Hz, 1H), 4.12 (d, *J* = 4.8 Hz, 1H), 4.06-4.00 (m, 2H), 3.84-3.75 (m, 3H), 3.68-3.63 (m, 2H), 3.58-3.56 (m, 2H), 2.08 (s, 3H), 2.07 (s, 3H), 2.07 (s, 3H), 2.06 (s, 6H), 2.02 (s, 3H), 2.00 (s, 6H), 1.99 (s, 3H), 1.96 (s, 3H). ^{13}C NMR (126 MHz, $CDCl_3$) δ 171.01, 170.88, 170.78, 170.58, 169.71, 169.61, 169.53, 169.37, 169.33, 169.11, 169.00, 156.04, 136.38, 135.30, 128.84, 128.82, 128.78, 128.55, 128.43, 101.28, 100.97, 100.87, 79.23, 78.39, 73.07, 72.93, 72.80, 72.06, 71.88, 71.80, 71.04, 69.13, 68.45, 68.30, 68.22, 67.94, 67.36, 62.30, 62.17, 61.87, 54.67, 21.16, 20.99, 20.93, 20.88, 20.82, 20.73, 20.71, 20.62. ESI HRMS: Calcd. for $C_{56}H_{69}NO_{30}$ $[M+Na]^+$ 1258.3798; obs. $[M+Na]^+$ 1258.3825

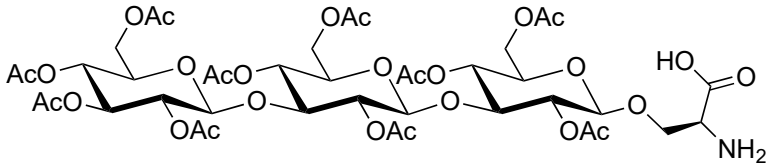

***O*-β-Decacetyl -D-Laminaritriosyl L-Serine, 2.1g**

To a solution of **2.12g** (184 mg, 0.15 mmol) in MeOH (5 mL) was added 20% (w/w on carbon, dry basis) palladium hydroxide (18 mg, 10% w/w). The atmosphere of the reaction vessel was then flushed thrice with hydrogen and stirred under a H_2 balloon at room temperature for 3 h. The reaction mixture was filtered through a 0.2 μm PTFE syringe filter and concentrated in vacuo. The resulting white residue was triturated with 3 × 5 mL diethyl ether and dried under high vacuum to afford **1c** as a white solid (113 mg, 100%). ^{1}H NMR (500 MHz, CD_3OD): δ 7.96 (br, 3H), 6.23 (d, *J* = 3.8 Hz, 0.33H), 5.58 (d, *J* = 6.0 Hz, 0.67H), 5.13-5.06 (m, 3H), 4.93-4.88 (m, 4H), 4.57-4.51 (m, 2H), 4.42-4.40 (m, 2H), 4.34 (m, 2H), 4.21 (m, 1H), 4.10-4.01 (m, 3H), 3.95 (m, 1H), 3.86-3.79 (m, 2H), 3.72-3.66 (m, 2H), 2.26-2.20 (s, 6H), 2.11-2.05 (m, 12H), 2.04-1.99 (m, 9H), 1.99 (s, 3H), 1.96 (s, 3H), 1.83 (s, 3H). ^{13}C NMR (126 MHz, CD_3OD): δ 170.86, 170.76, 170.56, 169.54, 169.42, 108.15, 73.02, 72.50, 71.91, 71.78, 71.19, 68.79, 68.16, 67.94, 61.89, 29.95, 29.39, 28.07, 24.17, 22.44, 21.27, 21.01, 20.93, 20.81, 20.70, 18.88. ESI HRMS: Calcd. for $C_{41}H_{57}NO_{28}$ $[M+H]^+$ 1012.3178, $[M+Na]^+$ 1034.2998; obs. $[M+H]^+$ 1012.3149, $[M+Na]^+$ 1034.2972

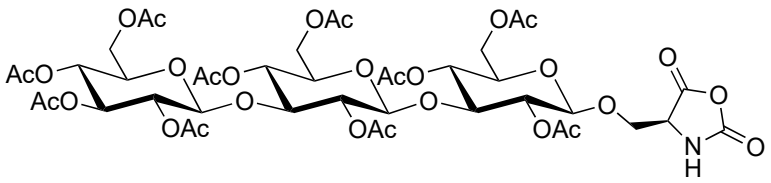

***O*-β-Decacetyl-D-Laminaritriosyl L-Serine *N*-Carboxyanhydride (βGlc3-Ser NCA), 2.2g**

Compound **2.1g** (53 mg, 0.052 mmol) was suspended in anhydrous THF (1.3 mL, 45 mM) under N_2 in an oven-dried 50 mL round-bottom flask with a stir bar. To this stirred suspension was added α-pinene (33 μL, 0.21 mmol, 4.0 equiv.), followed by a solution of 15% (w/w) phosgene in toluene (74 μL, 0.10 mmol, 2.0 equiv.). **Caution: Phosgene is extremely hazardous and all manipulations must be performed in a well-ventilated chemical fume hood with proper personal protection and necessary precautions taken to avoid exposure.** As the phosgene was added, the suspension cleared. The reaction mixture was stirred at room temperature under static N_2 and the flask was sealed with Parafilm. The reaction mixture was monitored by FTIR and allowed to stir until no further increase of the *N*-carboxyanhydride IR peaks at 1861 and 1791 cm^{-1} was observed, 76 h. The mixture was concentrated under high vacuum for 1 h using two sequential liquid nitrogen-cooled traps to condense solvent, byproducts, and phosgene. The collected condensate was quenched with ammonium hydroxide to consume residual phosgene prior to disposal. The crude NCA was dissolved in a minimal amount of 5% (v/v) anhydrous THF in anhydrous DCM and purified by flash chromatography on anhydrous silica gel (5–40% anhydrous THF in anhydrous DCM). Fractions were monitored by TLC with $KMnO_4$ and IR. Product containing fractions were concentrated in vacuo to afford **2.2g** as a white solid (60 mg, 62%). The products were afforded in a 1:4 α:β anomeric ratio by ^{1}H NMR analysis. ^{1}H NMR (500 MHz, $CDCl_3$): δ 7.35 (m, 1H), 6.79 (s, 1H), 5.10-5.05 (m, 2H), 4.94-4.80 (m, 5H), 4.56 (dd, J = 8.0, 3.0 Hz, 1H), 4.47-4.42 (m, 3H), 4.37 (m, 1H), 4.31 (dd, J = 12.0, 3.8 Hz, 1H), 4.14 (m, 1H), 4.09-3.99 (m, 3H), 3.93 (m, 1H), 3.87-3.81 (m, 3H), 3.77 (m, 1H), 3.71-3.63 (m, 2H), 3.51 (m, 1H), 2.16 (s, 3H), 2.13 (s, 3H), 2.09 (s, 3H), 2.08 (s, 3H), 2.05 (s, 6H), 2.03 (s, 3H), 1.99 (s, 6H), 1.95 (s, 3H). ^{13}C NMR (126 MHz, $CDCl_3$): δ 171.54, 170.99, 170.87, 170.77, 170.55, 169.75, 169.56, 169.45, 169.36, 169.24, 167.80, 152.04, 101.25, 101.19, 100.99, 100.86, 84.54, 79.24, 78.63, 78.16, 74.54, 73.03, 72.78, 72.65, 72.23, 71.88, 71.80, 71.10, 68.37, 68.16, 62.35, 62.10, 61.85, 58.91, 21.20, 21.12, 20.98, 20.92, 20.80, 20.70, 20.62. FTIR-ATR ν_{max}/cm^{-1} 1861, 1791, 1748, 1371, 1224, 1040. ESI HRMS: Calcd. for $C_{42}H_{55}NO_{29}$ $[M+Na]^+$ 1060.2798; obs. $[M+Na]^+$ 1060.2779

General procedure for polymerization of glycosylated Ser NCAs

All polymerization reactions were performed in a N_2-filled glove box. To a solution of NCA in DMF or THF (50 mg/mL) was rapidly added a solution of initiator via syringe. The reaction was stirred at 20 ºC and polymerization progress was monitored by FTIR. Polymerizations were generally complete within 2 h. Aliquots were removed for GPC analysis immediately upon polymerization completion. Reactions were dried under reduced pressure, diluted with minimal THF, then precipitated into acidic water (1 mM HCl, pH 3) to remove the metal initiator. Polymers were collected by centrifugation and dried under reduced pressure to yield peracetylated glycopolypeptides as white solids (87–99% yield). Glycopolypeptides initiated with $(PMe_3)_4Co$ initiator in THF have an N-terminal amino group and a glyco-Ser amino acid side chain group at

the C-terminal chain initiation site.[45] Glycopolypeptides initiated with azidopropyl-Leu-Ni initiator (**4**) in DMF have an N-terminal terminal amino group and an azidopropyl-Leu group at the C-terminal chain initiation site.[50] Polymer absolute molecular weights were determined for some polymers using ^{1}H NMR by integrations calibrated to the azidopropyl-Leu end group for low molecular weight polypeptides, or to polypeptides endcapped with PEG-isocyanate according to literature protocols.[45] Briefly, low dispersity, 1 kDa amino-terminal PEG was converted to PEG-isocyanate (PEG-NCO) via treatment with phosgene. Peracetylated polypeptides were treated with 3.0 eq of PEG-NCO per polypeptide chain in THF for 16 h at room temperature. Polypeptides were deprotected and dialyzed as described in section 'General Glycopolypeptide Deprotection Procedure'. Glycopolypeptide integrations were compared to the ethylene glycol peak at δ3.66 ppm, correlating to 88 H, as previously reported.[50] These samples were used for GPC calibration, allowing for subsequent determination of polymer molecular weights by GPC. An example spectrum of a polymer that was quantified relative to the leucine endgroup is shown in the Spectral Data section for poly(β-laminaribiosyl-L-Ser). Example spectra of endcapped polypeptides are shown in the appendix for poly(α-mannopyranosyl-L-Ser)**,** poly(α-mannobiosyl-L-Ser), and poly(β-lactosyl-L-Ser). Samples with a DP of 200-300 were used for GPC calibration, allowing for subsequent determination of polymer molecular weights by GPC.

Kinetic study of the polymerization rate of glyco-Ser NCAs

A kinetics study was performed to check that the rates of polymerization are comparable across different NCA monomers, supporting the premise that our copolymers are indeed random in their distribution of residues rather than tapered or block-like. ATR-FTIR was used to monitor conversion of NCA to polypeptide, based on comparison of the initial and reaction concentrations of NCA anhydride carbonyl peaks at ca. 1790 cm^{-1} and 1850 cm^{-1}, and appearance of polypeptide peaks at ca. 1650 cm^{-1} and 1540 cm^{-1}.[63-64] The glycosyl acetate peak at ca. 1750 cm^{-1} was used as an internal standard since this concentration does not change over the course of the polymerization. The polymerizations of NCAs α-Man-Ser **2d** and α-Man2-Ser **2e** were compared to TFA-Lys NCA polymerization. Polymerization was initiated at an M:I ratio of 75:1 using $(PMe_3)_4Co$ initiator in THF as described in the section 'General Procedure for Polymerization of glycosylated Ser NCAs'. Two μL-scale aliquots of the polymerization reactions were analyzed by ATR-FTIR at various time points after addition of initiator. Studies were performed in duplicate.

The polymerization rate constants ($k_{p,obs}$) were calculated by plots of natural logarithm of monomer concentration versus time, and linear fitting of the data using the following equation:

$$[-\ln(M_t/M_i)=k_{p,obs}t]$$

where M_t = concentration of monomer at time (t), M_i =initial concentration of monomer, $k_{p,obs}$= rate constant, and t = time. Reaction half-lives were calculated from the equation $t_{1/2} = (\ln 2)/k_{p,obs}$.

General glycopolypeptide deprotection procedure

To a solution of peracetylated glycopeptide in 1:1 MeOH:H_2O (10 mg/mL) was added K_2CO_3 and the reaction was stirred for 16 h at room temperature, with formation of a white precipitate for some glycopeptides. Reactions were neutralized with 0.1 M HCl then condensed under reduced

pressure. The solid glycopolypeptides were dissolved in water and transferred to 3500 Da molecular weight cutoff (MWCO) dialysis cassettes and dialyzed against 4 L of deionized water for 3 days, with water changes twice per day. Dialyzed polymers were lyophilized to dryness to give glycopolypeptides **3a-f** as white fluffy solids. (~90% yield after dialysis). PEG-endcapped glycopolypeptides were deprotected using the same conditions.

General procedure for copolymerizations

All polymerization reactions were performed in a dinitrogen-filled glove box. To a solution of NCA in DMF or THF (50 mg/mL) was added L-Ala NCA and *t*Bu-L-Glu NCA as a solution in the same solvent (50 mg/mL) in the desired molar ratios. Transition metal initiator was rapidly added as a solution via syringe. The reaction was stirred at 20 ºC and polymerization progress was monitored by ATR-IR for the disappearance of NCA peaks at 1790 and 1850 cm^{-1} and the formation of an amide bond via the C=O stretch at 1650 cm^{-1}. Polymerizations were generally complete within 2 h. Aliquots were removed for GPC analysis immediately upon polymerization completion. Reactions were dried under reduced pressure, diluted with minimal THF, then precipitated into acidic water (pH = 3, 1 mM HCl). Polymers were collected by centrifugation and dried under reduced pressure.

Copolypeptide deprotection

Acetate groups were removed as described in the general glycopolypeptide deprotection procedure. For copolypeptides containing alanine, one part THF was added to the deprotection reaction to increase solubility. After acetate deprotection, solutions were condensed under reduced pressure. *t*Bu-L-Glu/glyco-Ser copolypeptides were redissolved in trifluoroacetic acid (TFA) (10 mg/mL) and stirred at room temperature for 1 h. The TFA was evaporated and the solid residue was redissolved in minimal 0.1 M $NaHCO_3$ to deprotonate the Glu residues, and the copolypeptides were taken up in water and dialyzed to give poly(glyco-Ser-*stat*-L-Glu)s as fluffy white solids (92-99% yield). Alternatively, acetate deprotection could be performed after *t*Bu-L-Glu deprotection by dissolving the residue obtained after TFA evaporation in the acetate deprotection solvent mixture and proceeding as described in the general glycopolypeptide deprotection procedure. In this case, saturated K_2CO_3 was used to account for residual acidity; no β-elimination was observed by ^1H NMR in products deprotected in this manner despite the increased concentration of K_2CO_3. Amino acid ratios were calculated by ^1H NMR integrations in D_2O as previously described.[50] Spectra were calibrated to the Ala methyl group at ca 1.4 ppm. Example spectra of statistical copolypeptides are shown in the appendix for poly(α-mannopyranosyl-L-Ser-*co*-Glu-*co*-Ala) and poly(α-mannobiosyl-L-Ser-*co*-Glu-*co*-Ala) at either 65% or 30% glycosylation and for poly(β-laminaribiosyl-L-Ser-*co*-Glu-*co*-Ala) and poly(α-laminaritriosyl-L-Ser-*co*-Glu-*co*-Ala) at 50% glycosylation.

2.9 References

1. Cobb, M., 60 years ago, Francis Crick changed the logic of biology. *PLoS Biol* **2017,** *15* (9), e2003243.

2. Kerscher, B.; Willment, J. A.; Brown, G. D., The Dectin-2 family of C-type lectin-like receptors: an update. *Int Immunol* **2013,** *25* (5), 271-7.

3. Lopez Aguilar, A.; Briard, J. G.; Yang, L.; Ovryn, B.; Macauley, M. S.; Wu, P., Tools for Studying Glycans: Recent Advances in Chemoenzymatic Glycan Labeling. *ACS Chem Biol* **2017,** *12* (3), 611-621.

4. Yang, Y.; Franc, V.; Heck, A. J. R., Glycoproteomics: A Balance between High-Throughput and In-Depth Analysis. *Trends Biotechnol* **2017,** *35* (7), 598-609.

5. Manz, C.; Pagel, K., Glycan analysis by ion mobility-mass spectrometry and gas-phase spectroscopy. *Curr Opin Chem Biol* **2017,** *42*, 16-24.

6. Lepenies, B.; Lee, J.; Sonkaria, S., Targeting C-type lectin receptors with multivalent carbohydrate ligands. *Adv Drug Deliv Rev* **2013,** *65* (9), 1271-81.

7. Chiodo, F.; Marradi, M.; Park, J.; Ram, A. F.; Penades, S.; van Die, I.; Tefsen, B., Galactofuranose-coated gold nanoparticles elicit a pro-inflammatory response in human monocyte-derived dendritic cells and are recognized by DC-SIGN. *ACS Chem Biol* **2014,** *9* (2), 383-9.

8. Garcia-Vallejo, J. J.; van Kooyk, Y., The physiological role of DC-SIGN: a tale of mice and men. *Trends Immunol* **2013,** *34* (10), 482-6.

9. Schnaar, R. L.; Lee, Y. C., Polyacrylamide gels copolymerized with active esters. New medium for affinity systems. *Biochemistry* **2002,** *14* (7), 1535-1541.

10. Kanai, M.; Mortell, K. H.; Kiessling, L. L., Varying the Size of Multivalent Ligands: The Dependence of Concanavalin A Binding on Neoglycopolymer Length. *Journal of the American Chemical Society* **1997,** *119* (41), 9931-9932.

11. Mortell, K. H.; Weatherman, R. V.; Kiessling, L. L., Recognition Specificity of Neoglycopolymers Prepared by Ring-Opening Metathesis Polymerization. *Journal of the American Chemical Society* **1996,** *118* (9), 2297-2298.

12. Mayer, S.; Raulf, M. K.; Lepenies, B., C-type lectins: their network and roles in pathogen recognition and immunity. *Histochem Cell Biol* **2017,** *147* (2), 223-237.

13. Sharpe, A. H., Introduction to checkpoint inhibitors and cancer immunotherapy. *Immunological Reviews* **2017,** *276* (1), 5-8.

14. Pardoll, D. M., The blockade of immune checkpoints in cancer immunotherapy. *Nat Rev Cancer* **2012,** *12* (4), 252-64.

15. Li, K.; Qu, S.; Chen, X.; Wu, Q.; Shi, M., Promising Targets for Cancer Immunotherapy: TLRs, RLRs, and STING-Mediated Innate Immune Pathways. *Int J Mol Sci* **2017,** *18* (2).

16. Shi, M.; Chen, X.; Ye, K.; Yao, Y.; Li, Y., Application potential of toll-like receptors in cancer immunotherapy: Systematic review. *Medicine (Baltimore)* **2016,** *95* (25), e3951.

17. Goldberg, J. L.; Sondel, P. M., Enhancing Cancer Immunotherapy Via Activation of Innate Immunity. *Semin Oncol* **2015,** *42* (4), 562-72.

18. Corrales, L.; Gajewski, T. F., Endogenous and pharmacologic targeting of the STING pathway in cancer immunotherapy. *Cytokine* **2016,** *77*, 245-7.

19. Chiefari, J.; Chong, Y. K.; Ercole, F.; Krstina, J.; Jeffery, J.; Le, T. P. T.; Mayadunne, R. T. A.; Meijs, G. F.; Moad, C. L.; Moad, G.; Rizzardo, E.; Thang, S. H., Living Free-Radical Polymerization by Reversible Addition−Fragmentation Chain Transfer: The RAFT Process. *Macromolecules* **1998,** *31* (16), 5559-5562.

20. Moad, G.; Chiefari, J.; Chong, Y. K.; Krstina, J.; Mayadunne, R. T. A.; Postma, A.; Rizzardo, E.; Thang, S. H., Living free radical polymerization with reversible addition - fragmentation chain transfer (the life of RAFT). *Polymer International* **2000,** *49* (9), 993-1001.

21. Rabuka, D.; Parthasarathy, R.; Lee, G. S.; Chen, X.; Groves, J. T.; Bertozzi, C. R., Hierarchical assembly of model cell surfaces: synthesis of mucin mimetic polymers and their display on supported bilayers. *J Am Chem Soc* **2007,** *129* (17), 5462-71.

22. Godula, K.; Umbel, M. L.; Rabuka, D.; Botyanszki, Z.; Bertozzi, C. R.; Parthasarathy, R., Control of the molecular orientation of membrane-anchored biomimetic glycopolymers. *J Am Chem Soc* **2009,** *131* (29), 10263-8.

23. Miura, Y.; Hoshino, Y.; Seto, H., Glycopolymer Nanobiotechnology. *Chem Rev* **2016,** *116* (4), 1673-92.

24. Hudak, J. E.; Bertozzi, C. R., Glycotherapy: new advances inspire a reemergence of glycans in medicine. *Chem Biol* **2014,** *21* (1), 16-37.

25. Khalil, D. N.; Smith, E. L.; Brentjens, R. J.; Wolchok, J. D., The future of cancer treatment: immunomodulation, CARs and combination immunotherapy. *Nat Rev Clin Oncol* **2016,** *13* (5), 273-90.

26. Jackson, H. J.; Rafiq, S.; Brentjens, R. J., Driving CAR T-cells forward. *Nat Rev Clin Oncol* **2016,** *13* (6), 370-83.

27. Harris, D. T.; Kranz, D. M., Adoptive T Cell Therapies: A Comparison of T Cell Receptors and Chimeric Antigen Receptors. *Trends Pharmacol Sci* **2016,** *37* (3), 220-30.

28. Feng, D.; Shaikh, A. S.; Wang, F., Recent Advance in Tumor-associated Carbohydrate Antigens (TACAs)-based Antitumor Vaccines. *ACS Chem Biol* **2016,** *11* (4), 850-63.

29. Raokoganty, R.; Reddish, M.; Michaellongenecker, B., Glycopeptide-and carbohydratebased synthetic vaccines for the immunotherapy of cancer. *Drug Discovery Today* **1996,** *1* (5), 190-198.

30. Stergiou, N.; Glaffig, M.; Jonuleit, H.; Schmitt, E.; Kunz, H., Immunization with a Synthetic Human MUC1 Glycopeptide Vaccine against Tumor-Associated MUC1 Breaks Tolerance in Human MUC1 Transgenic Mice. *ChemMedChem* **2017,** *12* (17), 1424-1428.

31. McDonald, D. M.; Byrne, S. N.; Payne, R. J., Synthetic self-adjuvanting glycopeptide cancer vaccines. *Front Chem* **2015,** *3*, 60.

32. Xiao, H.; Woods, E. C.; Vukojicic, P.; Bertozzi, C. R., Precision glycocalyx editing as a strategy for cancer immunotherapy. *Proc Natl Acad Sci U S A* **2016,** *113* (37), 10304-9.

33. Mitchell, S. A.; Pratt, M. R.; Hruby, V. J.; Polt, R., Solid-Phase Synthesis of O-Linked Glycopeptide Analogues of Enkephalin. *The Journal of Organic Chemistry* **2001,** *66* (7), 2327-2342.

34. Xin, H.; Dziadek, S.; Bundle, D. R.; Cutler, J. E., Synthetic glycopeptide vaccines combining beta-mannan and peptide epitopes induce protection against candidiasis. *Proc Natl Acad Sci U S A* **2008,** *105* (36), 13526-31.

35. Kuduk, S. D.; Schwarz, J. B.; Chen, X.-T.; Glunz, P. W.; Sames, D.; Ragupathi, G.; Livingston, P. O.; Danishefsky, S. J., Synthetic and Immunological Studies on Clustered Modes of Mucin-Related Tn and TF O-Linked Antigens: The Preparation of a Glycopeptide-Based Vaccine for Clinical Trials against Prostate Cancer†. *Journal of the American Chemical Society* **1998,** *120* (48), 12474-12485.

36. Gamblin, D. P.; Scanlan, E. M.; Davis, B. G., Glycoprotein synthesis: an update. *Chem Rev* **2009,** *109* (1), 131-63.

37. Leuchs, H., Ueber die Glycin-carbonsäure. *Berichte der deutschen chemischen Gesellschaft* **1906,** *39* (1), 857-861.

38. Wessely, F., Untersuchungen über α-Amino-N-Carbonsäureanhydride. I. *Hoppe-Seyler´s Zeitschrift für physiologische Chemie* **1925,** *146* (1-3), 72-90.

39. Curtius, T.; Sieber, W., Umwandlung von Malonsäure in Glykokoll und von Methyl-malonsäure in α-Alanin. *Berichte der deutschen chemischen Gesellschaft (A and B Series)* **1921,** *54* (7), 1430-1437.

40. Curtius, T.; Hochschwender, K.; Meier, H.; Lehmann, W.; Benckiser, A.; Schenck, M.; Wirbatz, W.; Gaier, J.; Mühlhäusser, W., Umwandlung von alkylierten Malonsäuren in α-Aminosäuren. *Journal für Praktische Chemie* **1930,** *125* (1), 211-302.

41. Behrendt, R.; White, P.; Offer, J., Advances in Fmoc solid-phase peptide synthesis. *J Pept Sci* **2016,** *22* (1), 4-27.

42. Kricheldorf, H. R., Polypeptides and 100 years of chemistry of alpha-amino acid N-carboxyanhydrides. *Angew Chem Int Ed Engl* **2006,** *45* (35), 5752-84.

43. Deming, T. J., Transition Metal−Amine Initiators for Preparation of Well-Defined Poly(γ-benzyll-glutamate). *Journal of the American Chemical Society* **1997,** *119* (11), 2759-2760.

44. Cheng, J.; Deming, T. J., Synthesis of polypeptides by ring-opening polymerization of alpha-amino acid N-carboxyanhydrides. *Top Curr Chem* **2012,** *310*, 1-26.

45. Curtin, S. A.; Deming, T. J., Initiators for End-Group Functionalized Polypeptides via Tandem Addition Reactions. *Journal of the American Chemical Society* **1999,** *121* (32), 7427-7428.

46. Kramer, J. R.; Deming, T. J., Recent advances in glycopolypeptide synthesis. *Polym. Chem.* **2014,** *5* (3), 671-682.

47. Gibson, M. I.; Hunt, G. J.; Cameron, N. R., Improved synthesis of O-linked, and first synthesis of S- linked, carbohydrate functionalised N-carboxyanhydrides (glycoNCAs). *Org Biomol Chem* **2007,** *5* (17), 2756-7.

48. Aoi, K.; Tsutsumiuchi, K.; Okada, M., Glycopeptide Synthesis by an .alpha.-Amino Acid N-Carboxyanhydride (NCA) Method: Ring-Opening Polymerization of a Sugar-Substituted NCA. *Macromolecules* **1994,** *27* (3), 875-877.

49. Tsutsumiuchi, K.; Aoi, K.; Okada, M., Synthesis of Polyoxazoline−(Glyco)peptide Block Copolymers by Ring-Opening Polymerization of (Sugar-Substituted) α-Amino AcidN-Carboxyanhydrides with Polyoxazoline Macroinitiators. *Macromolecules* **1997,** *30* (14), 4013-4017.

50. Kramer, J. R.; Onoa, B.; Bustamante, C.; Bertozzi, C. R., Chemically tunable mucin chimeras assembled on living cells. *Proc Natl Acad Sci U S A* **2015,** *112* (41), 12574-9.

51. Bell, C.; Anderson, J.; Ganguly, T.; Prescott, J.; Capila, I.; Lansing, J. C.; Sachleben, R.; Iyer, M.; Fier, I.; Roach, J.; Storey, K.; Miller, P.; Hall, S.; Kantor, D.; Greenberg, B. M.; Nair, K.; Glajch, J., Development of Glatopa(R) (Glatiramer Acetate): The First FDA-Approved Generic Disease-Modifying Therapy for Relapsing Forms of Multiple Sclerosis. *J Pharm Pract* **2017**, 897190017725984.

52. Boons, G. J. H., K. J., *Organic Synthesis with Carbohydrates*. Blackwell Science, Inc.: Malden, MA, 2000.

53. Szabò, L.; Li, Y.; Polt, R., O-glycopeptides: a simple β-stereoselective glycosidation of serine and threonine via a favorable hydrogen bonding pattern. *Tetrahedron Letters* **1991,** *32* (5), 585-588.

54. Chen, L.; Tan, Z., A convenient and efficient synthetic approach to mono-, di-, and tri-O-mannosylated Fmoc amino acids. *Tetrahedron Letters* **2013,** *54* (17), 2190-2193.

55. Wang, L.-X.; Sakairi, N.; Kuzuhara, H., Peracetylated laminaribiose: preparation by specific degradation of curdlan and its chemical conversion into N-acetylhyalobiuronic acid. *Carbohydrate Research* **1991,** *219*, 133-148.

56. Deming, T. J.; Curtin, S. A., Chain Initiation Efficiency in Cobalt- and Nickel-Mediated Polypeptide Synthesis. *Journal of the American Chemical Society* **2000,** *122* (24), 5710-5717.

57. Coltart, D. M.; Royyuru, A. K.; Williams, L. J.; Glunz, P. W.; Sames, D.; Kuduk, S. D.; Schwarz, J. B.; Chen, X.-T.; Danishefsky, S. J.; Live, D. H., Principles of Mucin Architecture: Structural Studies on Synthetic Glycopeptides Bearing Clustered Mono-, Di-, Tri-, and Hexasaccharide Glycodomains. *Journal of the American Chemical Society* **2002,** *124* (33), 9833-9844.

58. Kelly, S.; Price, N., The Use of Circular Dichroism in the Investigation of Protein Structure and Function. *Current Protein & Peptide Science* **2000,** *1* (4), 349-384.

59. Klein, H.-F.; Karsch, H. H., Methylkobaltverbindungen mit nicht chelatisierenden Liganden, I. Methyltetrakis(trimethylphosphin)kobalt und seine Derivate. *Chemische Berichte* **1975,** *108* (3), 944-955.

60. Varon, D.; Lioy, E.; Patarroyo, M. E.; Schratt, X.; Unverzagt, C., *Australian Journal of Chemistry* **2002,** *55* (2), 161.

61. Ogawa, T.; Yamamoto, H., Synthesis of linear d-mannotetraose and d-mannohexaose, partial structures of the cell-surface d-mannan of Candida albicans and Candida utilis. *Carbohydrate Research* **1982,** *104* (2), 271-283.

62. Marca, E.; Valero-Gonzalez, J.; Delso, I.; Tejero, T.; Hurtado-Guerrero, R.; Merino, P., Synthesis of O- and C-glycosides derived from beta-(1,3)-D-glucans. *Carbohydr Res* **2013,** *382*, 9-18.

63. Habraken, G. J. M.; Wilsens, K. H. R. M.; Koning, C. E.; Heise, A., Optimization of N-carboxyanhydride (NCA) polymerization by variation of reaction temperature and pressure. *Polymer Chemistry* **2011,** *2* (6), 1322.

64. Zou, J.; Fan, J.; He, X.; Zhang, S.; Wang, H.; Wooley, K. L., A facile glovebox-free strategy to significantly accelerate the syntheses of well-defined polypeptides by N-carboxyanhydride (NCA) ring opening polymerizations. *Macromolecules* **2013,** *46* (10), 4223-4226.

Chapter 3

Exploring glycopolypeptides as agonists for Dectin-1 and Dectin-2

This work was adapted from Zhou, M. N.; Delaveris, C. S.; Kramer, J. R.; Kenkel, J. A.; Engleman, E. G.; Bertozzi, C. R. N-carboxyanhydride polymerization of glycopolypeptides that activate antigen presenting cells through Dectin-1 and -2. *Angew. Chemie Int. Ed.* **2018**.

3.1 C-type lectin receptors as therapeutically interesting targets for glycopolypeptides

Our previous work with GalNAc-Ser glycopolypeptides was aimed at mimicking mammalian mucin structures, which feature heavily glycosylated O-GalNAc-Ser/Thr cores.[1] As an alternative angle, I decided to focus my efforts instead into mimicking microbial, and particularly pathogen-associated, carbohydrate patterns. Microbes, particularly bacteria and fungi, display a variety of glycans and glycoconjugates that differ from human host structures. As detailed in Chapter 1, the innate immune system employs glycan-binding proteins, including C-type lectin receptors (CLRs), to recognize pathogen-associated glycan motifs and trigger immune cell activation.[2] Many CLRs are expressed on antigen-presenting cells, and thus have been investigated as targets for vaccine adjuvants and for antigen delivery.[3] These studies have primarily focused on dendritic cell-specific intercellular adhesion molecule-3-grabbing non-integrin (DC-SIGN)[4-5] and mannose receptor CD206[6-7], although interest in other CLRs is growing as they become better characterized.[8] CLRs may also be attractive targets for provoking an anticancer immune response in the typically immunosuppressive tumor microenvironment.[8] This strategy is currently under clinical investigation with other classes of innate immune receptors,[9-12] with the aim of complementing medicines that enhance adaptive immune mechanisms such as checkpoint inhibitors[13-14] and adoptive cell therapies[15-17].

Dectin-1 (Dec-1) and Dectin-2 (Dec-2) are CLRs expressed on antigen presenting cells such macrophages and dendritic cells that are best known for their roles in anti-fungal and -bacterial immunity. Dec-1 binds to microbial β-1,3-glucans, and is a key player in immunity against pathogenic fungi in mouse models (Fig. 1a).[18-19] Dec-1 signals through phosphorylation of its immune-receptor tyrosine activation motif (ITAM), leading to activation of NF-κB and AP-1, which, in turn, drives production of the proinflammatory cytokines TNFα and IL-6.[20] Engagement of Dec-1 also promotes phagocytosis of the pathogenic cell.[20] Interestingly, administration of particulate β-1,3-glucans from fungal extracts has been shown to improve anti-tumor T cell responses and delay tumor progression in mice.[21] Notably, smaller soluble glucans bind the receptor but do not result in immune cell activation, which is thought to require receptor clustering in a "phagocytic synapse".[22] Additionally, Dec-1 has recently been implicated in innate immune recognition of tumor-associated glycans and subsequent NK cell-mediated anti-tumor cytotoxicity, although the relevant glycan structures have not been fully characterized.[23] The macrophage and dendritic cell-associated Dec-2 has been less-thoroughly studied but also plays an important role in anti-fungal immunity, and might be similarly involved in anti-tumor innate immunity.[24-25] Dec-2 binds high-mannose glycans in a microarray format[26-27] as well as mannose-rich fungal and mycobacterial structures that are rich in mannosides[28-30]. Similar to Dec-1, Dec-2 activates immune cells through NF-κB and AP-1 upon receptor clustering, but lacks its own signaling domain and instead signals through an associated ITAM-possessing FcRγ subunit (Fig. 3.1).[30]

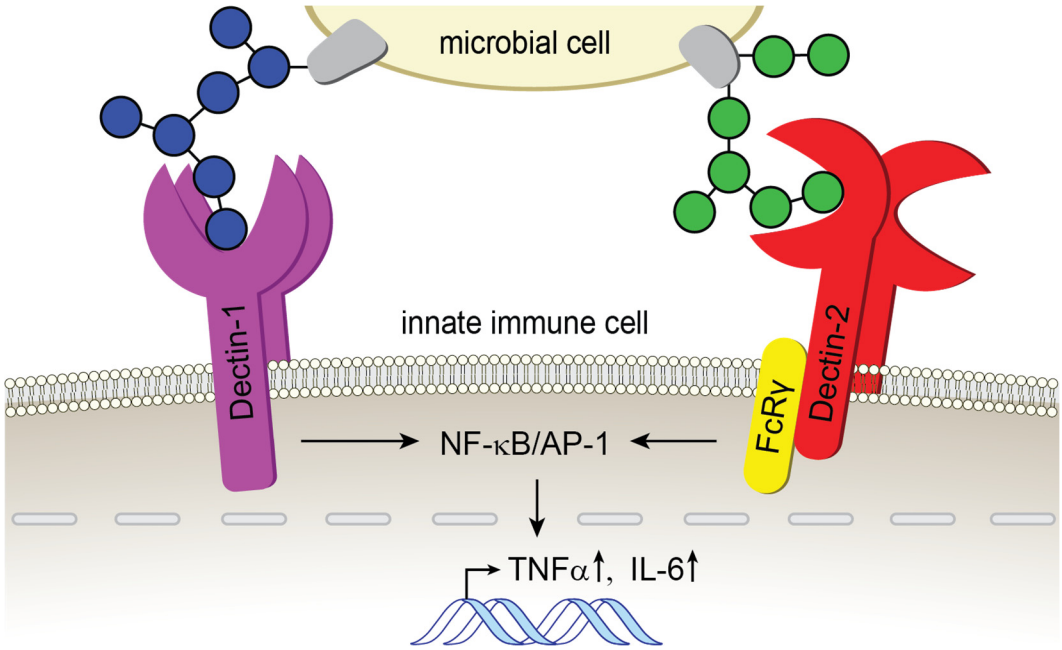

Figure 3.1. C-Type lectin receptors Dec-1 and Dec-2 recognize β-glucans and α-mannans, respectively, and induce expression of cytokines such as TNFα and IL-6 through activation of NF-κB and AP-1. Dec-1 signals through a cytoplasmic signaling domain, while Dec-2 requires an associated Fc receptor γ (FcRγ) subunit.

Previous work on Dec-1 and -2 has exclusively relied on heterogeneous extracts from microbes as a source of activating ligands. However, the investigation of Dec-1 and Dec-2 as translational targets for innate immune activation will require chemically-defined agonists. Here we report the development of fully synthetic glycopolypeptide-based agonists of Dec-1 and -2. Our design was inspired by a recent study of the fungal pathogen *Malassezia furfur* that identified heavily Ser-O-α-1,2-mannobiosylated glycopeptides as potent agonists of Dec-2 signaling.[28] Accordingly, we synthesized densely glycosylated polypeptides based on this motif. Natural Dec-1 ligands are rich in β-1,3-glucan structures, which we also integrated into glycopolypeptides to form multivalent arrays.

3.2 Exploring the impact of length and percent glycosylation on Dectin-2 activation *in vitro*

Our initial studies of CLR activation using glycopolypeptides focused on the α-1,2-mannobiose/Dectin-2 ligand/receptor pair. Our choice of glycan was motivated by a previous report that demonstrated that this specific disaccharide motif was the primary Dec-2 ligand present in the canonical Dec-2 agonist furfurman, a cell wall extract of the opportunistic fungal pathogen *Malassezia furfur*. For comparison, we also tested glycopolypeptides bearing the mannose monosaccharide. Work by Kiessling et al. has demonstrated that factors such as length and glycosylation density play a significant role in lectin binding and signaling; we therefore varied polymer lengths and glycosylation densities.[31] Polymers were synthesized as described in Chapter 2. Murine monocyte-derived dendritic cells (MDDCs) were exposed to a 25 μg/ml solution of polymer and analyzed for TNFα expression by ELISA (Fig. 3.2). Alternatively, cells were cultured

in wells that had been pretreated with glycopolypeptides by passive adsorption. An anti-Dec-2 blocking antibody was used to probe the Dec-2 dependence of any TNFα release.

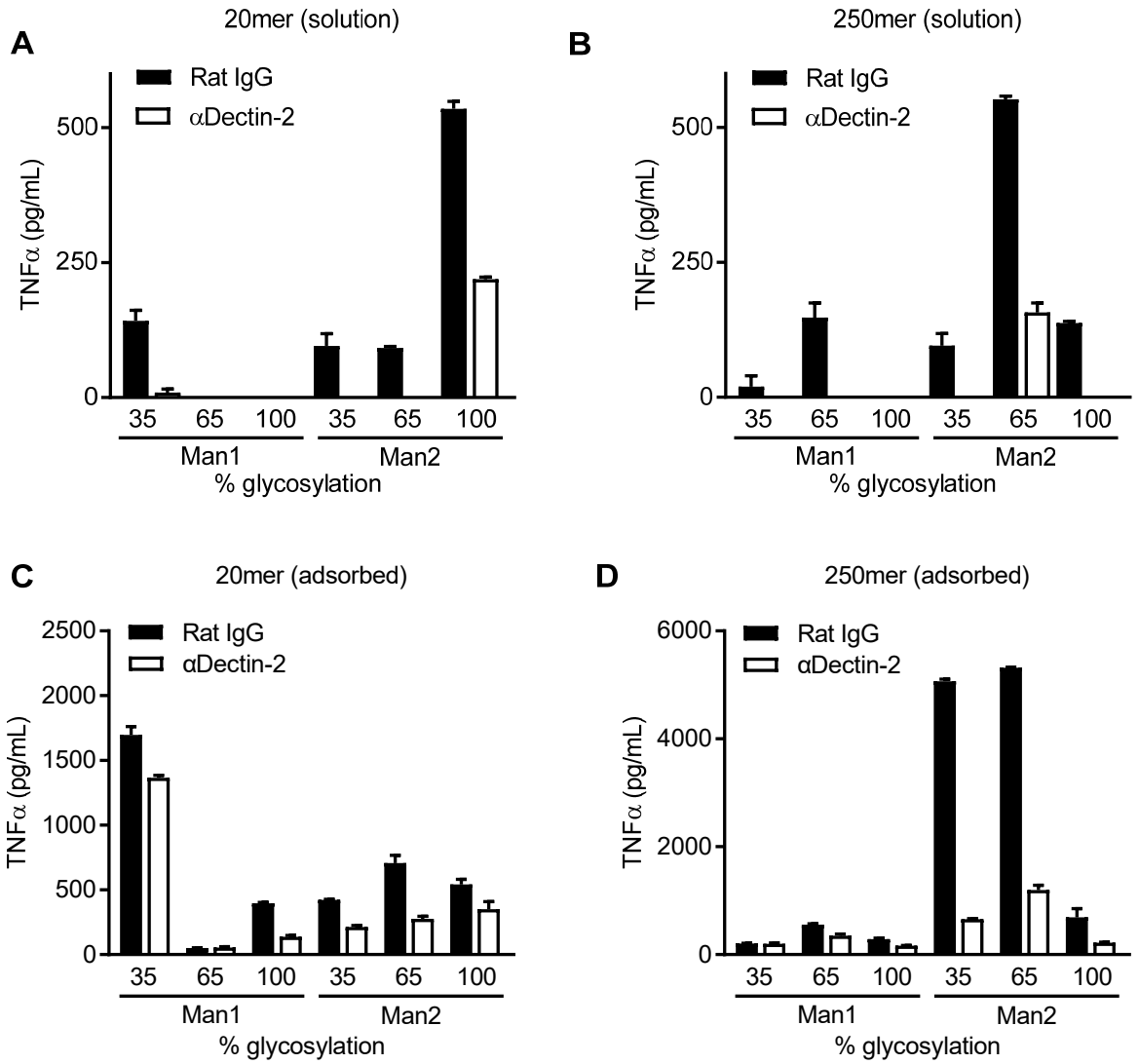

Figure 3.2. Activation of murine MDDCs upon incubation with mannosylated and mannobiosylated glycopolypeptides. A) Cells were grown in 25 μg/ml glycopolypeptide solutions. Glycopolypeptides tested were approximately 20 amino acid residues long; three glycosylation densities were tested for each polymer type. TNFα release was measured by ELISA as a measure of immunogenicity. Cells were pretreated with an anti-Dec-2 blocking antibody or an isotype control to determine the Dectin-2 dependence of the observed responses. B) The same experiment was performed using roughly 250 residue polypeptides to study the dependence of Dectin-2 stimulation on polymer length. C) Solutions of 20mer glycopolypeptides (200 μg/ml, 25 μl per well) were adsorbed onto 96-well plates prior to addition of cells. D) As with the solubilized polymer experiments, the experiment was conducted using 250mers. All data were measured in triplicate; error bars represent the standard error of the mean.

We were encouraged to observe Dec-2-specific TNFα release when cells were treated with some of our glycopolypeptides. As a general observation, mannobiosylated glycopolypeptides appeared to induce greater responses than corresponding mannosylated polymers. Furthermore, plate-adsorbed glycopolypeptides appeared more effective at stimulating monocytes than solubilized samples. Under these plate-adsorbed conditions, a notable dependence of TNFα release on polymer length was observed, with the longer polymers appearing much more effective than the shorter oligomers. This was perhaps surprising given that plate adsorption might be expected to negate any effects conferred by polymer length. It is worth noting that this initial experiment did not account for the possibility that polymers of different lengths and glycosylation densities might exhibit different binding affinities towards the assay plate, making it difficult to make conclusive comparisons between different polymers.

Because polymers in solution generally stimulated cells less effectively than plate-adsorbed glycopolypeptides, we hypothesized that rapid internalization of polymers could be impacting their ability to bind and activate cell-surface receptors. We therefore tested solution-phase polymers in the presence or absence of cytochalisin D, an inhibitor of actin polymerization and therefore actin-dependent internalization pathways (Fig. 3.3).[32] Interestingly, cytochalisin D did increase TNFα release for the majority of glycopolypeptides tested. This could indicate that rapid internalization of glycopolypeptides might interfere with signaling. Alternatively, given the mechanism of action of cytochalisin D, we cannot rule out the possibility that disrupting actin remodeling could impact Dec-2 presentation or biophysical characteristics of the interaction between glycopolypeptides and cell surface Dec-2.

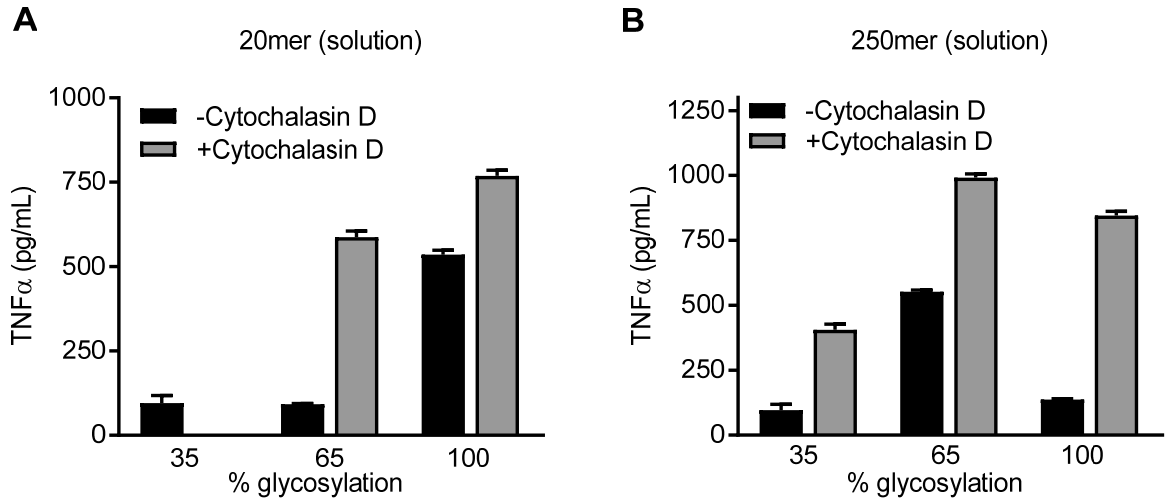

Figure 3.3. Activation of murine MDDCs using mannobiosylated glycopolypeptides of A) 20mer or B) 250mer target lengths, using the actin remodeling inhibitor cytochalasin D to probe the role of actin-dependent internalization pathways on cytokine release. All data were measured in triplicate; error bars represent the standard error of the mean.

Regardless, we were fairly confident that mannobiosylated glycopolypeptides were activating antigen-presenting cells primarily through Dec-2. As further confirmation, we repeated the experiment, this time comparing mannobiosylated and lactosylated glycopolypeptides in the plate-

adsorbed format (Fig. 3.4). To compromise between the improved activity of longer polymers and the more-reliable synthesis of shorter polymers, we used glycopolypeptides that were polymerized to a target length of 100 residues. In addition to TNFα, we measured expression of IL-6, which canonically induces a Th1-type immune response. Gratifyingly, we again observed a robust Dec-2 dependent response for mannobiosylated glycopolypeptides, whereas lactosylated control polymers induced negligible levels of either IL-6 or TNFα. Although more controls may be warranted in the future to further probe the structure-activity relationships between glycopolypeptide parameters and immune cell activation, these results illustrate that mannobiosylated glycopolymers are capable of inducing cytokine release through Dec-2.

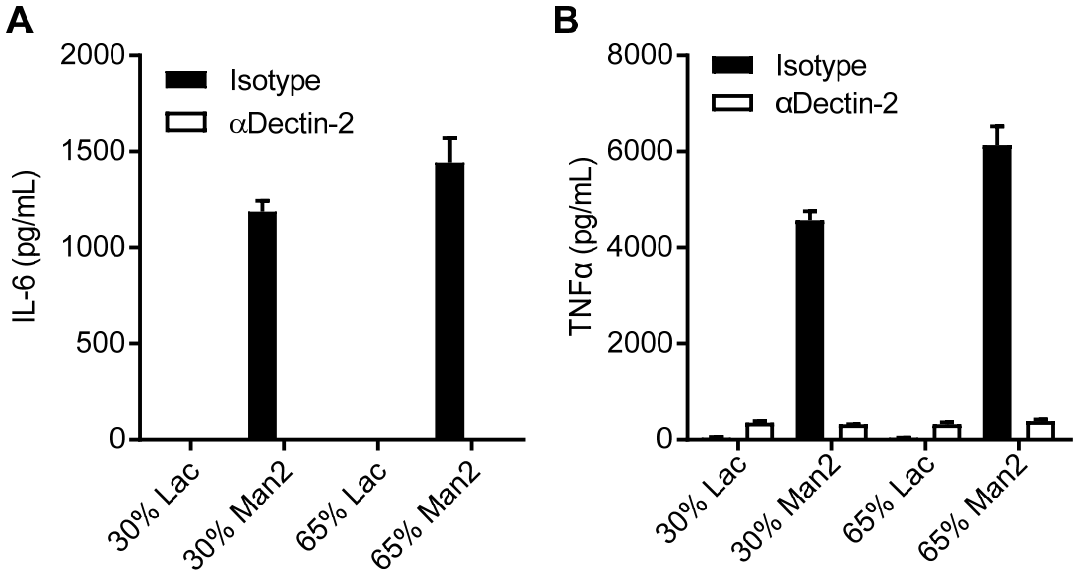

Figure 3.4. Mannosylated glycopolypeptides induce robust cytokine release in a cell culture model. Murine MDDCs were incubated for 20 hours with an αDec-2 blocking antibody or an isotype control antibody in plates that had been pretreated with Ser(Man2) or Ser(Lac) glycopolypeptides (Man2, Lac respectively) to confirm that A) IL-6 or B) TNFα release was Dec-2-dependent. Data were measured in duplicates, error bars indicate standard error of the mean.

3.3 Dec-1 and Dec-2 activation *in vitro* using glycopolypeptide-conjugated beads

Immunostimulatory C-type lectins often induce phagocytic behavior in addition to cytokine expression. While studies of free and plate-adsorbed polymers provide insight into immune cell activation via cytokine expression, successful implementation of innate immune-activating glycopolypeptides in the context of cancer immunotherapy will likely require a phagocytic response for tumor neoantigen processing and presentation to T cells via MHC receptors. We therefore sought to generate glycopolypeptide-decorated particles in the low-micron size range in order to mimic bacterial or fungal cells. To create a particulate architecture analogous to natural dectin ligands on microbial cells, we covalently attached Glc2- or Man2-glycopolypeptides to fluorescent, 0.8 μm diameter polystyrene beads (Fig. 3.5). Poly(ethylene glycol) (PEG) and Lac-glycopolypeptide conjugated beads were used as controls. Polymerizations were performed using Ni(II) catalyst **2.4**, which installs a C-terminal azide group for post-polymerization

functionalization that is chemically orthogonal to the N-terminal amino group (Scheme 1).[1] Amino functionalized beads were treated with a bicyclo[6,1,0]non-4-yn-9-yl (BCN) *N*-hydroxysuccinimidyl ester and then conjugated to the azide-terminated polypeptides or azido-PEG. Because steric crowding could inhibit receptor binding to fully glycosylated homopolymers, we used 50% and 65% glycosylated polypeptides for Ser(Glc2) and Ser(Man/Lac), respectively. Glycopolypeptides were copolymerized with a 1:1 Ala:Glu blend, all to approximately 100 residues.

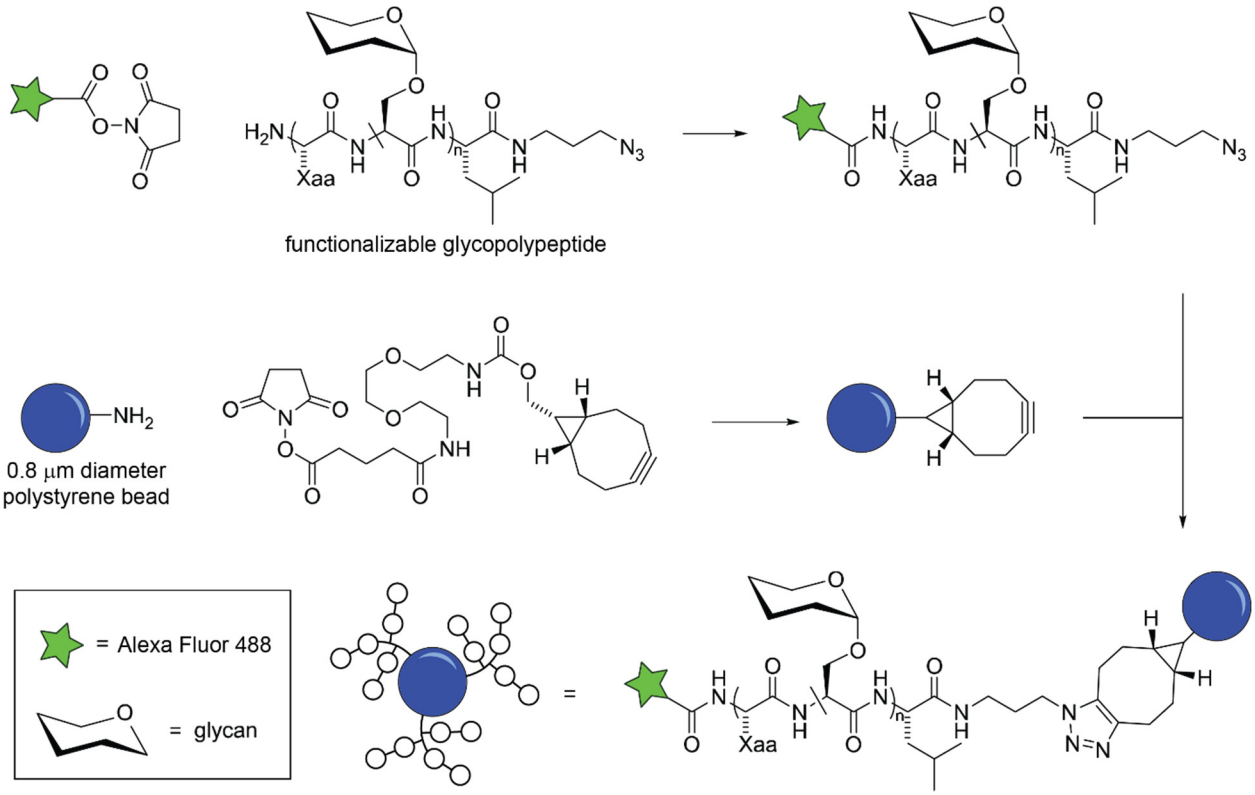

Figure 3.5. Covalent attachment of glycopolypeptides to fluorescent polystyrene beads for cell culture evaluation of immune activation and phagocytosis. Glycopolypeptides synthesized using azide-functionalized catalyst 4 were labeled with Alexa Fluor 488 NHS ester and then conjugated to fluorescent BCN-functionalized beads.

Successful loading of glycopolypeptides onto beads was measured via fluorescence intensity of polypeptides labeled with fluorophores at the N-terminus using a 488 nm dye that was fluorescently orthogonal to the red fluorescence of the beads—dye labeling of the polymers was confirmed prior to bead conjugation by measuring fluorescence signal of free polymers in solution (Figure 3.6b,d). As expected, beads that had been reacted with fluorescent glycopolypeptides exhibited greater relative fluorescence at 488 nm compared to those that were reacted with the PEG-N_3 control (Figure 3.6a,c).

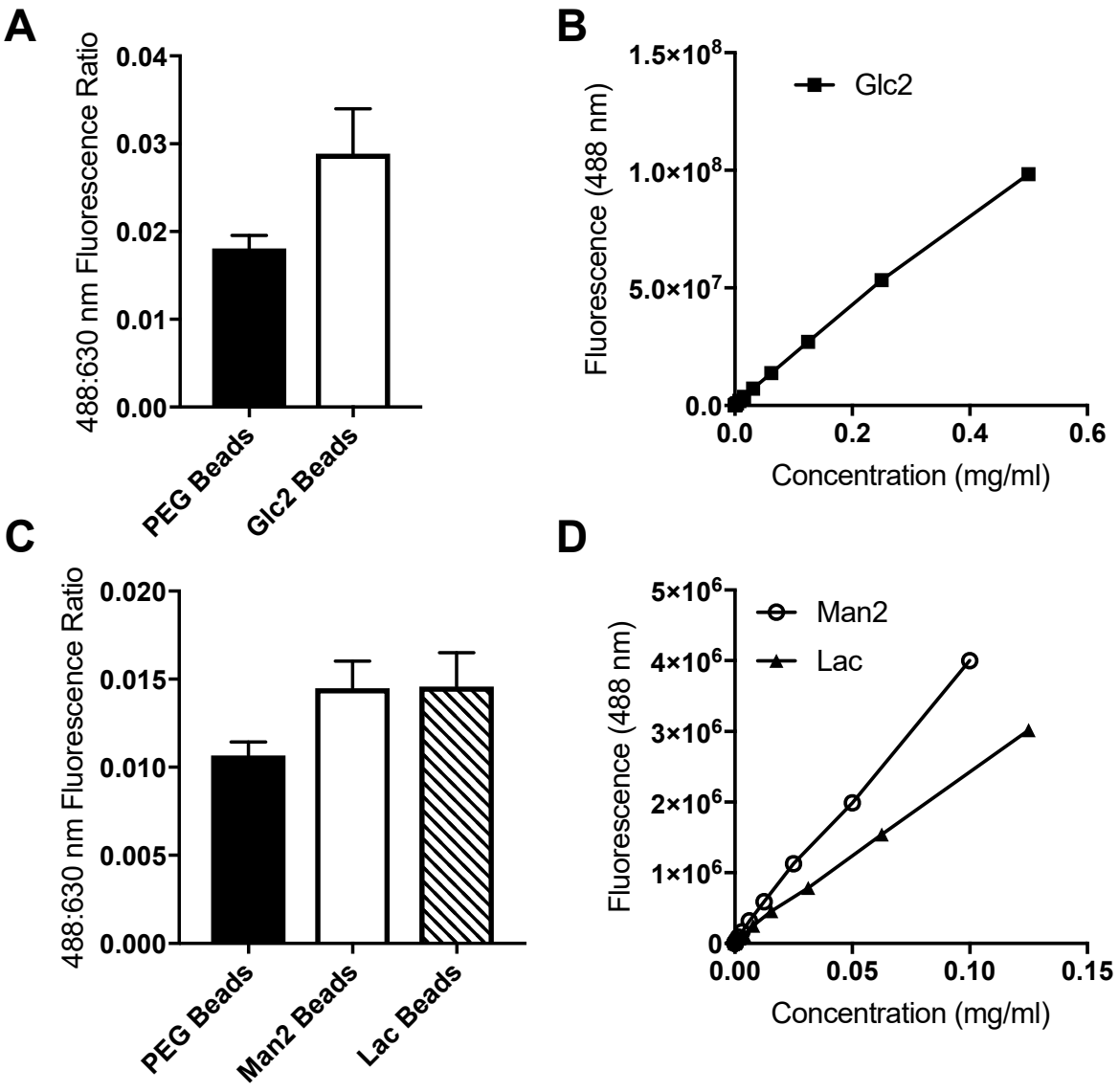

Figure 3.6. Quantification of polymer loading on beads. Comparison of relative polymer loadings on beads after click reaction of azide-terminated polymers with BCN-labeled beads. A and C) Polymers were reacted with Alexa Fluor 488 NHS ester prior to BCN conjugation, whereas the polystyrene beads contained Nile Red. Relative polymer loading was determined by comparing polymer excitation/emission at 488/520 nm to bead excitation/emission at 630/660 nm. PEG-labeled beads represent background fluorescence at 488/520 nm. All glycopolypeptide-labeled beads gave statistically significant polymer signal above background, suggesting successful polymer-bead conjugation. Polymer loadings for mannobiosylated vs. lactosylated polymers did not appear to drastically differ, suggesting that the difference in phagocytosis behavior was more likely due to glycan structure. B and D) Fluorescence at 488 nm vs. concentration of polymers before conjugation shows a linear increase of fluorescence with concentration of polymer (given in mg/mL; all polymers have same calc. molecular weight with comparable dispersities). Data are representative of technical sextuplicate; error bars represent standard deviation of the mean.

We used a commercial reporter cell line, RAW-Blue, to study immune cell activation through Dec-1. RAW-Blue cells possess an NF-κB-dependent secreted alkaline phosphatase (SEAP), the expression of which can be detected using colorimetric substrates (Fig 3.7). Since RAW-Blue cells do not express Dec-2, we used both the Dec-2-expressing murine immature dendritic cell line JAWSII and murine monocyte-derived dendritic cells to probe this receptor. Proinflammatory cytokines TNFα and IL-6 were detected by ELISA, and microbead phagocytosis was studied using flow cytometry and fluorescence microscopy (Fig 3.7).

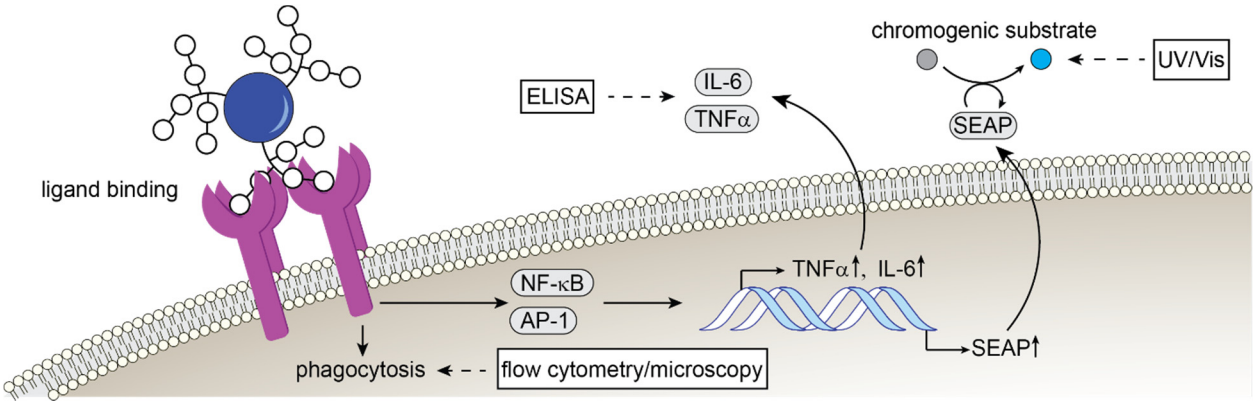

Figure 3.7. Glycopolypeptide-bead conjugates induce a variety of cellular responses upon engagement with CLRs. Cytokine secretion was detected by ELISA, and phagocytosis could be observed by fluorescence microscopy and quantified by flow cytometry. Alternatively, NF-kB- and AP-1-induced expression of a secreted alkaline phosphatase (SEAP) in the macrophage reporter cell line RAW Blue can be detected using a commercial chromogenic substrate.

Although dendritic cells generally phagocytose material in the low μm range, we observed that uptake of Man2-glycopolymer beads by JAWSII cells could be inhibited by pre-exposure to an anti-Dec-2 blocking antibody (Figs. 3.8 and 3.9). This effect was not observed with either the PEG- or Lac-glycopolymer-coated beads, suggesting that the mannobiosylated polymers indeed induced phagocytosis as expected. Bead internalization was also visualized by confocal microscopy (Fig. 3.8b-e). Although the changes appeared modest, quantification of phagocytosis by flow cytometry showed an approximately 30% increase in the relative size of the phagocytic population for cells exposed to Man2-Ser glycopolypeptide beads compared to PEG beads, and a 10% increase compared to the Lac-Ser glycopolypeptide beads (Fig. 3.9).

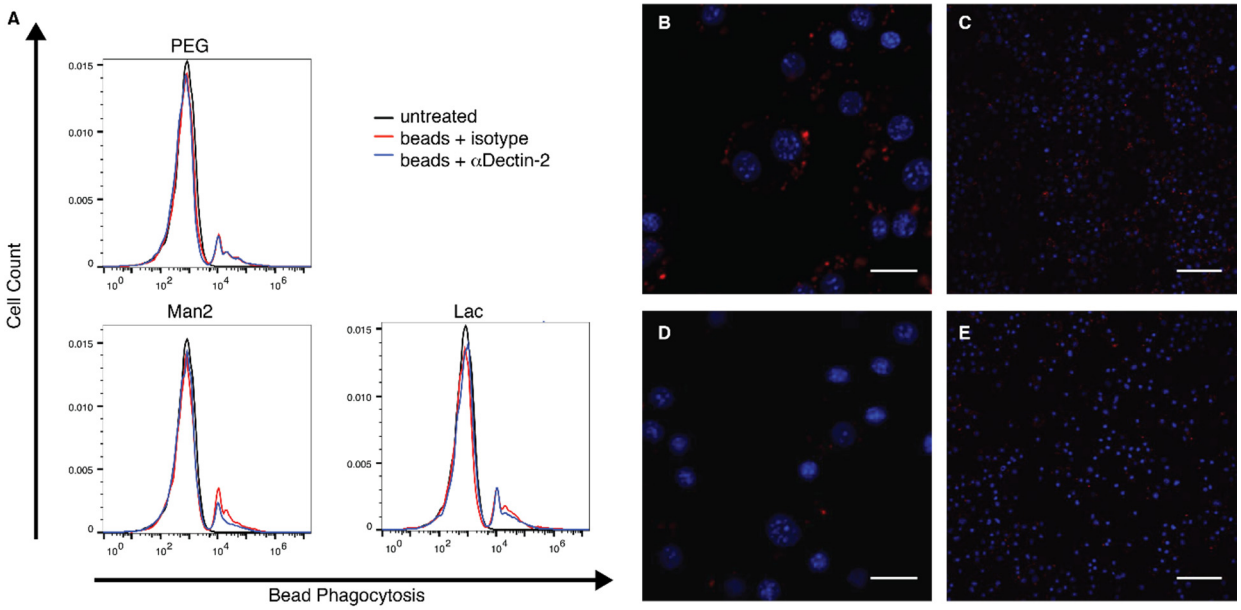

Figure 3.8. Phagocytosis of Lac and Man2 beads by JAWSII. A) Representative histograms of phagocytosis by JAWSII cells for PEG, Man2, and Lac beads in the presence of isotype or blocking αDectin-2 antibodies (5 μg/mL). Phagocytosis was measured via fluorescence in the 647 nm channel, which corresponds to the emission range of the fluorescent beads. Cells treated with only vehicle are represented in black, beads + isotype antibody are shown in red, and beads + αDectin-2 antibody are shown in blue. The peaks to the right of the mode are cells that have phagocytosed at least one fluorescent bead. B-E) Representative confocal images of JAWSII cells showing cell nuclei (blue, Hoechst 33258) and beads (red) for Man2 beads (B,C) and Lac beads (D,E). Scale bars for B,D are 20 μm and for C,E are 100 μm. Data are representative of at least three independent experiments.

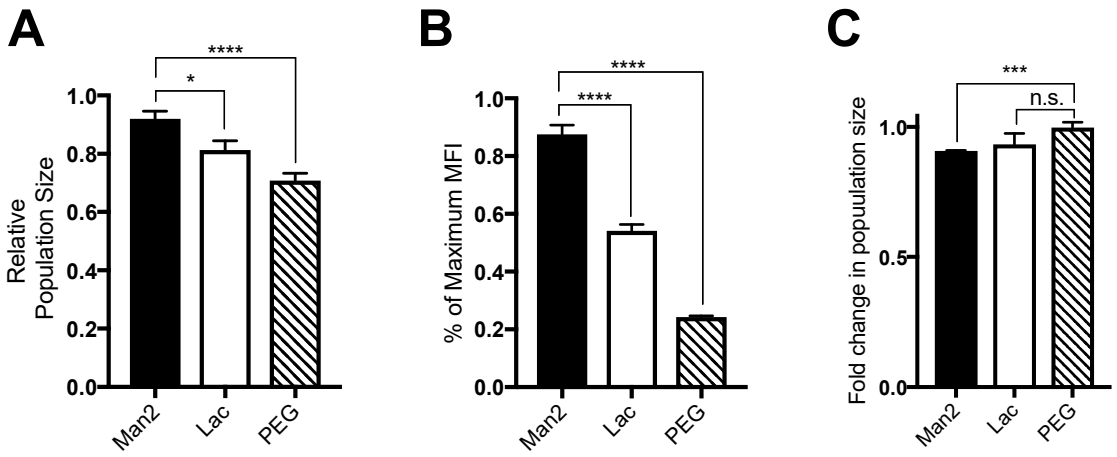

Figure 3.9. Quantification of JAWSII phagocytosis. The relative phagocytosis of Man2 (black), Lac (white), and PEG (black) conjugated beads by JAWSII cells. A) A larger proportion of the total population of JAWSII cells in each experiment phagocytose Man2 beads when compared to Lac or PEG. B) Of the population that has phagocytosed any beads, the populations treated with Man2 beads had phagocytosed more beads, indicating that the rate of phagocytosis is faster for Man2 beads by nearly two-fold for Lac and five-fold for PEG. C) When pretreated with αDectin-

2, Man2 beads selectively saw reduction in phagocytic population relative to isotype. Data are technical triplicate of biological triplicate, presented as SEM.

To further characterize the nature of the immunostimulatory effect of the glycopolypeptide-conjugated microbeads, we sought to confirm that these pro-phagocytic conjugates also induced cytokine release as expected from Figs 3.2-4. Indeed, when treated with Glc2- or Glc3-glycopolypeptide-conjugated beads, RAW-Blue cells activated NF-κB in a Dec-1-dependent manner (Fig. 3.10a-c). Promisingly, beads displaying Glc2- and Glc3-glycopolymers elicited a comparable response to the canonical Dec-1 agonist curdlan, derived from bacterial extracts.[33] Likewise, when JAWSII cells were incubated with Man2-glycopolymer-coated beads, we observed dose-dependent TNFα secretion (Fig. 3.10d). Unfortunately, the anti-Dec-2 blocking antibody has been reported as a partial agonist, and indeed we observed low-level TNFα expression in JAWSII cells, complicating analysis (Fig. 3.10e).[34] Regardless, because the Man2-glycopolypeptide-conjugated beads induced some Dec-2-dependent phagocytosis, and because the corresponding unconjugated glycopolypeptides robustly activated murine monocyte-derived cells (Figs 3.2-4), we remain confident that both the glucosylated and mannobiosylated microbe-inspired glycopolypeptides effectively mimic canonical CLR agonists and induce expected immunological outcomes.

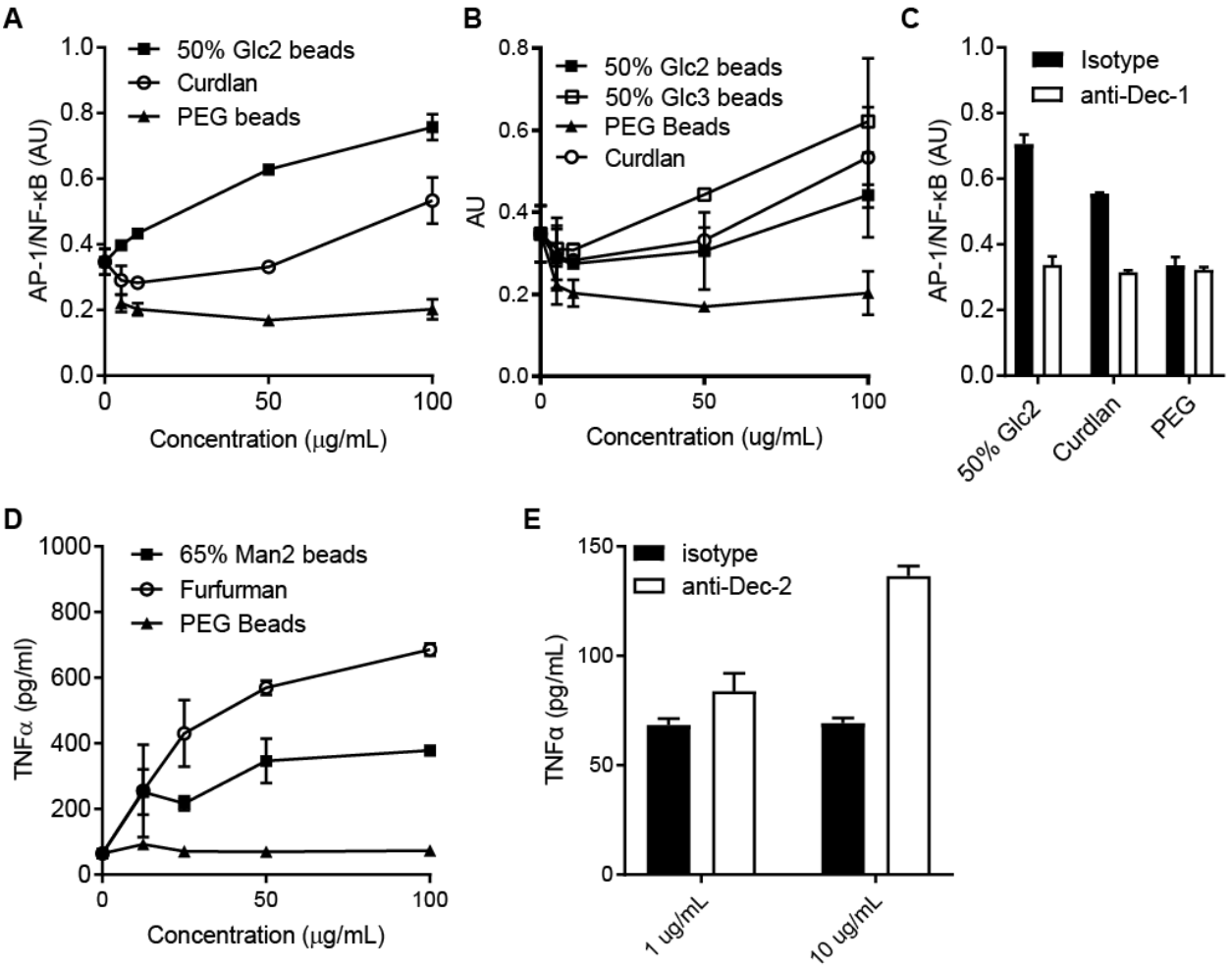

Figure 3.10. Glucosylated and mannosylated glycopolypeptides induce receptor-specific inflammatory responses in cell culture. A) Dose-response curve showing AP-1/NF-kB activation in RAW Blue cells when exposed to Glc2 glycopolypeptide-decorated beads. Cells were incubated with beads for 16 h, after which supernatants aliquots were mixed with the chromogenic substrate, incubated for four hours, and then absorbance measured at 620-655 nm. PEG-coated beads and the known agonist curdlan were used as a negative and positive control, respectively. B) The experiment was repeated with the inclusion of Glc3 glycopolypeptide-decorated beads for comparison. C) The same beads and cells were tested using the same general protocol in the presence of an anti-Dec-1 blocking antibody or an isotype control antibody to confirm that activation was Dec-1 dependent. D) JAWSII cells were similarly incubated with Man2 glycopolypeptide-decorated beads, Dec-2 agonist furfurman, or PEG-beads for 16 h, and dose-response relationships were measured via TNFa ELISA. E) The anti-Dec-2 blocking antibody induces TNFα release, complicating analysis of the dependence of cytokine release on Dec-2 signaling. A similar effect can be seen in Fig. 3.4b, albeit much less pronounced in that model system. Data were measured in triplicate, error bars indicate standard error of the mean.

3.4 Summary and Outlook

In the previous chapter, I successfully demonstrated that NCA polymerization is amenable to a variety of glycosylated structures besides the GalNAc-serine motif we had previously reported. As

we had not previously tested any NCA glycopolypeptides for biological activity, it was also important to demonstrate that this methodology could be employed to design probes and ligands for specific lectin receptors. In this chapter, I presented work confirming that the NCA-derived glycopolypeptides can induce expected biological outcomes in cell culture. As a model system, we synthesized glycopolypeptides bearing glucosylated and mannosylated immunostimulatory motifs, as these structures are widely-reported CLR agonists and *in vitro* assays of immune activation are readily accessible. As hoped, we found that rationally-designed glycopolypeptides activated murine innate immune cells through the predicted receptor interactions.

A natural next step would be to investigate *in vivo* properties of these materials to determine their utility in more biologically-relevant model systems. In the following chapter, I will present additional work using the Ser(Man2) glycopolypeptide scaffold demonstrating that the *in vitro* results presented here translate to an *in vivo* system. In particular, the ability of this structure to robustly activate Dec-2 makes it intriguing in a cancer immunotherapy context, where APC activation is a promising strategy for inducing antitumor innate and adaptive immune responses.

3.5 Materials and Methods

General Materials and Methods

Amine-functionalized, 0.8 μm fluorescent polystyrene beads were obtained from Spherotech. 384-Well black flat-bottom plates were purchased from Corning and fluorescence readings taken using a Molecular Devices SpectraMax i3x plate reader. PBS buffer, MEMα media, and heat-inactivated fetal bovine serum were obtained from Corning-Mediatech. Murine recombinant (rm) GM-CSF was purchased from Peprotech. Curdlan was purchased through Fisher Scientific. Rat anti-mouse Dectin-2 (clone 2E4.11D) and respective FITC conjugate were purchased from BioRad. Rat IgG2a isotype control was purchased from BD Biosciences. Flow cytometry was performed on a BD Biosciences Accuri C6. Confocal microscopy images were recorded on a Nikon A1R+ Resonant Scanning Confocal Microscope. TNFα and IL-6 ELISA kits were purchased from eBiosciences. QuantiBlue assay media was purchased from Invivogen. ELISA and QuantiBlue assays are absorbance-based and were read using a Molecular Devices SpectraMax i3x plate reader. Mouse Monocyte Enrichment Kit was purchased from STEMCELL Technologies. Procedures used to harvest murine monocytes were approved by the Institutional Animal Care and Use Committee of Stanford University. All experiments and protocols involving these primary murine cells were conducted exclusively by Dr. Justin Kenkel at Stanford University.

General procedure for glycopolypeptide end-group modification with fluorophores and conjugation to beads

Purified, deprotected glycopolypeptides bearing azide end groups were dissolved in 1X PBS (pH 7.4) at 10 mg/mL, and were then combined with a 0.33X volume of Alexa Fluor 488 NHS ester solution (1.55 mM in DMSO) in 1.5 ml Eppendorf tubes to label the N-terminal amine. The reaction mixtures were covered in foil to limit photobleaching and incubated at 4 °C for 16 h. Samples were purified by spin filtration using 3000 MWCO centrifuge filters, adding 450 μl sterile ddH_2O after each cycle (5 × 20 min at 10000 rcf). Filtrate was observed to be colorless by visual

inspection after two washes. The resulting solution was lyophilized to give functionalized glycopolypeptides as colored fluffy solids.

Amino functionalized, 0.8 μm polystyrene beads were obtained from the supplier as a 1% w/v suspension in H_2O. To functionalize, 0.5 ml of the well-mixed suspension was added to an equal volume of 1X PBS (pH 8.0) in a 2 mL Eppendorf tube, followed by 200 μl BCN-NHS ester (10 mM in DMSO). The blue suspension was covered in foil to limit photobleaching and allowed to react on a rotisserie mixer for 20 h at room temperature. Excess BCN reagent was removed by repeated centrifugation (3 × 15 min at 5000 rcf), replacing the supernatant with 1 mL 1X PBS (pH 7.4) after each cycle. Bead concentration was determined by absorbance at 600 nm relative to a standard curve. Azide-functionalized glycopolypeptides or azide-terminated 5 kDa PEG (1 mg/mL in ddH_2O) and BCN-functionalized beads (4 mg/mL in 1X PBS) were combined (1:1 by mass) and allowed to mix by rotisserie for 16 h at room temperature. Conjugated beads were isolated as described for the BCN-labeled beads. Fluorescence quantification of polymer loading was performed in 384-well format using black, flat-bottomed plates. Samples (5 μl per well) were measured in sextuplicate, exciting at 488 and 630 nm and measuring emission at 520 and 660 nm to quantify polymer and beads, respectively.

Cell lines and cell culture

JAWSII cells were purchased from American Type Culture Collection (ATCC). JAWSII cells were cultured in MEMα media supplemented with 20% heat-inactivated fetal bovine serum (FBS), supplemented with 5 ng/mL rmGM-CSF. Cells were subcultured per ATCC recommendation, subculturing at a 1:2 ratio once a week. RAW-Blue cells were purchased from Invivogen. RAW-Blue cells were cultured in DMEM supplemented with 10% FBS and supplier recommended antibiotics. Cells were subcultured at 1:5 ratio once every three days. Monocytes were isolated from the bone marrow of naïve C57BL/6 mice with the Mouse Monocyte Enrichment Kit according to the manufacturer's instructions, and cultured for 24 h in complete medium (RPMI with 10% heat-inactivated FBS, 2 mM L-glutamine) supplemented with 50 ng/mL of recombinant murine GM-CSF to generate monocyte-derived dendritic cells

Stimulation of RAW-Blue cells and NFκB reporter assay

Cells were stimulated and analyzed per manufacturer instructions for RAW-Blue and QuantiBlue assay. In brief, ~100,000 cells per well of a flat-bottom 96-well plate were treated with 20 μL of agonist to the reported final concentrations. Cells were incubated for 16 h and 50 μL aliquots of the supernatant were added to 150 μL 1X QuantiBlue, which was then incubated at 37 ºC in the dark for 4 h, including media-only blanks to control for any potential phosphatase in the media. SEAP concentrations were determined by plate reader at 620-655 nm.

Stimulation of JAWSII cells and quantification by ELISA

JAWSII media was supplemented with an additional 20 ng/mL rmGM-CSF 24 h prior to treatment with polymer-coated beads. JAWSII cells were treated with 20 μL agonist to the reported final concentrations of agonists and incubated for 16 h. The supernatants were then analyzed by TNFα ELISA, following the manufacturer's instructions.

Stimulation of murine monocyte-derived dendritic cells and quantification by ELISA

For plate-adsorbed conditions, glycopolypeptide solutions (200 μg/mL in PBS; 5 μg/well) were evaporated onto the surface of 96-well plates, followed by washing with PBS. The cells were pretreated for 30 min with isotype control or αDectin-2 antibodies (20 μg/mL), then stimulated with either plate-adsorbed glycopeptides or glycopolypeptide solutions (20 μg/ml) for 20 h. The levels of TNFα and IL-6 in cleared supernatants were measured by ELISA, following the manufacturer's instructions.

Flow cytometry

JAWSII media was supplemented with an additional 20 ng/mL rmGM-CSF 24 h prior to treatment. For inhibition assays, cells were pretreated with 5 μg/mL either αDectin-2 or isotype, and incubated for 30 min prior to addition of beads. Cells in a ~60% surface-confluent 6-well plate were treated to a final concentration of 10 μg/well of polymer-coated beads from stock solutions of approximately 1 mg/mL in PBS. The plates were incubated for 30 min at 37 °C. The wells were then washed 5 × 1 mL room temperature PBS. The cells were then lifted by incubating briefly with 10 mM EDTA in PBS followed by vigorous pipetting, pelleted at 400 rcf for 5 min, resuspended in 200 μL/well ice-cold 2% BSA in PBS, and analyzed by flow cytometry.

Fluorescence Microscopy

JAWSII cells were plated on German #1 borosilicate glass coverslips in media supplemented with 25 ng/mL GM-CSF and allowed to adhere overnight. Wells were treated with 10 μg/mL of polymer-coated bead and incubated at 37 ºC for 15 min. The media was aspirated and the wells were washed 3 × 400 μL PBS to remove excess beads. The cells were then fixed on ice in 1% PFA in PBS for 20 min. If used, cells were then stained for 30 min on ice in permeabilization buffer (5% BSA and 0.1% Triton-X100 in PBS) with 5 μM Hoescht. The cells were washed 3 × 400 μL PBS and then coated with 200 uL/well 2% BSA in PBS. Plates were imaged immediately.

3.6 References

1. Kramer, J. R.; Onoa, B.; Bustamante, C.; Bertozzi, C. R., Chemically tunable mucin chimeras assembled on living cells. *Proc Natl Acad Sci U S A* **2015,** *112* (41), 12574-9.

2. Kerscher, B.; Willment, J. A.; Brown, G. D., The Dectin-2 family of C-type lectin-like receptors: an update. *Int Immunol* **2013,** *25* (5), 271-7.

3. Lepenies, B.; Lee, J.; Sonkaria, S., Targeting C-type lectin receptors with multivalent carbohydrate ligands. *Adv Drug Deliv Rev* **2013,** *65* (9), 1271-81.

4. Chiodo, F.; Marradi, M.; Park, J.; Ram, A. F.; Penades, S.; van Die, I.; Tefsen, B., Galactofuranose-coated gold nanoparticles elicit a pro-inflammatory response in human monocyte-derived dendritic cells and are recognized by DC-SIGN. *ACS Chem Biol* **2014,** *9* (2), 383-9.

5. Garcia-Vallejo, J. J.; van Kooyk, Y., The physiological role of DC-SIGN: a tale of mice and men. *Trends Immunol* **2013,** *34* (10), 482-6.

6. Singh, S. K.; Streng-Ouwehand, I.; Litjens, M.; Kalay, H.; Burgdorf, S.; Saeland, E.; Kurts, C.; Unger, W. W.; van Kooyk, Y., Design of neo-glycoconjugates that target the mannose receptor and enhance TLR-independent cross-presentation and Th1 polarization. *Eur J Immunol* **2011,** *41* (4), 916-25.

7. Lam, J. S.; Mansour, M. K.; Specht, C. A.; Levitz, S. M., A Model Vaccine Exploiting Fungal Mannosylation to Increase Antigen Immunogenicity. *The Journal of Immunology* **2005,** *175* (11), 7496-7503.

8. Mayer, S.; Raulf, M. K.; Lepenies, B., C-type lectins: their network and roles in pathogen recognition and immunity. *Histochem Cell Biol* **2017,** *147* (2), 223-237.

9. Li, K.; Qu, S.; Chen, X.; Wu, Q.; Shi, M., Promising Targets for Cancer Immunotherapy: TLRs, RLRs, and STING-Mediated Innate Immune Pathways. *Int J Mol Sci* **2017,** *18* (2).

10. Shi, M.; Chen, X.; Ye, K.; Yao, Y.; Li, Y., Application potential of toll-like receptors in cancer immunotherapy: Systematic review. *Medicine (Baltimore)* **2016,** *95* (25), e3951.

11. Goldberg, J. L.; Sondel, P. M., Enhancing Cancer Immunotherapy Via Activation of Innate Immunity. *Semin Oncol* **2015,** *42* (4), 562-72.

12. Corrales, L.; Gajewski, T. F., Endogenous and pharmacologic targeting of the STING pathway in cancer immunotherapy. *Cytokine* **2016,** *77*, 245-7.

13. Sharpe, A. H., Introduction to checkpoint inhibitors and cancer immunotherapy. *Immunological Reviews* **2017,** *276* (1), 5-8.

14. Pardoll, D. M., The blockade of immune checkpoints in cancer immunotherapy. *Nat Rev Cancer* **2012,** *12* (4), 252-64.

15. Khalil, D. N.; Smith, E. L.; Brentjens, R. J.; Wolchok, J. D., The future of cancer treatment: immunomodulation, CARs and combination immunotherapy. *Nat Rev Clin Oncol* **2016,** *13* (5), 273-90.

16. Jackson, H. J.; Rafiq, S.; Brentjens, R. J., Driving CAR T-cells forward. *Nat Rev Clin Oncol* **2016,** *13* (6), 370-83.

17. Harris, D. T.; Kranz, D. M., Adoptive T Cell Therapies: A Comparison of T Cell Receptors and Chimeric Antigen Receptors. *Trends Pharmacol Sci* **2016,** *37* (3), 220-30.

18. Brown, G. D.; Taylor, P. R.; Reid, D. M.; Willment, J. A.; Williams, D. L.; Martinez-Pomares, L.; Wong, S. Y. C.; Gordon, S., Dectin-1 Is A Major β-Glucan Receptor On Macrophages. *The Journal of Experimental Medicine* **2002,** *196* (3), 407-412.

19. Drummond, R. A.; Brown, G. D., The role of Dectin-1 in the host defence against fungal infections. *Curr Opin Microbiol* **2011,** *14* (4), 392-9.

20. Brown, G. D., Dectin-1: a signalling non-TLR pattern-recognition receptor. *Nat Rev Immunol* **2006,** *6* (1), 33-43.

21. Goodridge, H. S.; Reyes, C. N.; Becker, C. A.; Katsumoto, T. R.; Ma, J.; Wolf, A. J.; Bose, N.; Chan, A. S.; Magee, A. S.; Danielson, M. E.; Weiss, A.; Vasilakos, J. P.; Underhill, D. M., Activation of the innate immune receptor Dectin-1 upon formation of a 'phagocytic synapse'. *Nature* **2011,** *472* (7344), 471-5.

22. Walachowski, S.; Tabouret, G.; Foucras, G., Triggering Dectin-1-Pathway Alone Is Not Sufficient to Induce Cytokine Production by Murine Macrophages. *PLoS One* **2016,** *11* (2), e0148464.

23. Chiba, S.; Ikushima, H.; Ueki, H.; Yanai, H.; Kimura, Y.; Hangai, S.; Nishio, J.; Negishi, H.; Tamura, T.; Saijo, S.; Iwakura, Y.; Taniguchi, T., Recognition of tumor cells by Dectin-1 orchestrates innate immune cells for anti-tumor responses. *Elife* **2014,** *3*, e04177.

24. Ifrim, D. C.; Quintin, J.; Courjol, F.; Verschueren, I.; van Krieken, J. H.; Koentgen, F.; Fradin, C.; Gow, N. A.; Joosten, L. A.; van der Meer, J. W.; van de Veerdonk, F.; Netea, M. G., The Role of Dectin-2 for Host Defense Against Disseminated Candidiasis. *J Interferon Cytokine Res* **2016,** *36* (4), 267-76.

25. Kimura, Y.; Inoue, A.; Hangai, S.; Saijo, S.; Negishi, H.; Nishio, J.; Yamasaki, S.; Iwakura, Y.; Yanai, H.; Taniguchi, T., The innate immune receptor Dectin-2 mediates the phagocytosis of cancer cells by Kupffer cells for the suppression of liver metastasis. *Proc Natl Acad Sci U S A* **2016,** *113* (49), 14097-14102.

26. McGreal, E. P.; Rosas, M.; Brown, G. D.; Zamze, S.; Wong, S. Y.; Gordon, S.; Martinez-Pomares, L.; Taylor, P. R., The carbohydrate-recognition domain of Dectin-2 is a C-type lectin with specificity for high mannose. *Glycobiology* **2006,** *16* (5), 422-30.

27. Zheng, R. B.; Jegouzo, S. A. F.; Joe, M.; Bai, Y.; Tran, H. A.; Shen, K.; Saupe, J.; Xia, L.; Ahmed, M. F.; Liu, Y. H.; Patil, P. S.; Tripathi, A.; Hung, S. C.; Taylor, M. E.; Lowary, T. L.; Drickamer, K., Insights into Interactions of Mycobacteria with the Host Innate Immune System from a Novel Array of Synthetic Mycobacterial Glycans. *ACS Chem Biol* **2017**.

28. Ishikawa, T.; Itoh, F.; Yoshida, S.; Saijo, S.; Matsuzawa, T.; Gonoi, T.; Saito, T.; Okawa, Y.; Shibata, N.; Miyamoto, T.; Yamasaki, S., Identification of distinct ligands for the C-type lectin receptors Mincle and Dectin-2 in the pathogenic fungus Malassezia. *Cell Host Microbe* **2013,** *13* (4), 477-88.

29. Sato, K.; Yang, X. L.; Yudate, T.; Chung, J. S.; Wu, J.; Luby-Phelps, K.; Kimberly, R. P.; Underhill, D.; Cruz, P. D., Jr.; Ariizumi, K., Dectin-2 is a pattern recognition receptor for fungi that couples with the Fc receptor gamma chain to induce innate immune responses. *J Biol Chem* **2006,** *281* (50), 38854-66.

30. Feinberg, H.; Jegouzo, S. A. F.; Rex, M. J.; Drickamer, K.; Weis, W. I.; Taylor, M. E., Mechanism of pathogen recognition by human dectin-2. *J Biol Chem* **2017,** *292* (32), 13402-13414.

31. Kiessling, L. L.; Grim, J. C., Glycopolymer probes of signal transduction. *Chem Soc Rev* **2013,** *42* (10), 4476-91.

32. Dutta, D.; Donaldson, J. G., Search for inhibitors of endocytosis: Intended specificity and unintended consequences. *Cell Logist* **2012,** *2* (4), 203-208.

33. Kankkunen, P.; Teirila, L.; Rintahaka, J.; Alenius, H.; Wolff, H.; Matikainen, S., (1,3)-beta-glucans activate both dectin-1 and NLRP3 inflammasome in human macrophages. *J. Immunol.* **2010,** *184* (11), 6335-42.

34. Robinson, M. J.; Osorio, F.; Rosas, M.; Freitas, R. P.; Schweighoffer, E.; Gross, O.; Verbeek, J. S.; Ruland, J.; Tybulewicz, V.; Brown, G. D.; Moita, L. F.; Taylor, P. R.; Reis e Sousa, C., Dectin-2 is a Syk-coupled pattern recognition receptor crucial for Th17 responses to fungal infection. *J Exp Med* **2009,** *206* (9), 2037-51.

Chapter 4

Mannobiosylated glycopolypeptides and conjugates for cancer immunotherapy

This work was performed in collaboration with Dr. Justin Kenkel, Shelley Ackerman, Dr. Edgar Engleman, and Melissa Gray

4.1 Dectin-2 is highly expressed in PDAC-associated immune cells

As discussed in Chapter 1, tumors are generally highly infiltrated with immune cells representing a variety of lineages and roles. However, cancer cells induce an immunosuppressive environment to prevent activation of an antitumor response. Therefore, while dendritic cells and macrophages, which would normally be key to an effective immune response, reside within tumors in high numbers, the cocktail of suppressive cytokines such as IL-10 and TGF-β renders them ineffective.[1] The relative effectiveness of intratumoral injections of immune adjuvants, including early work using bacterial cultures, as well as more modern dendritic cell-based therapies such as sipuleucel-T, suggest that activation of a competent APC response is a viable immunotherapy approach.[2-5] Whereas sipuleucel-T and other adoptive cell therapies generally rely on prior knowledge of an appropriate cancer-specific antigen, an antigen-agnostic approach would be more generalizable. Engleman et al. recently demonstrated that allogeneic IgG antibodies in combination with dendritic cell stimuli could induce an antitumor T-cell response both in mice and using human patient cells *in vitro*.[6] This observation suggests that many tumors likely do express neoantigens that can be exploited for immunotherapy, and that tumor-associated APCs can be activated by counteracting the immunosuppressive signaling in the tumor microenvironment. We therefore hypothesized that sufficient activation of phagocytic APC receptors might allow for uptake of tumor material, presentation of neoantigens, and induction of a desired T cell response.

Key to this strategy is the identification of activating receptors that are highly expressed on tumor-associated macrophages and dendritic cells. In the course of their research, the Engleman laboratory discovered that the C-type lectin Dectin-2 is highly expressed on immune cells associated with a variety of pancreatic ductal adenocarcinomas (PDAC) (Fig. 4.1). Immunofluorescence staining of Dec-2 in both the LMP and Panc02 murine PDAC models showed high Dec-2 expression in both primary tumors and metastatic sites. Likewise, immunohistochemical staining revealed high Dec-2 expression in the *Pdx1-Cre; Kras*$^{LSLG12D/+}$; *Cdkn2a*$^{-/-}$ genetically engineered mouse model (GEMM) of spontaneous PDAC, as well as in primary human lung cancer tissue. Notably, Dec-2 is an immune-activating PRR that is primarily expressed on dendritic cells and some macrophage lines, making it an intriguing potential immunotherapy target. Its natural ligand preference is for bacterial and fungal mannans, with specificity towards the alpha-1,2-mannobiose structure.[7] It remains somewhat unclear why the receptor is expressed to such a high degree in tumors, as the alpha-1,2-mannobiose motif is not normally found on fully processed human N- or O-glycans. It is possible that the receptor is expressed in response to the presence of the disaccharide as a DAMP, as oligomannans are initially installed onto N-glycan dolichol phosphate donors prior to removal in the ER after transfer to the protein. We did consider the possibility, therefore, that Dec-2 expression in the tumor environment might imply that Dec-2 activation is insufficient for induction of a robust antitumor response. Nevertheless, we decided to investigate whether or not Dec-2 agonists might be able to push the cytokine balance in the tumor microenvironment towards immune activation.

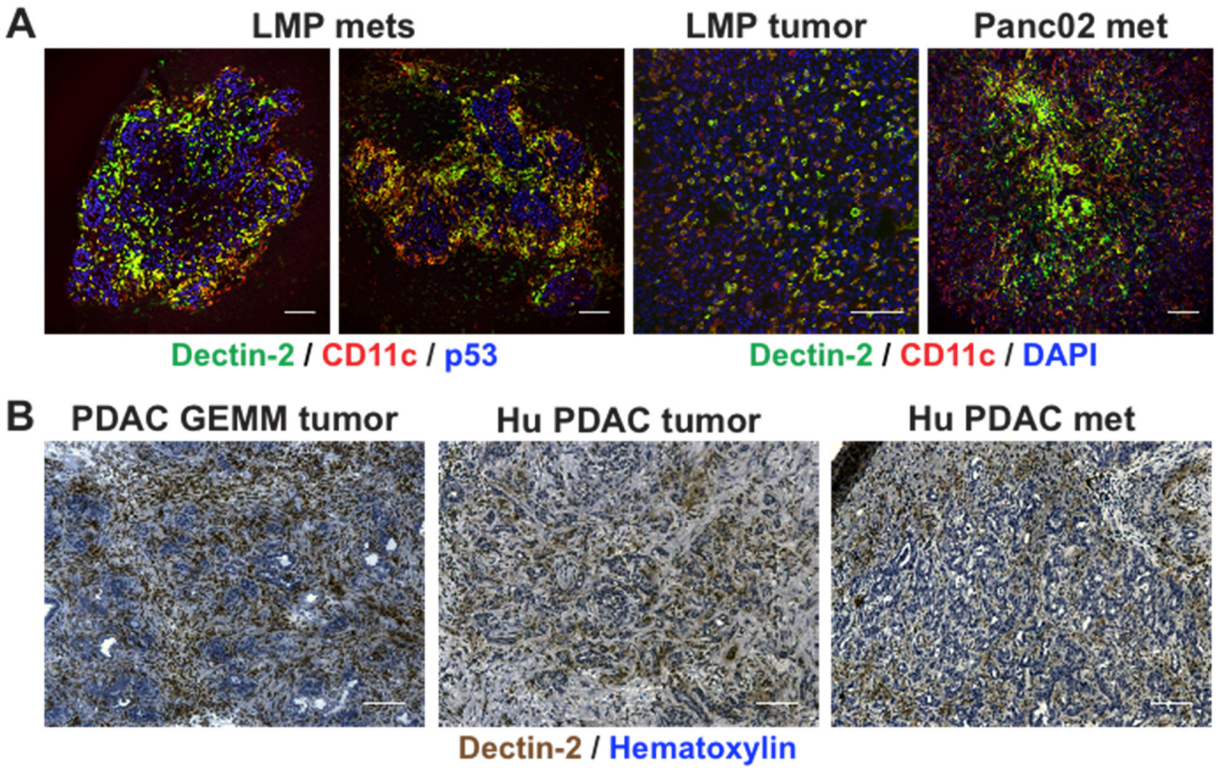

Figure 4.1. Tumor-associated myeloid cells express high levels of Dectin-2. (A,B) Tissues from murine and human (Hu) PDAC were stained with the indicated antibodies and imaged by fluorescence (A) or light (B) microscopy. (A) Primary pancreatic tumor tissues and metastatic liver samples from immunocompetent mice injected with the LMP[8] or Panc02 murine tumor cell line. LMP cells (originally obtained from *Pdx1-Cre; Kras*$^{LSL\text{-}G12D/+}$*; Trp53*$^{LSL\text{-}R172H/+}$ mice and used throughout these studies) are marked by the accumulation of mutant p53. (B) Primary tumor and metastatic tissues from human PDAC and a genetically engineered mouse model (GEMM) of PDAC (*Pdx1-Cre; Kras*$^{LSLG12D/+}$; *Cdkn2a*$^{-/-}$). Scale bar, 100 μm.

In Chapters 2 and 3, I described the synthesis of Dec-2-activating mannobiosylated glycopolypeptides by NCA polymerization. Here, I present our work using these polymers in the context of cancer immunotherapy. In addition to testing free polymers, I investigated the possibility of enhancing their therapeutic potential through conjugation to either synergistic costimulants or to tumor-targeting antibodies. Because Dec-2 was observed in a variety of PDAC tumor types, and because of the Engleman lab's expertise in that disease area, our model systems focused on murine PDAC tumor models. In particular, *in vivo* experiments were based on the LMP model, and *in vitro* experiments with immune cells used isolated murine monocytes that were cultured in tumor-conditioned media to induce tumor associated monocyte (TAM)-like differentiation. In principle, this should generate a population of innate immune cells that includes dendritic cells and macrophages similar to those found in PDAC tumors, and presumably a more biologically relevant model system than commercial cell lines.

4.2 Antitumor activity of Ser(Man2) glycopolypeptides in a murine model of pancreatic cancer.

The cell culture experiments described in Chapter 3 demonstrated that mannobiosylated glycopolypeptides induce cytokine expression and phagocytosis in antigen-presenting cells. These observations were particularly intriguing because they suggested that the glycopolypeptides might be able to induce the robust APC response that would likely be necessary for sustained and effective antitumor activity. Specifically, activation of tumor-associated dendritic cells should result in downstream priming of tumor-specific CD4+ T cells, a key APC function, which have been shown to be sufficient for tumor rejection.[9] As an initial proof of concept, we tested our glycopolypeptides in a murine pancreatic tumor model. Although free polymers lack a tumor-targeting mechanism and might therefore induce nonspecific inflammation, we hypothesized that we might still achieve some level of tumor growth inhibition.

Based on our *in vitro* experiments, we chose to test 65% Ser(Man2) polypeptides of 100-residue target lengths, **4.1a,** with the remainder of the copolymer consisting of an equal blend of alanine and glutamate. We were surprised to find that, even with systemic administration by intravenous injection, the free glycopolypeptides clearly inhibited tumor growth (Figure 4.2). Notably, a relatively aggressive dosing regimen of 20 mg/kg every 48 hours was required to achieve an approximately 50% reduction in tumor growth over the course of the experiment relative to the control. Furthermore, toxicity, likely due to cytokine release syndrome, was observed at higher dosages during preliminary tests to determine the optimal dosing regimen. Therefore, while these results were encouraging, it was clear that either increased immunogenicity or a tumor targeting mechanism might be necessary to achieve a sufficient antitumor response without unacceptable toxicity.

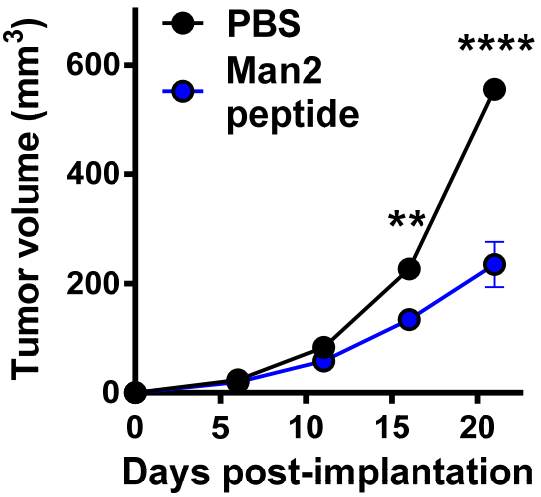

Figure 4.2. Mannobiosylated glycopolypeptides inhibit tumor growth in the LMP murine PDAC model. Polymer (65:17.5:17.5 mannobiose-serine:alanine:glutamate, 100mer target length, **4.1a**) was administered intravenously at 20 mg/kg every 48 hours starting 10 days after implantation. The PBS negative control treatment was performed in biological quadruplicate; the

glycopolypeptide treatment was performed in biological quintuplicate. Error bars represent standard error of the mean.

4.3 Conjugation of a TLR7/8 agonist to Ser(Man2) glycopolypeptides.

It has been well established that simultaneous activation of different immune receptors, particularly through covalent linkage of agonists, can result in a synergistic boost in cytokine release. This has been most frequently demonstrated using various permutations of TLR agonists, though TLR and C-type lectin stimulation have been combined to successfully induce Th1 polarization of dendritic cells.[10-12] We hypothesized that covalent conjugation between immunostimulatory glycopolypeptides and other immune agonists would similarly induce a stronger immune response than either component alone. Because a variety of well-validated small-molecule TLR agonists have been developed via traditional medicinal chemical techniques, and because antigen-presenting cells express both CLRs and TLRs, I aimed to conjugate Ser(Man2) glycopolypeptides to a TLR agonist.

One of the best-developed small molecule TLR agonist scaffolds is the imidazoquinoline class of TLR7 and/or TLR8 agonists, which was first disclosed by Gerster in 1985.[13] These endosomal TLRs recognize viral RNA, and the imidazoquinolines are thought to act as mimics of nucleotide purines.[14] Notable examples include the FDA-approved TLR7 agonist imiquimod and the investigational TLR7/8 agonist resiquimod (Fig. 4.3). Structure-activity relationship studies have been carried out to identify the key structural features for activity and selectivity.[15] Activation of TLR8 in particular has been shown to robustly induce expression of a variety of cytokines, including IL-12, the primary driver of a Th1-type CD4+ T cell response, as well as more general pro-inflammatory cytokines like TNFα and IL-6.[16] Although a complex systemic response is ultimately necessary for effective tumor rejection, there is evidence that a Th1 response, which results in direct cytotoxicity, is preferred over a humoral Th2 response for cancer immunotherapy.[9, 17] For my work, I used a functionalizable imidazoquinoline, T785 (**4.2**), which bears a primary amine that is not involved in TLR binding and is therefore well suited for conjugation chemistry.

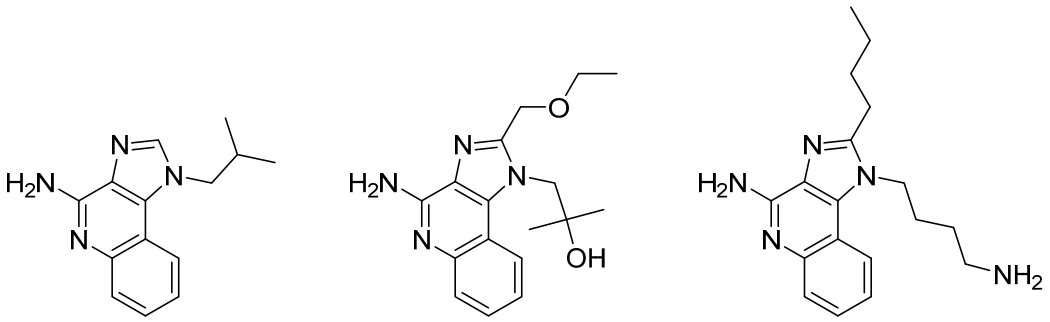

Figure 4.3. Structures of representative imidazoquinoline TLR7/8 agonists. Imiquimod is a TLR7 agonist that is approved for topical use against warts, actinic keratosis, and basal cell carcinoma. Resiquimod is an investigational topical treatment for various skin lesions, and has been reported to stimulate both TLR7 and TLR8. T785 similarly induces signaling through both TLR7 and TLR8, and features a primary amine for easy functionalization. SAR studies on the scaffold have suggested that effective TLR8 activation requires C-2 functionalization, explaining the respective activity profiles of the three compounds.[15]

Conjugation of **4.2** with similarly amine-functionalized glycopolypeptides required modification of both molecules to afford a pair of reactive handles. Fully deprotected glycopolypeptide **4.1a** was subjected to an N-succidimidyl S-acetylthioacetate linker to install an N-terminal protected thiol. Mild aqueous thioacetate deprotection using hydroxylamine hydrochloride afforded the free thiol **4.5**, which I immediately reacted with maleimide-functionalized T785 derivative to avoid loss of reactivity via thiol oxidation, affording product **4.6**.

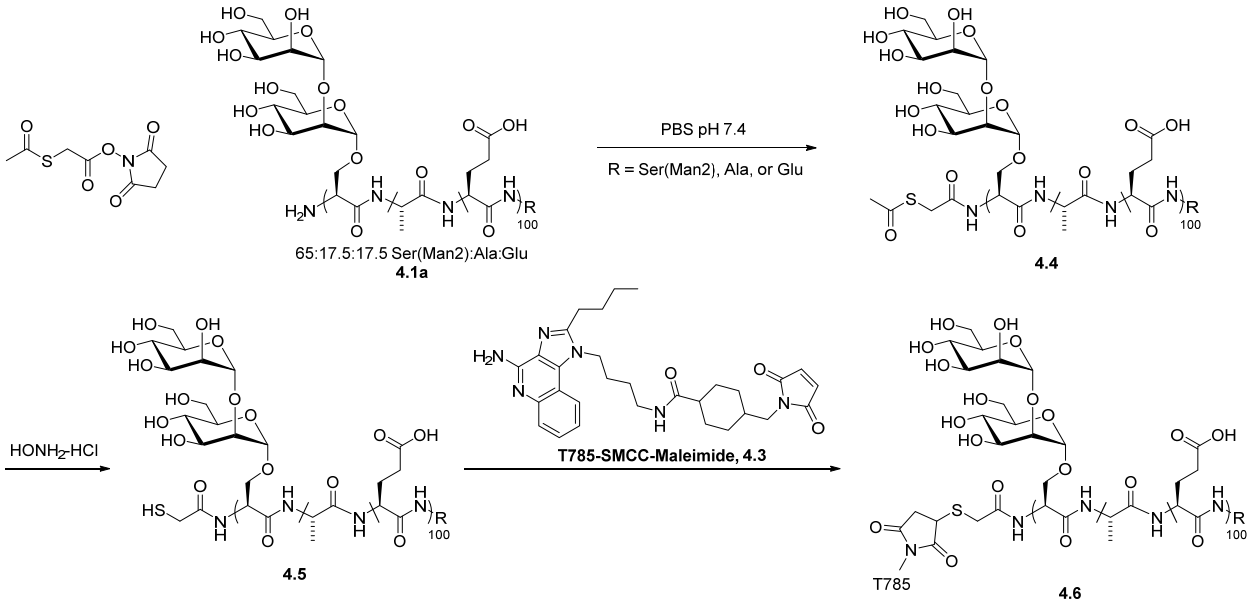

Scheme 4.1. Conjugation of glycopolypeptides to a maleimide-functionalized TLR7/8 agonist. Labeling of the N-terminus with a commercially-available NHS ester afforded a protected thiol, which was conjugated to the maleimide immediately after deprotection.

4.4 Biological activity of T785-glycopolypeptide conjugates

T785-Man2 glycopolypeptide conjugate **4.6** was first tested in cell culture using primary murine monocytes that were pre-exposed to tumor-conditioned media to induce a TAM-like phenotype. For comparison, cells were also treated with either polymer (**4.1a**) or T785 (**4.3**) alone, as well as with an unconjugated mixture of the two species. Remarkably, the conjugates induced very high cytokine expression at the concentrations tested relative to either free polymer or T785 (Fig. 4.4). Moreover, the bulk of this effect could be blocked with an anti-Dec-2 antibody, indicating a receptor-specific effect. In addition to TNFα, we checked expression of additional cytokines to probe the nature of the cellular response. Robust IL-12 signal, observed via detection of both the active p70 heterodimer and the p40 subunit, suggested a bias towards Th1 signaling. Increased TNFα and IL-6 indicated an expected pro-inflammatory response consistent with activation of TLR7/8 and/or Dec-2.[15, 18]

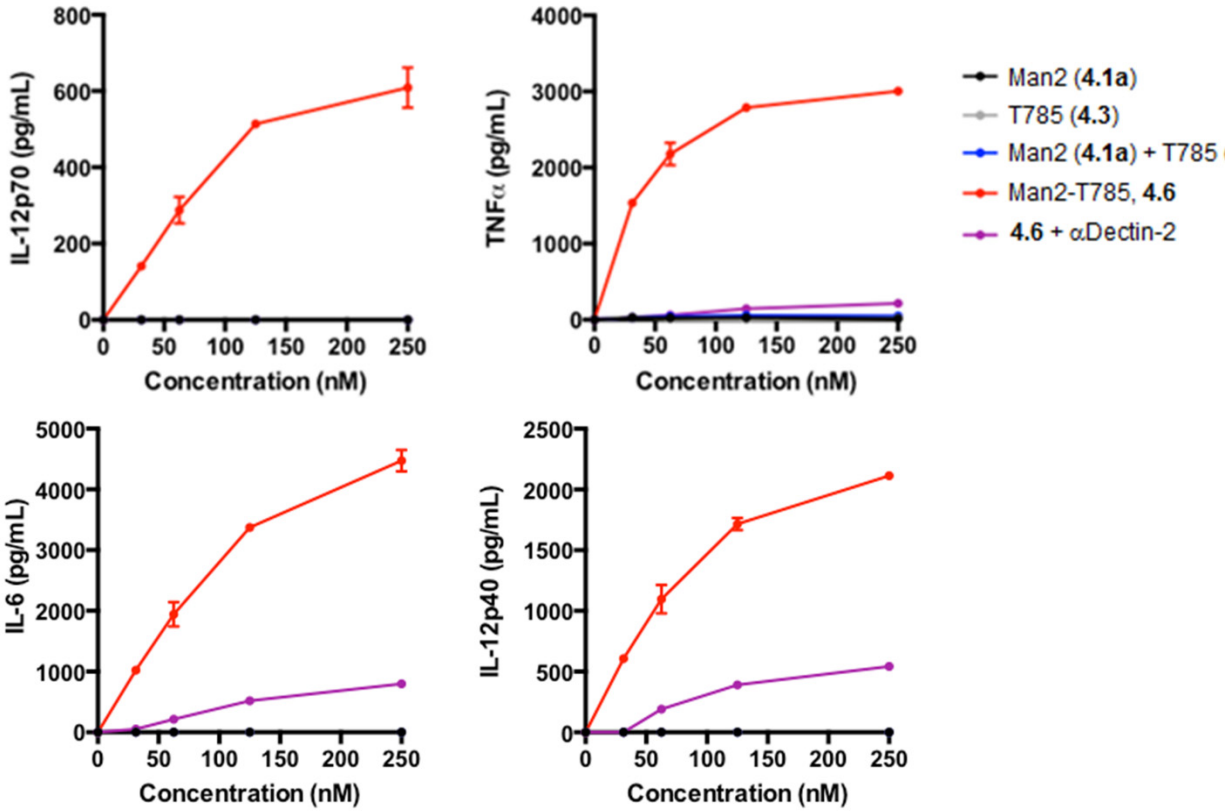

Figure 4.4. Glycopolypeptide conjugate **4.6** induces robust cytokine expression *in vitro*. Murine monocytes were isolated and incubated with tumor-conditioned media to induce a TAM-like phenotype prior to exposure to varying concentrations of agonists. Cytokine expression was detected by ELISA. Man2 (black) and T785 (grey) represent the Ser(Man2) glycopolypeptide **4.1a** and T785 maleimide **4.3**, respectively. Man2 + T785 (blue) indicates an unconjugated mixture of the two agonists. Conjugation via thiol-maleimide chemistry (Man2-T785, red) results in release of high levels of IL-12p70, TNFα, IL6, and IL-12p40 compared to the controls. Inclusion of an anti-Dec-2 blocking antibody (αDectin-2, purple) inhibits this effect, suggesting a Dec-2-dependent effect. Treatments were conducted in duplicate, error bars represent the standard error of the mean.

In addition to cytokine expression, we assayed expression of key cell surface markers associated with antigen-presenting cells (Fig. 4.5). CD40 is a constitutively expressed protein found on APCs, including macrophages, dendritic cells, and B cells, that is bound and activated by CD154 (CD40-L) on helper T lymphocytes.[19] Upregulation of CD40 expression in dendritic cells is known to occur upon exposure to various TLR agonists, including imiquimod. The observed dose-dependent increase in CD40 by ELISA upon exposure to our conjugate was therefore expected. Likewise, CD86 is a costimulatory cell-surface molecule expressed on APCs that is required for effective T cell activation.[20] Again, TLR7 agonists have been reported to upregulate CD86 expression, as has Dec-2 activation.[21-22] We therefore concluded that the observed receptor upregulation was consistent with expected patterns.

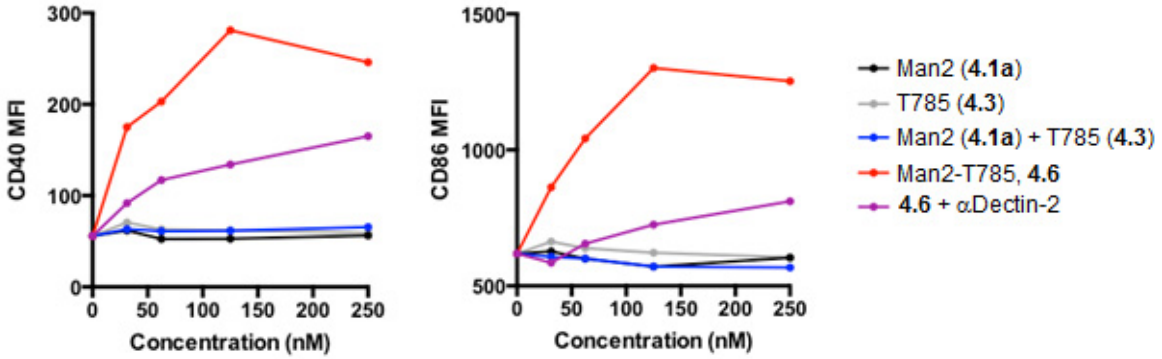

Figure 4.5. Glycopolypeptide conjugate **4.6** induces expression of APC cell-surface markers *in vitro*. Murine monocytes were isolated and incubated with tumor-conditioned media to induce a TAM-like phenotype prior to exposure to varying concentrations of agonists. Cell-surface markers were detected by flow cytometry analysis. Man2 (black) and T785 (grey) represent the Ser(Man2) glycopolypeptide **4.1a** and T785 maleimide **4.3**, respectively. Man2 + T785 (blue) indicates an unconjugated mixture of the two agonists. Conjugation of the two via thiol-maleimide chemistry (Man2-T785, red) results in release of high expression of CD40 and CD86 compared to controls. Inclusion of an anti-Dec-2 blocking antibody (αDectin-2, purple) inhibits this effect, suggesting a Dec-2-dependent effect. Data points represent n = 1.

Encouraged by this *in vitro* evidence of synergistic immune activation upon conjugation of T785 to Ser(Man2) glycopolypeptides, we moved to the LMP murine model in which we had previously observed an antitumor effect with unconjugated glycopolypeptides. At a substantially lower dose of three 250 μg intratumoral injections, the free glycopolypeptide had an insignificant effect on tumor growth (Fig. 4.6). In contrast, the conjugates inhibited tumor growth in this model, confirming that the increased immunogenicity observed *in vitro* translated to an *in vivo* antitumor effect.

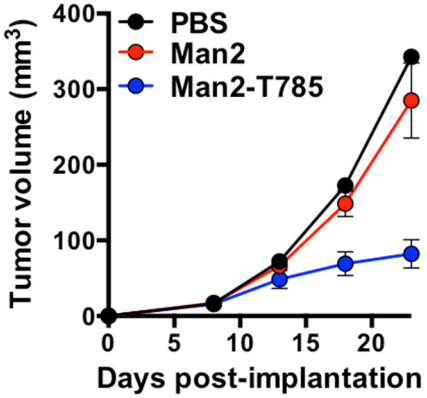

Figure 4.6. T785-Ser(Man2) glycopeptides conjugates inhibit tumor growth in the LMP murine PDAC model. Man2 represents unconjugated glycopolypeptide **4.1a**, Man2-T785 represents the thiol-maleimide conjugate **4.6**. The conjugate was administered twice intratumorally at 250 μg per dose (days 10 and 12), the unconjugated polymer was administered one additional time on day 14. The PBS negative control treatment was performed in biological quadruplicate; other conditions were performed in biological quintuplicate. Error bars represent the standard error of the mean.

These initial results provide encouraging evidence that conjugating our polymeric Dec-2 ligands to other immunostimulants might enhance their potential therapeutic efficacy. However, because the cytokine and cell surface receptor profiles we observed would also be consistent with TLR7/8 activation alone, we cannot currently rule out the possibility that the Dectin-2 ligand is serving primarily as a delivery vector rather than by activating Dectin-2 signaling. In fact, targeting dendritic cell surface receptors to deliver TLR agonists has been reported in the literature.[23-24] It may be of interest in future work to examine the role of Dectin-2 signaling in explaining the synergistic immunogenicity of the glycopolypeptide-T785 conjugates. Conversely, Dec-2 activation, while less-thoroughly investigated than TLR7/8, also appears to activate TNFα, IL-12, and IL-6.[18, 25] Because of the significant overlap between the potential assayable readouts of the TLR7 and Dec-2 signaling pathways, as well as the confounding effects of secondary immune activation resulting from downstream cytokine release, future experiments may require complementary models such as Dec-2 mutants incapable of signaling.

4.5 Nonspecific lysine conjugation of glycopolypeptides to an anti-EpCAM antibody

Perhaps the greatest challenge in implementing immunostimulatory cancer therapeutics is avoiding the inherent toxicity associated with inducing an inflammatory immune response. Even for recently approved checkpoint inhibitors and CAR-T therapies, cytokine release syndrome remains a prominent side effect.[26] While this is arguably preferable to the cancer itself and can be managed in many cases, improving anticancer selectivity is still an important goal. As inspiration, we turned to the active field of antibody-drug conjugates, which has put significant resources behind developing technologies for conjugating small molecules onto tumor-targeted antibodies.[27] Rather than introducing a cytotoxic payload, our conjugates are designed to bring APC-activating glycopolypeptides to the tumor site. Optimally, specifically coating tumor cells with fungal cell wall carbohydrates would induce specific phagocytosis of those cells in addition to pro-inflammatory cytokine release in the tumor microenvironment. At the very least, we anticipated that some measure of tumor-directed specificity could be derived simply from accumulation of the immunostimulatory conjugate in the tumor area.

A myriad of techniques have been developed for attaching payloads to antibodies; a full discussion of the field is beyond the scope of this dissertation, but has been well reviewed elsewhere.[27-29] Broadly speaking, conjugation strategies either make use of native reactive handles, such as thiols and amines found on amino acid residues, or engineer the antibody to introduce bioorthogonal reactive groups that allow for a greater degree of control over conjugation parameters. While the latter strategy has some significant advantages, including good control over the sites and degree of functionalization, it generally requires significantly more optimization to implement. Because I was concerned that the size and degree of glycosylation of the glycopolypeptides might interfere with conjugation, I first tested a proof of concept system based on nonspecific conjugation to native solvent-exposed lysines. Proteins generally display multiple chemically-similar functionalizable lysine residues; one unfortunate result of nonspecific lysine labeling is therefore a distribution of products with different degrees and sites of conjugation. However, the strategy requires no antibody engineering, and a variety of efficient, bifunctional amine-reactive linkers are commercially available. In particular, amine-reactive N-hydroxysuccinimide (NHS) esters represent one of the most widely used reagent classes due to their combination of reactivity under mild aqueous conditions and relative stability to hydrolysis given proper storage.

Conjugation reactions involving two macromolecules, such as a polymer and an antibody, generally require very efficient and rapid chemistries. Furthermore, direct conjugation of a polymer to lysines on an antibody would require the synthesis of an NHS ester or similar reactive handle on the polymer, rather than leveraging the commercial availability of a wide variety of NHS ester reagents for bioconjugation. Thus, I decided to instead modify antibodies of interest with bicyclo[6,1,0]non-4-yn-9-yl *N*-hydroxysuccinimidyl ester (BCN-NHS, **4.9**) in order to install a "click" handle for rapid ligation.[30] My choice of tumor-targeting antibody was informed by the observation of high Dec-2 expression in the context of pancreatic tumors. PDAC tumors, as well as a variety of other cancers, are known to overexpress Epithelial Cell Adhesion Molecule (EpCAM), and monoclonal antibodies against that target are known.[31] Towards this end, the well-validated Rat anti-Mouse EpCAM IgG2a (clone G8.8) was a suitable model antibody. Glycopolypeptides were reacted with a tetrazine NHS ester to install the click handle, while antibodies were conjugated to varying amounts of BCN-NHS (Scheme 4.2). Conjugation was then easily achieved by incubating the functionalized glycopolypeptide and antibody under mild aqueous conditions.

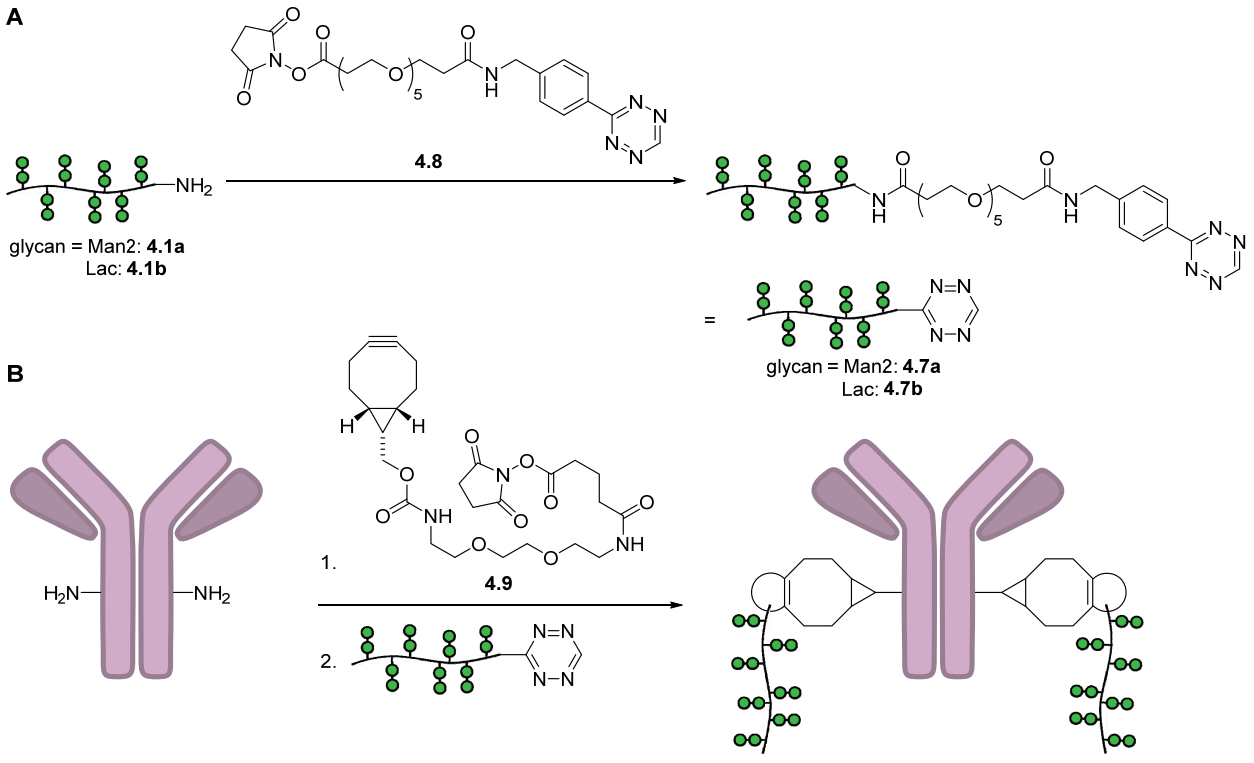

Scheme 4.2. Generalized schematics illustrating synthetic strategy for antibody-glycopolypeptide conjugation via tetrazine-cyclooctyne click chemistry. A) Polymers, representing either Dec-2 agonist **4.1a** or a lactosylated negative control **4.1b** were modified using tetrazine NHS ester **4.8** to introduce the tetrazine moiety with a PEG spacer. B) In parallel, antibody was reacted with commercial bifunctional linker **4.9** via NHS ester chemistry, installing a reactive BCN group onto solvent-exposed lysines along with a short PEG spacer. Incubation of the functionalized antibody and glycopolypeptide results in conjugation to give either the potential Dec-2-agonist construct or a lactosylated negative control.

Because antibodies can have dozens of modifiable lysine residues, it was important to establish an optimal degree of BCN labeling.[27] A 1 mg/ml solution of antibody was reacted overnight with a 5-50 fold excess of BCN NHS ester, followed by purification by centrifuge filtration to remove excess BCN reagent. SDS-PAGE of the modified antibodies showed a slight upward shift of the light and heavy chain bands with increasing degree of functionalization, as well as higher molecular weight bands that might be due to crosslinking between BCN-modified antibody subunits and exposed nucleophilic residues (Fig. 4.7a). At the highest (50:1) BCN:antibody ratio, significant protein loss was observed due to precipitation, and the conjugates were difficult to detect by Coommassie stain. To check for the presence of active BCN on the functionalized antibodies, I reacted them with an excess of a tetramethylrhodamine-azide dye, which should efficiently and specifically react with the cyclooctyne. After purification by centrifuge filtration, I did indeed observe fluorescence of antibody bands for all samples that had been reacted with the dye (Fig. 4.7b). Even the 50:1 BCN:antibody sample, which gave only faint signals by Coommassie staining, exhibited strong fluorescence and a band pattern consistent with a functionalized antibody. As controls, antibody samples that were not exposed to the dye or BCN did not fluoresce. Dye quantification for the 10:1 and 25:1 samples indicated the presence of approximately 5 and 3 BCN moieties per antibody on average, respectively, assuming quantitative efficiency of the BCN-azide click reaction. Based on these results, and to simplify the number of tested conditions moving forward, I limited glycopolypeptide conjugation reactions to the 25:1 and 10:1 BCN:antibody samples.

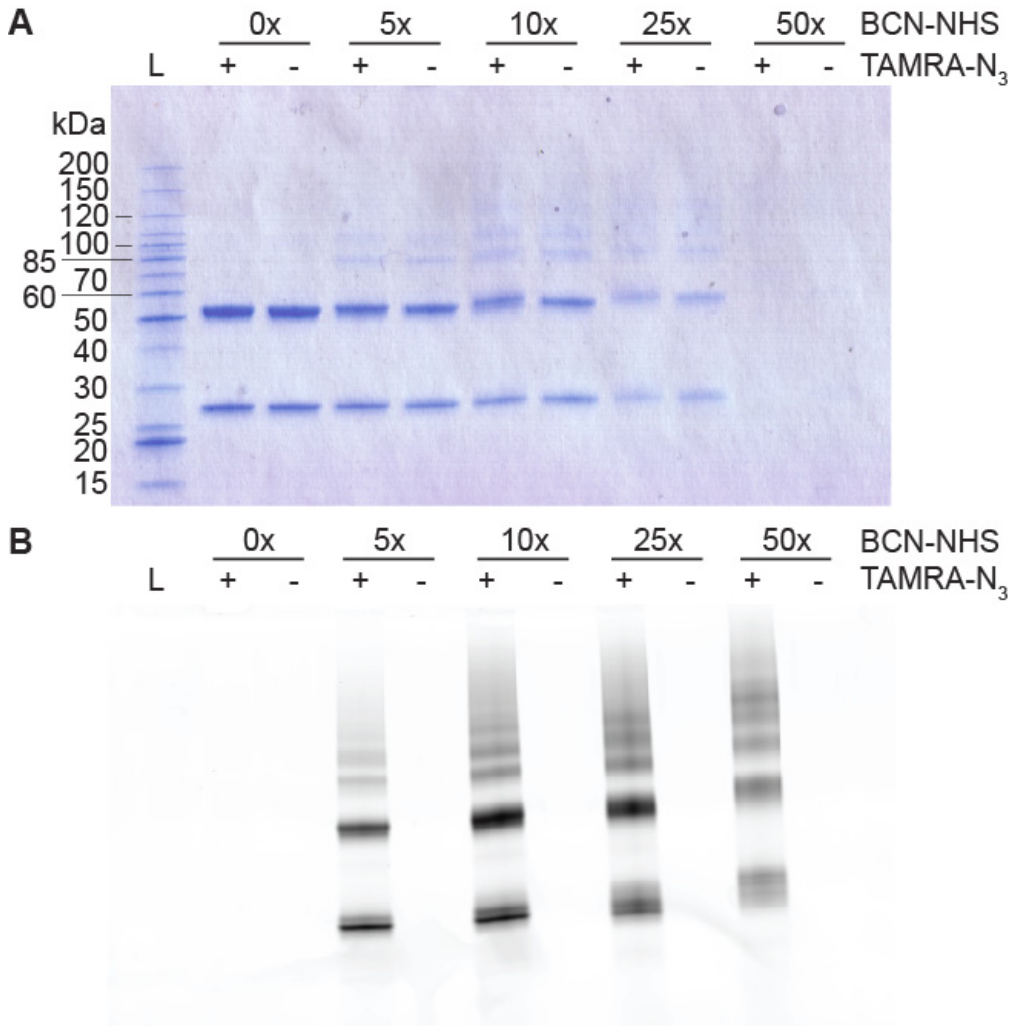

Figure 4.7. SDS-PAGE and western blot analysis of BCN-antibody conjugates. Antibodies were conjugated to varying amounts of BCN-NHS, and then reacted with a tetramethylrhodamine-azide (TAMRA-N_3) dye for analysis. A) Coommassie staining showed subtle changes in band patterns with increasing levels of BCN intensity; significant sample loss occurred with the 50x sample, resulting in low protein levels. The fluorophore had no observed effect. B) Successful BCN conjugation was determined by western blot analysis via fluorescence of the TAMRA dye. Unmodified antibody (0x) gave no dye signal, whereas TAMRA-specific fluorescence was observed for all BCN-labeled antibodies. L: protein molecular weight ladder.

Although SDS-PAGE in conjunction with fluorescence imaging allowed for confirmation of BCN labeling, it proved unreliable when analyzing glycopolypeptide conjugation reactions. Test reactions using low-dispersity 5 kDa PEG-N_3 showed a banding pattern consistent with the addition of discrete numbers of polymer chains (Figure 4.8a). Increasing the BCN:antibody ratio clearly resulted in less unmodified antibody after reaction with the polymer, based on the relative intensities of the light and heavy chain bands at ca. 27 and 55 kDa, respectively. However, the analogous experiment using NCA-derived glycopolypeptides was more difficult to interpret. I first reacted Ser(Man2) glycopolypeptide **4.1a** or the lactosylated analog **4.1b** with tetrazine NHS ester **4.8** to introduce a cyclooctyne-reactive moiety. The modified glycopolypeptides and antibodies were then conjugated overnight prior to purification by spin filtration. As observed previously,

increasing BCN:antibody ratios resulted in high-molecular weight bands and streaking, primarily around 75 kDa and above (Fig. 4.8b). Rather than introducing additional discrete bands as with the PEG-N_3 reagent, conjugation to glycopolypeptides resulted in smearing. Although the degree of smearing appeared to correlate with increasing BCN:antibody ratios, possibly indicating successful conjugation, these SDS-PAGE results remain ambiguous.

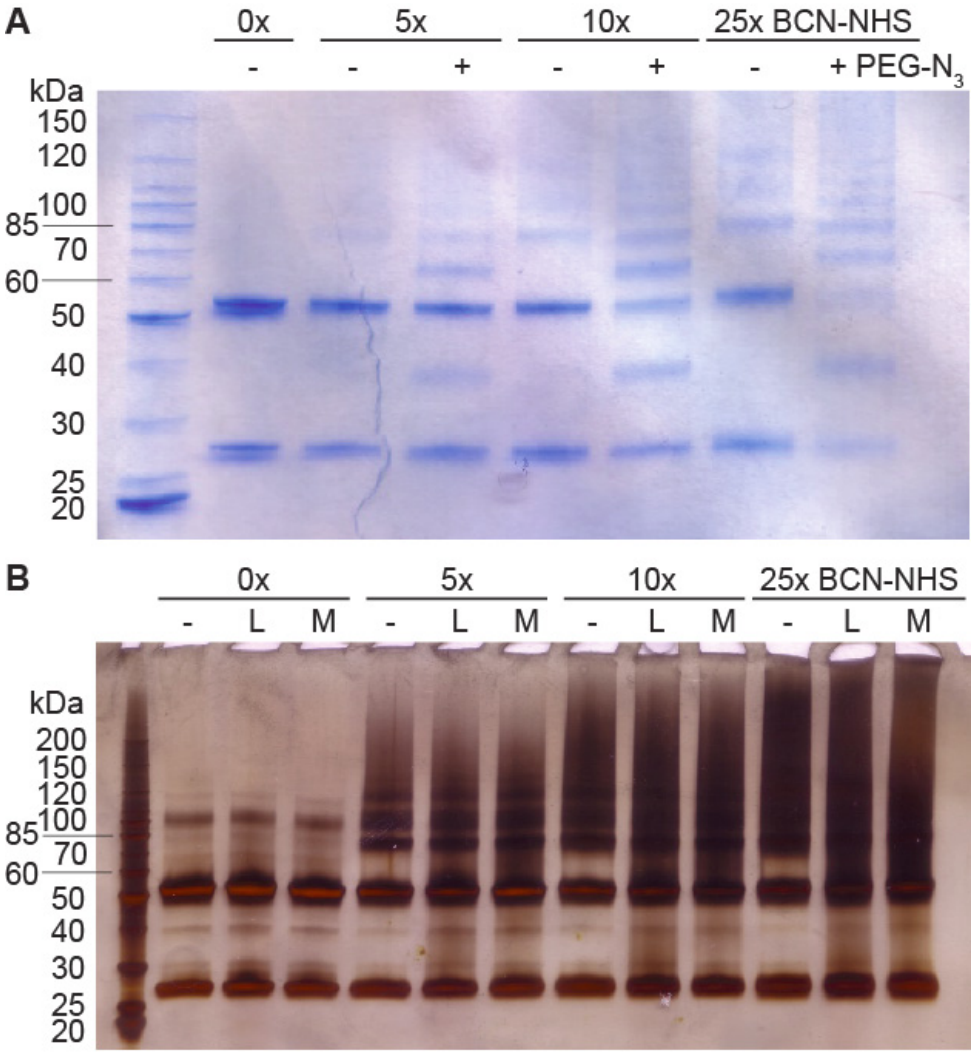

Figure 4.8. SDS-PAGE analysis of PEG- and glycopolypeptide-antibody conjugates demonstrate that polymer homogeneity is necessary for unambiguous analysis. A) Reaction of BCN-labeled anti-EpCAM antibodies with a low-dispersity 5 kDa PEG-N_3 reagent shows band patterns consistent with successful conjugation. Three BCN:antibody ratios were tested, ranging from 5:1 to 25:1. Qualitative analysis of the bands around 50 and 25 kDa, representing the unconjugated heavy and light chains, respectively, suggests a decrease in unconjugated antibody with increasing BCN. Visualization was performed using a colloidal Coomassie stain. B) In contrast, the analogous experiment with glycopolypeptides **4.7b** or **4.7a** (L and M, respectively) was more difficult to interpret. Rather than clear bands, conjugation appeared to result in streaking, likely due to the heterogeneity of the glycopolypeptides compared to the commercial PEG reagent. Visualization was performed using silver stain.

SDS-PAGE relies on denaturation of protein samples with an anionic detergent, normalizing charge density across the length of the protein and allowing for separation based almost exclusively on size alone. Native PAGE, in contrast, separates proteins based both on their pI and their size. Because of the anionic nature of the glycopolypeptides, which are comprised of approximately 18% glutamate, I therefore reasoned that native PAGE might give clearer results. Indeed, capping lysines, which are generally protonated and positively charged around physiological pH, with neutral BCN groups resulted in a marked downward gel shift proportional to the BCN:antibody ratio (Fig. 4.9a). Interestingly, reaction of BCN-labeled antibodies with 5kDa PEG-N_3 caused an upward gel shift despite the fact that PEG is not generally considered a charged species (Fig. 4.9a). In contrast, reaction with tetrazine-labeled glycopolypeptides resulted in a further downwards gel shift as expected due to increased negative charge. Although not a quantitative analysis, the relative clarity of the gel shift, supported the conclusion that the antibodies had been successfully conjugated to glycopolypeptides. As an additional analysis, I fluorophore-labeled polypeptide **4.1a** with a commercial Cy5-DBCO dye prior to conjugation to the 10:1 and 25:1 BCN:antibody samples. Subsequent fluorescence quantification, using a standard curve derived from unconjugated, fluorophore-labeled glycopolypeptides, indicated approximately 1.1 and 0.7 polypeptide chains per antibody on average for the 25:1 and 10:1 samples, respectively.

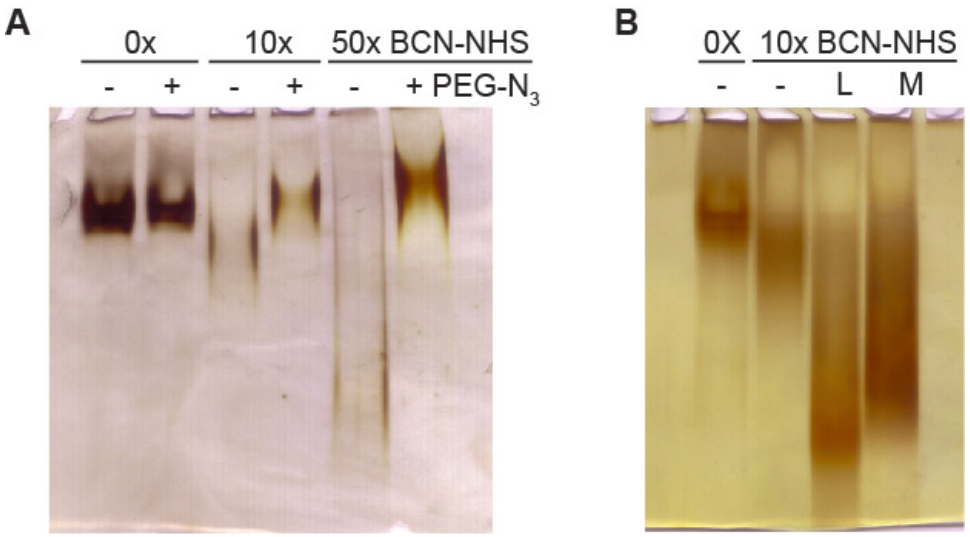

Figure 4.9. Native PAGE analysis of PEG- and glycopolypeptide-antibody conjugates show clear gel shifts for both polymer classes. A) Reaction of BCN-labeled anti-EpCAM antibodies with a low-dispersity 5 kDa PEG-N_3 reagent shows a distinct gel shift upon conjugation. Two BCN:antibody ratios, 5:1 and 50:1, were used for this experiment. Notably, BCN conjugation results in a significant gel shift as well, due to capping of positively-charged lysine residues. B) The analogous experiment with glycopolypeptides **4.7b** or **4.7a** (L and M, respectively) showed clear downward gel shifts upon conjugation despite significant band smearing. Both gels were visualized by silver stain.

4.6 Biological activity of αEpCAM-Ser(Man2) glycopolypeptide conjugates.

With antibody-glycopolypeptide conjugates successfully synthesized by nonspecific lysine modification, we then tested their ability to activate murine monocytes *in vitro*. Interestingly, unlike free polymers, mannobiosylated glycopolypeptide-antibody conjugates were relatively effective at inducing TNFα release without the need for plate adsorption (Fig 4.10a). The effect appeared to be Dec-2 dependent, and inclusion of tumor cells did not appreciably impact cytokine release (Fig 4.10b). Antibody by itself was ineffective at stimulating cytokine release, suggesting that the glycopolypeptide was predominantly responsible for signaling. Without further experiments, it is difficult to say for sure why antibody conjugation would boost immunogenicity in the absence of EpCAM-expressing cancer cells. It is possible that some population of the isolated monocytes, which are murine in origin, express enough EpCAM to bind the conjugate, resulting in cell surface-mediated enhancement of receptor activation as with attachment to a surface. Alternatively, the monocytes might bind the rat antibody via promiscuous Fc recognition or some other mechanism, effectively increasing delivery of the mannobiosylated payload to APC Dec-2. Along these lines, murine Fc receptors (FcR) are known to bind non-murine Fc domains, including Rat IgG2a, with nontrivial binding affinities.[32]

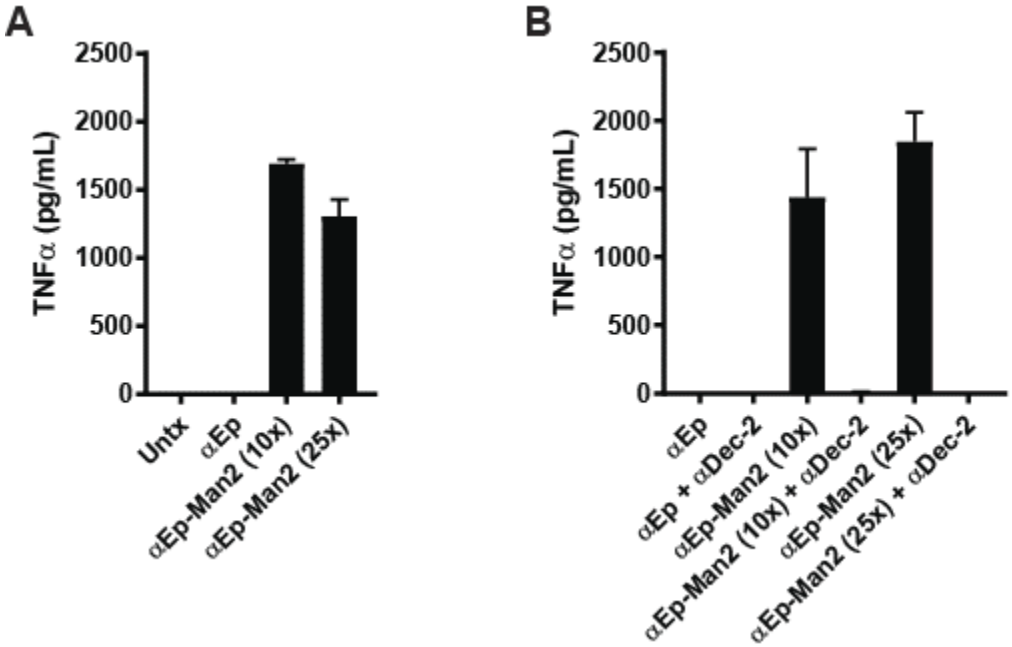

Figure 4.10. αEpCAM-Ser(Man2) glycopolypeptide conjugates stimulate cytokine release in murine monocytes. Cells were pretreated with tumor-conditioned media to induce differentiation into a TAM-like phenotype. Conjugates were synthesized using αEpCAM antibodies that had been labeled with either a 10:1 or 25:1 ratio of BCN:antibody and then conjugated to tetrazine-functionalized glycopolypeptide **4.7a** to afford the constructs αEp-Man2 (10x) and αEp-Man2 (25x), respectively. A) Unlike free glycopolypeptides, the conjugates induced TNFα release without the need for plate adsorption. B) The activated monocytes were also co-cultured with tumor cells did not significantly impact Dec-2-dependent TNFα activation. Data reflect biological triplicates, error bars represent standard error of the mean.

These initial assays demonstrated that the conjugates were able to activate monocytes through Dec-2; however, they did not show whether or not covalent linkage of the glycopolypeptide and antibody were necessary for a robust response. To answer this question, we carried out a studies using either the conjugate or a mixture of free antibody and polymer (Fig. 4.11). As expected, in solution the unconjugated mixture only weakly induced TNFα release in the concentration range tested and induced no detectible IL-12p40 or IL-6. In contrast, we again observed robust, Dec-2-specific activity with the conjugate.

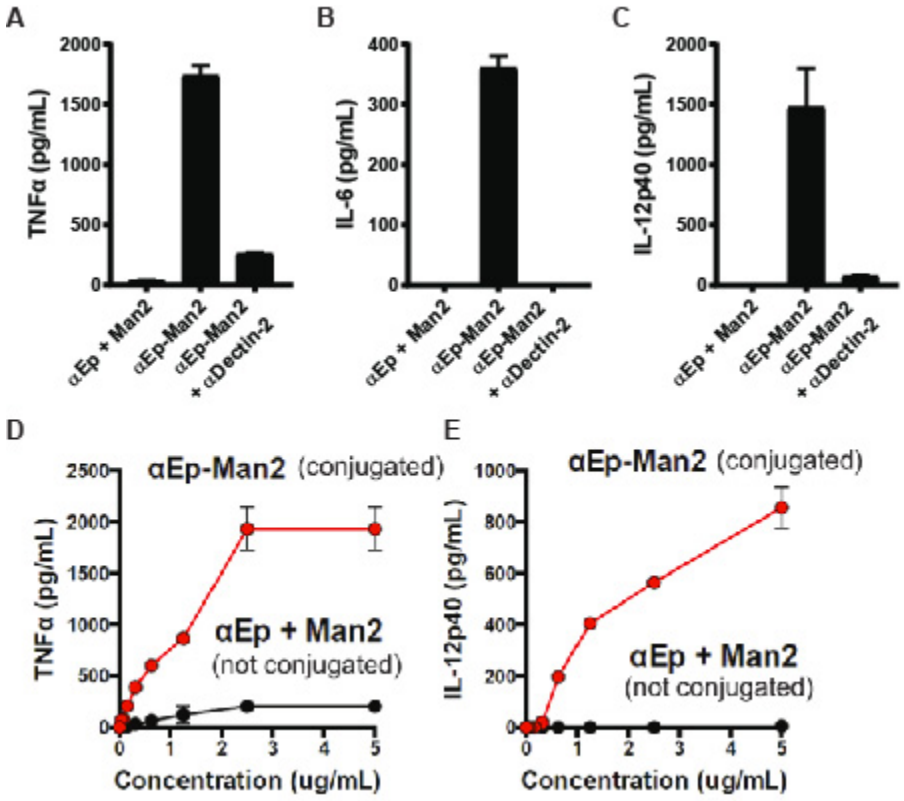

Figure 4.11. Efficient immune cell activation requires covalent conjugation of the αEpCAM antibody and Ser(Man2) glycopolypeptide. Monocytes were pretreated with granulocyte-macrophage colony-stimulating factor (GM-CSF) to induce differentiation into a TAM-like phenotype. Conjugates were synthesized using αEpCAM antibodies that had been labeled with a 10:1 ratio of BCN:antibody and then conjugated to tetrazine-functionalized glycopolypeptide **4.7a** to afford the desired construct (αEp-Man2). A-C) Conjugates induce robust cytokine release, whereas an unconjugated mixture of antibody and glycopolypeptide (αEp + Man2) is ineffective at the same concentration. Inclusion of an anti-Dec-2 blocking antibody demonstrated the Dec-2 dependence of stimulation. D,E) Dose-response studies using the same conditions similarly demonstrate that conjugation is necessary for robust monocyte activation across a range of concentrations. Results reflect biological triplicates, error bars represent standard error of the mean.

Improved stimulation of cytokine release in solution form is itself an interesting result; however, measuring phagocytic behavior in a monocyte/tumor cell coculture system is an important piece of evidence that activated cells might be capable of antigen presentation. To probe endocytic

behavior, we prelabeled tumor cells with the dye 5(6)-carboxyfluorescein succinimidyl ester (CFSE) and then incubated them with TAM-like immune cells derived from murine monocytes. Uptake of fluorescently-labeled tumor material by the monocyte-derived immune cells would be expected to increase their fluorescence, providing a readout on endocytic activity. The unconjugated αEpCAM antibody induced a 30% increase in endocytosis, again possibly due to binding of the rat IgG2a via FcR promiscuity (Fig. 4.12). However, conjugation of the antibody to glycopolypeptide **4.7a** resulted in even greater fluorescence, corresponding to an approximately 2-fold increase in phagocytic cell population within the gated region compared to the untreated control. Inclusion of the anti-dectin-2 blocking antibody resulted in an overall shift in the cell population back towards lower fluorescence and therefore less endocytosis. We are therefore fairly confident that the antibody-glycopolypeptide conjugates induce upregulation of endocytosis in murine APCs. Work is ongoing to probe the *in vivo* activity of the conjugates to determine efficacy and study whether antibody conjugation increases on-target immunogenicity.

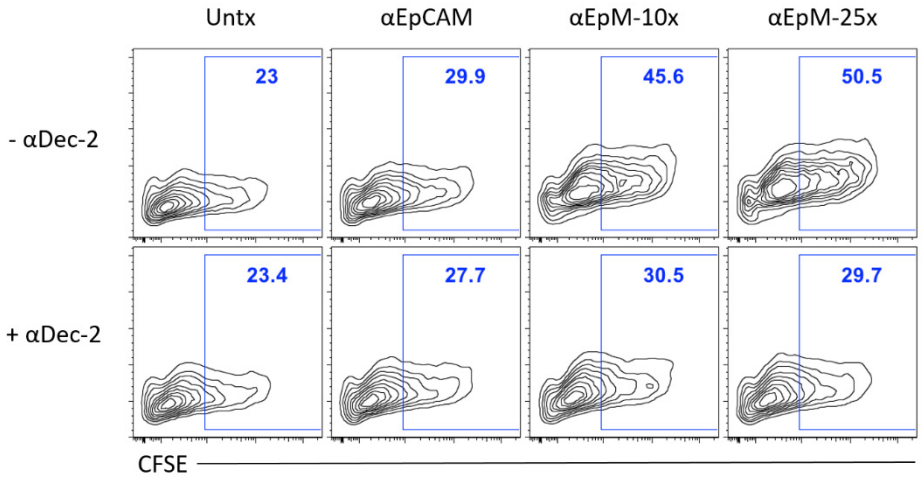

Figure 4.12. Uptake of fluorescently-labeled tumor cells by primary murine monocyte-derived immune cells in cell culture. Tumor tissue was labeled with 5(6)-carboxyfluorescein succinimidyl ester (CFSE) prior to co-incubation with the murine immune cells. Top panels: A slight increase in tumor cell endocytosis by the immune cells was observed via CFSE signal in the presence of an unmodified Rat anti-Mouse EpCAM IgG2a (αEpCAM) compared to the untreated control (Untx). Incubation with glycopolypeptide-antibody conjugates αEpM-10x or αEpM-25x enhanced this anti-tumor activity. The αEpM-10x and αEpM-25x conjugates differ in their extent of conjugation; αEpM-10x was labeled with a 10:1 BCN-NHS ester:antibody ratio prior to conjugation with tetrazine-modified glycopolypeptide **4.7a**, whereas αEpM-25x used a 25:1 ratio. Bottom panels: The same conditions were tested in the presence of an anti-Dec-2 blocking antibody to determine the receptor specificity of this effect. Notably, in the presence of the blocking antibody, the αEpM-10x and αEpM-25x show reduced tumor cell uptake by the immune cells on par with the unconjugated αEpCAM antibody alone, suggesting that the increase in CFSE signal observed with the conjugates was Dec-2-dependent.

4.7 Developing a site-specific glycopolypeptide-antibody conjugate using the aldehyde-tag technology

Although nonspecific lysine labeling effectively produced glycopolypeptide-conjugated antibodies capable of inducing *in vitro* immune cell activation, site-specific modification will likely be a more promising approach for robust therapeutic applications. By improving control over the degree and sites of labeling, optimized site-specific conjugates tend to exhibit higher activity, simpler analysis, more-reproducible synthesis, and lower immunogenicity.[27, 33] A variety of approaches to engineering site-specific modifications are possible, including introduction of artificial amino acids, engineering in protein tags, or modification of specific native cysteine residues.[28-29] The aldehyde tag technology, developed by the Bertozzi lab, employs a small five amino acid peptide tag to introduce a cysteine at an arbitrary site in the protein (Scheme 4.3).[33] This peptide tag is a recognition sequence for the formylglycine-generating enzyme (FGE), which specifically converts the cysteine residue into formylglycine. The resulting aldehyde exhibits privileged reactivity with various alpha-effect nucleophiles, allowing for selective conjugation. The technology benefits from the small size of the tag and the ability to introduce the consensus sequence wherever desired, allowing for optimization of the conjugation site for efficacy and stability of the conjugate. Unlike artificial amino acid incorporation, generation of the reactive amino acid residue requires only routine cloning protocols and a source of recombinant FGE.

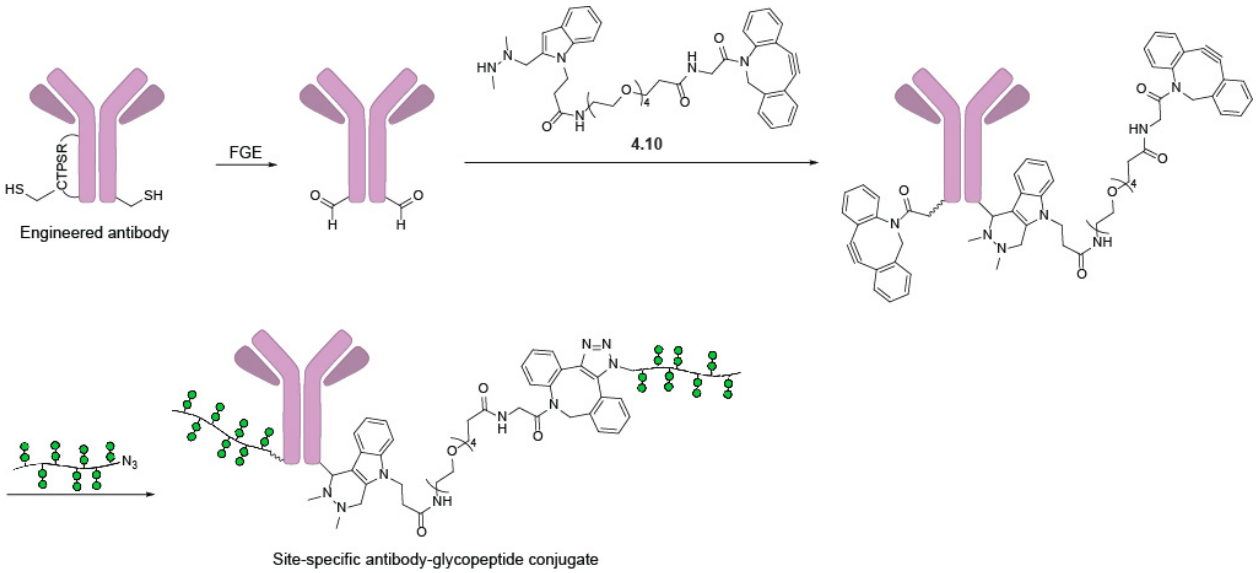

Scheme 4.3. Site-specific conjugation of azide-functionalized glycopolypeptides to antibodies via the aldehyde tag technology and hydrazino-Pictet-Spengler (HIPS) ligation. Engineering of the CXPXR consensus sequence into the antibody of interest allows for conversion of the cysteine to a formylglycine residue using the formylglycine-generating enzyme (FGE). Reaction with the cyclooctyne-functionalized HIPS linker **4.10** allows for installation of one copper-free click handle onto each heavy chain subunit. Incubation of the functionalized antibody with an azide-bearing glycopolypeptide affords the desired conjugate.

Previous work in our lab has utilized an azide-functionalized HIPS linker to conjugate antibodies site-specifically with cyclooctyne-bearing partners, including macromolecules as large as the 83 kDa *V. cholerae* sialidase.[34-35] Because the glycopolypeptides can be azide-functionalized, I

decided to investigate the viability of a cyclooctyne-functionalized HIPS linker. Carboxylic acid-functionalized, Fmoc-protected dimethylhydrazinyl indole **4.11** is a reported intermediate in the synthesis of the azide-functionalized HIPS linker. Amide coupling with commercially-available amino-PEG4-DBCO **4.13** afforded the FMOC-protected linker **4.12**, which could be deprotected with piperidine or *t*-butylamine to afford the desired product **4.10** as determined by LC-MS and ^{1}H-NMR. Deprotected HIPS linkers are known to degrade upon extended exposure to air and light, as well as during extensive chromatographic purification.[36] As such, while the product was assessed to contain various impurities, I judged that it might be practical to test the partially-purified material in bioconjugation reactions based on experimental precedent with the corresponding azide derivative as well as small molecule drug conjugates.[34, 36] A prudent future direction would be to scale up synthesis of this DBCO-modified linker and fully purify and characterize the product.

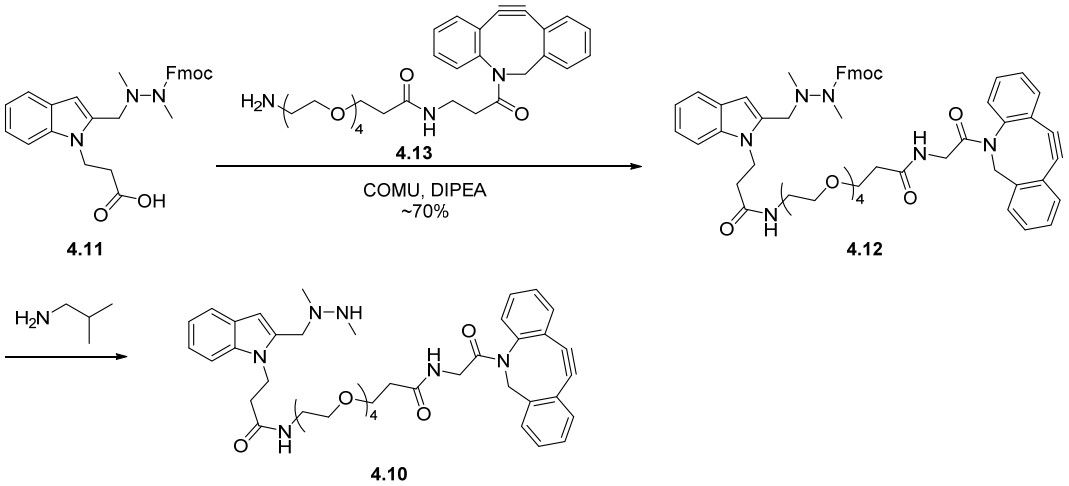

Scheme 4.4. Synthesis of HIPS-DBCO linker from reported intermediate **4.11**. Conjugation of the carboxylic acid with DBCO-amine **4.13** gave the Fmoc-protected, cyclooctyne-functionalized intermediate **4.12**, which was deprotected with amine bases to give the desired linker **4.10**.

Nevertheless, formylglycine-modified trastuzumab was reacted with the linker in an attempt to generate the desired site-specifically DBCO-modified antibody. Based on previous work, the aldehyde tag was installed on the heavy chain at the C-terminus to avoid interfering with variable region or Fc binding interactions.[35] Briefly, antibody was incubated at 37 °C with an 8-fold excess of linker for 72 hours at pH 5.5. After purification by buffer exchange, samples were analyzed by western blot and by ESI-MS. For western blot detection, an aliquot of purified sample was reacted with azide-biotin to allow for visualization using a fluorophore-conjugated streptavidin. A streptococcal sialidase (46 kDa) that had been reacted with maleimide-DBCO was used as a previously-validated positive control, and the corresponding unreacted sialidase was used as a negative control. Total protein staining demonstrated successful western blot transfer and comparable protein loading across lanes (Fig. 4.13a). Anti-biotin staining demonstrated robust DBCO labeling on the positive control and no signal for the negative control, as well as faint but clear labeling on the trastuzumab heavy chain (50 kDa) as hoped. Mass spectrometry analysis of the conjugate was less conclusive. A mass of 50028 Da was observed for the formylglycine-modified heavy chain, approximately 34 Da greater than expected. After reaction with the DBCO

linker, an increase in mass to 50798 Da was observed, approximately 54 Da greater than expected. Although the discrepancy in MS data has not yet been accounted for, the observation of an approximately expected increase in mass, along with the western blot data, suggested to us that the HIPS-DBCO linker was likely successfully modifying the aldehyde-tagged antibody.

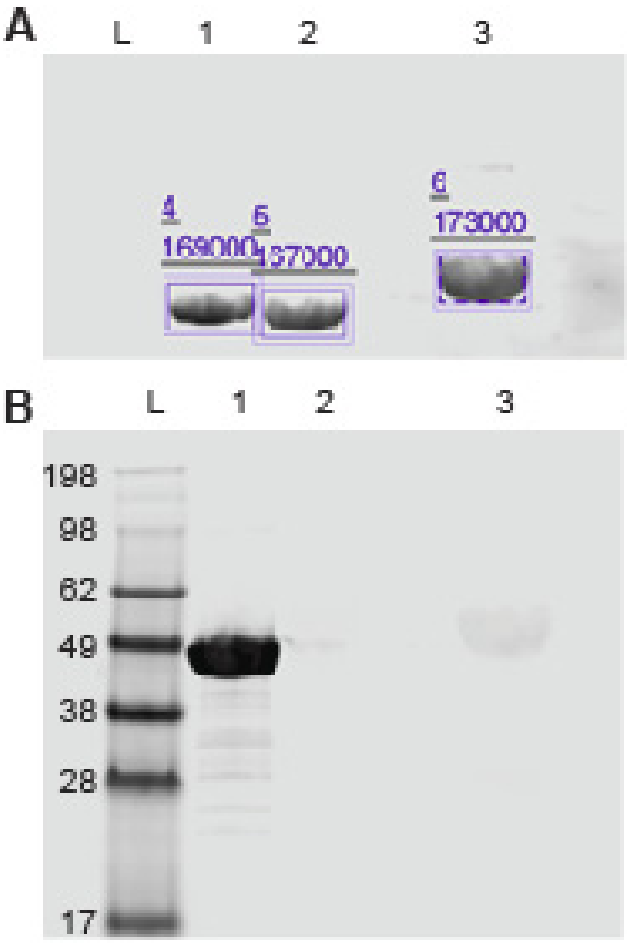

Figure 4.13. Western blot analysis of site-specifically DBCO-modified trastuzumab. After reaction with HIPS-DBCO linker **4.10** and purification, tagged trastuzumab was reacted with an azide-biotin reagent for detection of DBCO modification. A) Total protein stain shows comparable levels of protein in the three sample lanes. Lane 1 represents a streptococcal sialidase (46 kDa expected) that was reacted with maleimide-DBCO and which had been previously-validated as a positive control for DBCO labeling. Lane 2 represents the corresponding unreacted sialidase, a negative control. The DBCO-modified trastuzumab sample is shown in lane 3. B) Anti-biotin staining using fluorescent streptavidin reveals robust DBCO labeling for the positive control (lane 1) and no labeling for the negative control (lane 2). The trastuzumab sample (lane 3) shows faint but clear labeling, suggesting some degree of DBCO functionalization.

As these preliminary results suggested probable DBCO functionalization of aldehyde-tagged trastuzumab, I attempted to generate site-specific glycopolypeptide-trastuzumab conjugates by click chemistry. Glycopolypeptides were synthesized using azidophenylalanine benzyl amide, an amine NCA initiator that will be discussed in more detail in Chapter 5, and which introduces a C-terminal azide for reaction with the antibody DBCO modification. Analysis of polymers

synthesized using this nucleophile initiator compared to those using the Ni(II) initiator **4** strongly suggested a higher degree of functional azide labeling using the amine initiator. I began by labeling a 100 residue target length, 65:17.5:17.5 Ser(Man2):Ala:Glu polypeptide analogous to **4.1a** at the amine terminus with a Cy5.5 fluorophore to facilitate analysis. After 72 hour incubation at 4 °C with the DBCO-functionalized antibody and Protein A column purification, I analyzed the purified sample by western blot following SDS-PAGE or native PAGE. As I had observed in Fig. 4.8b, conjugation of glycopolypeptides to antibody resulted in the development of a streaky staining pattern by SDS-PAGE, particularly above the heavy chain band around 55 kDa (Fig. 4.14a). No notable light-chain modification was observed, consistent with the location of the tag at the heavy chain C-terminus. Interestingly, this smear did not stain efficiently with the anti-human IgG monoclonal primary antibody, apparent as a lack of colocalized 800 nm fluorescence relative to the unconjugated control. However, strong 700 nm fluorescence was observed in this region. Because this band, while diffuse, did not correlate with the fluorescently-labeled polymer control, it seemed plausible that it represented heavy chain-glycopolypeptide conjugate. The lack of 800 nm signal could suggest interference by the glycopolypeptide with binding of the primary antibody.

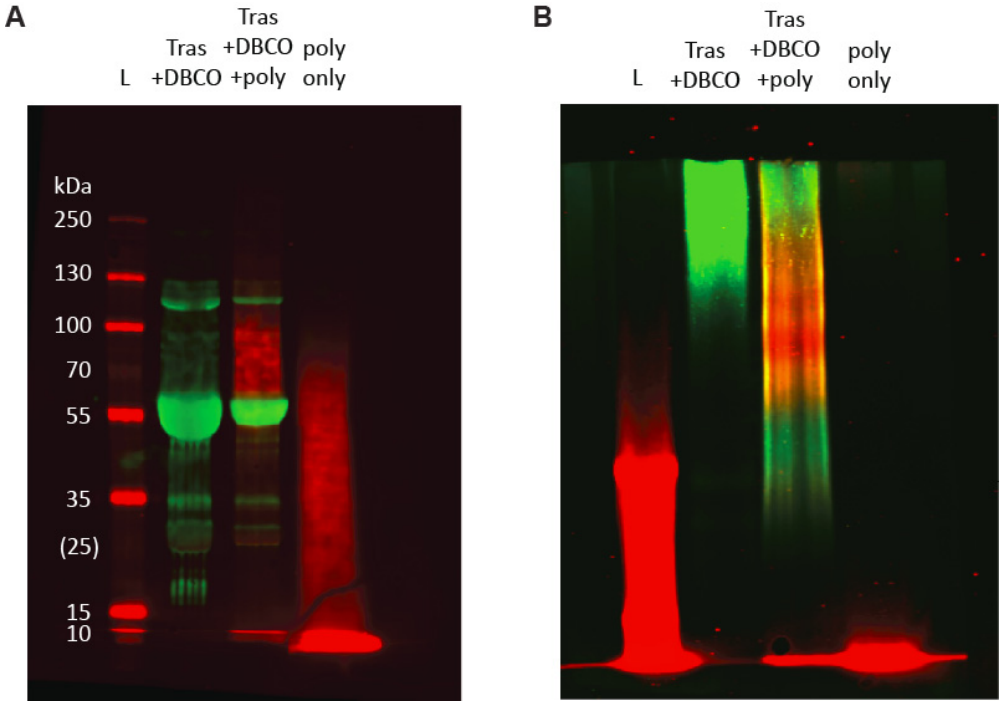

Figure 4.14. Western blot analysis of glycopolypeptide-antibody conjugation. Site-specifically DBCO-labeled trastuzumab was reacted with azide-functionalized glycopolypeptide (65% Ser(Man2), 100mer target length) that had previously been modified at the N-terminus with a Cy5.5 dye (Tras +DBCO +poly). As controls, the DBCO-modified antibody (Tras +DBCO) and unconjugated, fluorophore-labeled glycopolypeptide (poly only) were also loaded. Gels were run under either A) denaturing or B) native conditions. Red signal represents fluorescence at 700 nm, which includes Cy5.5 fluorescence. Blots were also stained with a monoclonal mouse anti-human IgG primary antibody, followed by detection using an 800 nm fluorescent goat anti-mouse secondary antibody, represented as green signal.

Successful conjugation was further supported by the native gel pattern, which showed a downward shift in the 800 nm fluorescence antibody band, consistent with conjugation to negatively-charged polymer (Fig. 4.14b). Furthermore, this band colocalized with a 700 nm fluorescence band that did not appear in the glycopolypeptide-only lane. It therefore seemed likely that this represented a fluorophore-glycopolypeptide-trastuzumab conjugate. However, it was not clear why the anti-IgG detection antibodies would stain the conjugates under native but not denaturing conditions. As an additional control, I repeated the analysis with the inclusion of a sample in which the glycopolypeptide was incubated with trastuzumab bearing formylglycine but not the DBCO click moiety, followed again by Protein A column purification (Fig. 4.15). The resulting gel patterns were highly unexpected: no clear difference was observed between the 700 nm fluorescence patterns for the +DBCO and –DBCO samples under denaturing or native conditions. Furthermore, in this particular blot I observed an apparent anti-correlation between the 700 and 800 nm signals by native PAGE, and a downshifted region of 800 nm fluorescence that was specific to the +DBCO sample.

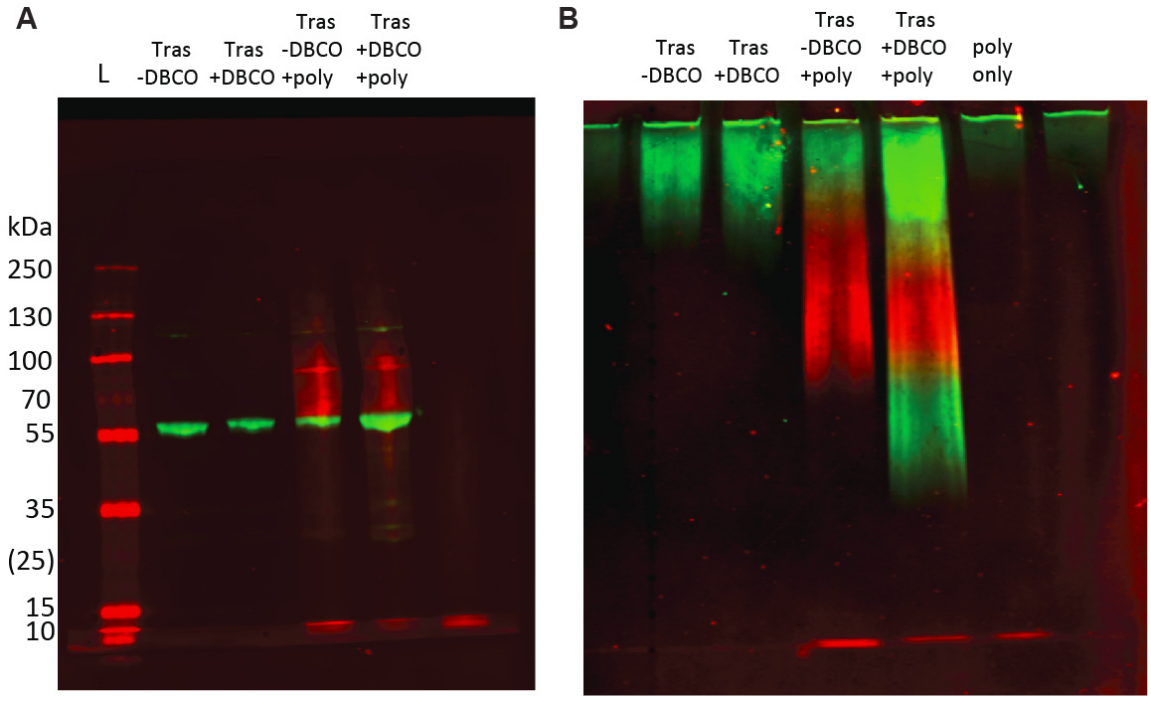

Figure 4.15. Western blot analysis of glycopolypeptide-antibody conjugation. Site-specifically DBCO-labeled trastuzumab was reacted with azide-functionalized glycopolypeptide (65% Ser(Man2), 100mer target length) that had previously been modified at the N-terminus with a Cy5.5 dye (Tras +DBCO +poly). As controls, the DBCO-modified antibody (Tras +DBCO) and unconjugated, fluorophore-labeled glycopolypeptide (poly only) were also loaded. An additional control was also included in which the conjugation reaction was performed using non-DBCO-labeled trastuzumab (Tras –DBCO +poly). Gels were run under either A) denaturing or B) native conditions. Red signal represents fluorescence at 700 nm, which includes Cy5.5 fluorescence. Blots were also stained with a monoclonal mouse anti-human IgG primary antibody, followed by detection using an 800 nm fluorescent goat anti-mouse secondary antibody, represented as green signal.

As a final attempt to characterize the nature of the trastuzumab-glycopolypeptide conjugation, I repeated the reaction using a Ser(Man2) homopolymer of 20mer target length (~7 kDa average mass) in an attempt to remove extraneous variables. The polymerization was again conducted using azidophenylalanine benzyl amide, but the glycopolypeptides were not labeled with Cy5.5 to avoid any potential dye-associated side reactions or interactions. Instead, detection of the highly mannosylated structures was achieved using biotinylated concanavalin A (ConA), which was detected using 800 nm fluorescent streptavidin. Trastuzumab was detected with a polyclonal, 700 nm fluorescent goat anti-human IgG primary antibody. As these glycopolypeptides were not fluorophore labeled, total protein analysis using a 700 nm fluorescent stain was also possible. Under these conditions, a band was observed by total protein, anti-human IgG, and ConA staining above the 50 kDa heavy chain band, as would be expected for a glycopolypeptide-heavy chain conjugate (Fig. 4.16a-c). Unlike the previous experiment, however, no such band appeared in the absence of antibody DBCO-labeling (Fig. 4.16e). Unfortunately, native PAGE analysis was complicated by the fact that ConA, which binds both glucosylated and mannosylated glycans, clearly stained both heavy chain glycosylation and mannosylated glycopolypeptide. Without additional data, we cannot conclusively claim that the observed gel shifts represent true glycopolypeptide-trastuzumab conjugates.

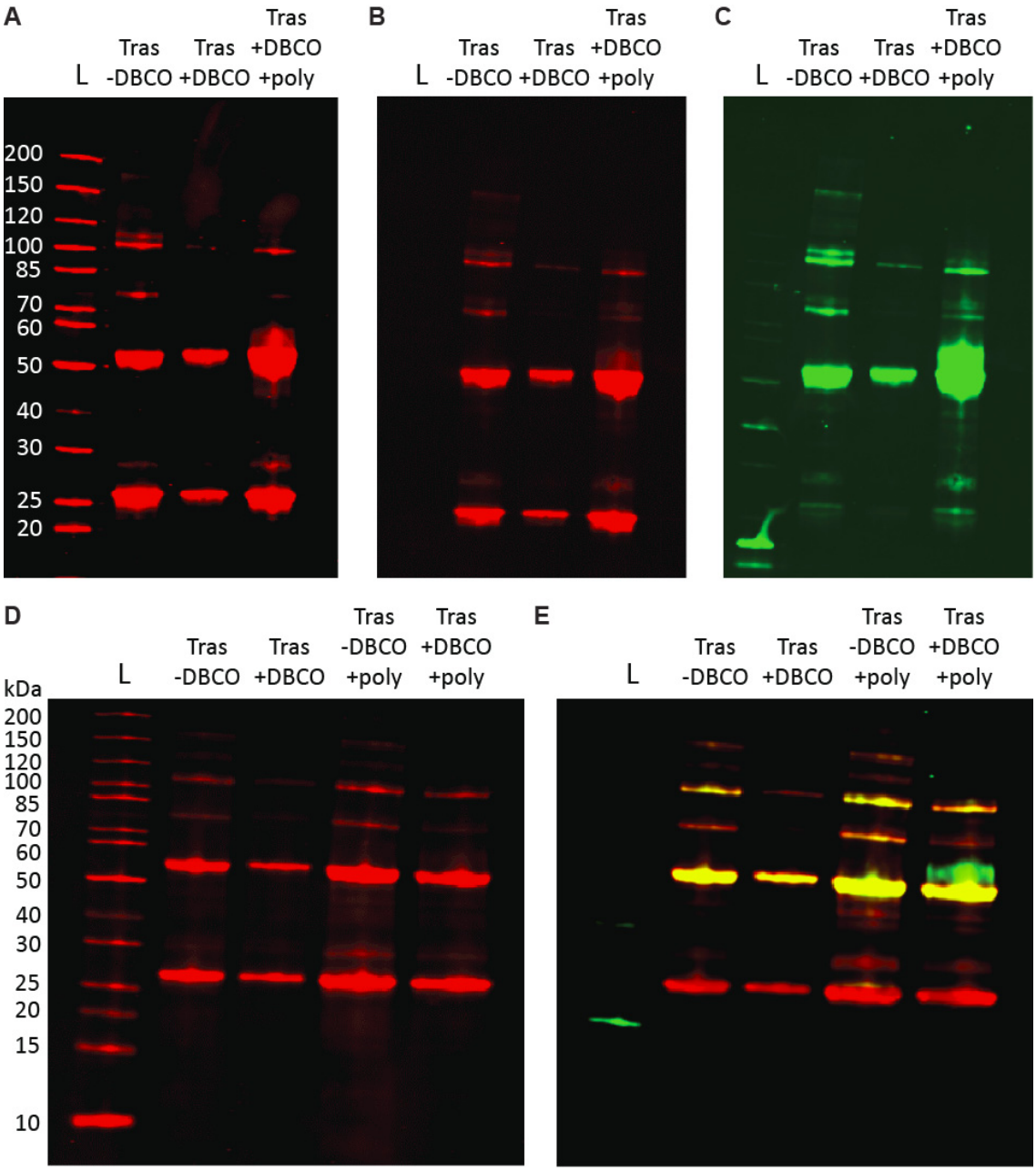

Figure 4.16. Western blot analysis of glycopolypeptide-antibody conjugation after SDS-PAGE. Site-specifically DBCO-labeled trastuzumab was reacted with azide-functionalized glycopolypeptide (100% Ser(Man2), 20mer target length) (Tras +DBCO +poly). As controls, the DBCO-modified antibody (Tras +DBCO) and unmodified antibody (Tras –DBCO) were also loaded. A) Total protein staining of putative conjugates and relevant controls. B) Western blot detection using a 700 nm fluorescent, polyclonal goat anti-human IgG antibody. C) Staining with biotin-labeled concanavalin A, followed by detection with an 800 nm fluorescent streptavidin reagent. D-E) The analysis was repeated with the inclusion of a control lane in which the conjugation reaction was performed using non-DBCO-labeled trastuzumab (Tras –DBCO +poly). All other lane labels are consistent with A-C).

Although these initial results do not definitively demonstrate successful conjugation, I remain optimistic that the HIPS/click chemistry strategy can yield the desired structures. In particular, reaction of DBCO-labeled antibody with the shorter mannobiose-serine homopolymer resulted in a glycosylated band by SDS-PAGE of approximately the expected size that was not observed in the absence of cyclooctyne (Fig 4.16e). Nevertheless, additional experiments will be necessary to definitively demonstrate that the HIPS/click reaction strategy successfully affords site-specific conjugates. Chromatographic analytical techniques, such as hydrophobic interaction, ion exchange, and size exclusion chromatography, may aid in purifying and analyzing the products of these reactions. Mass spectrometry, a key tool in the antibody-drug conjugate field, may not be readily amenable to analysis of these highly-glycosylated structures, and the inherent length dispersity of the glycopolypeptides will likely impede characterization. However, mass spectrometry analysis may be possible after chemical or enzymatic deglycosylation, and should be considered. On a different note, trastuzumab was chosen as a model enzyme in these experiments because of our previous experience with that particular aldehyde-tagged antibody. In order to compare site-specific conjugates with nonspecific lysine conjugation, it will likely be necessary to generate site-specific anti-EpCAM antibody-glycopolypeptides conjugates as well. Subsequent *in vivo* experiments should help to establish whether the site-specific approach indeed confers improved pharmacological properties on these novel immunogenic constructs.

4.8 Summary and outlook

A robust T cell response has generally been recognized as a key component of successful tumor rejection by the immune system; as such, cancer immunotherapies such as CAR-T cells and immune checkpoint inhibitors often focus directly on T cell populations.[17, 37-39] As an alternative, it has become increasingly clear that activation of antigen presenting cells can also result in downstream T cell-mediated tumor rejection.[6] With this in mind, we anticipated that antigen-agnostic APC activation could allow for uptake of tumor tissue and neoantigen presentation in the lymph nodes to induce adaptive immune tumor rejection, and therefore a highly generalizable cancer immunotherapy strategy. The key to our approach was the identification of an activating CLR, Dectin-2, that was highly expressed in the tumor microenvironment, and which we could stimulate using the Ser(Man2) glycopolypeptide ligands described in previous chapters. In the previous chapter, we demonstrated that the glycopolypeptides were able to activate antigen-presenting cells *in vitro* through Dec-2, giving credence to our proposed mechanism of action. Here, we investigated the *in vivo* activity of these Dec-2-activating glycopolypeptides in a murine PDAC cancer model.

Our initial results demonstrated that unmodified Ser(Man2) glycopolypeptides did reduce tumor growth in the animal model. However, a relatively aggressive dosing regimen was required, raising concerns about potential side effects if translated to a clinical setting. To address these concerns, we investigated two complementary approaches: conjugation of the glycopolypeptides to the synergistic TLR agonist T785 and conjugation to tumor-targeting antibodies. Our results clearly demonstrated a marked increase in immunogenicity upon conjugation to the TLR agonist, suggesting that a multi-receptor approach might allow for better potency *in vivo*. Conjugation to an anti-EpCAM antibody similarly improved APC activation *in vitro*, although additional *in vivo* experiments will be necessary to determine the impact of a tumor-targeting moiety on the therapeutic window. Given our results, we believe Dec-2 targeting to be a promising and

unexplored direction for cancer immunotherapy. Additional optimization of conjugation chemistry and strategy, including site-specific antibody constructs and alternative synergistic agonists, will help to focus our research on the key variables necessary to maximize *in vivo* efficacy while minimizing unnecessary synthetic and analytical complexity.

4.9 Materials and Methods

General Materials and Methods

T785 amine **4.2** and T785 maleimide **4.3** were provided by the Edgar Engleman lab and used without further purification. PBS buffer was obtained from Corning-Mediatech. Murine recombinant (rm) GM-CSF was purchased from Peprotech. Rat anti-mouse Dectin-2 (clone 2E4.11D) was purchased from BioRad. Flow cytometry was performed on a BD Biosciences Accuri C6. TNFα, IL-6, IL-12p40, and IL-12p70 ELISA kits were purchased from eBiosciences. Mouse Monocyte Enrichment Kit was purchased from STEMCELL Technologies. Procedures used to harvest murine monocytes were approved by the Institutional Animal Care and Use Committee of Stanford University. All experiments and protocols involving these primary murine cells were conducted exclusively by Dr. Justin Kenkel at Stanford University. Rat anti-Mouse EpCAM IgG2a (clone G8.8) was provided by the Edgar Engleman lab, and produced by them via hybridoma. Bicyclo[6,1,0]non-4-yn-9-yl N-hydroxysuccinimidyl ester (BCN-NHS) bearing a short PEG linker was obtained from Berry & Associates (Click-easy BCN N-hydroxysuccinimide ester II). Tetrazine-PEG5-NHS ester was obtained from Jena Biosciences. N-succidimidyl S-thioacetate was purchased from ThermoFisher Scientific. All NHS esters were stored as stock solutions in DMSO at -80 °C; thawed aliquots were not reused to protect against hydrolysis. 384-Well black flat-bottom plates were purchased from Corning and fluorescence readings taken using a Molecular Devices SpectraMax i3x plate reader. Aldehyde-tagged trastuzumab was a gift from Catalent Pharma Solutions. Near-IR western blot visualization was performed on a Li-COR Odyssey imaging system. High-resolution protein ESI mass spectrometry was performed by the Stanford University Mass Spectrometry laboratory.

LMP murine model and *in vivo* treatment protocol

The PDAC cell line, LMP, was established from liver metastases obtained from *Pdx1-Cre*; *Kras*$^{LSL\text{-}G12D/+}$; *Trp53*$^{LSL\text{-}R172H/+}$ mice on a B6/129 background, as described.[8, 40] Eight-week-old B6/129 (C57BL/6J x 129S1/SvImJ F1) mice were injected s.c. with 5x10^5 LMP cells suspended in PBS. For the experiment shown in Fig. 4.2, mice with established tumors (15-30 mm^2) were treated by intravenous injection every other day with 65% Man2 100mer **4.1a** (20 mg/kg i.v.) or vehicle (PBS) for 2 weeks. For the experiment shown in figure 4.6, mice with established tumors were treated with intratumoral injections of the T785-glycopolypeptide **4.6** twice at 250 μg per dose (days 8 and 10), or with the unconjugated glycopolypeptide **4.1a** using the same doses and treatment days as well as an additional dose on day 12. Tumors were measured by caliper every 5 d, and tumor volumes were estimated using the formula $V = (L \times W^2)/2$.

Synthesis of T785-glycopolypeptide conjugate 4.6 by maleimide-thiol ligation

Fully deprotected glycopolypeptides to be conjugated were dissolved to 1 mg/ml in 1x PBS [pH 7.4] and allowed to mix at ambient temperature overnight with a 5-10 fold excess of *N*-succinimidyl S-acetylthioacetate. Thioester-modified polymers were purified from excess thioacetate-labeling reagent via centrifuge spin filtration, using 3 kDa or 10 kDa MWCO filters as appropriate for the length of the polymers used and washing with additional 1X PBS [pH 7.4]. To the concentrated, purified solution of glycopolypeptide (~25-50 µl volume) was added 500 µl deacetylation solution (50 mM Hydroxylamine, 2.5 mM EDTA in PBS [pH 7.4]). The solution was allowed to incubate at ambient temperature for 2-4 hours. The deprotected thiol-bearing glycopolypeptide was again purified by spin filtration, washing with 10 mM EDTA in PBS [pH 7.4]. The solution was diluted to at least 0.5 ml with additional 10 mM EDTA in PBS [pH 7.4] and combined with a solution of T785 maleimide in DMSO (at least 5X excess T785 relative to theoretical equivalents of glycopolypeptide). Additional reaction buffer and/or DMSO were added as necessary to fully dissolve the relatively hydrophobic maleimide. The reaction was allowed to proceed overnight, followed by final purification by extensive spin filtration, washing with Milli-Q deionized water to remove excess salts. The resulting aqueous solution was lyophilized to afford the desired T785-glycopolypeptide conjugate as a pale fluffy solid.

Monocyte cell culture and ELISA

Bone marrow monocytes from naïve B6/129 mice were isolated by immunomagnetic negative selection according to the manufacturer's instructions (EasySep Mouse Monocyte Isolation Kit, Stemcell Technologies). Monocytes were cultured in the presence of LMP tumor conditioned medium for 24 hr prior to coculture with CFSE-labeled LMP cells (1:4 tumor:monocyte). Unconjugated αEpCAM antibody (clone G8.8) or antibody-glycopeptide conjugate were added at a final concentration of 10 µg/mL. CFSE uptake and costimulatory molecule expression by monocytes ($CD45^+EpCAM^-$) were evaluated by flow cytometry after 18 hr. Cytokine levels in coculture supernatants were determined by ELISA (eBioscience).

BCN-functionalization of EpCAM antibody

Rat anti-mouse EpCAM IgG2a clone G8.8 was diluted to approximately 1 mg/ml in PBS [pH 7.4]. BCN-NHS was stored at -80 °C as a 10 mg/ml stock in DMSO. An appropriate volume of BCN-NHS stock was added to the antibody solution, and the reaction was incubated on a rotary mixer overnight at ambient temperature. The reaction mixture was analyzed by native PAGE to qualitatively characterize BCN conjugation, and purified by repeated spin filtration to afford the BCN-labeled antibody as a solution in PBS [pH 7.4]. Concentration was determined by A280 using a NanoDrop instrument, assuming the standard IgG extinction coefficient and mass as defined by the NanoDrop software.

Polymer conjugation to tetrazine

Fully deprotected glycopolypeptide was dissolved in PBS [pH 7.4] to 1 mg/ml. To this solution was added a stock solution of tetrazine-PEG5-NHS ester (MW 604.61, 10 mM) in DMSO. The mixture was incubated on a rotary mixer overnight at ambient temperature. The tetrazine-labeled

product was purified into Milli-Q deionized water by extensive spin filtration and lyophilized to afford a faintly pink, fluffy solid.

Conjugation of tetrazine-labeled polymer and antibody

BCN-labeled antibody was diluted in PBS [pH 7.4] to 1-5 mg/ml and combined with a 2-5 fold excess of tetrazine-labeled polymer (10 mg/ml as a solution in PBS [pH 7.4]). The solution was allowed to incubate overnight on a rotary mixer at ambient temperature. The reaction mixture was analyzed by native PAGE to qualitatively characterize polymer conjugation and conjugates purified by extensive spin filtration using a 30 kDa MWCO filter to remove excess glycopolypeptide. Samples were analyzed by SDS-PAGE and/or native PAGE.

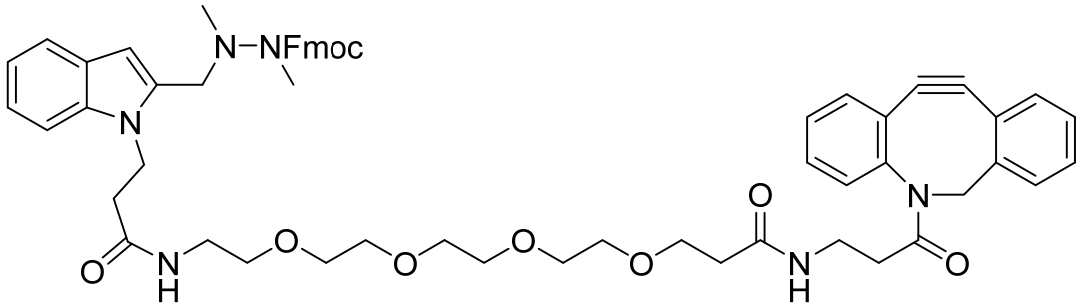

N-(3-[2-azatricyclo[10.4.0.0^{4,9}]hexadeca-1(12),4,6,8,13,15-hexaen-10-yn-2-yl]-3-oxopropyl)-1-[3-(2-[[([[(9H-fluoren-9-yl)methoxy]carbonyl}(methyl)amino)(methyl)amino]methyl]-1H-indol-1-yl)propanamido]-3,6,9,12-tetraoxapentadecan-15-amide, 4.10

3-(2-((2-(((9H-fluoren-9-yl)methoxy)carbonyl)-1,2-dimethylhydrazineyl)methyl)-1H-indol-1-yl)propanoic acid (**4.11**) was synthesized as described previously.[34] The indole (100 mg, 0.2067 mmol, 1 equiv.) was dissolved in 25 ml dry dichloromethane with (1-Cyano-2-ethoxy-2-oxoethylidenaminooxy)dimethylamino-morpholino-carbenium hexafluorophosphate (COMU) (88.5 mg, 0.2067 mmol, 1 equiv.) in an oven-dried round-bottom flask with a stir bar. The solution was briefly purged with dry N_2, and then the DBCO amine **4.13** (108 mg, 0.2067 mmol, 1 equiv.) was added as a solution in minimal dry dichloromethane. 2,6-Lutidine (47.7 µl, 0.4134 mmol, 0.925 g/ml, 2 equiv.) was then added, causing the reaction solution to immediately turn yellow. The reaction was allowed to proceed at room temperature for several hours, with product formation monitored by TLC and LC-MS. The reaction solution was washed three times with water to remove salts, then the organic fraction was dried over $MgSO_4$, filtered, and concentrated to a yellow residue which was purified by column chromatography (30-75% EtOAc in hexanes). The desired product did not elute readily using the described solvent gradient, and was eluted from the column using methanol to afford a yellow solid that was observed to contain product (approx.. 150 mg, 75%) by LC-MS and carried on without further purification.

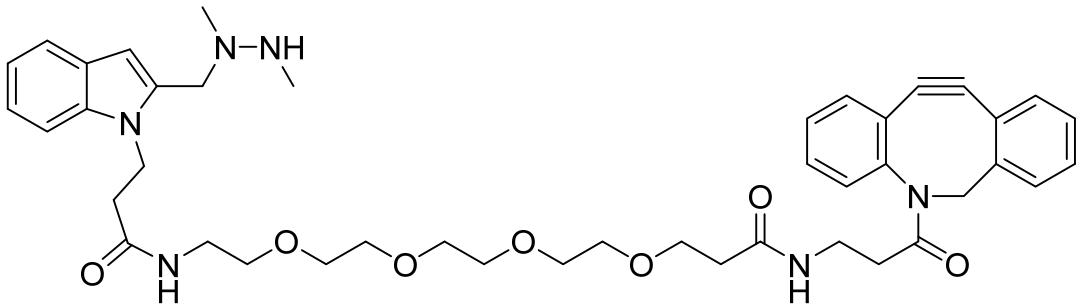

N-(3-[2-azatricyclo[10.4.0.0⁴,⁹]hexadeca-1(12),4,6,8,13,15-hexaen-10-yn-2-yl]-3-oxopropyl)-1-(3-[2-[(1,2-dimethylhydrazin-1-yl)methyl]-1H-indol-1-yl]propanamido)-3,6,9,12-tetraoxapentadecan-15-amide, 4.10

Fmoc-protected DBCO-conjugated starting material **4.10** was dissolved in 50% *t*-butylamine in THF. The reaction was monitored by TLC and allowed to proceed for 2 hours at ambient temperature. The reaction mixture was concentrated and the product repeatedly precipitated from dry diethyl ether, monitoring residual Fmoc-derived side products by TLC, to afford a yellow powder that was divided into approx. 2 mg aliquots that were purged with dry N_2 and stored at -80 C. ^{1}H-NMR analysis confirmed the loss of the Fmoc protecting group via the disappearance of the aryl peak at 7.9 ppm. Product mass, along with the presence of unidentified impurities, was confirmed by LC-MS. Due to the known instability of the 2-((1,2-dimethylhydrazinyl)methyl)-1*H*-indole core to air, light, and repeated chromatography, the material was carried on for conjugation without additional purification. ESI LRMS: Calcd. for $C_{43}H_{54}N_6O_7$ $[M+H]^+$ 767.41; obs. $[M+H]^+$ 767.0.

Conjugation of HIPS-DBCO linker 4.10 to aldehyde-tagged trastuzumab

Aldehyde-tagged trastuzumab was diluted to 10 mg/ml in citrate buffer (50 mM sodium citrate, 50 mM sodium chloride, 0.085% Triton X-100, pH 5.5). HIPS-DBCO **4.10** was dissolved in DMA to give a 30.7 mM stock solution, and a sufficient volume was added to the antibody solution to afford an 8:1 molar ratio of HIPS-DBCO to antibody. The reaction was allowed to proceed at 37 °C for 72 hours with gentle mixing. Note that the linker appears to precipitate from the reaction solution, indicating that additional optimization of reaction conditions may be desirable. Product was purified by buffer exchange on a Zeba Spin desalting column. To test DBCO labeling, a small aliquot was removed after purification and reacted with an azide-biotin reagent for 2 hours at 37 °C. Anti-biotin western blot analysis confirmed the presence of biotin, suggesting successful conjugation of DBCO onto the aldehyde-tagged samples.

Conjugation of azide-terminated glycopolypeptides to DBCO-labeled trastuzumab

Azide-terminated glycopolypeptides were synthesized as described in Chapter 5 using azidophenylalanine benzyl amide as the initiator and labeled at the N-terminus with Cy5.5 NHS ester where applicable. DBCO-labeled antibodies were diluted to approximately 1 mg/ml in PBS [pH 7.4] and combined with a 2-5 fold excess of glycopolypeptide. Samples were incubated overnight at ambient temperature on a rotary mixer before purification by Protein A column, eluting with PBS [pH 7.4]. Purified samples were analyzed by native PAGE and western blot.

4.10 References

1. Kerkar, S. P.; Restifo, N. P., Cellular constituents of immune escape within the tumor microenvironment. *Cancer Res* **2012,** *72* (13), 3125-30.

2. Coley, W. B., II. Contribution to the Knowledge of Sarcoma. *Ann Surg* **1891,** *14* (3), 199-220.

3. Lee, S.; Margolin, K., Cytokines in cancer immunotherapy. *Cancers (Basel)* **2011,** *3* (4), 3856-93.

4. Marabelle, A.; Kohrt, H.; Caux, C.; Levy, R., Intratumoral immunization: a new paradigm for cancer therapy. *Clin Cancer Res* **2014,** *20* (7), 1747-56.

5. Kantoff, P. W.; Higano, C. S.; Shore, N. D.; Berger, E. R.; Small, E. J.; Penson, D. F.; Redfern, C. H.; Ferrari, A. C.; Dreicer, R.; Sims, R. B.; Xu, Y.; Frohlich, M. W.; Schellhammer, P. F.; Investigators, I. S., Sipuleucel-T immunotherapy for castration-resistant prostate cancer. *N Engl J Med* **2010,** *363* (5), 411-22.

6. Carmi, Y.; Spitzer, M. H.; Linde, I. L.; Burt, B. M.; Prestwood, T. R.; Perlman, N.; Davidson, M. G.; Kenkel, J. A.; Segal, E.; Pusapati, G. V.; Bhattacharya, N.; Engleman, E. G., Allogeneic IgG combined with dendritic cell stimuli induce antitumour T-cell immunity. *Nature* **2015,** *521* (7550), 99-104.

7. Ishikawa, T.; Itoh, F.; Yoshida, S.; Saijo, S.; Matsuzawa, T.; Gonoi, T.; Saito, T.; Okawa, Y.; Shibata, N.; Miyamoto, T.; Yamasaki, S., Identification of distinct ligands for the C-type lectin receptors Mincle and Dectin-2 in the pathogenic fungus Malassezia. *Cell Host Microbe* **2013,** *13* (4), 477-88.

8. Tseng, W. W.; Winer, D.; Kenkel, J. A.; Choi, O.; Shain, A. H.; Pollack, J. R.; French, R.; Lowy, A. M.; Engleman, E. G., Development of an orthotopic model of invasive pancreatic cancer in an immunocompetent murine host. *Clin Cancer Res* **2010,** *16* (14), 3684-95.

9. Spitzer, M. H.; Carmi, Y.; Reticker-Flynn, N. E.; Kwek, S. S.; Madhireddy, D.; Martins, M. M.; Gherardini, P. F.; Prestwood, T. R.; Chabon, J.; Bendall, S. C.; Fong, L.; Nolan, G. P.; Engleman, E. G., Systemic Immunity Is Required for Effective Cancer Immunotherapy. *Cell* **2017,** *168* (3), 487-502 e15.

10. van Haren, S. D.; Dowling, D. J.; Foppen, W.; Christensen, D.; Andersen, P.; Reed, S. G.; Hershberg, R. M.; Baden, L. R.; Levy, O., Age-Specific Adjuvant Synergy: Dual TLR7/8 and Mincle Activation of Human Newborn Dendritic Cells Enables Th1 Polarization. *J Immunol* **2016,** *197* (11), 4413-4424.

11. Tom, J. K.; Dotsey, E. Y.; Wong, H. Y.; Stutts, L.; Moore, T.; Davies, D. H.; Felgner, P. L.; Esser-Kahn, A. P., Modulation of Innate Immune Responses via Covalently Linked TLR Agonists. *ACS Cent Sci* **2015,** *1* (8), 439-448.

12. Ryu, K. A.; Slowinska, K.; Moore, T.; Esser-Kahn, A., Immune Response Modulation of Conjugated Agonists with Changing Linker Length. *ACS Chem Biol* **2016,** *11* (12), 3347-3352.

13. Gerster, J. F. 1H-Imidazo[4,5-c]quinolines and 1H-imidazo[4,5-c]quinolin-4-amines. EP 0145340, 1985.

14. Heil, F.; Hemmi, H.; Hochrein, H.; Ampenberger, F.; Kirschning, C.; Akira, S.; Lipford, G.; Wagner, H.; Bauer, S., Species-specific recognition of single-stranded RNA via toll-like receptor 7 and 8. *Science* **2004,** *303* (5663), 1526-9.

15. Shi, C.; Xiong, Z.; Chittepu, P.; Aldrich, C. C.; Ohlfest, J. R.; Ferguson, D. M., Discovery of Imidazoquinolines with Toll-Like Receptor 7/8 Independent Cytokine Induction. *ACS Med Chem Lett* **2012,** *3* (6), 501-504.

16. Ghosh, T. K.; Mickelson, D. J.; Fink, J.; Solberg, J. C.; Inglefield, J. R.; Hook, D.; Gupta, S. K.; Gibson, S.; Alkan, S. S., Toll-like receptor (TLR) 2-9 agonists-induced cytokines and chemokines: I. Comparison with T cell receptor-induced responses. *Cell Immunol* **2006,** *243* (1), 48-57.

17. Knutson, K. L.; Disis, M. L., Tumor antigen-specific T helper cells in cancer immunity and immunotherapy. *Cancer Immunol Immunother* **2005,** *54* (8), 721-8.

18. Saijo, S.; Iwakura, Y., Dectin-1 and Dectin-2 in innate immunity against fungi. *Int Immunol* **2011,** *23* (8), 467-72.

19. Ma, D. Y.; Clark, E. A., The role of CD40 and CD154/CD40L in dendritic cells. *Semin Immunol* **2009,** *21* (5), 265-72.

20. Guermonprez, P.; Valladeau, J.; Zitvogel, L.; Thery, C.; Amigorena, S., Antigen presentation and T cell stimulation by dendritic cells. *Annu Rev Immunol* **2002,** *20*, 621-67.

21. Agrawal, S.; Gupta, S., TLR1/2, TLR7, and TLR9 signals directly activate human peripheral blood naive and memory B cell subsets to produce cytokines, chemokines, and hematopoietic growth factors. *J Clin Immunol* **2011,** *31* (1), 89-98.

22. Rizzetto, L.; De Filippo, C.; Rivero, D.; Riccadonna, S.; Beltrame, L.; Cavalieri, D., Systems biology of host-mycobiota interactions: dissecting Dectin-1 and Dectin-2 signalling in immune cells with DC-ATLAS. *Immunobiology* **2013,** *218* (11), 1428-37.

23. Klauber, T. C. B.; Laursen, J. M.; Zucker, D.; Brix, S.; Jensen, S. S.; Andresen, T. L., Delivery of TLR7 agonist to monocytes and dendritic cells by DCIR targeted liposomes induces robust production of anti-cancer cytokines. *Acta Biomater* **2017,** *53*, 367-377.

24. Chen, P.; Liu, X.; Sun, Y.; Zhou, P.; Wang, Y.; Zhang, Y., Dendritic cell targeted vaccines: Recent progresses and challenges. *Hum Vaccin Immunother* **2016,** *12* (3), 612-22.

25. Ifrim, D. C.; Quintin, J.; Courjol, F.; Verschueren, I.; van Krieken, J. H.; Koentgen, F.; Fradin, C.; Gow, N. A.; Joosten, L. A.; van der Meer, J. W.; van de Veerdonk, F.; Netea, M. G., The Role of Dectin-2 for Host Defense Against Disseminated Candidiasis. *J Interferon Cytokine Res* **2016,** *36* (4), 267-76.

26. Weber, J. S.; Yang, J. C.; Atkins, M. B.; Disis, M. L., Toxicities of Immunotherapy for the Practitioner. *J Clin Oncol* **2015,** *33* (18), 2092-9.

27. Agarwal, P.; Bertozzi, C. R., Site-specific antibody-drug conjugates: the nexus of bioorthogonal chemistry, protein engineering, and drug development. *Bioconjug Chem* **2015,** *26* (2), 176-92.

28. Jain, N.; Smith, S. W.; Ghone, S.; Tomczuk, B., Current ADC Linker Chemistry. *Pharm Res* **2015,** *32* (11), 3526-40.

29. McCombs, J. R.; Owen, S. C., Antibody drug conjugates: design and selection of linker, payload and conjugation chemistry. *AAPS J* **2015,** *17* (2), 339-51.

30. Patterson, D. M.; Nazarova, L. A.; Prescher, J. A., Finding the right (bioorthogonal) chemistry. *ACS Chem Biol* **2014,** *9* (3), 592-605.

31. Munz, M.; Baeuerle, P. A.; Gires, O., The emerging role of EpCAM in cancer and stem cell signaling. *Cancer Res* **2009,** *69* (14), 5627-9.

32. Ober, R. J.; Radu, C. G.; Ghetie, V.; Ward, E. S., Differences in promiscuity for antibody–FcRn interactions across species: implications for therapeutic antibodies. *International Immunology* **2001,** *13* (12), 1551-1559.

33. Rabuka, D.; Rush, J. S.; deHart, G. W.; Wu, P.; Bertozzi, C. R., Site-specific chemical protein conjugation using genetically encoded aldehyde tags. *Nat Protoc* **2012,** *7* (6), 1052-67.

34. Drake, P. M.; Albers, A. E.; Baker, J.; Banas, S.; Barfield, R. M.; Bhat, A. S.; de Hart, G. W.; Garofalo, A. W.; Holder, P.; Jones, L. C.; Kudirka, R.; McFarland, J.; Zmolek, W.; Rabuka, D., Aldehyde tag coupled with HIPS chemistry enables the production of ADCs conjugated site-specifically to different antibody regions with distinct in vivo efficacy and PK outcomes. *Bioconjug Chem* **2014,** *25* (7), 1331-41.

35. Xiao, H.; Woods, E. C.; Vukojicic, P.; Bertozzi, C. R., Precision glycocalyx editing as a strategy for cancer immunotherapy. *Proc Natl Acad Sci U S A* **2016,** *113* (37), 10304-9.

36. Pijnenborg, J. F. Rituximab-sialidase conjugation for improved drug efficacy. Stanford University, Stanford, CA, 2017.

37. Pardoll, D. M., The blockade of immune checkpoints in cancer immunotherapy. *Nat Rev Cancer* **2012,** *12* (4), 252-64.

38. Jackson, H. J.; Rafiq, S.; Brentjens, R. J., Driving CAR T-cells forward. *Nat Rev Clin Oncol* **2016,** *13* (6), 370-83.

39. Harris, D. T.; Kranz, D. M., Adoptive T Cell Therapies: A Comparison of T Cell Receptors and Chimeric Antigen Receptors. *Trends Pharmacol Sci* **2016,** *37* (3), 220-30.

40. Hingorani, S. R.; Wang, L.; Multani, A. S.; Combs, C.; Deramaudt, T. B.; Hruban, R. H.; Rustgi, A. K.; Chang, S.; Tuveson, D. A., Trp53R172H and KrasG12D cooperate to promote chromosomal instability and widely metastatic pancreatic ductal adenocarcinoma in mice. *Cancer Cell* **2005,** *7* (5), 469-83.

Chapter 5

Further study of NCA initiators for dual-end-functionalized glycopolypeptides

This work was performed in collaboration with Corleone Delaveris, Dr. Justin Kenkel, and Dr. Jana Maclaren

5.1 Installing C-terminal functionality using Ni(II) NCA initiators

One of the key advantages of synthetic glycopolypeptides over natural extracts is the ability to chemically install additional functionality in a predictable and well-characterized manner. NCA polymerization using Ni(0) or Co(0) initiators as described in Chapter 2 affords a reactive amine terminus. Unfortunately, the proposed mechanism of polymerization results in loss of the C-terminal carboxylic acid through decarboxylation during the initiation phase.[1] Introduction of a second functional handle would allow for conjugation of glycopolypeptides to a second small molecule or protein. For example, combining the improved immunostimulatory properties of a TLR agonist-glycopolypeptide conjugate with a tumor-specific antibody might allow for optimization of on-target efficacy as demonstrated in Chapter 4. As described briefly in Chapter 2, Deming et al. first reported in 1999 a panel of Ni(II) initiators capable of efficiently polymerizing NCAs while installing C-terminal functionality (Scheme 5.1).[2] Reaction of alloc-protected amino amides with Ni(0) species at elevated temperatures afforded metal complexes capable of initiating NCA polymerization while installing the desired C-terminal group. A Ni(II) amido-amidate structure was proposed based on IR and MS of the metal complex and NMR and MALDI-MS analysis of monopeptide and polypeptide products. Given the proposed polymerization mechanism using Ni(0) initiators, such a structure would represent an analog of the propagating species and therefore seemed consistent with the available data. Notably, crystal structures of the isolated initiators were not obtained, and direct NMR analysis of the initiator was difficult due to paramagnetism of the isolated material. However, we were still attracted by the possibility of introducing glycopolypeptide C-terminal functionality in a quantitative manner.

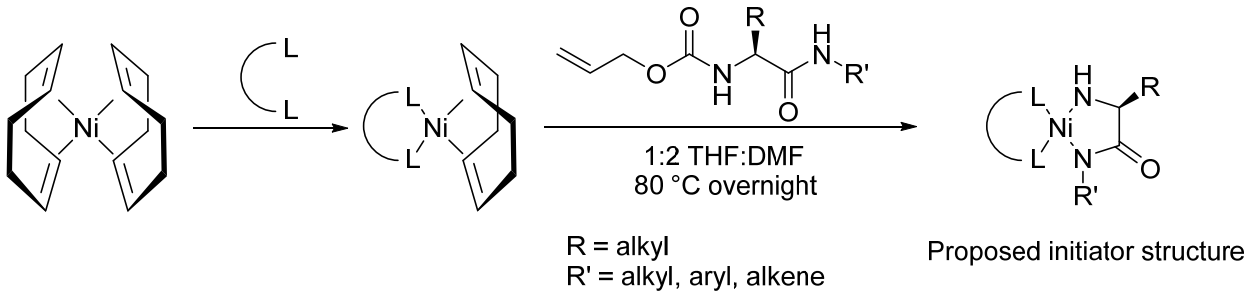

Scheme 5.1. Generalized route to Ni(II) amido amidates proposed by Deming et al.[2]

In our earlier publication, we reported the synthesis of Ni(II) initiator **2.4** based on the Deming et al. publication.[3] Featuring a C-terminal azide, the initiator was synthesized in an analogous fashion using N_α-alloc-leucine azidopropyl amide **5.1** and the phosphine ligand 1,2-bis(dimethylphosphino)ethane (dmpe) (Scheme 5.2). The crude orange reaction mixture was used directly for polymerization, as Deming had reported no notable difference using isolated initiator versus the crude reaction mixture and because we had been advised that the isolated material was difficult to purify and handle.[2] Direct analysis of the initiator was not performed at the time, and the resulting glycopolypeptides were treated under the assumption that quantitative azide labeling had been achieved, as might be supposed based on the Deming report. Indeed, reaction of *N*-acetylgalactosamine-serine glycopolypeptides with cyclooctyne-functionalized dyes afforded fluorescent polymers after workup. I was also able to decorate cyclooctyne-functionalized polystyrene beads with azide-bearing glycopolypeptides as described in Chapter 3, although I used equal mass equivalents of beads and polypeptides to maximize the effective polypeptide:bead

ratio. Unfortunately, during subsequent studies it became clear to me and colleagues that glycopolypeptides derived from initiator **2.4** were not fully azide functionalized. In this chapter, I detail some of our experiments corroborating this observation, as well as my attempts to further characterize and optimize dual-functionalized initiators.

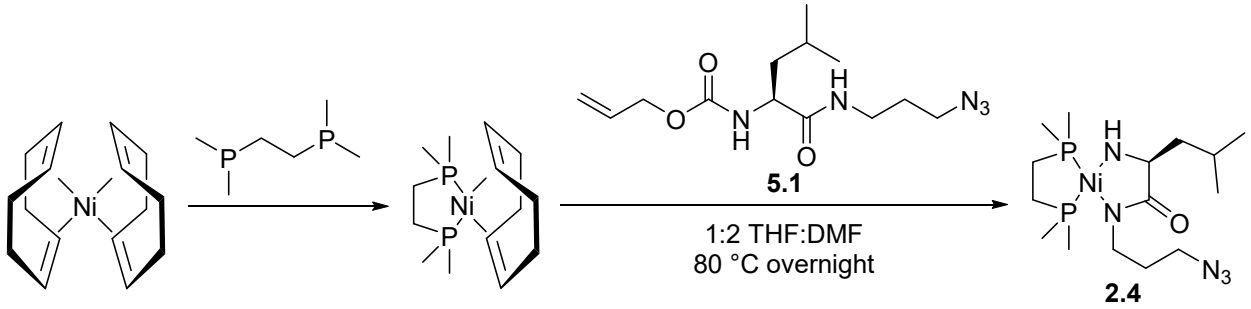

Scheme 5.2. Synthetic route to Ni(II) amido amidate **2.4**, first reported by our lab as an initiator for polymerizing azide-terminated polypeptides.[3]

5.2 Analyzing azide functionalization on Ni(II) initiator 2.4

In my hands, one of the first indications that azide-based conjugation was not labeling all polymer chains was the qualitative observation that dye-labeling reactions using cyclooctyne-functionalized dyes afforded polymers that were only faintly colored after workup, whereas the relative amount of free dye visibly removed during washing steps seemed incommensurate with the reaction stoichiometries. Subsequent plate reader fluorescence measurements of a 100mer target length glycopolypeptide (65:17.5:17.5 Ser(Man2):Ala:Glu) that had been reacted with a Cy5-DBCO dye compared to a standard curve of free dye suggested a labeling efficiency of approximately 2%. Although the precise length of the polypeptide was not determined at the time, it was clear from these initial observations that the majority of polymer chains were likely not reacting with the small molecule azide. Consultation with colleagues revealed that similar problems had been observed when attempting to conjugate glycopolypeptides derived from **2.4** to other cyclooctyne-functionalized reaction partners, including lipids and antibodies, as well as to terminal alkynes via copper-catalyzed cycloaddition.

Difficulty conjugating glycopolypeptides via azide-alkyne click reactions could be either due to chemical degradation of the azide handle or to impaired reactivity due to reduced accessibility or slower kinetics in a macromolecular context. Further optimization therefore required additional characterization of the initiator. Deming et al. reported that NMR characterization of the Ni complexes was not possible, with spectral characteristics consistent with the presence of paramagnetic species.[2] I also consistently observed a high degree of peak broadening that made attempts to characterize the initiators by NMR unfruitful. Interestingly, square planar Ni(II) complexes are generally expected to be diamagnetic, and NMR spectra for a variety of square planar Ni(II) complexes have been reported.[4-5] Nevertheless, as Ni(II) amido-amidate species are not widely known in the literature, I could not determine from this observation alone if the paramagnetism was due to an unusual electronic configuration, an unexpected ligand geometry, or even the presence of other paramagnetic species in the initiator mixture.

The azide is well-known for its distinctive IR stretch at 2100 cm^{-1}, which is often employed to monitor azide-alkyne click reactions.[6] As a simple test, I compared the IR spectra of the N_{α}-alloc-

leucine azidopropyl amide starting material with the products obtained after initial reaction with dmpeNi(COD) at ambient temperature and after formation of the final initiator solution upon heating at 80 °C. As expected, N_α-alloc-leucine azidopropyl amide exhibits a strong azide stretch at 2100 cm^{-1}, as well as characteristic amide and carbamate peaks at 1670 and 1650 cm^{-1}, respectively (Fig. 5.1a). Per Deming et al., combining the Ni(0) starting material and N_α-alloc-leucine azidopropyl amide, which induces a rapid color change from yellow to green, likely results in formation of an initial oxidative addition product which is not a competent NCA initiator.[2] Interestingly, FTIR-ATR analysis of this intermediate did give an azide peak (Fig. 5.1b). Loss of the carbamate peak at 1700 cm^{-1} corroborated the mechanistic proposal of an initial reaction between the allyl carbamate and Ni center. Consistent with the Deming report, a prominent peak at 1570 cm^{-1} was observed after heating to form the orange product, likely corresponding to the amidate C=O stretch (Fig. 5.1c). However, any potential azide peak was faint at best, and indistinguishable from the baseline noise often observed in the 2000-2200 cm^{-1} region, a known artifact attributable to the diamond ATR crystal.[7-8]

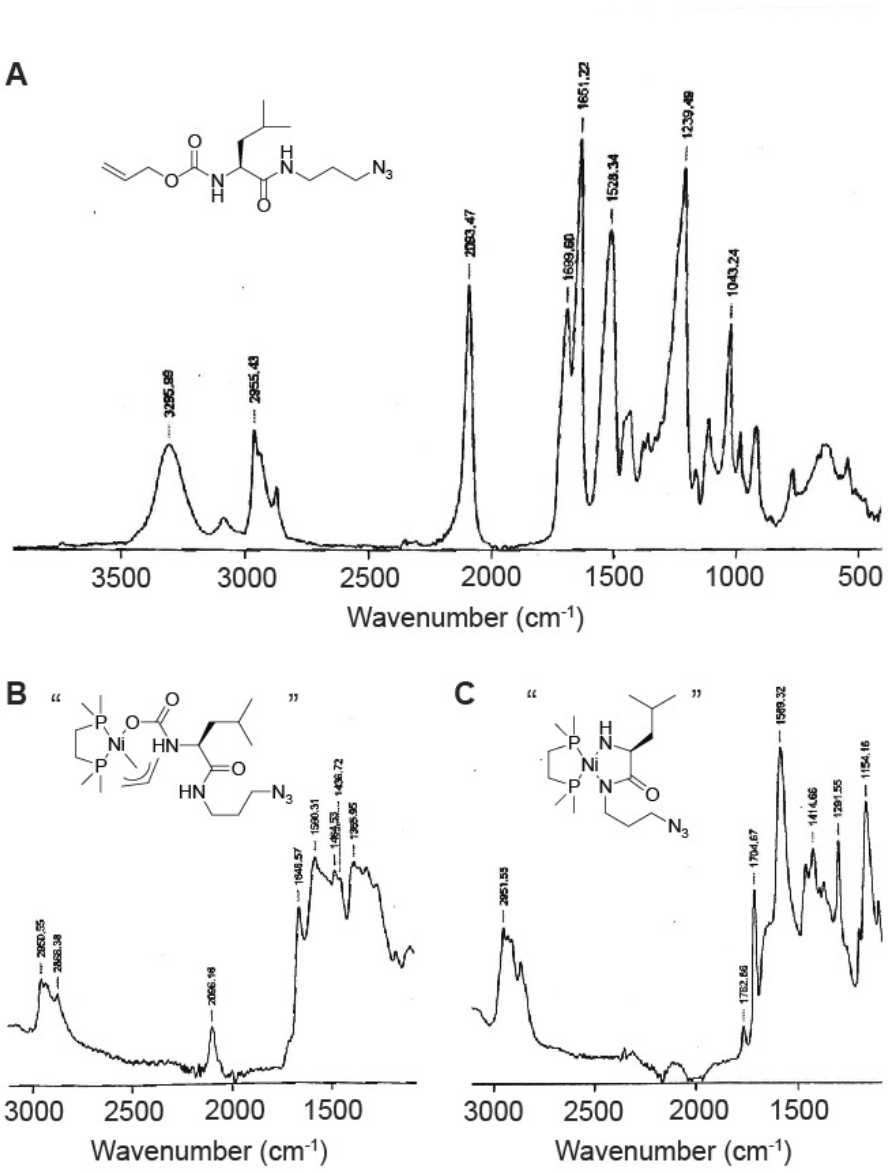

Figure 5.1. FTIR-ATR spectra demonstrating partial loss of azide during the synthesis of initiator **2.4**. A) FTIR spectrum of the N_{α}-alloc-leucine azidopropylamide starting material, with clear peaks around 2100 (azide stretch), 1700 (carbamate stretch), and 1650 (amide stretch) cm^{-1}. B) Initial reaction of **5.1** with dmpeNi(COD) affords a green solution that retains an azide peak. C) However, upon heating to afford the final orange initiator solution, significant loss of the azide signal is observed along with appearance of the expected amidate peak at 1570 cm^{-1}.

Due to technical constraints, I was unable to obtain meaningful IR spectra under air free conditions; I therefore could not rule out the possibility that the observed loss of the azide peak was due to decomposition of the Ni complex during the course of analysis. Furthermore, disappearance of the azide peak could be due to a non-destructive interaction between the Ni center and N1, the most electron-rich of the three azide nitrogens, which could possibly shift the corroesponding IR peak. As a complementary analysis, I therefore attempted LC-MS analysis of the products obtained after

acidic aqueous workup of the initiator solution, a protocol we routinely use during glycopolypeptide workup, and which Deming et al. have employed to characterize reaction products for mechanistic studies.[2-3] Quenching the initiator solution with aqueous HCl, followed by reverse-phase LC-MS analysis on a C18 silica column afforded a complex LC trace (Fig 5.2a). However, I was able to identify masses corresponding to both the expected leucine azidopropyl amide as well as leucine aminopropyl amine, indicating partial reduction of the azide and supporting the hypothesis that the initiator solution contains a mixture of Ni species (Fig. 5.2b).

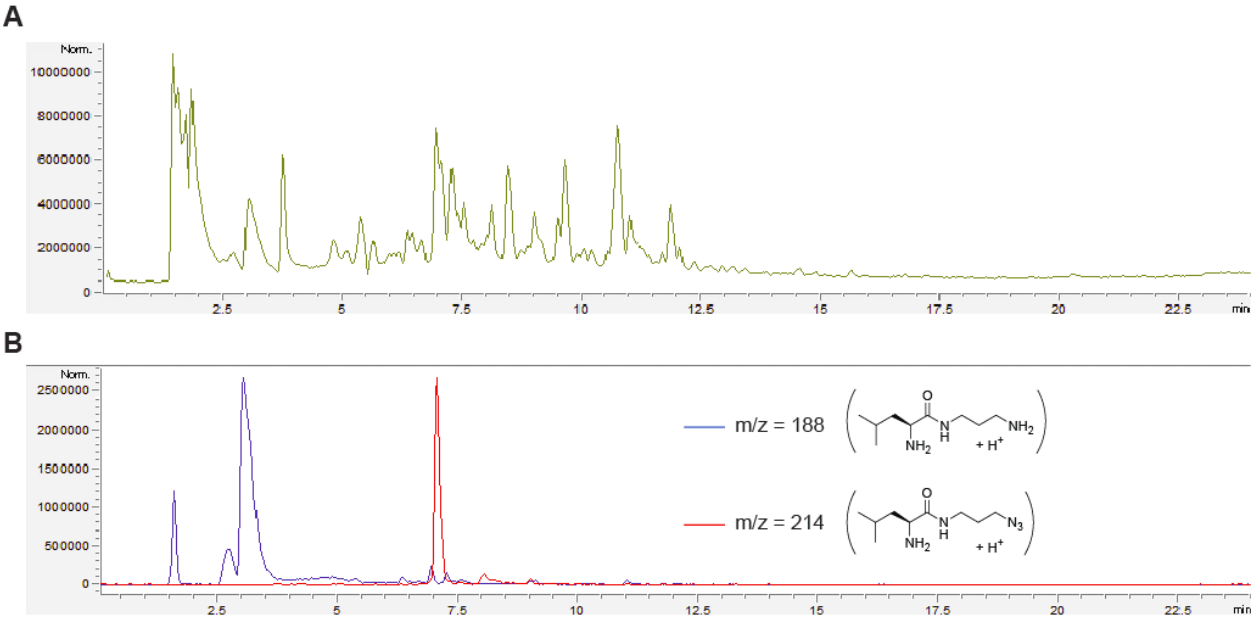

Figure 5.2. LC-MS traces obtained from initiator **2.4** after acidic aqueous workup, demonstrating partial reduction of the azide functional group. For both panels, the Y-axis represents detection via ESI-MS in positive ion mode. A) MS total ion trace showing a complex mixture of products present in the quenched initiator solution. B) MS ion traces corresponding to the expected leucine azidopropyl amide (red) as well as the reduced leucine aminopropyl amide (blue), indicating significant loss of the desired azide functionality. The LC method was run using a gradient of 95-5% H_2O in acetonitrile with 0.1% TFA on a C18 silica column.

5.3 Attempted synthesis of the 2,2′-bipyridine analog of 2.4 and crystallization of an unexpected product

Given clear evidence that azide reduction was occurring, I considered options for redesigning the initiator. Upon further consideration of the synthetic route to **2.4**, it became clear that the dmpe ligand was likely reacting with the azide, as phosphines are well-known to reduce azides through Staudinger-type chemistry.[9] Indeed, simple ^{31}P-NMR experiments demonstrated that free dmpe, which could conceivably exist at multiple points during initiator synthesis, polymerization, and workup, unsurprisingly reacted very efficiently with **5.1** to afford the phosphazene intermediate. It therefore seemed prudent to examine whether the ligand could be a primary cause for the loss of azide functionality. The original choice of phosphine ligands was based on literature reports that concluded that alkyl phosphines promoted the most efficient initiation out of the ligands

tested.[2, 10] However, a variety of amine ligands are effective enough sigma donors to promote reasonable reactivity at the metal center. I therefore attempted to synthesize **5.2**, the 2,2′-bipyridine (bpy) analog of **2.4**, via an analogous protocol (Scheme 5.3). Test-scale reactions suggested that the resulting initiator solution was also capable of initiating NCA polymerizations, with no notable qualitative difference in reaction rate compared to the phosphine analog. Dispersity of a Ser(Man2) glycopolypeptide polymerized at a 25:1 monomer:initiator (M:I) ratio was measured at 1.19 using bpy as the ligand; the same reaction using DMPE gave a similar dispersity of 1.15, suggesting that change of ligand did not negatively impact the polymer length distribution.

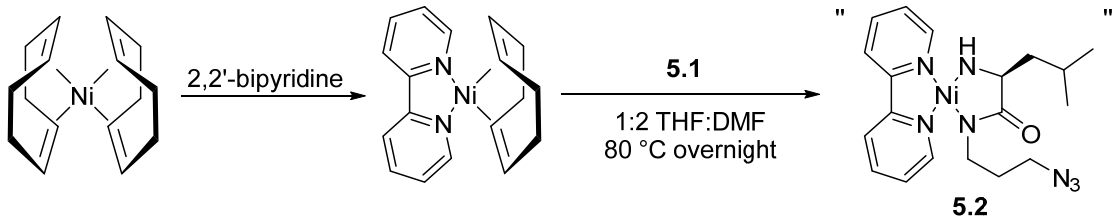

Scheme 5.3. Synthetic route to Ni(II) amido amidate **5.2**, bearing a 2,2'-bipyridine ligand to avoid Staudinger-type reduction of the azide functional group.

I again attempted a fluorescence-based approach to quantifying reactive azide termini. For simplicity, I synthesized a relatively short 25:1 M:I homopolymer of Ser(Man2). ^{1}H-NMR of the resulting glycopolypeptide allowed for integration of the mannobiose anomeric protons against the leucine methyl protons to give an approximate molecular weight of 16 kDa. Overnight reaction with 1.5 equivalents of Cy5-DBCO, followed by extensive purification by spin filtration, again produced pale blue products after lyophilization along with a concerning amount of visible free dye in the filtrate. Plate reader analysis confirmed innefficient dye conjugation, with only approximately 1% chain functionalization measured.

Consistent with the fluorescence experiment, FTIR analysis again showed loss of the azide peak at 2100 cm^{-1} upon heating (Fig. 5.3b) despite its presence in the putative single oxidative-addition intermediate (Fig. 5.3a). Interestingly, however, acidic workup of a separate batch of the initiator solution gave material that did display an azide signal, albeit with a reduced relative peak size compared with the N_{α}-alloc-leucine azidopropyl amide (Fig. 5.3c,d). Because the two samples were synthesized and analyzed separately on different days, it was unfortunately not possible to directly compare the two to determine if the discrepancy was due to batch-to-batch inconsistency in azide labeling or due to the differences in sample handling prior to FTIR analysis. It remains theoretically possible that prolonged exposure of the unquenched initiator solution to ambient air or moisture could promote reaction of the azide, though the mechanism by which this would occur is unclear.

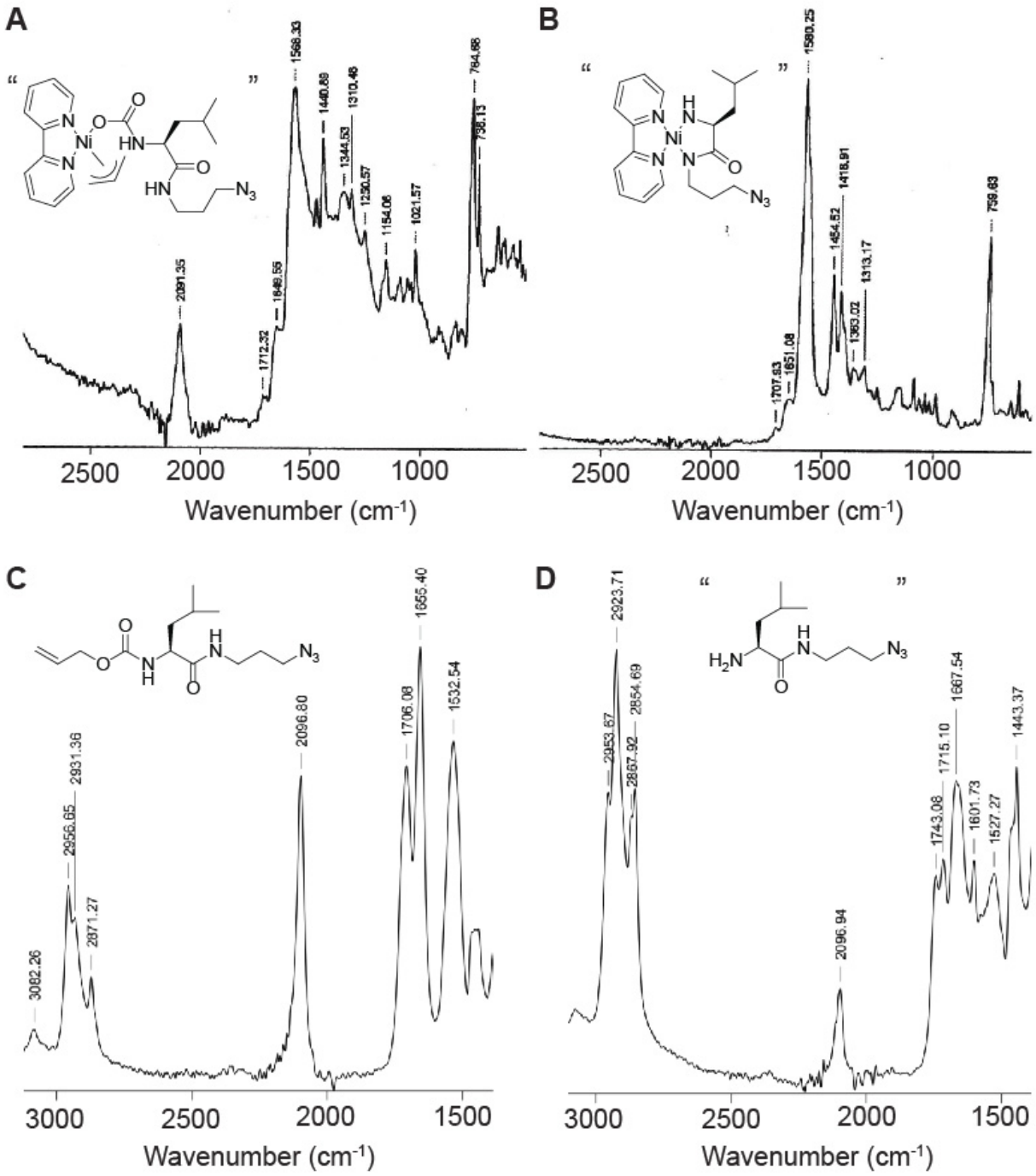

Figure 5.3. FTIR-ATR spectra demonstrating partial loss of azide during the synthesis of initiator **5.2**. A) As observed during the synthesis of initiator **2.4**, the intermediate formed during the reaction of **5.2** with bpyNi(COD) affords a green solution that retains an azide peak at 2100 cm^{-1}. B) Heating to afford the final orange initiator solution, significant loss of the azide signal is observed along with appearance of the expected amidate peak at 1580 cm^{-1}. During the course of

a subsequent attempted synthesis of **5.2**, the FTIR spectrum of C) the amino acid-derived starting material was compared to that of D) a quenched and worked up sample of initiator solution.

Regardless, the accumulated data suggested that a large proportion of the azide was still degrading despite the absence of a phosphine ligand. Furthermore, the lack of direct structural characterization of any of the metal complexes present in the initiator solution made it difficult to propose decomposition mechanisms with certainty. I therefore sought to grow crystals from the initiator complex for X-ray diffraction (XRD) analysis. Deming et al. reported isolation of their initiators in solid form via precipitation from diethyl ether, followed by washing with THF, although they did not report XRD structural characterization.[2] Interestingly, I found that addition of either diethyl ether or THF to the crude solution of **5.2**, a 1:2 THF:DMF mixture, resulted in immediate precipitation of a white or off-white material. Further addition of ether or THF caused increasing coprecipitation of orange solid, suggesting the presence of multiple species. Unfortunately, identification of the white solid has proven unfruitful to date; I was unable to identify suitable crystallization conditions, NMR analysis was difficult due to insufficient isolated sample and apparent paramagnetism, and LC-MS results were inconclusive. To obtain crystals of the orange material, I first subjected the initiator solution to several cycles of minimal dilution with THF followed by filtration to remove as much of the lighter-colored precipitate as possible. Using this protocol, I obtained fragile orange/red crystals from the orange solution by vapor diffusion using THF as the countersolvent.

From one of the isolated crystals, I observed a highly unexpected crystal structure at 0.71 Å resolution (Fig. 5.4). Instead of the proposed mononuclear square planar configuration, the complex features two Ni centers bridged by azide-derived imines. No bpy ligands appear to be present, either coordinated as part of the complex or elsewhere in the crystal lattice. To achieve a net Ni(II) oxidation state for each metal center, the amines coordinate as doubly protonated neutral ligands rather than as metal amides, while the amino acid amide does appear to coordinate as the anionic amidate. The geometry around each Ni atom is approximately square planar, although the overall complex conformation is bent slightly along the imine nitrogens. Though unexpected in this case, complexes of this form are known in the literature. In particular, Soloshonok and Ueki described binuclear Ni(II) complexes derived from picolinic acid and *N*-benzylproline that adopt a strikingly similar puckered conformation.[5] Notably, those complexes were not observed to be paramagnetic, allowing for ^{1}H-NMR characterization. It is almost certainly the case, then, that the crystalline material I isolated does not represent the entire population of Ni species in the clearly paramagnetic initiator mixture. Unfortunately, the crystals rapidly physically degraded once removed from solvent, likely due to escape of THF from the crystal lattice, complicating sample handling. Coupled with low yields, this rendered isolation of suitable amounts of crystalline material for NMR analysis or test polymerizations impractical.

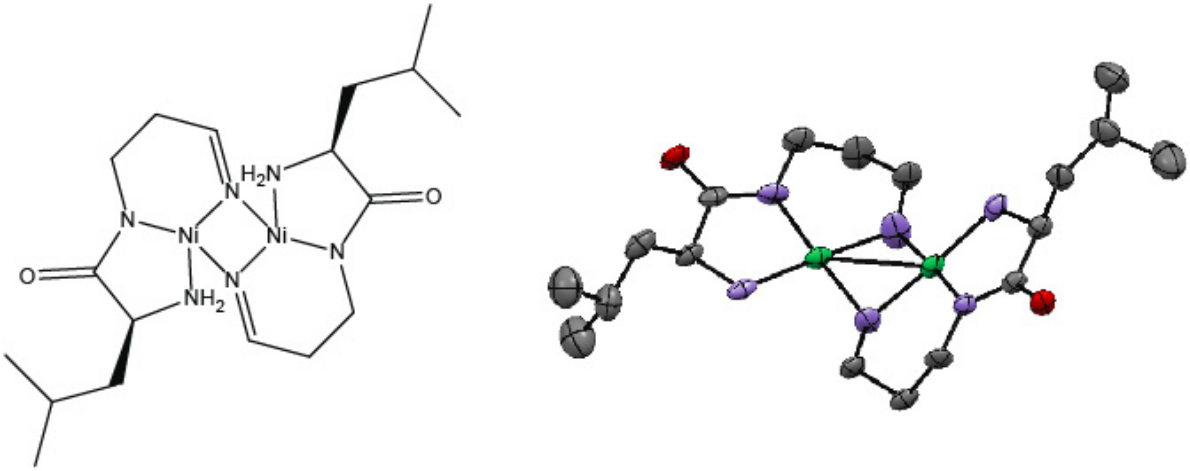

Figure 5.4. Solid state structure of an unexpected complex crystallized during attempted synthesis of NCA initiator **5.2**. Grey, purple, green, and red ellipsoids represent carbon, nitrogen, nickel, and oxygen, respectively. H atoms omitted, ellipsoids at 50% probability. Schematized structure depicted at left. CCDC 1819997.

These results raised a few concerns for further initiator development. Although the observed binuclear complex might not account for the majority of the Ni in the initiator mixture, the possibility that it might still be a competent initiator complicates our understanding of the overall polymerization mechanism and products. Canonically, transition metal-mediated NCA polymerization proceeds via the N-terminal derived metal amide; it is unclear whether the corresponding amine would serve the same purpose. The identity of the resulting C-terminal end group is therefore also unclear, although the absence of an azide renders this point somewhat irrelevant. Notably, formation of the bridging imine structure via reaction of the azide might only be possible due to the length of the arbitrarily-chosen propyl linker, which allows for formation of an energetically-favorable six-membered ring. With this in mind, I designed an alternative initiator structure in the hope that azide loss was driven by this coincidence and not by inherent reactivity of the azide with the Ni center.

5.4 Attempted synthesis and characterization of the azidophenylalanine-derived Ni(II) amido-amidate 5.6.

A variety of azide-functionalized amino acids are commercially available due to significant interest in incorporating unnatural amino acids into proteins for biological studies.[11] I therefore chose to base the redesigned initiator core on azidophenylalanine, a commercially available azide-bearing starting material. Due to the geometry and rigidity of the aryl side chain, I hypothesized that intramolecular azide reactivity would be unfavorable with this ligand. Synthesis of the alloc-protected intermediate was achieved analogously to the reported synthesis of **5.1**, beginning with base-mediated formation of the carbamate using allyl chloroformate (Scheme 5.4).[3] As no additional C-terminal functionality was necessary, I chose to block the carboxylic acid as the theoretically-inert isoamyl amide to give the pro-ligand **5.5**.

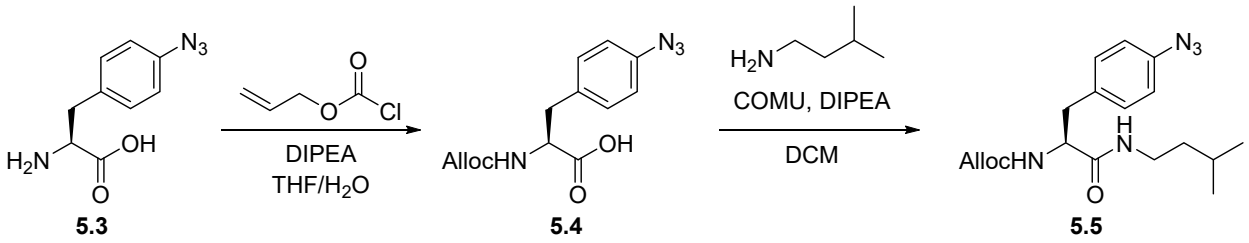

Scheme 5.4. Synthetic route for N_α-alloc-azidophenylalanine isoamyl amide **5.5**.

I reacted **5.5** with a freshly-made solution of bpyNi(COD) using the usual initiator formation conditions, again analyzing the reaction at various points for signs of azide retention (Scheme 5.5). Unfortunately, while **5.5** again gave a clear azide peak by FTIR-ATR (Fig. 5.5a), again no azide was observed during direct analysis of the initiator solution (Fig. 5.5b). This remained true for an aliquot of the initiator solution that was subjected to acidic aqueous workup (Fig. 5.5c). Attempts to crystallize Ni complexes from the initiator solution have been unsuccessful to date. While characterization of the products formed during attempted synthesis of **5.6** remain incomplete, it seems probable that the azide functional group is incompatible with Ni, and particularly Ni(0), under the elevated temperatures necessary to generate viable NCA initiator solutions.

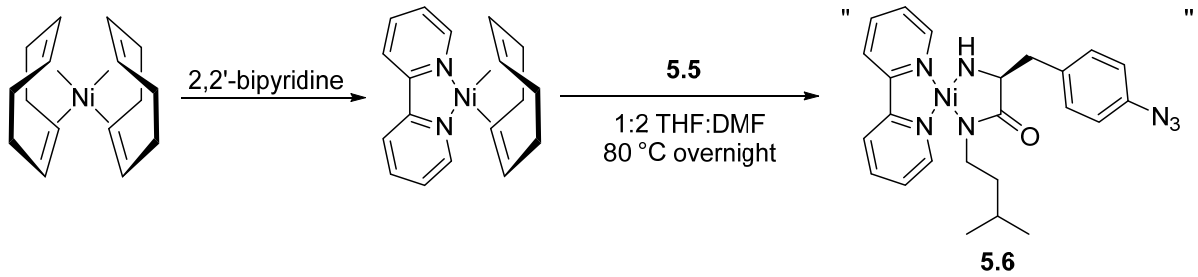

Scheme 5.5. Synthetic route for the attempted synthesis of Ni(II) amido-amidate NCA initiator **5.6**, adapted from the attempted syntheses of compounds **2.4** and **5.2**.

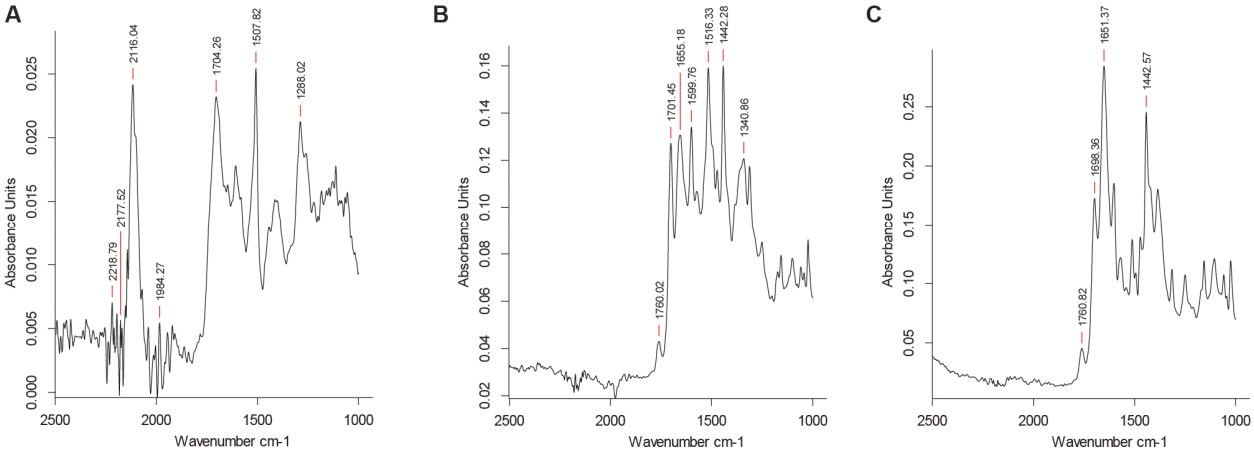

Figure 5.5. FTIR-ATR spectra demonstrating loss of azide during the attempted synthesis of initiator **5.5**. A) Alloc-azidophenylalanine *i*-amyl amide. B) Initiator solution. C) Initiator after acidic aqueous workup.

5.5 Synthesis and crystallization of a leucine isobutyl amide initiator

Concurrent with my attempts to optimize azide-functionalized initiators, I also attempted to further characterize simpler complexes similar to those reported by Deming et al.[2] By removing the reactive azide, I reasoned that I might gain additional insight into the nature of the putative Ni(II) amido-amidate initiators. Synthesis of N_α-alloc-leucine isobutyl amide was achieved analogously to the azidopropyl amide via COMU coupling of isobutylamine with N_α-alloc-leucine; subsequent reaction with a solution of bpyNi(COD) at 80 °C in the usual manner again afforded an orange solution that was capable of initiating NCA polymerization (Scheme 5.6). Interestingly, dilution of the solution with THF or diethyl ether again resulted in precipitation of a pale solid. Orange crystals formed from the initiator solution upon standing for several days in a N_2-filled glovebox, which were of sufficient quality for XRD analysis.

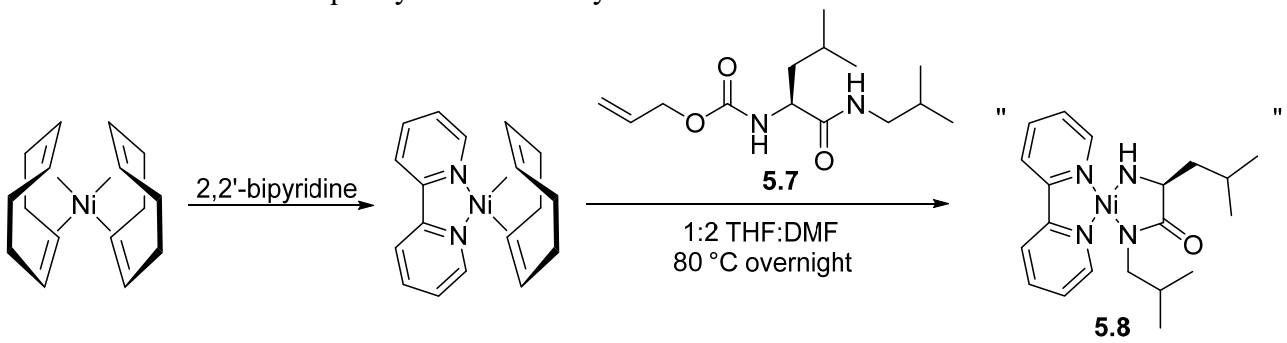

Scheme 5.6. Synthetic route for the attempted synthesis of Ni(II) amido-amidate NCA initiator **5.8**.

The observed structure differed significantly from both the expected product and the binuclear complex observed with the azidopropyl amide initiator (Fig. 5.6). Although the structure was a square planar complex, I again did not observe the bpy ligand. Instead, the Ni(II) center was unexpectedly coordinated to two leucine isobutyl amide ligands. Again, the amines were datively bound as neutral ligands rather than as the metal amides, while the amides were bound as the anionic amidates. Because a 1:1 ratio of Ni to N_α-alloc-leucine isobutyl amide was used during initiator synthesis, the observation of this particular structure implies that other Ni species, likely in the Ni(0) oxidation state, must exist in the initiator solution. This is consistent with the observation that the initiator complex again appeared to be paramagnetic by NMR, despite the fact that similar square planar amino-amidate Ni(II) complexes are known to be diamagnetic.[4] Although all crystallization experiments were performed under air-free conditions in a N_2-filled glovebox, it remains unclear whether the observed structures represent decomposition products that form over the course of several days or if they are relevant products of the initiator synthesis. Again, NMR analysis and accurate sample weighing of the crystalline material was not practical due to low yields; however, polymerization of a solution of alanine NCA was observed upon addition of several morphologically similar, THF-rinsed orange crystals that were manually isolated from the crystallization vial (Fig. 5.7). It is therefore possible that this species represents one of several viable initiating complexes present in the initiator solution.

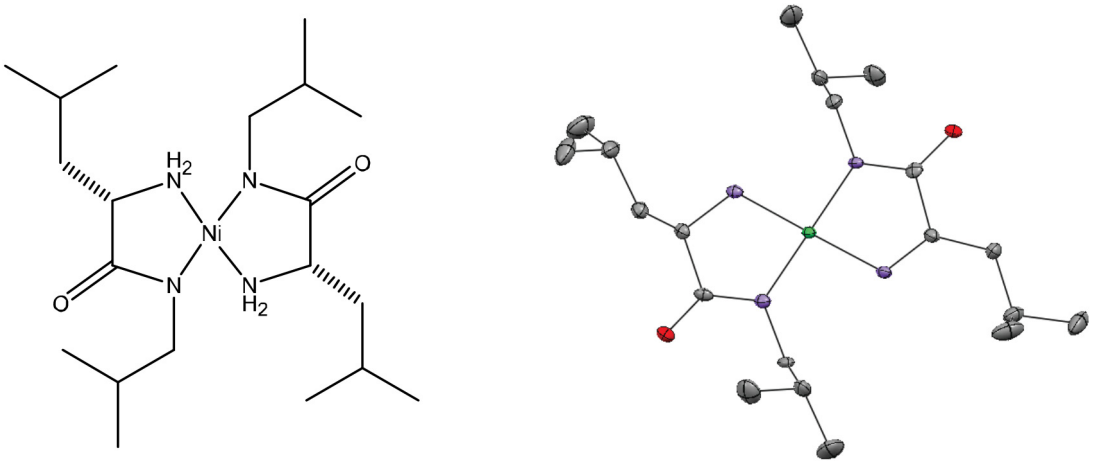

Figure 5.6. Solid state structure of an unexpected complex crystallized during attempted synthesis of NCA initiator **5.8**. Grey, purple, green, and red ellipsoids represent carbon, nitrogen, nickel, and oxygen, respectively. H atoms omitted, ellipsoids at 50% probability. Schematized structure depicted at left. CCDC 1819996.

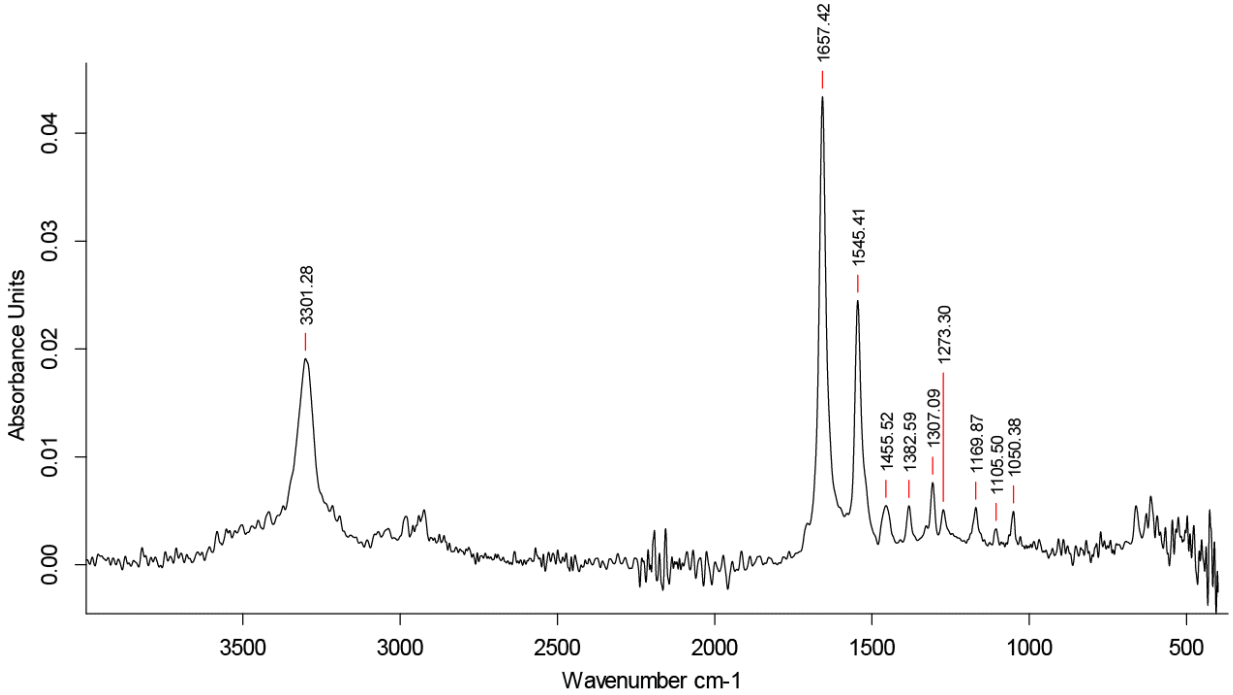

Figure 5.7. FTIR-ATR analysis of an alanine NCA polymerization reaction, initiated using the crystalline material depicted in Fig. 5.6. No NCA peaks around 1790 and 1850 cm^{-1} are observed, suggesting total consumption of the starting material. A prominent peak at 1660 cm^{-1}, corresponding to an amide carbonyl stretch, indicates formation of a peptide product.

5.6 Synthesis of Ni(II) amino-amidates as potential NCA initiators

Interestingly, literature precedent exist for the synthesis of amino-amidate Ni(II) complexes by a relatively mild route.[4] Although I was unsure of the relevance of these structures in the context of the Deming group's NCA initiator solutions, I decided to intentionally synthesize some of these

complexes in the hopes that I might be able to obtain azide-functionalized initiators. In their work, Escorihuela et al. reported benzyl amide-based complexes derived from a variety of amino acids, including phenylalanine.[4] Therefore, rather than proceeding through the azidopropyl amide, which requires synthesis and handling of a volatile organic azide, I aimed to make complexes derived from *p*-azidophenylalanine benzyl amide. Ligand synthesis using either amino acid was easily achieved via COMU coupling of benzyl amine to the boc-protected amino acid (Scheme 5.6). Acidic deprotection, followed by treatment with aqueous sodium hydroxide, afforded the free amine. Escorihuela et al. formally reported the synthesis of their complexes via refluxing of the ligand with Ni(II) acetate in methanolic potassium hydroxide. However, in their manuscript they also note that XRD-quality crystals were grown via slow evaporation from the reaction solution, presumably at ambient temperature. Because I had previously observed azide reduction in the presence of Ni at elevated temperatures, I focused my efforts on the latter strategy.

Indeed, mixing a green solution of nickel acetate and either ligand with methanolic potassium hydroxide reliably induced the formation of orange crystals over the course of minutes to hours depending on reaction concentration. Oddly, the isolated crystals were extremely insoluble in all solvents tested, despite the fact that NMR spectra and optical rotation measurements of the phenylalanine complex are reported in methanol.[4] Attempts to synthesize the complexes under refluxing conditions similarly yielded orange insoluble powder, stymying NMR and MS analyses and suggesting that the observed product might differ from the structure reported in the literature.

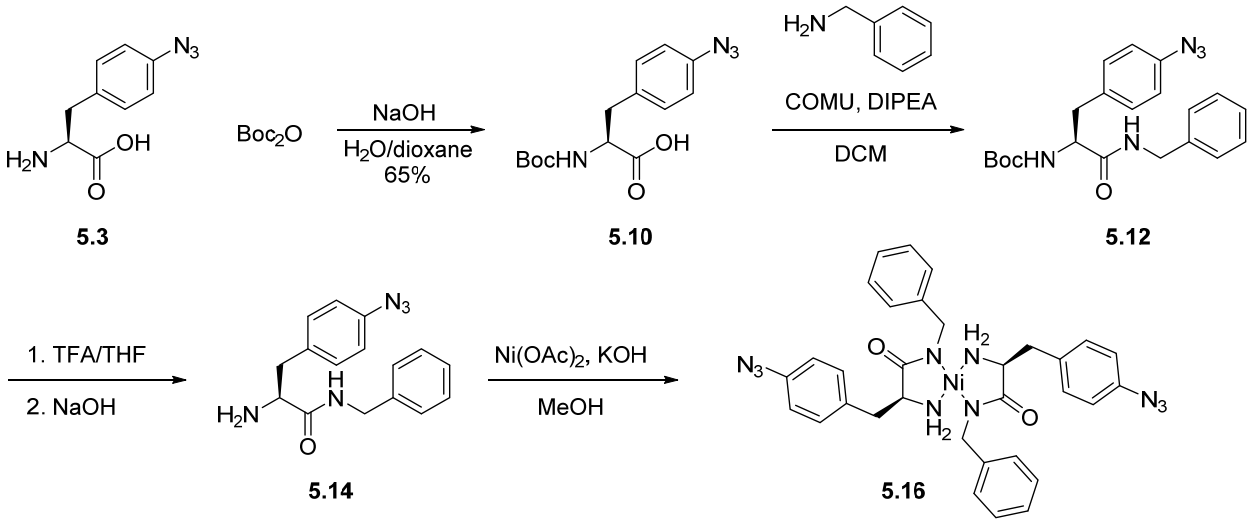

Scheme 5.7. Synthetic route to a Ni(II) amino-amidate complex, based on the work of Escorihuela et al.[4]

As I had hoped, I was able to observe an azide IR peak by FTIR-ATR, suggesting that the functional group is in fact stable to Ni(II) at room temperature (Fig. 5.8a). Although the crystalline material was not sufficiently soluble to prepare stock solutions at useful concentrations for NCA polymerization, addition of a small amount of the solid directly to a solution of Ser(Man2) monomer resulted in possible observed polymerization by FTIR-ATR after 12 hours (Fig. 5.8b). Additional characterization and experimentation will be necessary to fully determine whether this class of Ni(II) amino-amidates can act as effective initiators of NCA polymerization.

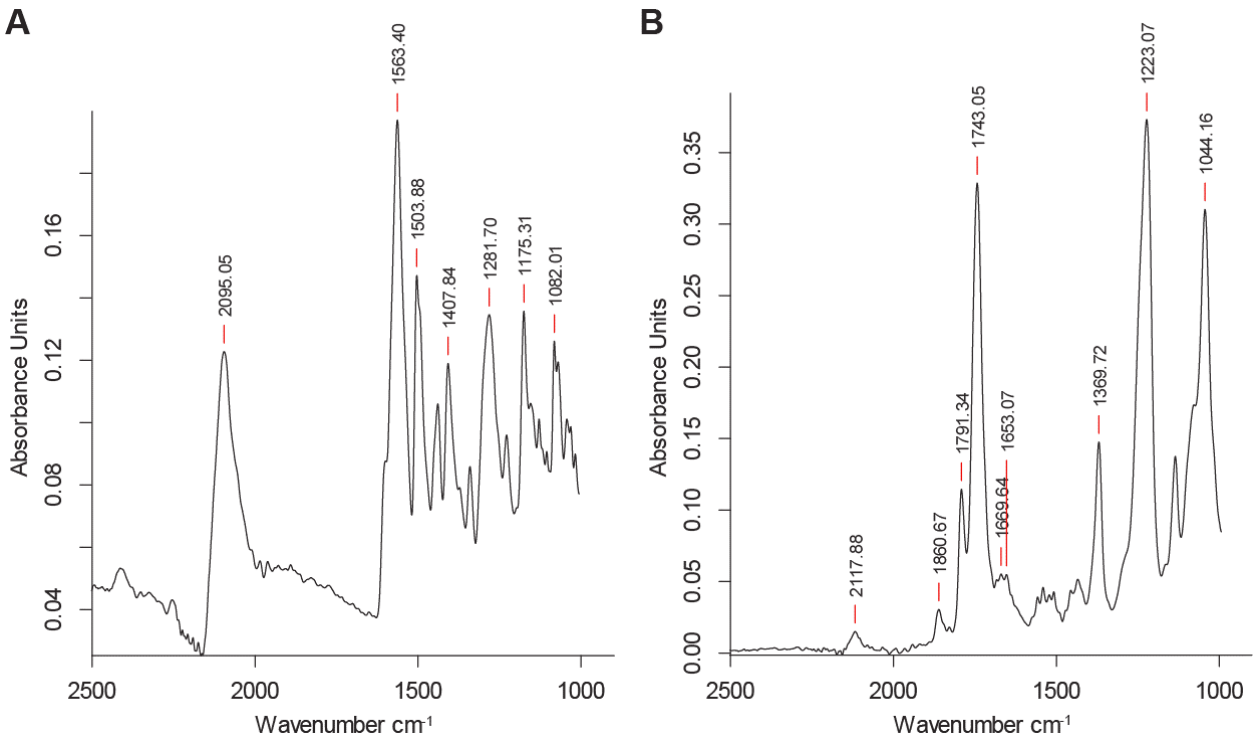

Figure 5.8. FTIR-ATR spectra of A) complex **5.16**, showing a clear azide peak around 2100 cm^{-1}, and B) a small-scale reaction in which crystalline **5.16** was added to a solution of Ser(Man2) NCA **2.3d**, showing possible amide signals around 1650 cm^{-1} indicating some degree of polymerization, as well as peaks at 1860 and 1740 cm^{-1} corresponding to unreacted NCA monomer. Notably, an azide peak at 2100 cm^{-1} remains clearly visible, suggesting that the functional group tolerates polymerization conditions and the presence of the Ni(II) complex.

5.7 Exploration of primary amines as initiators

The primary benefits of Ni and Co complexes are their rapid initiation kinetics, which improves polymer chain length dispersity, and short overall reaction times.[1] However, they require rigorous air-free conditions and often must be freshly prepared and immediately used, which limits scale-up potential. Furthermore, transition metals can introduce downstream toxicity concerns if the polypeptide products are to be used for therapeutic applications.[12] In light of the additional complications I encountered attempting to characterize and optimize Ni-based transition metal initiators, it seemed worth examining other initiator platforms for comparison. Although we had previously claimed the first successful polymerization of O-glycosylated NCA monomers, to the best of my knowledge other initiator systems had not been tested in combination with the improved monomer purification techniques that were key to our earlier success. As a starting point, I decided to investigate nucleophilic amines, the most common class of NCA initiators used in the field.

As an initial test, I tested whether or not T785 amine **4.2**, which I had on hand as a pure solid, could initiate polymerization. This amine was also an interesting potential initiator because it would allow for C-terminal installation of the biologically active T785 moiety without the need for an azide or any other post-polymerization conjugation reactions. For comparison, the maleimide conjugation strategy I described in Chapter 3 required installation of an N-terminal

thiol by reaction with a thioester NHS ester and subsequent nucleophilic deprotection, followed by reaction with the T785 maleimide, which is prepared in one step from **4.2** (Scheme 4.1). Direct T785 conjugation at the time of polymerization would therefore save three conjugation steps while introducing a reactive N-terminal amine that would avoid the need for azide functionalization for applications requiring additional functionalization. ^{1}H-NMR analysis of the crude product obtained upon mixing the amine with one equivalent of Ser(Man2) NCA confirmed that ring opening primarily occurred via attack by the primary amine and not through reaction with the aryl amine or aromatic ring nitrogens (Fig. 5.9). This gave me hope that I would be able to use T785 amine to synthesize glycopolypeptides bearing the C-terminal TLR7/8 agonist in a single reaction step, with predictable end group chemistry and essentially 100% functionalization.

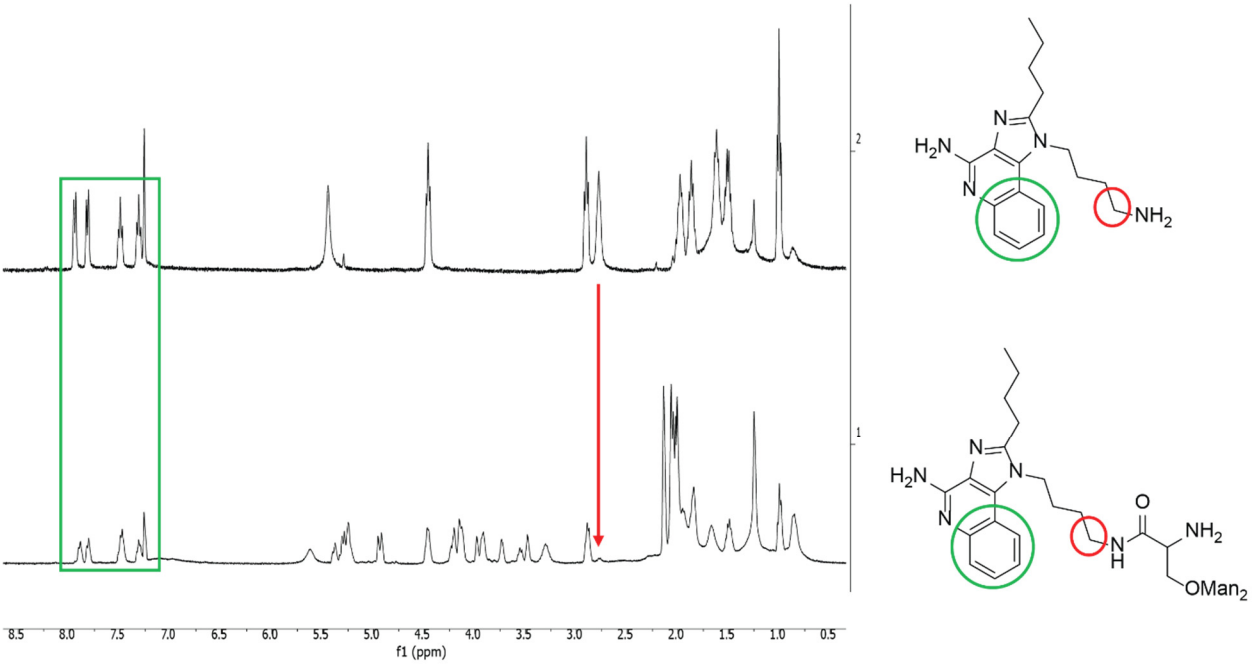

Figure 5.9. ^{1}H-NMR analysis of a 1:1 reaction of T785 amine **4.2** with mannobiose-serine NCA to confirm reactivity and determine the preferred site of reaction. The unreacted amine (top) exhibits key peaks at 2.78 ppm (red) and above 7.25 ppm (green) corresponding to the two protons alpha to the amine and to the aromatic protons, respectively. Overnight reaction with NCA monomer (bottom) results in almost complete disappearance of the 2.78 ppm signal, but little change to the aromatic protons, suggesting amide coupling via the primary amine.

Given that result, I attempted to synthesize a 65% glycosylated α-mannobiose-serine:alanine:glutamate polymer using a 1:100 initiator:monomer ratio to see if the amine was an effective initiator for polymerization and in the hopes that I would be able to compare the resulting polymer directly against the previous maleimide conjugate **4.6**. Gratifyingly, I found that the amine was again capable of initiating polymerization despite the higher M:I. Although FTIR monitoring indicated that the reaction required several days for complete monomer consumption, comparison to literature amine initiation protocols suggested that this reaction time scale was not unusual.[1, 13-14] Side chain deprotection, followed by purification via size exclusion techniques, afforded a white solid that exhibited ^{1}H-NMR peaks consistent with an approximately 1:100 T785:amino acid ratio

(Fig. 5.10). To the best of my knowledge, this result demonstrated for the first time that O-glycosylated NCA monomers can be polymerized using primary amine initiators.

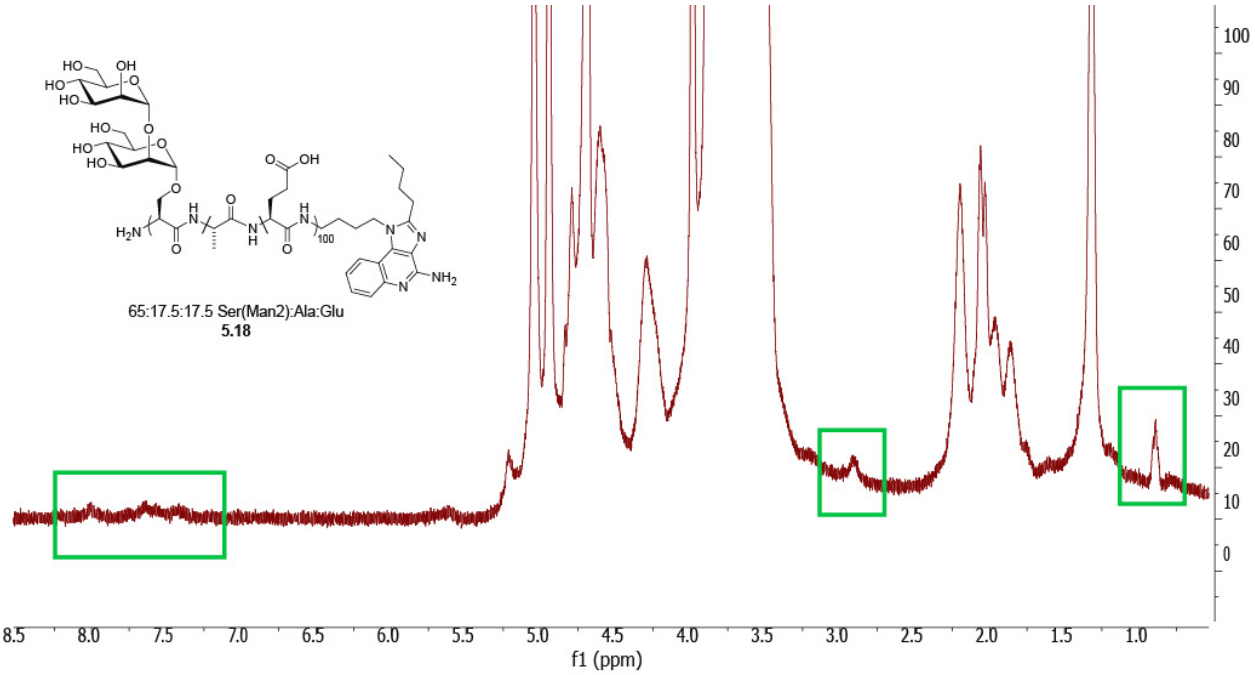

Figure 5.10. ^{1}H-NMR spectrum of purified glycopolypeptide **5.18** obtained using T785 amine **4.2** as the initiator. The areas indicated in green represent peaks associated with the TLR agonist. A 65:17.5:17.5 ratio of Ser(Man2):alanine:*t*-butyl glutamate NCA monomers and 1:100 initiator:monomer ratio were used for this reaction to allow for comparison of the product to the maleimide-based conjugate **4.6**.

Because the two T785 conjugation strategies install the TLR agonist at different ends of the chain using different linker chemistries, it was not safe to assume that the "direct conjugate" obtained using the amine initiator would activate immune cells to the same extent as the maleimide conjugate. Indeed, while the new glycopolypeptide conjugate did induce some TNFα and low levels of IL-12p40 in murine monocyte cultures, it was significantly outperformed by the maleimide conjugate. Furthermore, no detectable IL-12p70 was observed even at fairly high glycopolypeptide concentrations. Although additional experiments will be necessary to account for this discrepancy, it is likely that the different linker length might impact TLR binding. Research in antibody-drug conjugates has generated a significant amount of literature suggesting that even seemingly small changes in linker length, rigidity, and hydrophobicity can significantly impact biological outcomes in the context of macromolecular therapeutics.[15-16] Because of the step efficiency conferred by the direct conjugation approach, as well as the known hydrolytic instability of maleimide-based linkages in serum,[17-18] SAR studies on the structure of the amine, and particularly the linker, may be a fruitful area of investigation moving forward.

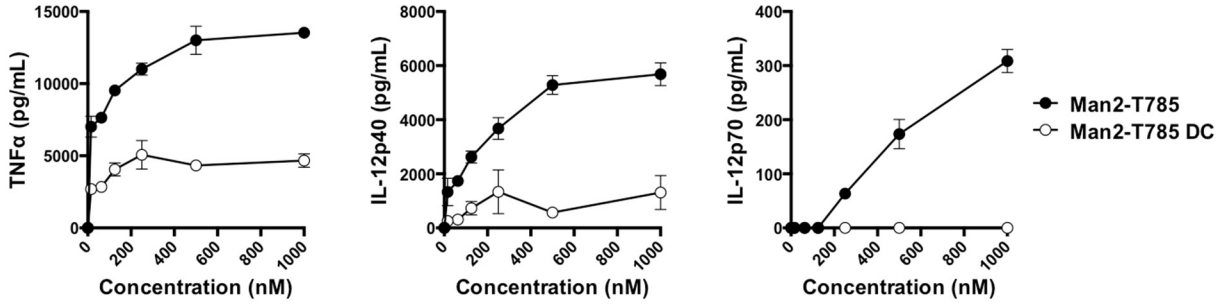

Figure 5.11. Comparison of cytokine expression *in vitro* using T785-conjugated glycopolypeptides **5.18** and **4.2**. Murine monocytes were isolated and incubated with tumor-conditioned media to induce a TAM-like phenotype prior to exposure to varying concentrations of agonists. Cytokine expression was detected by ELISA. Conjugate **4.2** (Man2-T785, black) induced robust cytokine expression as previously observed (Fig. 4.4). In contrast, **5.18** (Man2-T785 DC, white) induced some TNFa release, but low IL-12p40 expression and no detectable IL-12p70. Treatments were conducted in duplicate, error bars represent the standard error of the mean.

Although the T785 amine may be suitable for bypassing the need for an azide handle when TLR7/8 activation is desired, not all applications will be amenable to such an approach. Dual chain end modification with reactive chemical handles is therefore still an attractive goal for the amine-initiated NCA glycopolypeptide platform. Fortunately, amines are generally compatible with organic azides under mild conditions. Along these lines, azidophenylalanine benzyl amide was an obvious experimental initiator, given that I had already synthesized the compound during the course of my Ni(II) initiator experiments. I was pleased to find that two test reactions, representing a Ser(Man2) homopolymer (M:I = 20:1) and a 65% glycosylated polypeptide (M:I = 100:1, 65:17.5:17.5 Ser(Man2):Ala:Glu) went to completion over the course of several days, similar to the T785 amine-initiated reactions. Unlike any of the Ni(II)-derived polymers, the amine-initiated glycopolypeptides gave faint but detectable azide signals by IR (Fig. 5.12). Furthermore, the aryl groups provided a distinct group of ^{1}H-NMR peaks that allowed for length quantification of the shorter polymer at approximately 17 residues long on average. While quantitation for the 100mer target length polymer was less reliable due to low signal:noise of the end group peaks, integration of the end group peaks relative to the mannobiose anomeric proton peaks gave a calculated length of 97 residues.

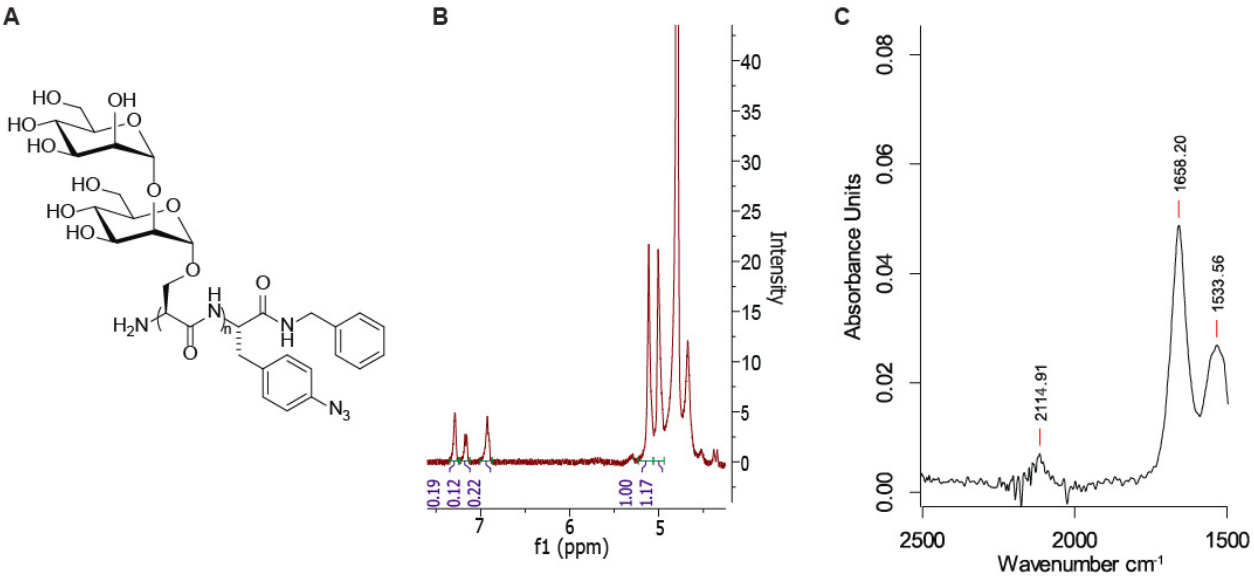

Figure 5.12. ^{1}H-NMR and FTIR analysis of a Ser(Man2) glycopolypeptide of 20 residue target length, polymerized using azidophenylalanine benzyl amide. A) Theoretical structure of the glycopolypeptide, showing the repeating monomer structure and azidophenylalanine benzyl amide end group. B) ^{1}H-NMR demonstrated the presence of aryl peaks around 7 ppm, likely corresponding to the desired end group. Integration of these peaks relative to the two anomeric proton peaks around 5 ppm suggested an average degree of polymerization of approximately 17 residues. C) FTIR of the glycopolypeptide, showing the amide peak around 1660 cm^{-1} as well as a peak around 2110 cm^{-1} that likely corresponds to the aryl azide. The relative peak areas reflect the approximately 20:1 ratio of polypeptide backbone amide bonds compared to azide end groups.

To provide additional evidence for the presence of the key reactive azide, I reacted the approximately 17-residue homopolymer with a cyclooctyne-functionalized Cy5 dye. After extensive purification by a combination of spin filtration, NAP-25 size exclusion chromatography, and ethanol trituration to remove excess dye, I analyzed the vibrantly blue samples by fluorescence at 646 nm in plate reader format. Comparison of glycopolypeptide fluorescence with a standard curve of free dye gave a calculated degree of functionalization of 80%, much higher than the ~1-2% functionalization observed when polymerizing with transition metal initiators. Taken together, the various analyses demonstrated a high degree of azide end group functionalization. Unfortunately, rigorous determination of molar mass dispersity for the amine-initiated glycopolypeptides by GPC was not possible at the time due to technical issues. If future experiments demonstrate relatively low molar mass dispersities by this approach, nucleophile-based initiation strategies will likely prove to be a key strategy for synthesizing dual end-labeled glycopolypeptides.

As a side note, a commercial amino-PEG$_4$-azide, used without additional purification, failed to efficiently polymerize NCAs. TLC analysis revealed the presence of at least one contaminating species, raising the possibility that a high degree of amine purity might be necessary for initiation. Because the PEG$_4$ amine is a highly polar, viscous liquid and therefore difficult to handle and purify, I elected to focus my attention on azidophenylalanine at the time instead. However, given that aryl azides are known photocrosslinking functional handles, and due to the relatively high cost of azidophenylalanine, alternative primary amine initiators should be pursued in the future. In

particular, relatively simple structures such as 4-(azidomethyl)benzylamine may be sufficient to combine ease of synthesis and handling with acceptable initiation rates, desired end group functionality, and a distinctive ^{1}H-NMR signature to aid in product characterization.

5.8 Summary and Outlook

Among the key features of the glyco-NCA platform is the ability to make end-functionalized glycopolypeptides to allow for conjugation to targeting agents, surfaces, small molecules, and other substrates of interest. Towards this end, reliable end-functionalization is key for the technology to be of practical use. Although our work in Chapter 2 demonstrated that transition metal initiators are effective at producing low dispersity glycopolypeptides, I found that the end-functionalization strategy using Ni(II) initiators lacking due to a fundamental incompatibility of azides with Ni under the initiator synthesis conditions. During the course of my experiments, I attempted to obtain clear structural characterization of a variety of Ni(II) initiators and worked towards developing an improved initiator design. Until structural characterization of a Ni(II) amido-amidate species can be obtained and the corresponding complex isolated in rigorously pure form, it may be wise to assume that the initiator solution generated by the Deming route consists of a mixture of Ni(II) and possibly Ni(0) complexes. Further work with Ni(II) amino-amidate complexes may also provide insight into alternative transition metal initiator structures for dual-end functionalization. Changing the desired reactive handle from an azide to other moieties may also improve compatibility with the Ni center, and is an ongoing research focus in the Bertozzi lab.

With that said, transition metal-free strategies for NCA polymerization look to be a promising direction in the future, particularly for therapeutic applications in which synthetic scalability and avoidance of transition metals are preferred. My initial experiments suggest that primary amines are capable of initiating NCA polymerization for glycosylated monomers, and optimization of primary amine scaffolds may prove fruitful. However, because unmodified amines afford relatively slow polymerization kinetics, and because molar mass dispersities were not determined for the first batch of amine-polymerized glycopolypeptides, we are continuing to explore alternative initiation strategies based on modern NCA polymerization technologies. Current areas of research include investigation of thiourea-based hydrogen-bond donors designed to activate NCA monomers,[19] Lewis acid catalysis to achieve a similar effect, and synthesis of highly reactive nucleophiles, e.g. via silylamines.

5.9 Materials, methods, and syntheses of new compounds

General Materials and Methods

Unless stated otherwise, reactions were conducted in oven-dried glassware under an atmosphere of nitrogen using anhydrous solvents. Tetrahydrofuran (THF) and dichloromethane (DCM) were purified by first purging with dry nitrogen, followed by passage through columns of activated alumina. Anhydrous *N*,*N*-dimethylformamide (DMF) was purchased and stored over activated 4 Å molecular sieves. Deionized water was purified to 18 MΩ-cm using a Millipore Milli-Q Biocel A10 purification unit. All commercially obtained reagents were used as received without further purification unless otherwise stated. Polymerizations were conducted as described in Chapter 2.

Flash chromatography was performed using Silicycle SiliaFlash P60 silica gel. Analytical thin layer chromatography was performed using glass-backed Analtech Uniplate silica gel plates containing a fluorescent indicator, and visualized using a combination of UV, anisaldehyde, $KMnO_4$, H_2SO_4, ninhydrin, and phosphomolybdic acid staining. NMR spectra were obtained on Varian spectrometers at room temperature at the Stanford Department of Chemistry NMR Facility. NMR spectra are reported relative to residual solvent signals. Data for ^1H NMR spectra are reported as follows: chemical shift (δ ppm), multiplicity, coupling constant (Hz) and integration. Splitting patterns are designated as follows: s, singlet; d, doublet; t, triplet; q, quartet; m, multiplet; br, broad. Data for ^{13}C NMR spectra are reported in terms of chemical shift. High-resolution mass spectrometry was performed at the Stanford University Mass Spectrometry core facility. All attenuated total reflectance (ATR) Fourier Transform infrared (FTIR) samples were recorded on a Bruker Alpha spectrometer. 384-Well black flat-bottom plates were purchased from Corning and fluorescence readings taken using a Molecular Devices SpectraMax i3x plate reader. TNFα, IL-12p40, and IL-12p70 ELISA kits were purchased from eBiosciences. ELISA assays are absorbance-based and were read using a Molecular Devices SpectraMax i3x plate reader. Mouse Monocyte Enrichment Kit was purchased from STEMCELL Technologies. Procedures used to harvest murine monocytes were approved by the Institutional Animal Care and Use Committee of Stanford University. Cell culture and ELISA protocols were performed as described in Chapter 3. XRD was performed at the Stanford University Nano Shared Facilities X-ray Lab on a Bruker D8 Venture using a Mo source; structures were solved by Dr. Jana Maclaren.

N-terminal glycopolypeptide labeling for analysis of azide functionalization

Cy5-DBCO was obtained from Click Chemistry Tools (Product number A130, 1211.60 Da as the triethylammonium salt) and dissolved to 10 mg/ml in DMSO. Glycopolypeptides were dissolved in 1× PBS at 1-10 mg/ml and reacted with a 5-10 fold excess of the Cy5-DBCO reagent at ambient temperature overnight. Samples were protected from light using aluminum foil. The bright blue reaction mixtures were purified using 0.5 ml centrifuge spin filters (3 kDa MWCO), washing with Milli-Q water at least two times after observation of a colorless filtrate. For additional removal of potential dye aggregates, samples were also purified by NAP-25 column, eluting with Milli-Q water, when indicated. Concentrated samples were lyophilized to yield blue fluffy solids. Where indicated, samples were further purified by trituration with ethanol, followed by removal of excess ethanol under vacuum, dissolution in minimal water, and lyophilization.

Generalized initiator synthesis protocol for putative Ni(II) amido-amidate species

The general initiator synthesis protocol was adapted from a previous publication.[3] Inside a dinitrogen filled glovebox, $Ni(COD)_2$ (2-15 mg, 1.0 equiv.) was dissolved to 145.5 mM in THF in a vial. Phosphine or amine ligand (1.0 equiv.) was added to the bright yellow $Ni(COD)_2$ solution, and the mixture was allowed to incubate for 10 minutes – 1 hour to allow for ligand displacement. The appropriate N_α-alloc-amino acid amide (1.0 eq) was then added as 72.75 mM solution in DMF. The resulting solutions were transferred to a pressure vessel, sealed, removed from the glovebox, and placed in an oil bath at 80 °C. After 12-16 hours at 80 °C, vessels were cooled to room

temperature and returned to the glovebox. The resulting initiator solutions were used directly in NCA polymerization reactions and/or analyzed as described above.

Crystallization and XRD analysis of a Ni(II) complex from the initiator solution corresponding to 5.2

Following synthesis of the orange initiator solution as described above, an aliquot was removed for XRD analysis. In a N_2-filled glovebox, the orange 1:2 THF:DMF solution was diluted ~25% with dry, N_2-purged THF, resulting in the observed precipitation of a white or off-white solid. The mixture was filtered through a 0.2 μm syringe filter and concentrated slightly *in vacuo*. The process was repeated several additional times, before transfer of the filtered solution to a clean 1 ml vial. Several orange crystals suitable for X-ray diffraction studies were obtained by vapor diffusion using THF as the countersolvent. These crystals were observed to physically decompose upon removal from THF; we hypothesize that this was due to evaporation of THF from the crystal lattice. CCDC 1819997.

Crystallization and XRD analysis of a Ni(II) complex from the initiator solution corresponding to 5.8, and test polymerization of Ala using isolated crystals

Following synthesis of the orange initiator solution as described above, an aliquot was removed for XRD analysis. Although vapor diffusion conditions were tested for crystallization, higher-quality crystals formed around the solvent line upon allowing the capped 1:2 THF:DMF solution to stand for several days. The excess solution was removed and the crystals washed briefly with THF prior to analysis. Crystals that were not used for XRD analysis were transferred to a microscope slide, and several morphologically-similar crystals were collected and transferred to a THF solution of ~2 mg alanine NCA (50 mg/ml). The reaction mixture was analyzed by FTIR-ATR after overnight incubation in a N_2-filled glovebox at ambient temperature. CCDC 1819996.

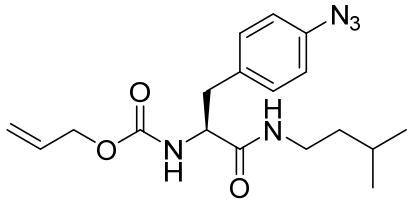

Allyl (S)-(3-(4-azidophenyl)-1-(isopentylamino)-1-oxopropan-2-yl)carbamate, 5.5

Azidophenylalanine (0.302 g, 1.46 mmol, 1 equiv.) was suspended in 25 ml dry THF. Allyl chloroformate (0.169 ml, 1.6 mmol, 1.134 g/ml, 1.1 equiv.) and DIPEA (2.77 ml, 1.6 mmol, 0.742 g/ml, 1.1 equiv.) were then added to the stirring mixture. Deionized water was slowly added until all solid had dissolved. After two hours, additional portions of allyl chloroformate (0.08 ml) and DIPEA (0.15 ml) were added to the stirring reaction, which was allowed to proceed until no starting amino acid remained by TLC analysis (ninhydrin stain) to give alloc-azidophenylalanine **5.4**. To the reaction mixture were added isoamyl amine (0.84 ml, 7.24 mmol, 0.751 g/ml, 5 equiv.), an additional portion of DIPEA (0.757 ml, 4.35 mmol, 0.742 g/ml, 3 equiv.), and COMU (1.24 g, 2.90 mmol, 2 equiv.). The reaction was allowed to proceed overnight. The reaction mixture was added to a separatory funnel along with EtOAc and 1 M HCl, and the organic fraction washed with two additional portions of 1 M HCl, followed by three portions of saturated sodium bicarbonate.

The organic fraction was dried over $MgSO_4$, filtered, and concentrated, and then purified by column chromatography to give an off-white solid. ^{1}H NMR (400 MHz, $CDCl_3$) δ 7.19 (d, J = 7.4 Hz, 2H), 6.96 (d, J = 7.9 Hz, 2H), 5.88 (dd, J = 15.3, 9.2 Hz, 1H), 5.58 (s, 1H), 5.38 – 5.14 (m, 2H), 4.67 – 4.48 (m, 2H), 4.27 (d, J = 7.5 Hz, 1H), 3.18 (s, 2H), 3.03 (qd, J = 13.8, 6.9 Hz, 2H), 1.43 (dd, J = 13.5, 6.9 Hz, 1H), 1.33 – 1.18 (m, 2H), 0.86 (d, J = 6.2 Hz, 6H). FTIR-ATR ν_{max}/cm^{-1} 2922.82, 2116.04 (azide stretch, s), 1704.26 (carbamate C=O stretch, s), 1507.82.

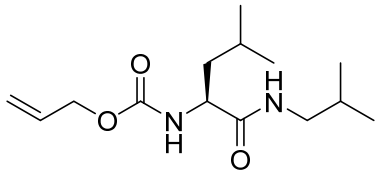

Allyl (S)-(1-(isobutylamino)-4-methyl-1-oxopentan-2-yl)carbamate (N_α-alloc-leucine isobutyl amide, 5.7)

N_α-alloc leucine (1.52 g, 7.06 mmol, 1 equiv.) was dissolved in 50 ml DCM in an oven-dried 100 ml round-bottom flask with stir bar. COMU (6.03 g, 14.1 mmol, 2 equiv.) was added, followed by DIPEA (3.66 ml, 21.1 mmol, 0.742 g/ml, 3 equiv.). The red solution was allowed to stir for one minute before the addition of isobutylamine (3.50 ml, 35.3 mmol, 0.736 g/ml, 5 equiv.). Although the reaction was conducted at ambient temperature, cooling is advised in the future as the reaction was observed to be highly exothermic. After overnight reaction, the reaction was transferred to a separatory funnel and washed 3x with 1 M aqueous HCl, 2x saturated $NaHCO_3$, then 1x deionized water. The organic fraction was concentrated and redissolved in diethyl ether, then washed again with 2x saturated $NaHCO_3$, 2x 1 M aqueous HCl, and finally 2x deionized water. The organic fraction, which remained red, was collected, dried over $MgSO_4$, filtered, and concentrated to a red solid. Column chromatography (25-33% EtOAc in hexanes) afforded a light orange solid, which was repeatedly washed with hexanes to give a white solid. ^{1}H NMR (300 MHz, $CDCl_3$) δ 6.38 – 6.18 (m, 1H), 5.88 (ddt, J = 17.3, 10.3, 5.6 Hz, 1H), 5.41 – 5.12 (m, 3H), 4.55 (dd, J = 5.3, 1.9 Hz, 2H), 4.12 (td, J = 7.7, 7.2, 3.3 Hz, 1H), 3.18 – 2.92 (m, 2H), 1.90 (s, 1H), 1.83 – 1.42 (m, 4H), 0.97 – 0.85 (m, 11H). ^{13}C NMR (75 MHz, $CDCl_3$) δ 172.33, 156.28, 132.63, 117.98, 77.58, 77.16, 76.74, 65.98, 53.72, 46.91, 41.54, 28.56, 24.83, 23.01-20.16 (12C).

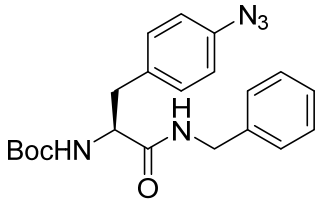

***tert*-Butyl (S)-(3-(4-azidophenyl)-1-(benzylamino)-1-oxopropan-2-yl)carbamate, 5.12**

Boc-protected azidophenyalanine **5.10** (482 mg, 1.57 mmol, 1 equiv.) was dissolved in 25 ml dry dichloromethane. Benzylamine (0.86 ml, 7.84 mmol, 0.981 g/ml, 5 equiv.) was added to the solution, followed by COMU (672 mg, 1.57 mmol, 1 equiv.). DIPEA (272 µl, 1.57 mmol, 0.742 g/ml, 1 equiv.) was added as an additional base. The reaction was allowed to react overnight, then transferred to a separatory funnel. The organic fraction was washed three times with saturated sodium bicarbonate, followed by one wash with water, and then dried over $MgSO_4$, filtered, and

concentrated under reduced pressure. The product was purified by column chromatography (30-50% EtOAc in hexanes) to give a yellow solid that was carried on without further analysis.

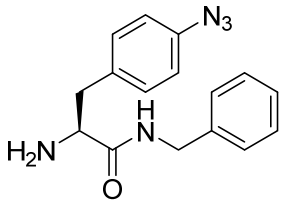

(S)-2-Amino-3-(4-azidophenyl)-N-benzylpropanamide, 5.14

Boc-protected amine **5.12** was dissolved in a 50:50 TFA:DCM mixture and allowed to stand for several hours. The reaction was concentrated, and the residue taken up in a 50:50 mixture of 10% aqueous NaOH and EtOAc. The mixture was transferred to a separatory funnel and the organic fraction washed two additional times with 10% NaOH. The organic fraction was dried over $MgSO_4$, filtered, and concentrated to a yellow residue. The product was precipitated from heptane to give an off-white solid. ^{1}H NMR (400 MHz, $CDCl_3$) δ 8.37 (s, 1H), 8.13 – 8.02 (m, 2H), 7.97 (dd, J = 14.1, 7.7 Hz, 4H), 7.72 (d, J = 7.9 Hz, 2H), 5.31 – 5.08 (m, 2H), 4.40 (dd, J = 8.6, 4.3 Hz, 1H), 3.97 (dd, J = 13.9, 4.2 Hz, 1H), 3.58 (dd, J = 13.8, 8.7 Hz, 1H), 2.15 (s, 2H). ^{13}C NMR (101 MHz, $CDCl_3$) δ 173.83, 138.65, 138.34, 134.47, 130.75 (2C), 128.64 (2C), 127.73 (2C), 127.43, 119.26 (2C), 77.48, 77.15, 76.84, 56.37, 43.14, 40.37.

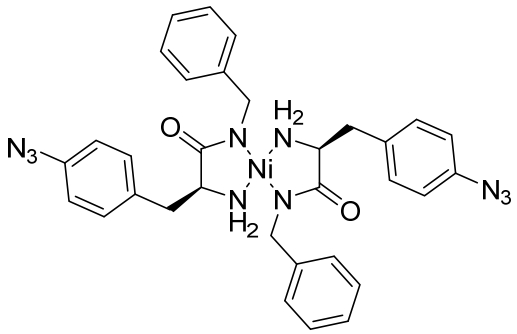

2:1 Ni complex of (S)-2-Amino-3-(4-azidophenyl)-N-benzylpropanamide, 5.16

Syntheses of Ni(II) amino-amidates such as 5.16 were based on the work of Escorihuela et al.[4] Ni(II) acetate tetrahydrate (1 equiv.) and azidophenylalanine benzyl amide (2 equiv.) were dissolved in methanol to give a green solution. To this mixture was added a solution of at least 2 equiv. methanolic KOH, resulting in an immediate color change to give an orange solution. Orange crystals were observed to slowly form in the solution, which were collected by filtration and washing with methanol to give highly insoluble crystalline material. NMR and LC-MS analyses were not feasible due to very low solubility in all tested solvents. FTIR-ATR ν_{max}/cm^{-1} 3311.64, 3287.33, 3069.50, 2095.05 (azide stretch, s), 1563.40 (amidate C=O stretch, s), 1503.88.

5.10 References

1. Cheng, J.; Deming, T. J., Synthesis of polypeptides by ring-opening polymerization of alpha-amino acid N-carboxyanhydrides. *Top Curr Chem* **2012,** *310*, 1-26.

2. Curtin, S. A.; Deming, T. J., Initiators for End-Group Functionalized Polypeptides via Tandem Addition Reactions. *Journal of the American Chemical Society* **1999,** *121* (32), 7427-7428.

3. Kramer, J. R.; Onoa, B.; Bustamante, C.; Bertozzi, C. R., Chemically tunable mucin chimeras assembled on living cells. *Proc Natl Acad Sci U S A* **2015,** *112* (41), 12574-9.

4. Escorihuela, J.; Altava, B.; Burguete, M. I.; Luis, S. V., C2 symmetrical nickel complexes derived from α-amino amides as efficient catalysts for the enantioselective addition of dialkylzinc reagents to aldehydes. *Tetrahedron* **2013,** *69* (2), 551-558.

5. Soloshonok, V. A.; Ueki, H., Design, synthesis, and characterization of binuclear Ni(II) complexes with inherent helical chirality. *J Am Chem Soc* **2007,** *129* (9), 2426-7.

6. Sun, S.; Wu, P., Mechanistic insights into Cu(I)-catalyzed azide-alkyne "click" cycloaddition monitored by real time infrared spectroscopy. *J Phys Chem A* **2010,** *114* (32), 8331-6.

7. Rodrigues, N. V. S.; Cardoso, E. M.; Andrade, M. V. O.; Donnici, C. L.; Sena, M. M., Analysis of Seized Cocaine Samples by using Chemometric Methods and FTIR Spectroscopy. *Journal of the Brazilian Chemical Society* **2013**.

8. *ATR accessories: an overview.* PerkinElmer Life and Analytical Sciences: Shelton, CT, 2004. https://shop.perkinelmer.com/Content/technicalinfo/tch_atraccessories.pdf (accessed Feb 1, 2018).

9. Gololobov, Y. G.; Zhmurova, I. N.; Kasukhin, L. F., Sixty years of staudinger reaction. *Tetrahedron* **1981,** *37* (3), 437-472.

10. Deming, T. J.; Curtin, S. A., Chain Initiation Efficiency in Cobalt- and Nickel-Mediated Polypeptide Synthesis. *Journal of the American Chemical Society* **2000,** *122* (24), 5710-5717.

11. Kim, C. H.; Axup, J. Y.; Schultz, P. G., Protein conjugation with genetically encoded unnatural amino acids. *Curr Opin Chem Biol* **2013,** *17* (3), 412-9.

12. *Elemental Impurities in Drug Products: Guidance for Industry.* US Food and Drug Administration, 2016. https://www.fda.gov/downloads/Drugs/Guidances/UCM509432.pdf (accessed Feb 1, 2018).

13. Conejos-Sánchez, I.; Duro-Castano, A.; Birke, A.; Barz, M.; Vicent, M. J., A controlled and versatile NCA polymerization method for the synthesis of polypeptides. *Polymer Chemistry* **2013,** *4* (11), 3182.

14. Zhao, W.; Gnanou, Y.; Hadjichristidis, N., Fast and living ring-opening polymerization of alpha-amino acid N-carboxyanhydrides triggered by an "alliance" of primary and secondary amines at room temperature. *Biomacromolecules* **2015,** *16* (4), 1352-7.

15. Buskas, T.; Li, Y.; Boons, G. J., The immunogenicity of the tumor-associated antigen Lewis(y) may be suppressed by a bifunctional cross-linker required for coupling to a carrier protein. *Chemistry* **2004,** *10* (14), 3517-24.

16. McCombs, J. R.; Owen, S. C., Antibody drug conjugates: design and selection of linker, payload and conjugation chemistry. *AAPS J* **2015,** *17* (2), 339-51.

17. Baldwin, A. D.; Kiick, K. L., Tunable degradation of maleimide-thiol adducts in reducing environments. *Bioconjug Chem* **2011,** *22* (10), 1946-53.

18. Ross, P. L.; Wolfe, J. L., Physical and Chemical Stability of Antibody Drug Conjugates: Current Status. *J Pharm Sci* **2016,** *105* (2), 391-397.

19. Zhao, W.; Gnanou, Y.; Hadjichristidis, N., Organocatalysis by hydrogen-bonding: a new approach to controlled/living polymerization of α-amino acid N-carboxyanhydrides. *Polymer Chemistry* **2015,** *6* (34), 6193-6201.

Appendix: Spectral Data

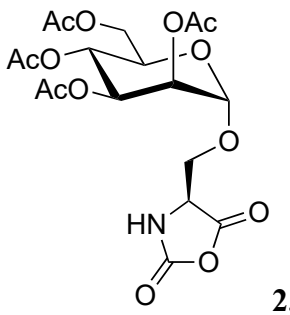
AcO
OAc
AcO
O
AcO
O
HN
O
O
O

2.2a

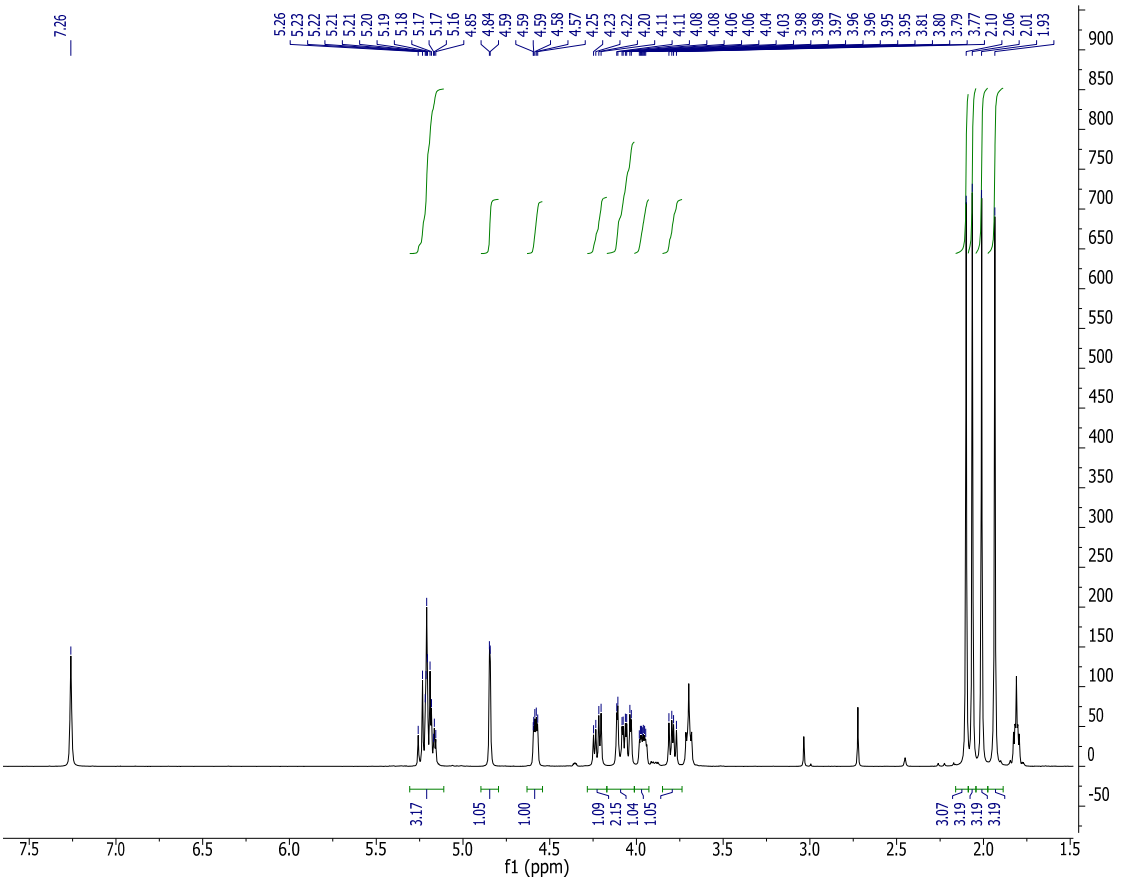
7.26
5.26
5.23
5.22
5.21
5.21
5.20
5.19
5.18
5.17
5.17
5.16
4.85
4.84
4.59
4.59
4.59
4.58
4.57
4.25
4.23
4.22
4.20
4.11
4.11
4.08
4.08
4.06
4.06
4.04
4.03
3.98
3.98
3.97
3.96
3.96
3.95
3.95
3.81
3.80
3.79
3.77
2.10
2.06
2.01
1.93
3.17
1.05
1.00
1.09
2.15
1.04
1.05
3.07
3.19
3.19
3.19
f1 (ppm)

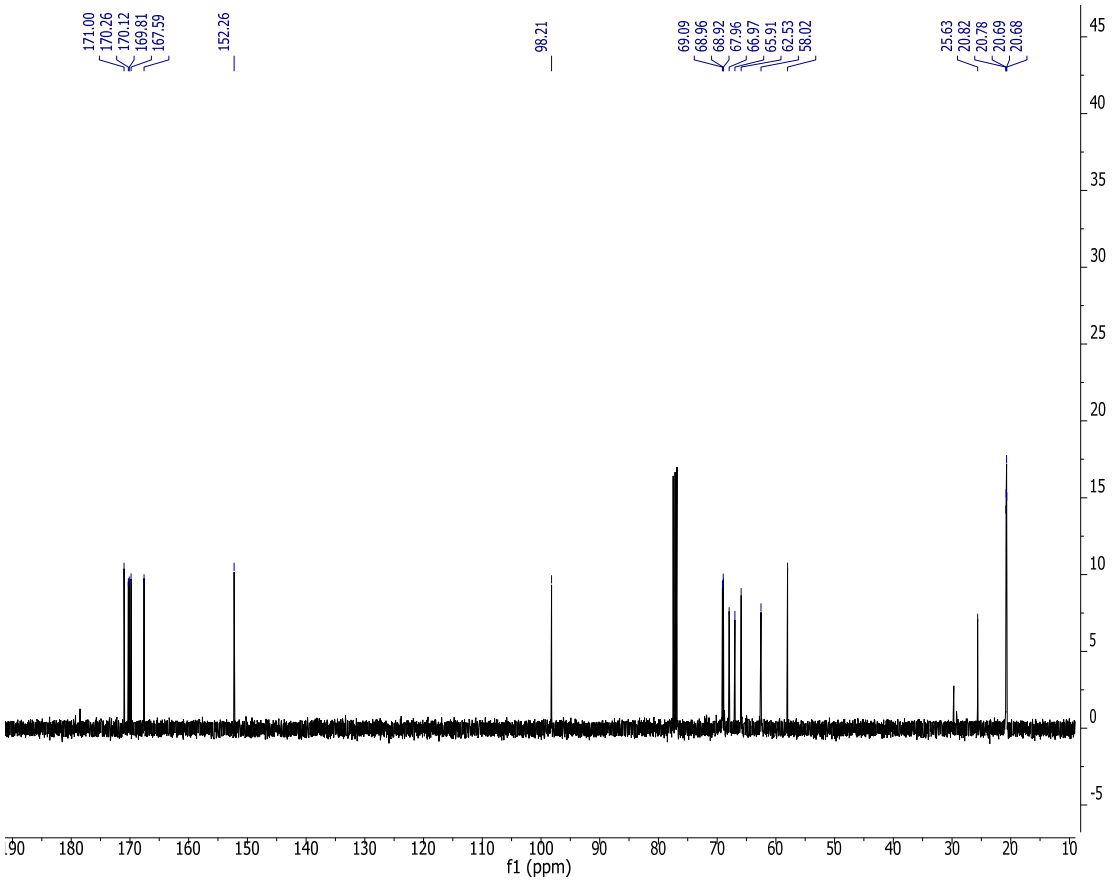
171.00
170.26
170.12
169.81
167.59
152.26
98.21
69.09
68.96
68.92
67.96
66.97
65.91
62.53
58.02
25.63
20.82
20.78
20.69
20.68
f1 (ppm)

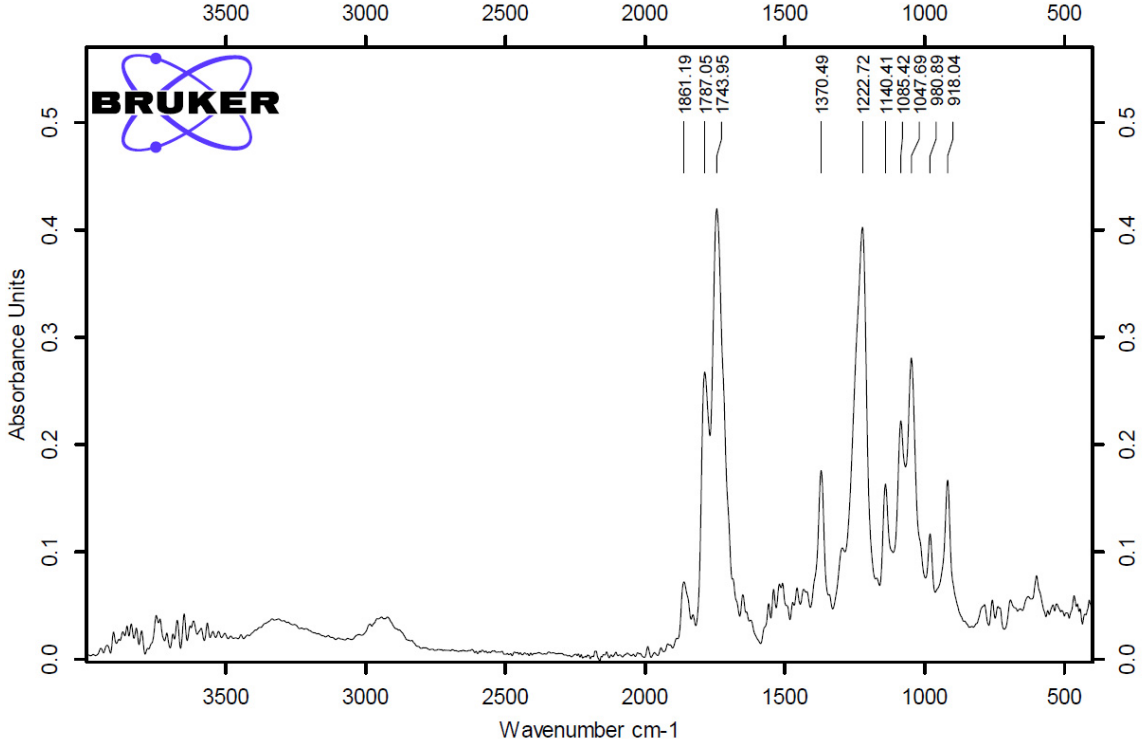
BRUKER
1861.19
1787.05
1743.95
1370.49
1222.72
1140.41
1085.42
1047.69
980.89
918.04
Absorbance Units
Wavenumber cm-1

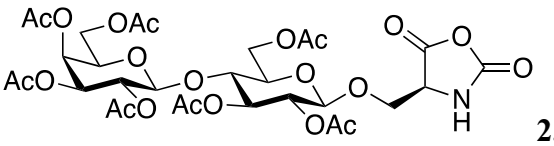
AcO
OAc
O
AcO
AcO
AcO
OAc
O
O
OAc
O
O
N
H
O
O

2.2b

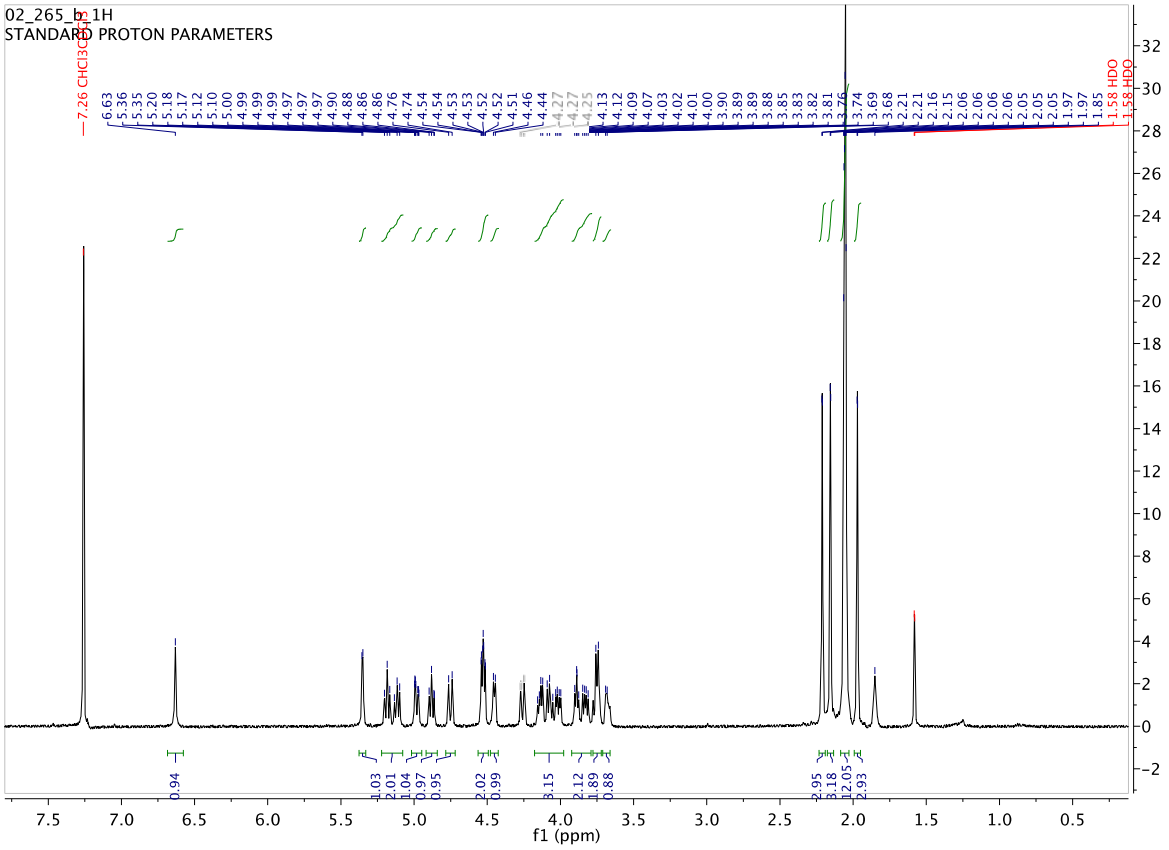
02_265_b 1H
STANDARD PROTON PARAMETERS
7.26 CHCl3
1.58 HDO
f1 (ppm)

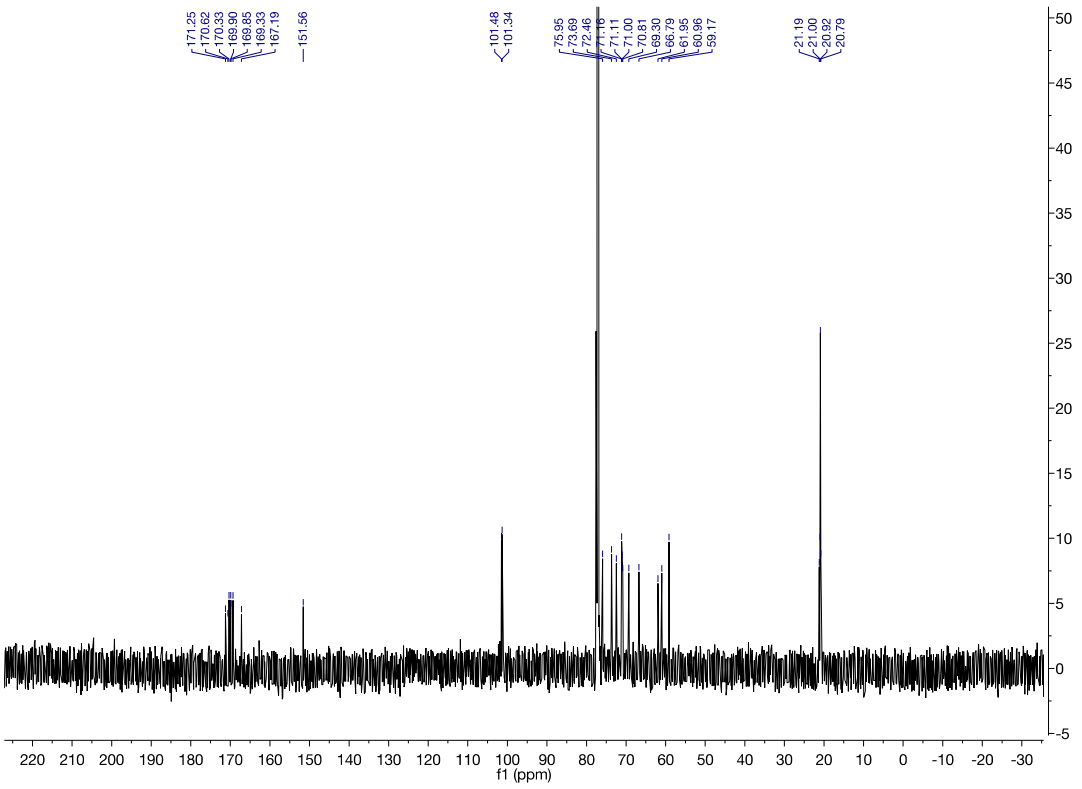
171.25
170.62
170.33
169.90
169.85
169.33
167.19
151.56
101.48
101.34
75.95
73.69
72.46
71.16
71.11
71.00
70.81
69.30
66.79
61.95
60.96
59.17
21.19
21.00
20.92
20.79
f1 (ppm)

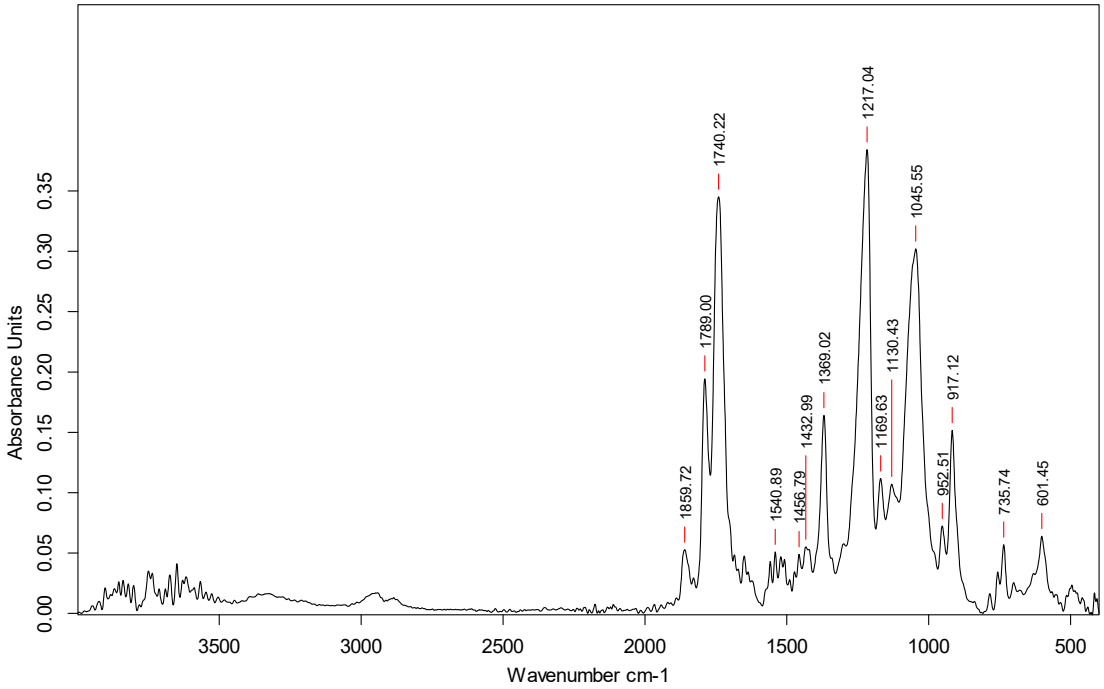
Absorbance Units
Wavenumber cm-1
1859.72
1789.00
1740.22
1540.89
1456.79
1432.99
1369.02
1217.04
1169.63
1130.43
1045.55
952.51
917.12
735.74
601.45

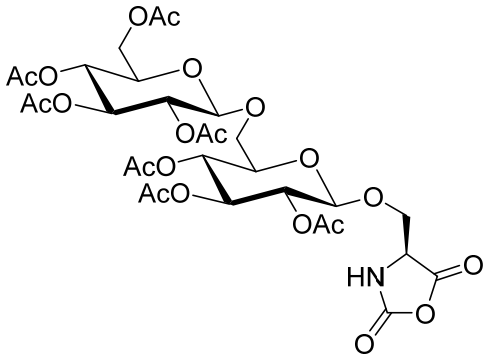
OAc
AcO
AcO
O
OAc
AcO
AcO
OAc
O
O
HN
O
O
O

2.2c

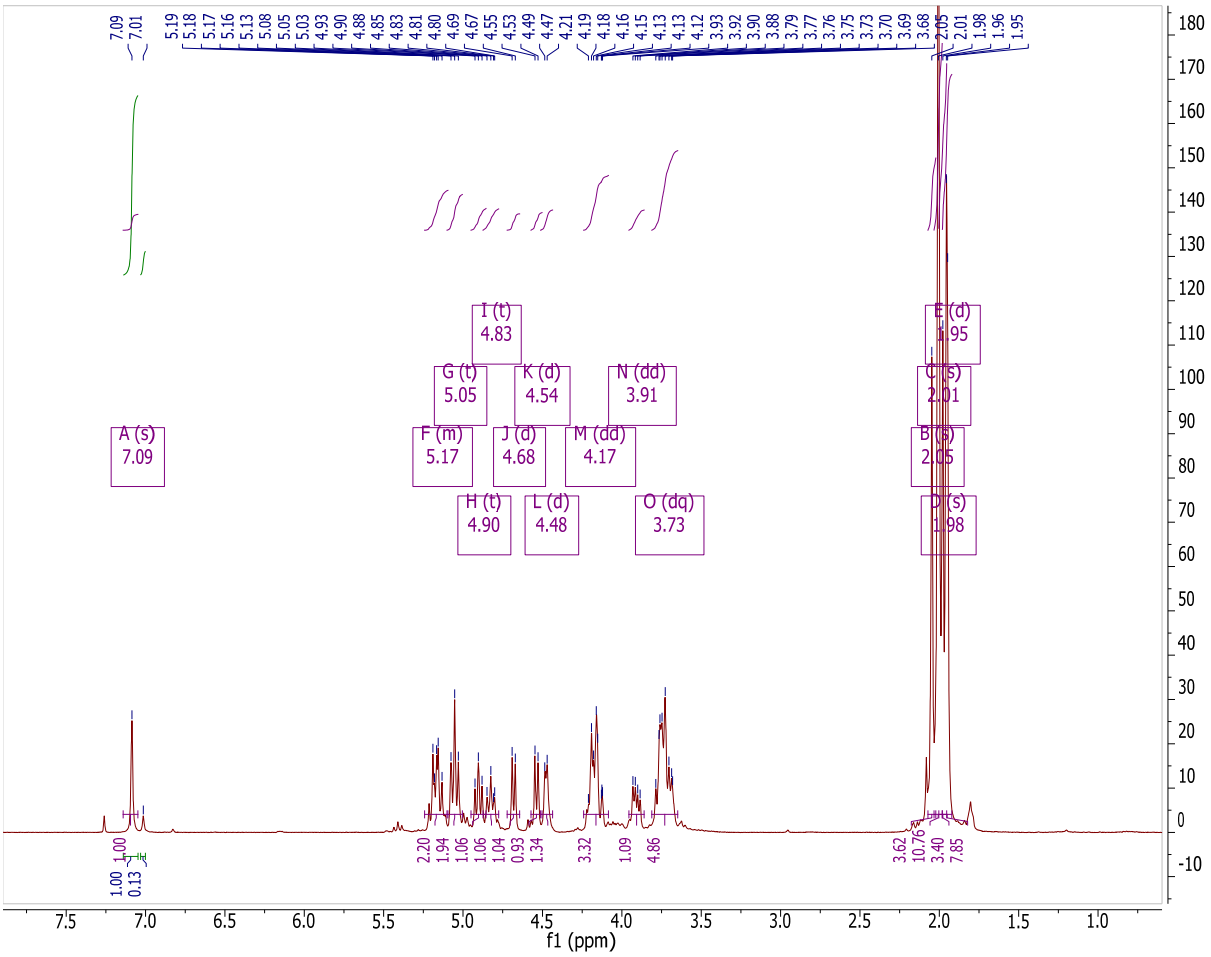
A (s) 7.09
F (m) 5.17
G (t) 5.05
H (t) 4.90
I (t) 4.83
J (d) 4.68
K (d) 4.54
L (d) 4.48
M (dd) 4.17
N (dd) 3.91
O (dq) 3.73
B (s) 2.05
C (s) 2.01
D (s) 1.98
E (d) 1.95
f1 (ppm)

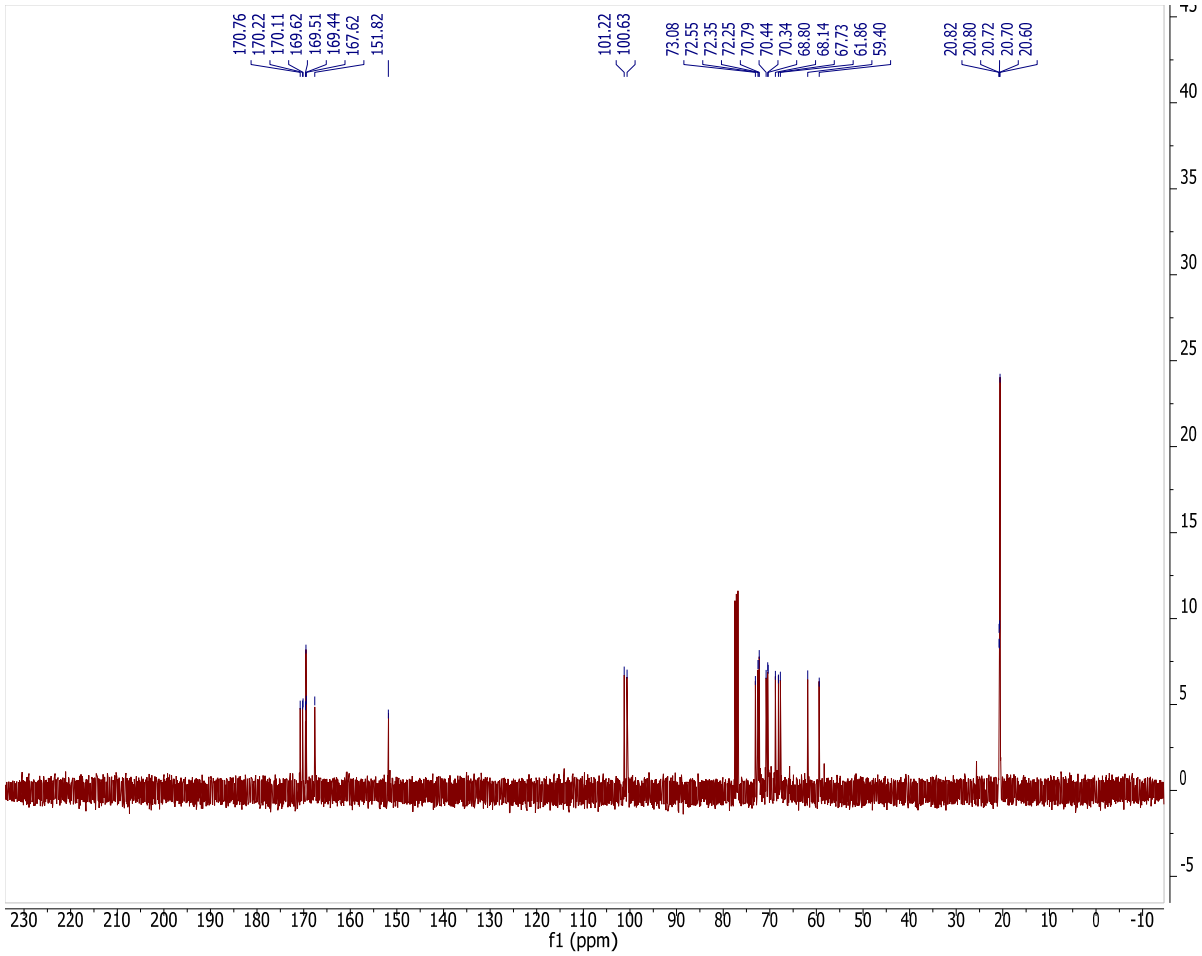
170.76
170.22
170.11
169.62
169.51
169.44
167.62
151.82
101.22
100.63
73.08
72.55
72.35
72.25
70.79
70.44
70.34
68.80
68.14
67.73
61.86
59.40
20.82
20.80
20.72
20.70
20.60
f1 (ppm)

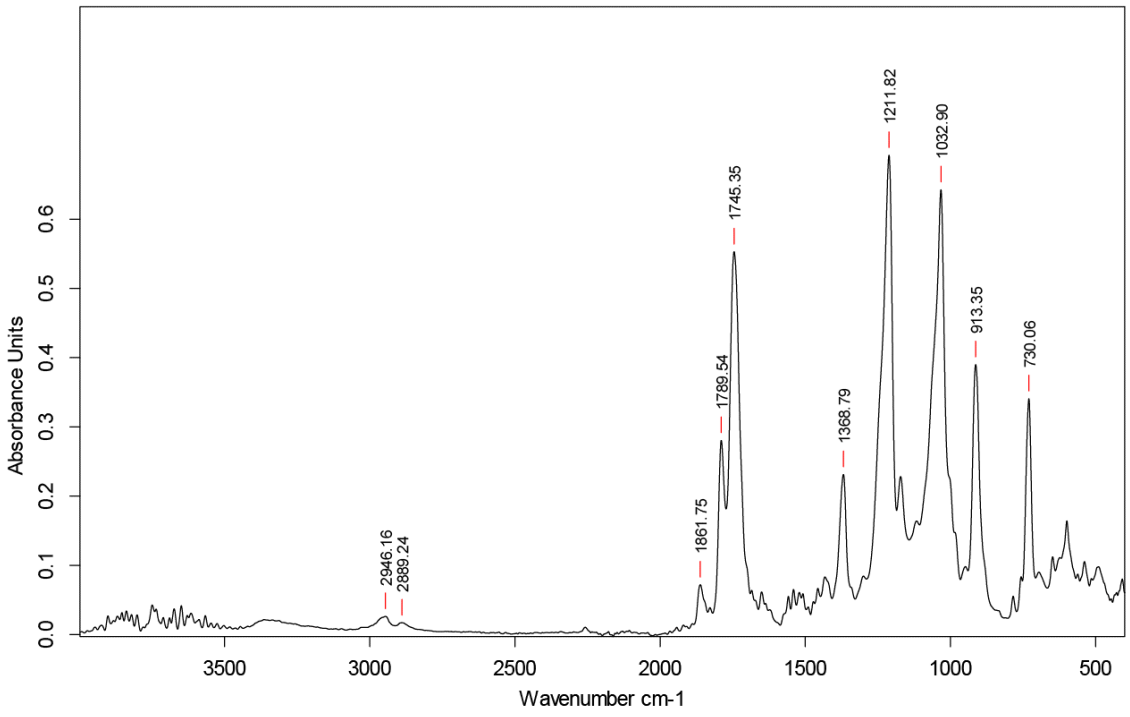
Absorbance Units
Wavenumber cm-1
2946.16
2889.24
1861.75
1789.54
1745.35
1368.79
1211.82
1032.90
913.35
730.06

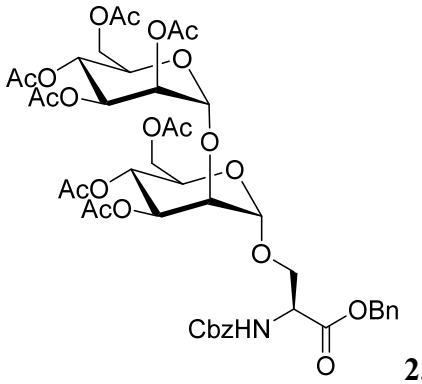

2.12d

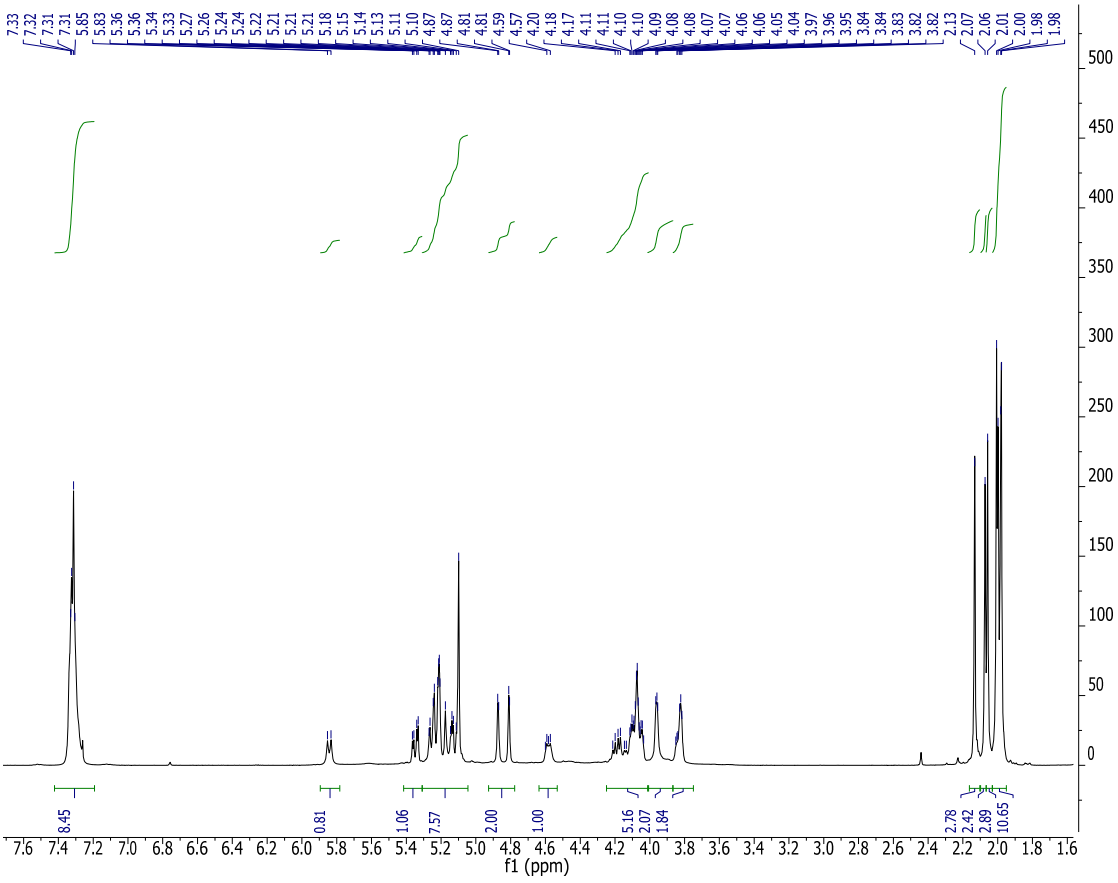

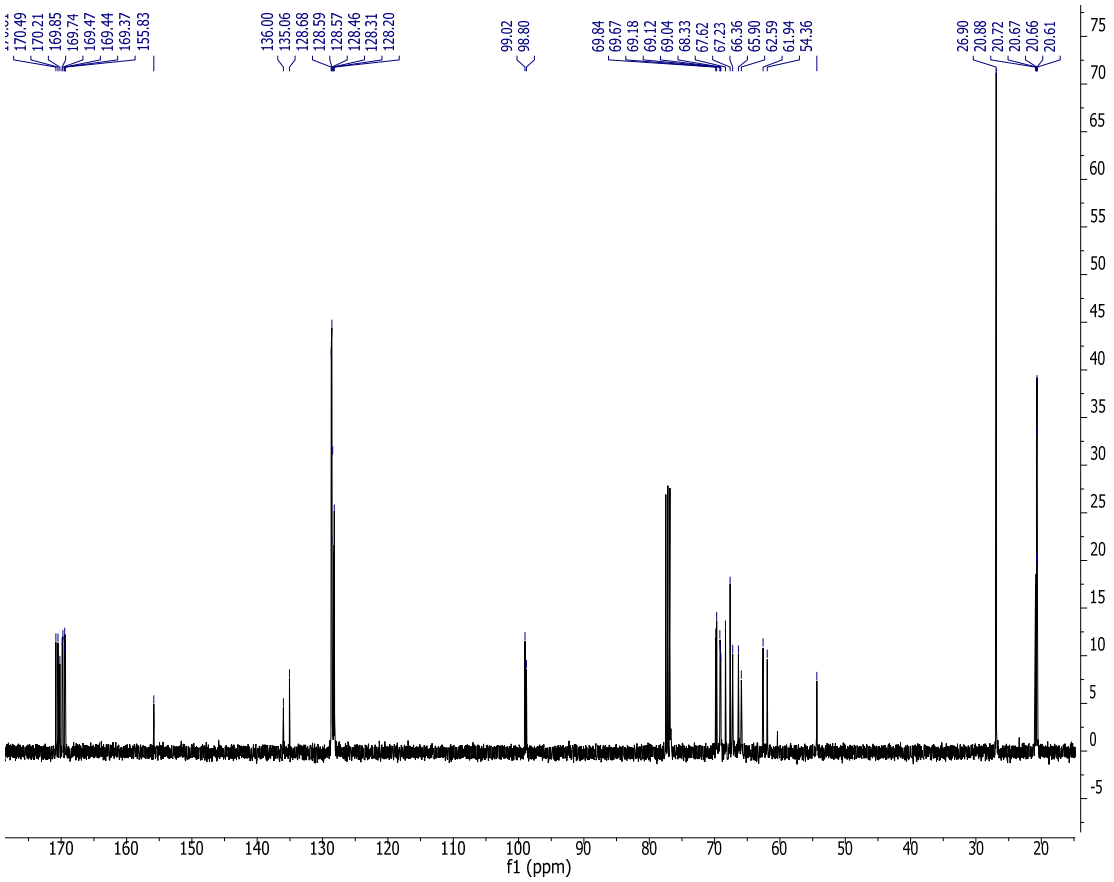
170.49
170.21
169.85
169.74
169.47
169.44
169.37
155.83
136.00
135.06
128.68
128.59
128.57
128.46
128.31
128.20
99.02
98.80
69.84
69.67
69.18
69.12
69.04
68.33
67.62
67.23
66.36
65.90
62.59
61.94
54.36
26.90
20.88
20.72
20.67
20.66
20.61
f1 (ppm)

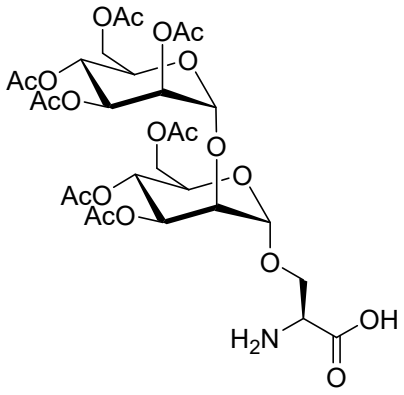
OAc
OAc
AcO
AcO
O
OAc
O
AcO
AcO
O
O
H2N
OH
O

2.1d

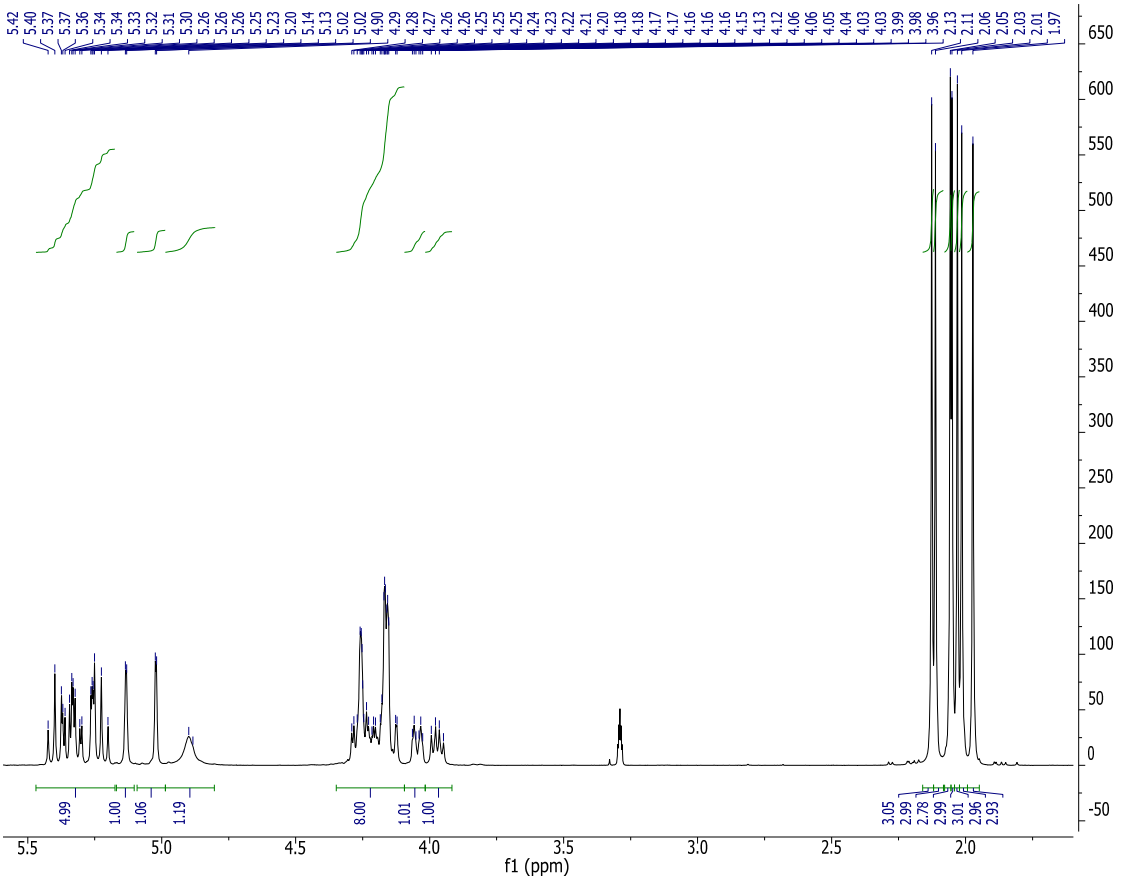
5.42 5.40 5.37 5.37 5.36 5.34 5.34 5.33 5.32 5.31 5.30 5.26 5.26 5.26 5.25 5.23 5.20 5.14 5.13 5.02 5.02 4.90 4.29 4.28 4.27 4.26 4.26 4.25 4.25 4.25 4.24 4.23 4.22 4.21 4.20 4.18 4.18 4.17 4.17 4.16 4.16 4.16 4.15 4.13 4.12 4.06 4.06 4.05 4.04 4.03 4.03 3.99 3.98 3.96 2.13 2.11 2.06 2.05 2.03 2.01 1.97
650 600 550 500 450 400 350 300 250 200 150 100 50 0 -50
4.99 1.00 1.06 1.19 8.00 1.01 1.00 3.05 2.99 2.78 2.99 3.01 2.96 2.93
5.5 5.0 4.5 4.0 3.5 3.0 2.5 2.0
f1 (ppm)

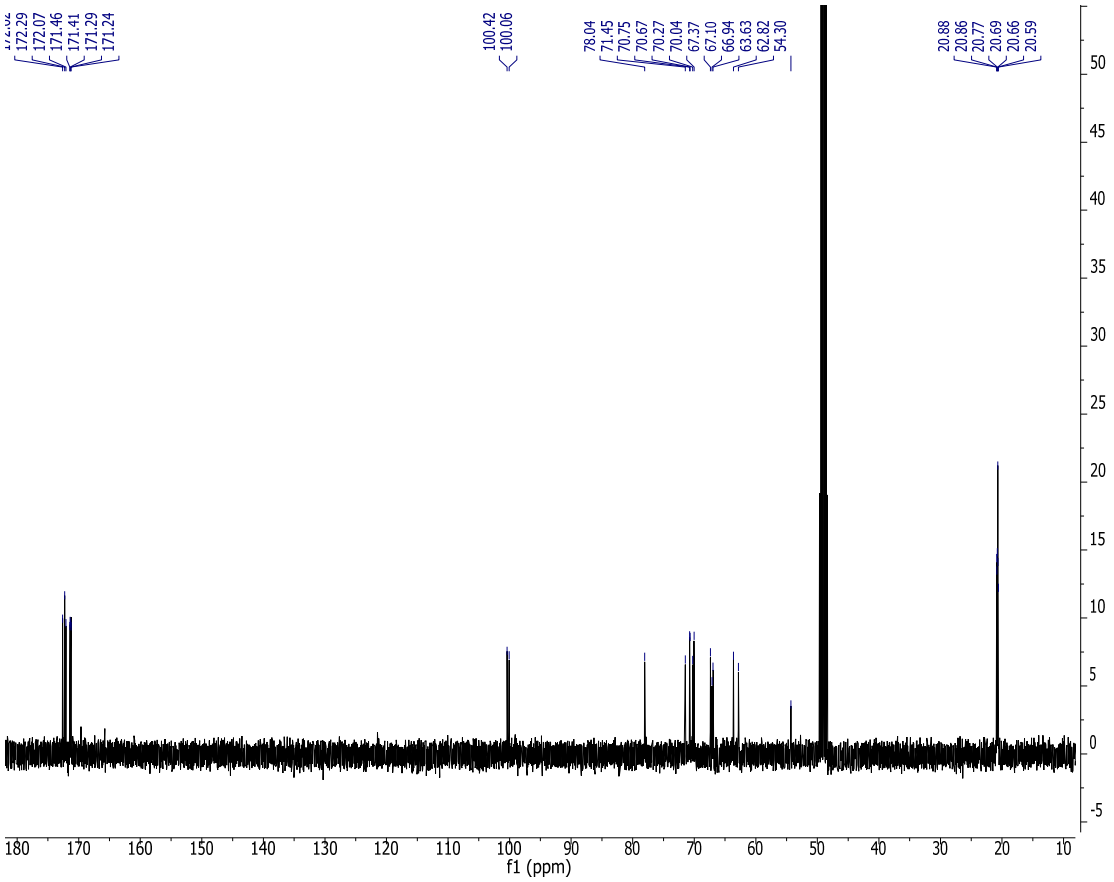
172.29
172.07
171.46
171.41
171.29
171.24
100.42
100.06
78.04
71.45
70.75
70.67
70.27
70.04
67.37
67.10
66.94
63.63
62.82
54.30
20.88
20.86
20.77
20.69
20.66
20.59
f1 (ppm)

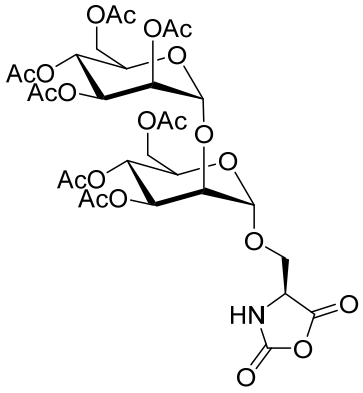

2.2d

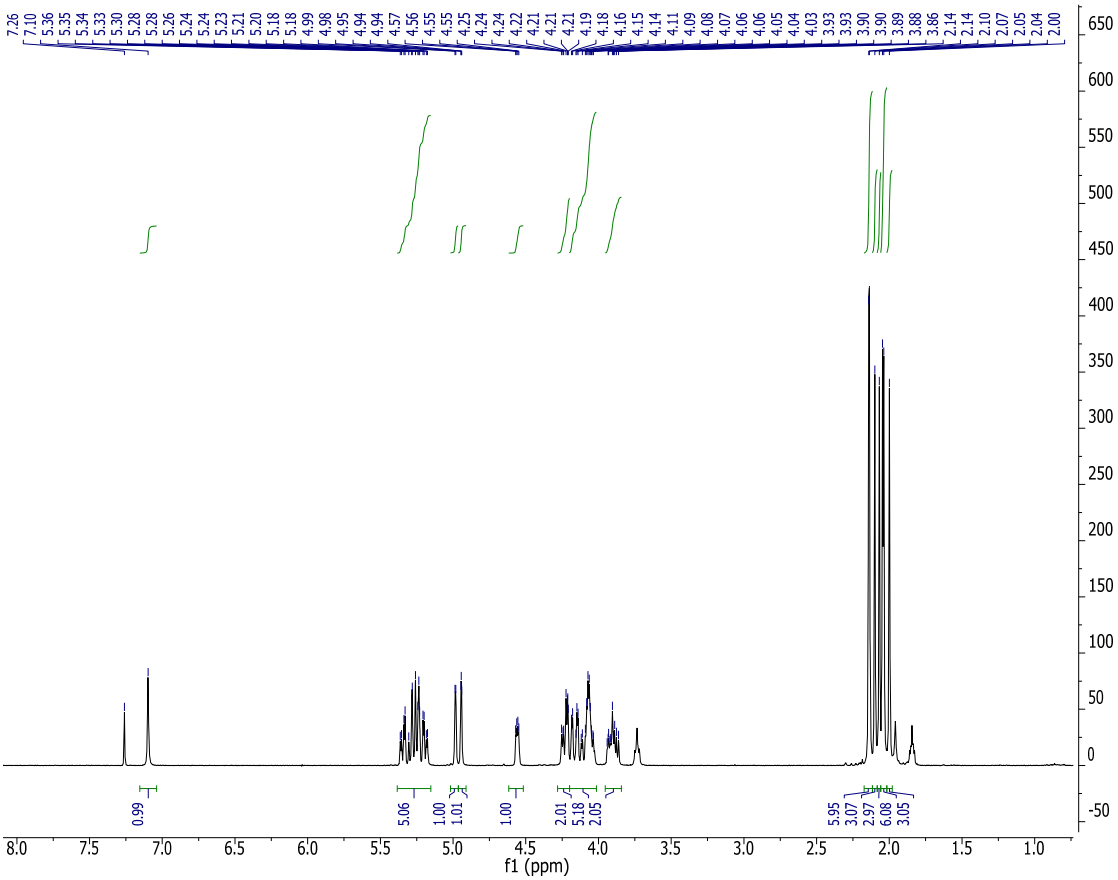

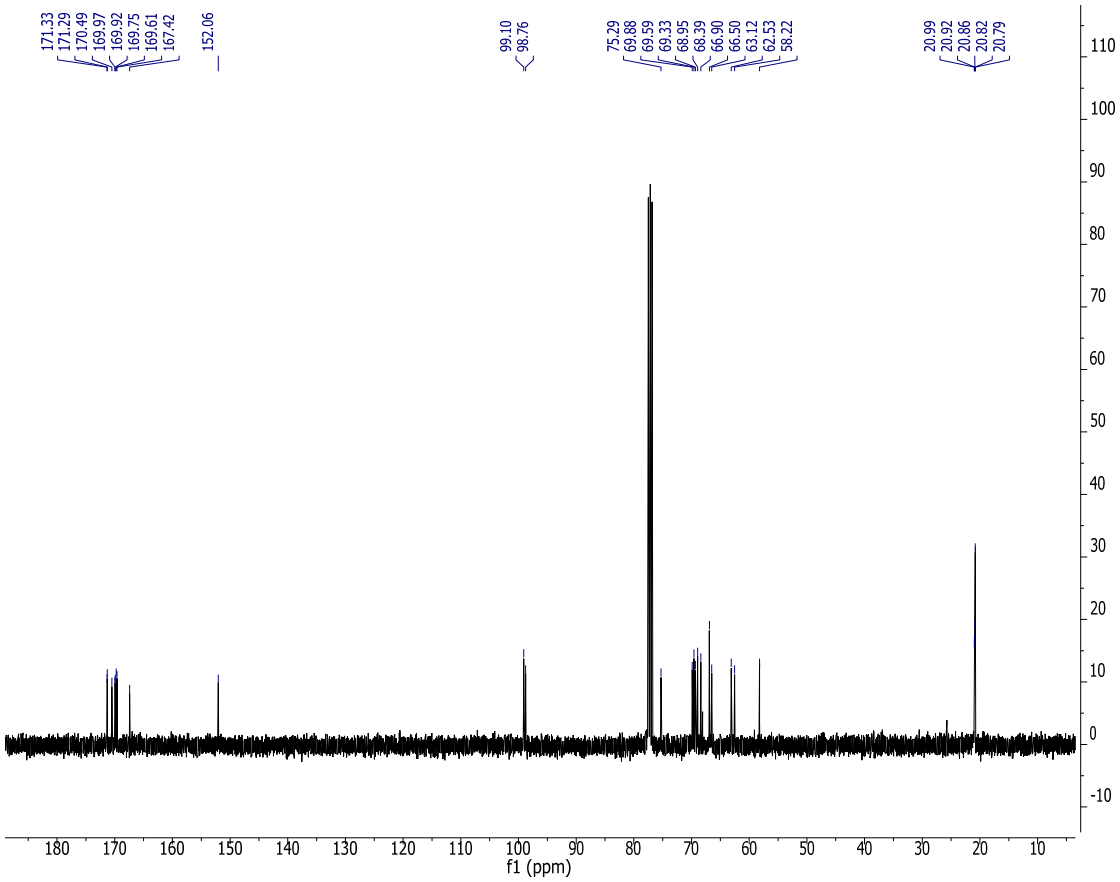
171.33
171.29
170.49
169.97
169.92
169.75
169.61
167.42
152.06
99.10
98.76
75.29
69.88
69.59
69.33
68.95
68.39
66.90
66.50
63.12
62.53
58.22
20.99
20.92
20.86
20.82
20.79
f1 (ppm)

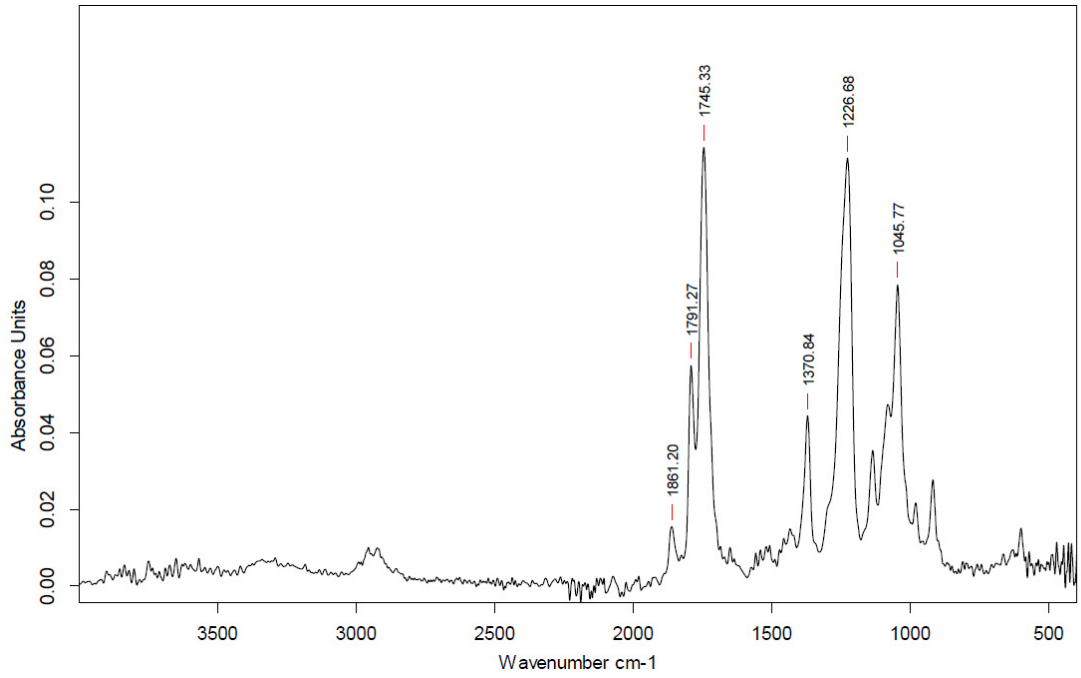
1861.20
1791.27
1745.33
1370.84
1226.68
1045.77
Absorbance Units
Wavenumber cm-1

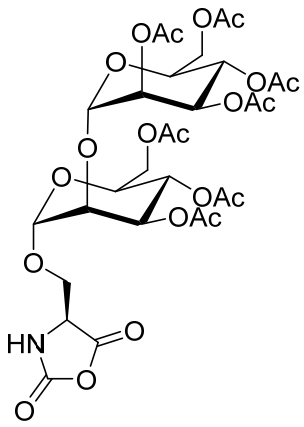
OAc
OAc
OAc
OAc
OAc
OAc
OAc
O
O
O
O
O
HN
O
O
O

2.2e

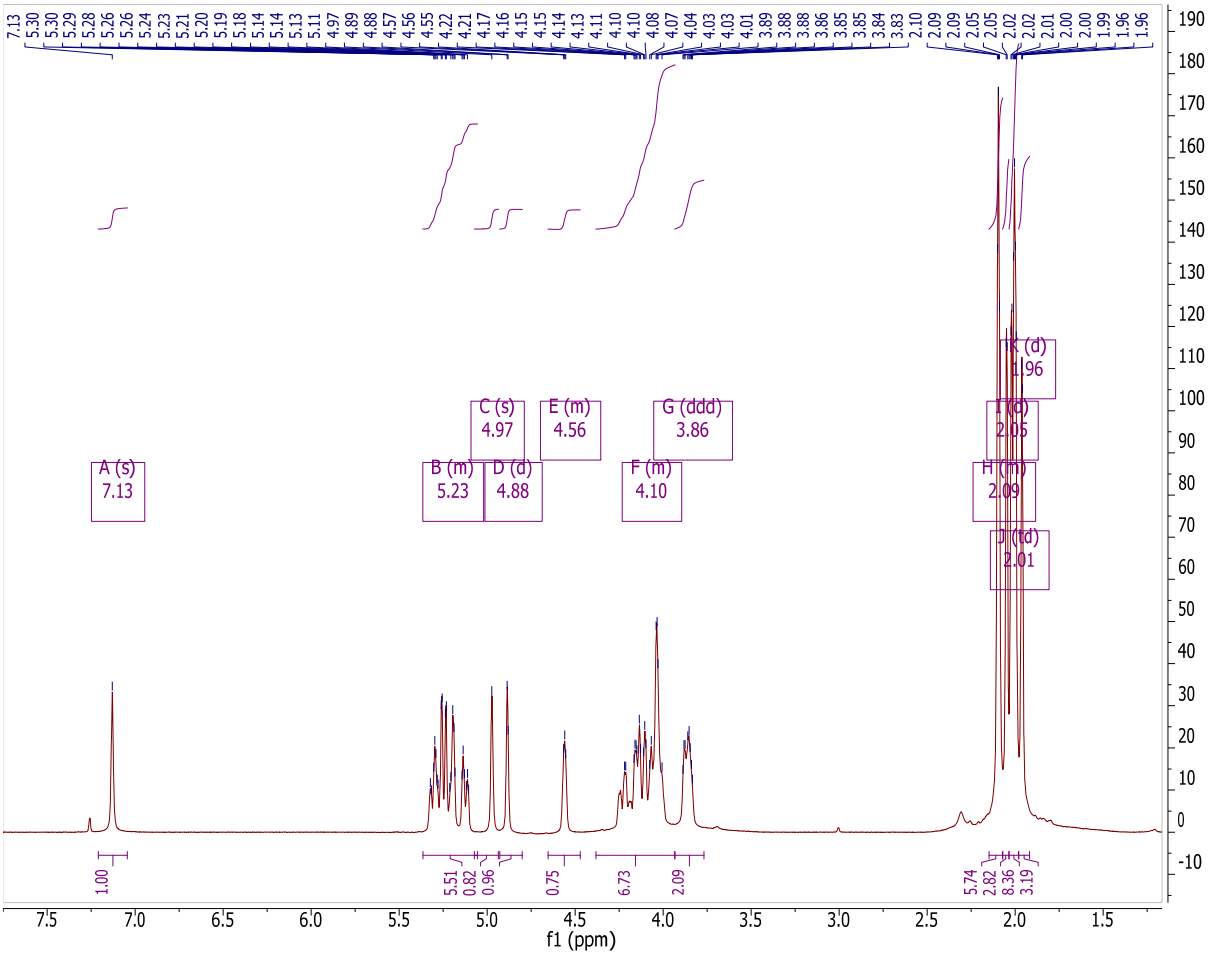
A (s) 7.13
B (m) 5.23
C (s) 4.97
D (d) 4.88
E (m) 4.56
F (m) 4.10
G (ddd) 3.86
H (m) 2.09
I (td) 2.05
J (td) 2.01
K (d) 1.96
1.00
5.51
0.82
0.96
0.75
6.73
2.09
5.74
2.82
8.36
3.19
f1 (ppm)

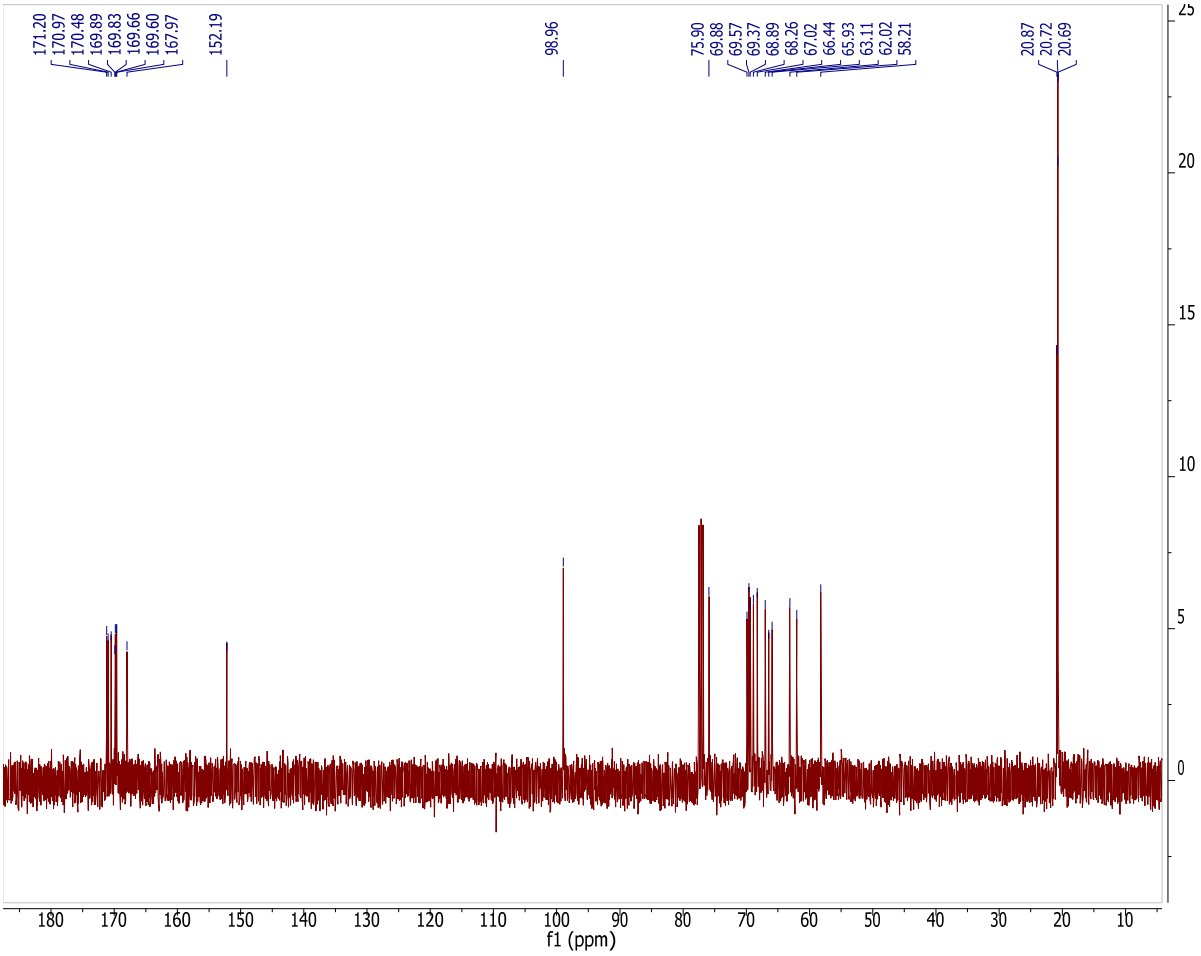
171.20
170.97
170.48
169.89
169.83
169.66
169.60
167.97
152.19
98.96
75.90
69.88
69.57
69.37
68.89
68.26
67.02
66.44
65.93
63.11
62.02
58.21
20.87
20.72
20.69
f1 (ppm)

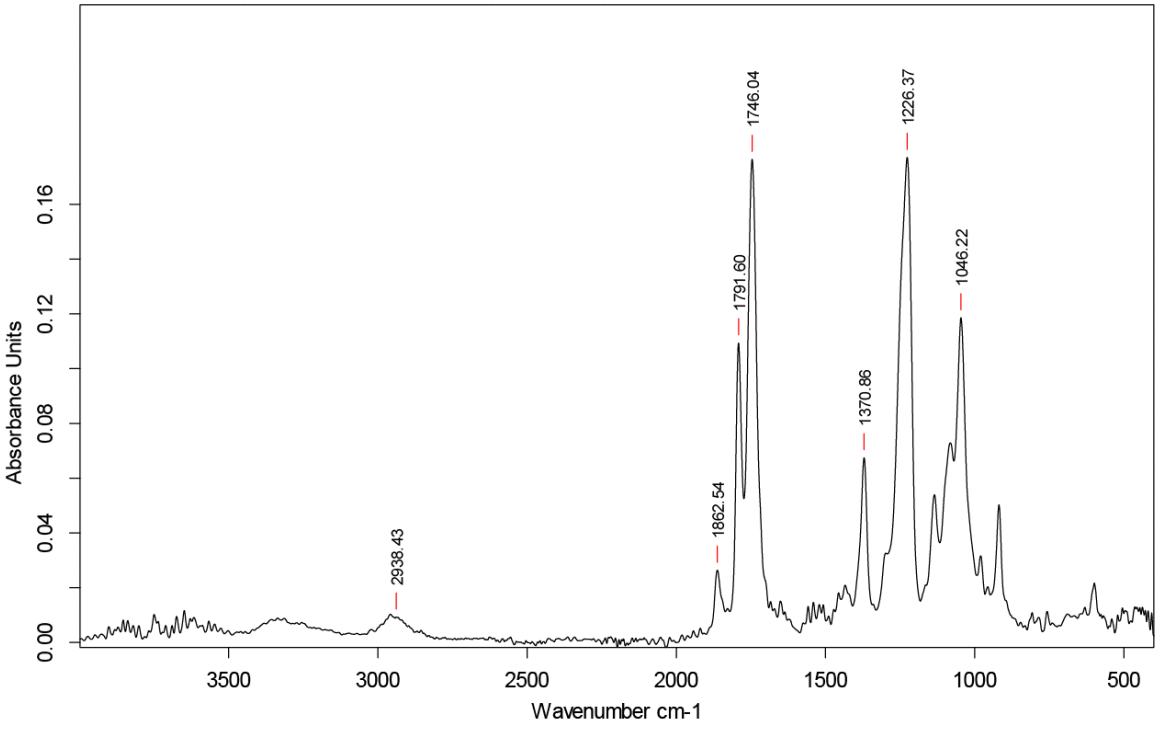
2938.43
1862.54
1791.60
1746.04
1370.86
1226.37
1046.22
Absorbance Units
Wavenumber cm-1

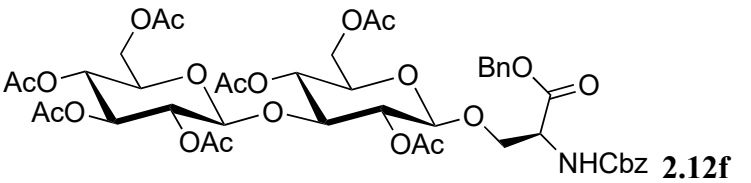
OAc
OAc
AcO
AcO
AcO
O
O
O
O
O
O
BnO
O
NHCbz

2.12f

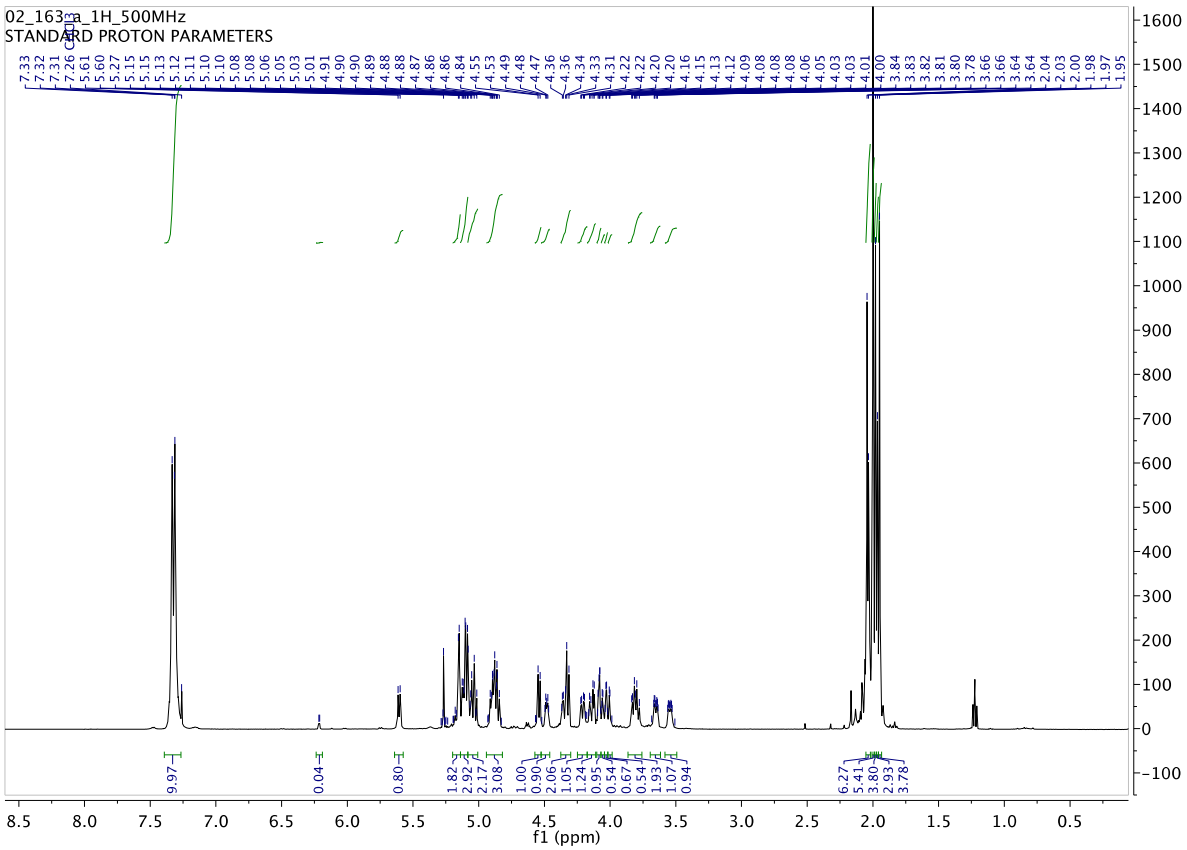
02_163a_1H_500MHz
STANDARD PROTON PARAMETERS
f1 (ppm)

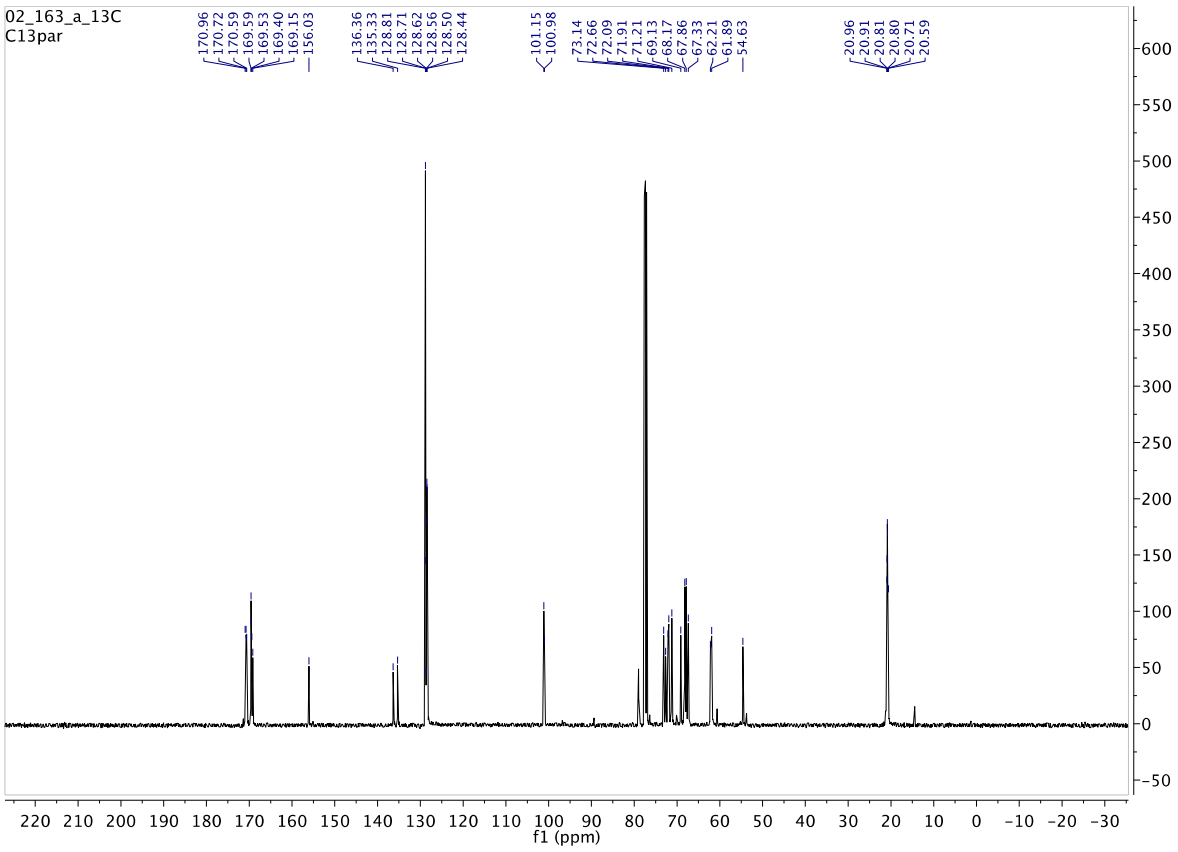
02_163_a_13C
C13par
170.96
170.72
170.59
169.59
169.53
169.40
169.15
156.03
136.36
135.33
128.81
128.71
128.62
128.56
128.50
128.44
101.15
100.98
73.14
72.66
72.09
71.91
71.21
69.13
68.17
67.86
67.33
62.21
61.89
54.63
20.96
20.91
20.81
20.80
20.71
20.59
f1 (ppm)

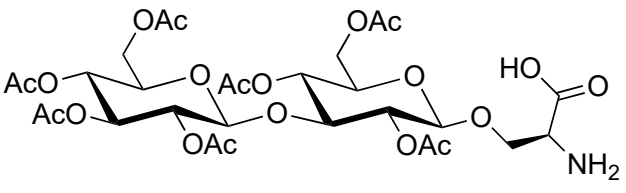
OAc
OAc
AcO
AcO
AcO
O
O
O
O
O
HO
O
NH2

2.1f

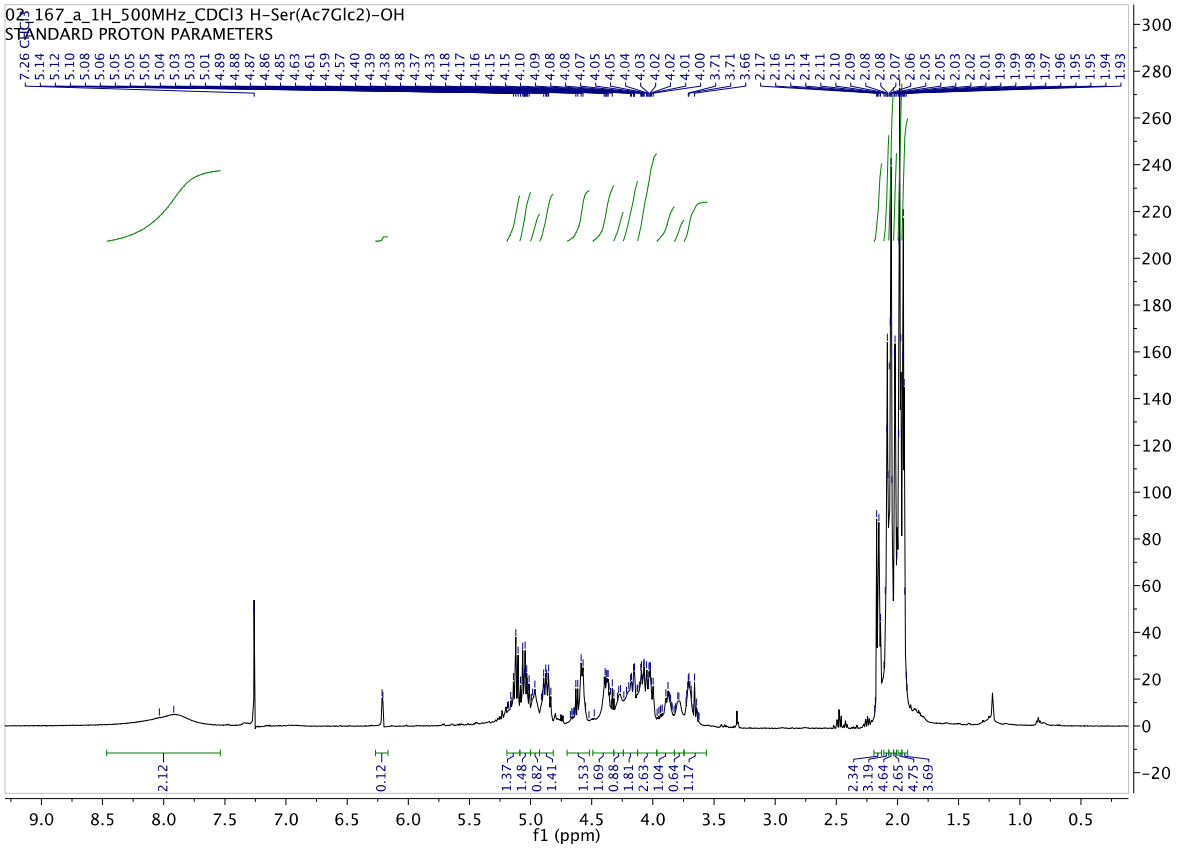
02_167_a_1H_500MHz_CDCl3 H-Ser(Ac7Glc2)-OH
STANDARD PROTON PARAMETERS
f1 (ppm)

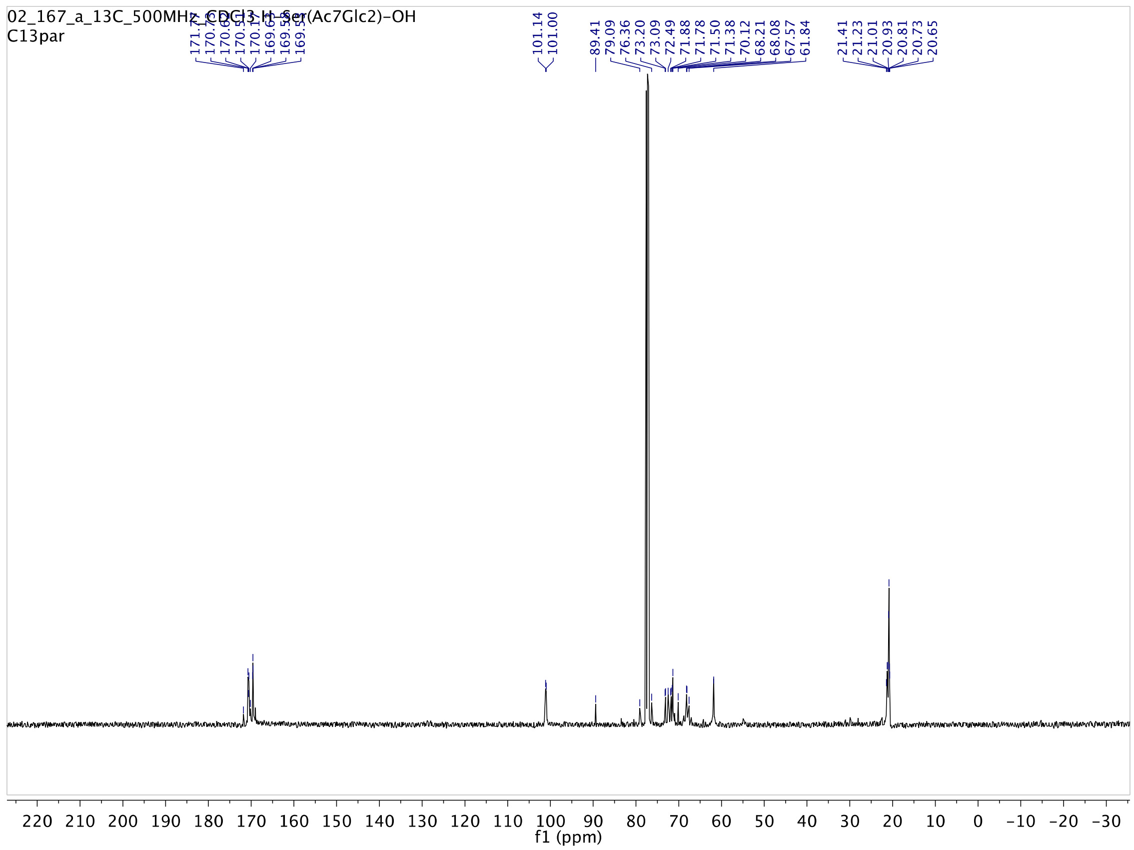
02_167_a_13C_500MHz_CDCl3-H-Ser(Ac7Glc2)-OH
C13par
101.14
101.00
89.41
79.09
76.36
73.20
73.09
72.49
71.88
71.78
71.50
71.38
70.12
68.21
68.08
67.57
61.84
21.41
21.23
21.01
20.93
20.81
20.73
20.65
f1 (ppm)

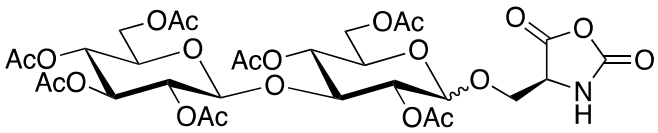

2.2f (1:3 α:β ratio)

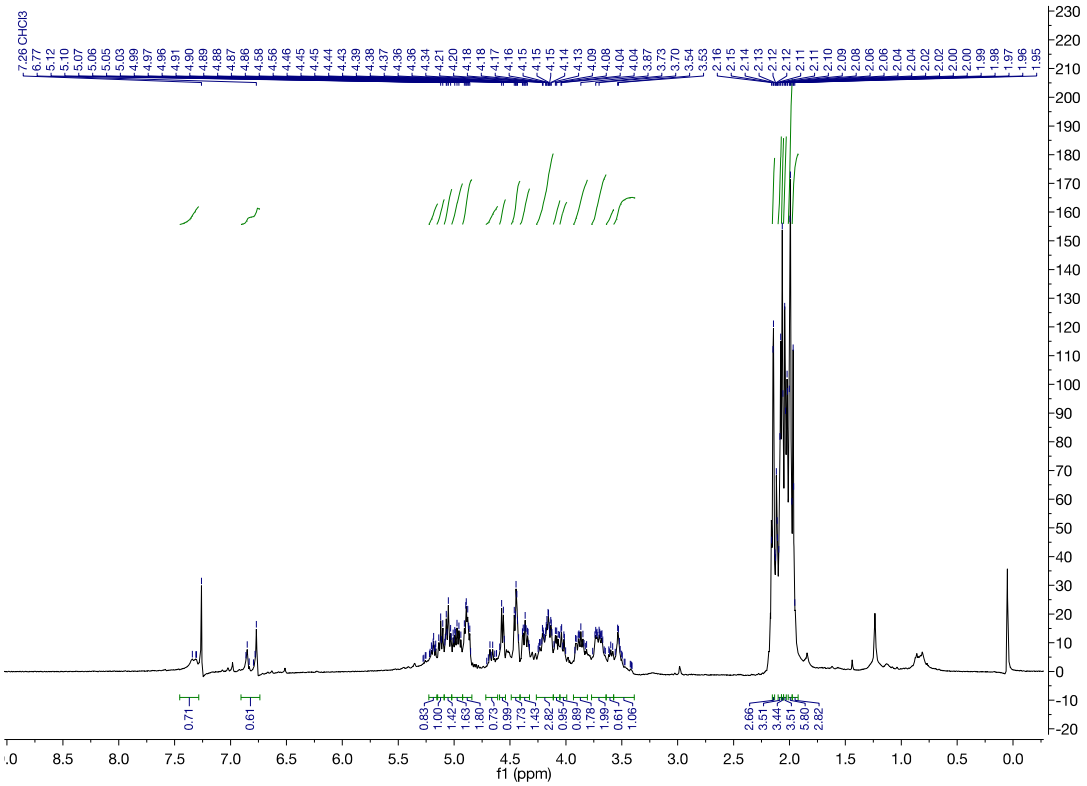

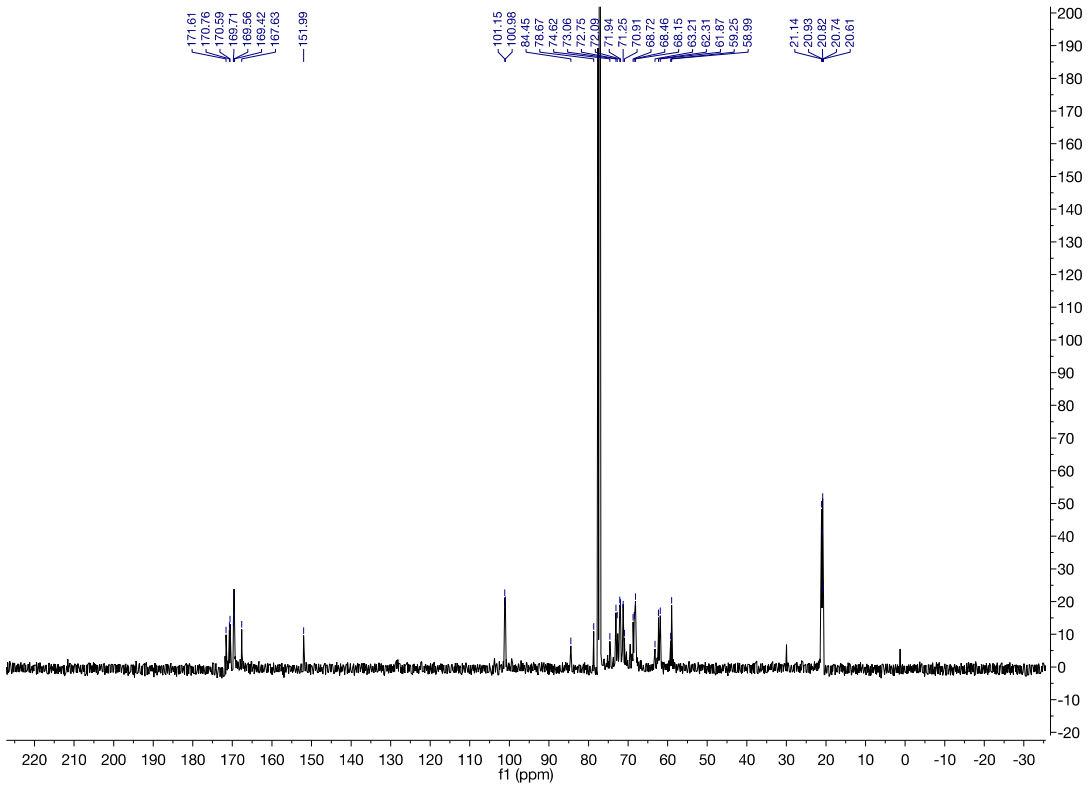
171.61
170.76
170.59
169.71
169.56
169.42
167.63
151.99
101.15
100.98
84.45
78.67
74.62
73.06
72.75
72.09
71.94
71.25
70.91
68.72
68.46
68.15
63.21
62.31
61.87
59.25
58.99
21.14
20.93
20.82
20.74
20.61
f1 (ppm)

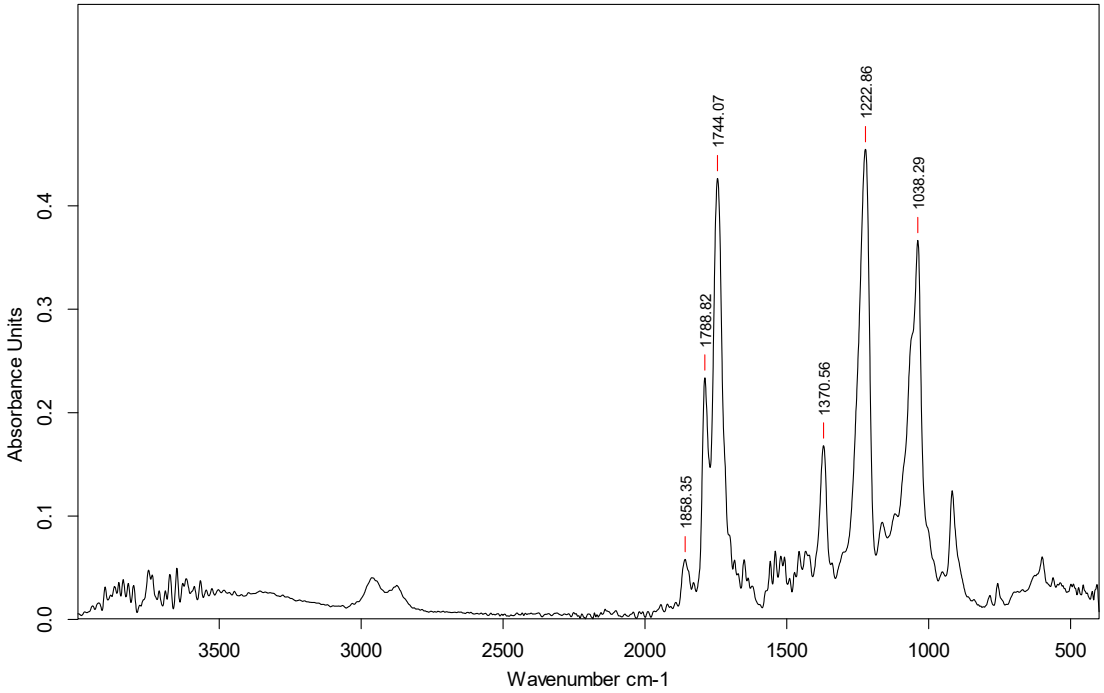
1858.35
1788.82
1744.07
1370.56
1222.86
1038.29
Absorbance Units
Wavenumber cm-1

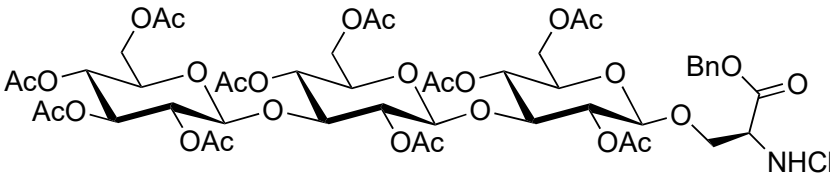
OAc
OAc
OAc
AcO
AcO
AcO
AcO
AcO
O
O
O
O
O
O
O
O
BnO
O
NHCbz

2.12g

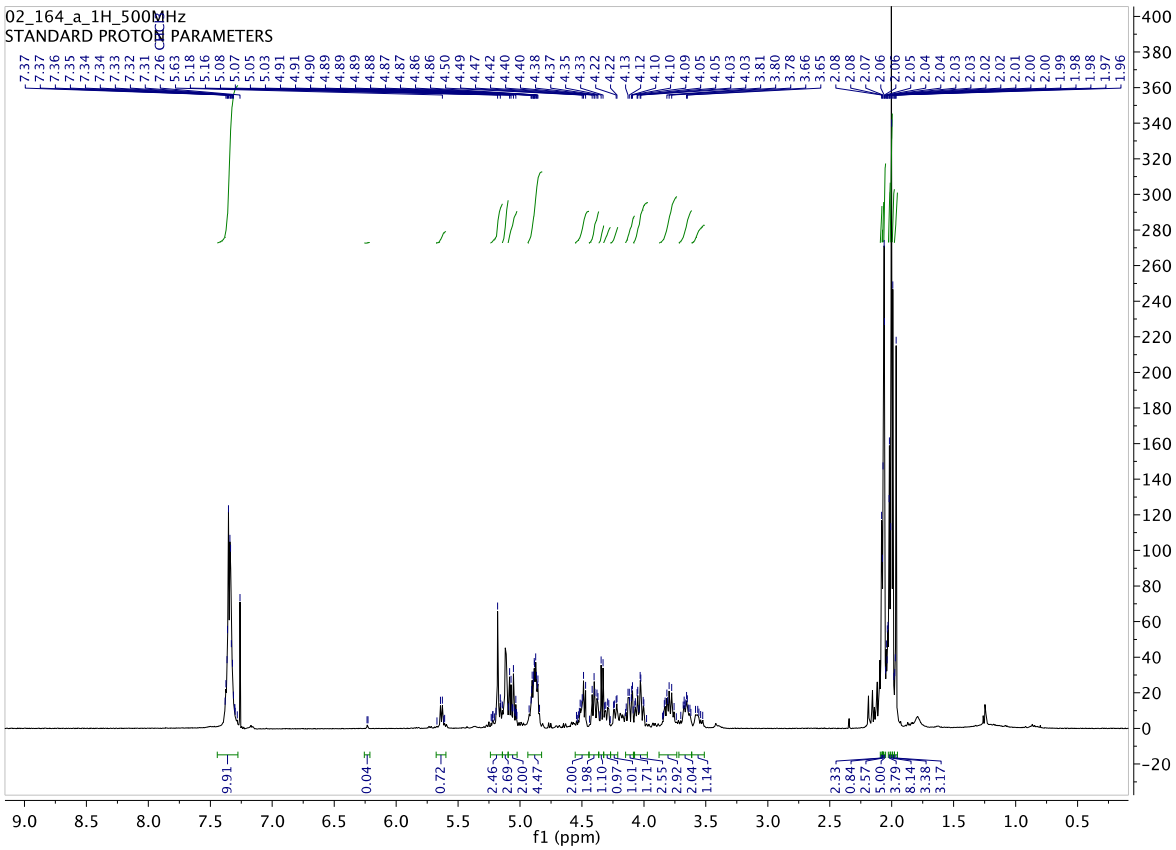
02_164_a_1H_500MHz
STANDARD PROTON PARAMETERS
f1 (ppm)

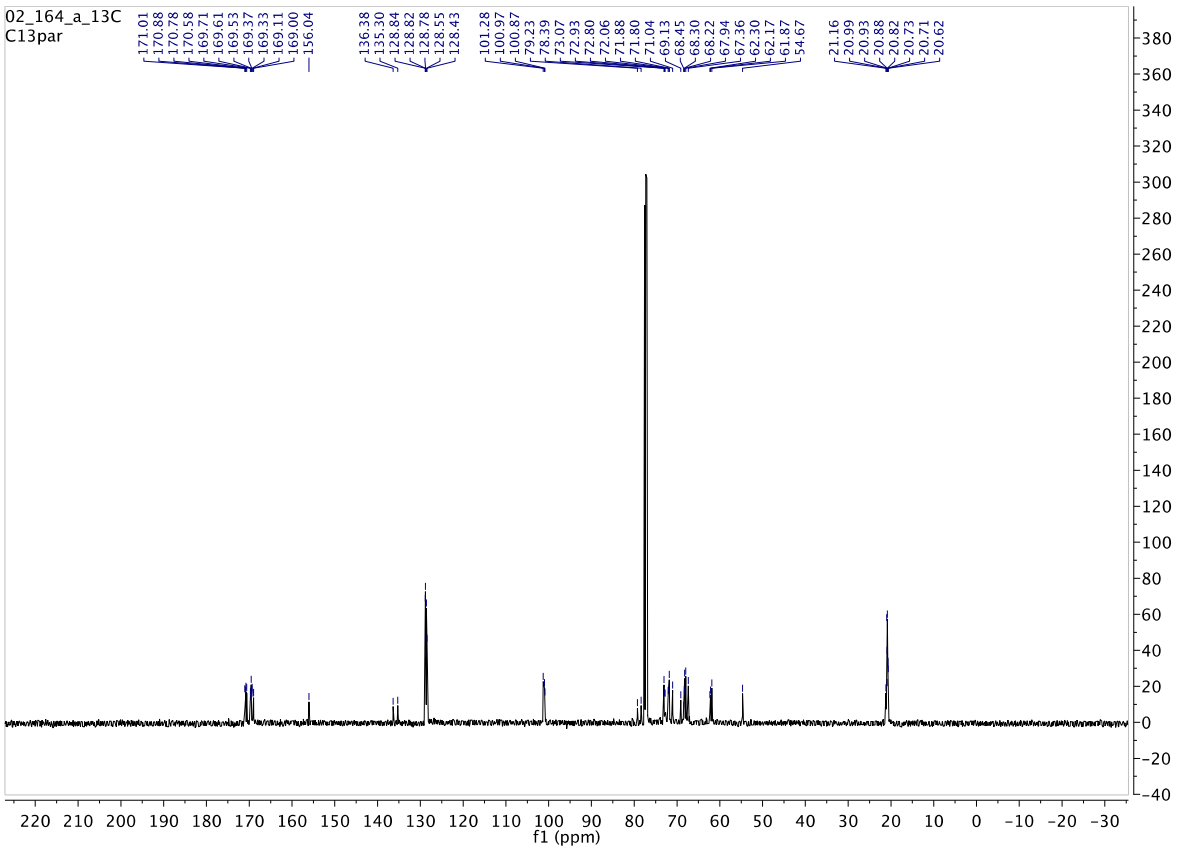
02_164_a_13C
C13par
171.01
170.88
170.78
170.58
169.71
169.61
169.53
169.37
169.33
169.11
169.00
156.04
136.38
135.30
128.84
128.82
128.78
128.55
128.43
101.28
100.97
100.87
79.23
78.39
73.07
72.93
72.80
72.06
71.88
71.80
71.04
69.13
68.45
68.30
68.22
67.94
67.36
62.30
62.17
61.87
54.67
21.16
20.99
20.93
20.88
20.82
20.73
20.71
20.62
f1 (ppm)

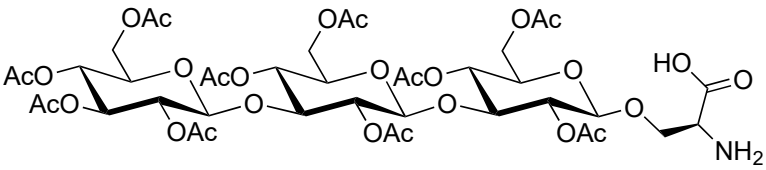
OAc
AcO
O
HO
NH2

2.1g

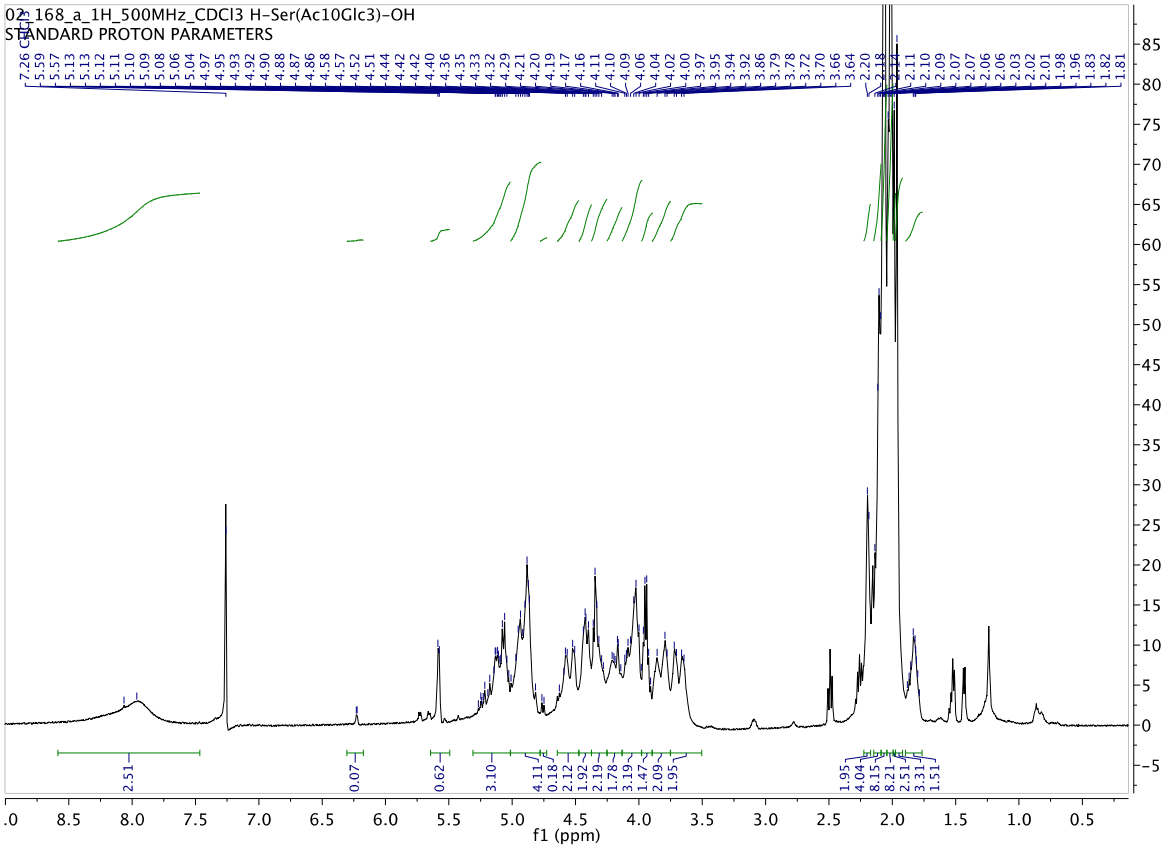
02_168_a_1H_500MHz_CDCl3 H-Ser(Ac10Glc3)-OH
STANDARD PROTON PARAMETERS
f1 (ppm)

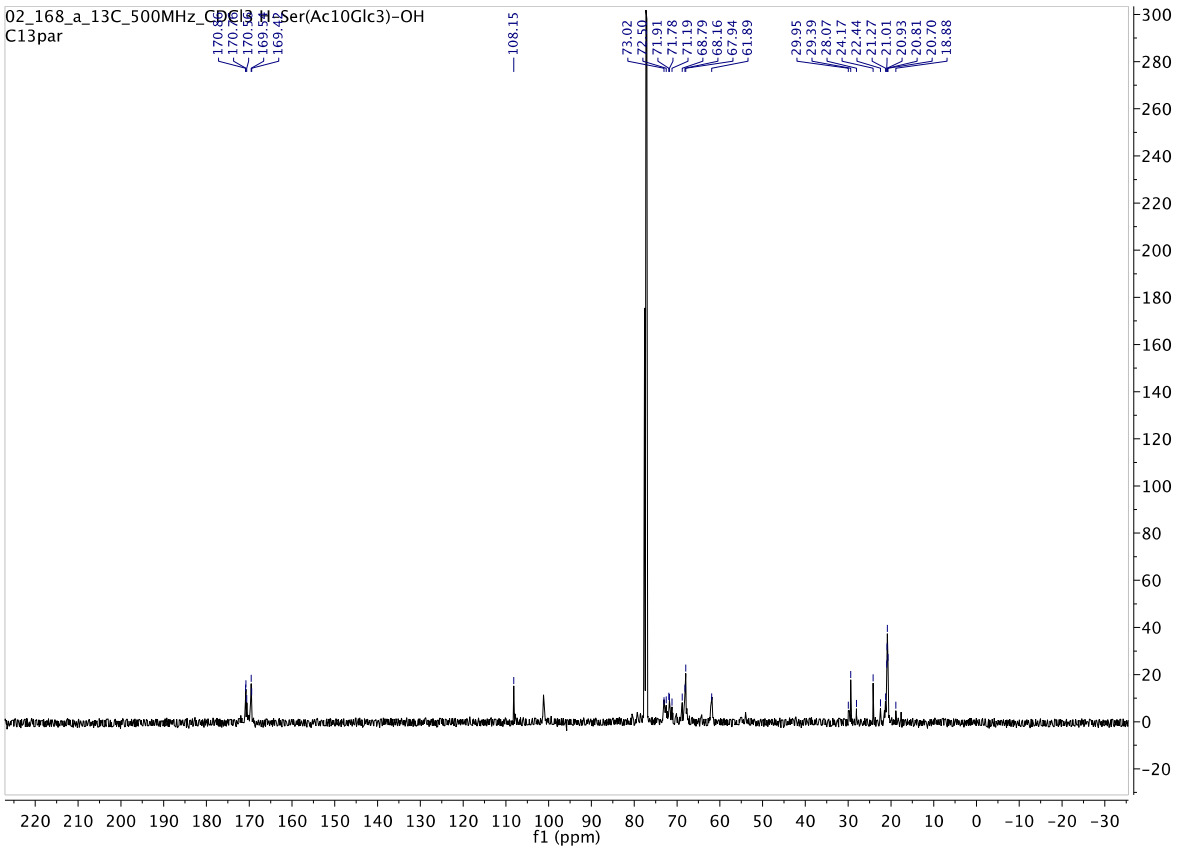
02_168_a_13C_500MHz_CDCl3 H-Ser(Ac10Glc3)-OH
C13par
170.88
170.70
170.50
169.54
169.41
108.15
73.02
72.50
71.91
71.78
71.19
68.79
68.16
67.94
61.89
29.95
29.39
28.07
24.17
22.44
21.27
21.01
20.93
20.81
20.70
18.88
f1 (ppm)

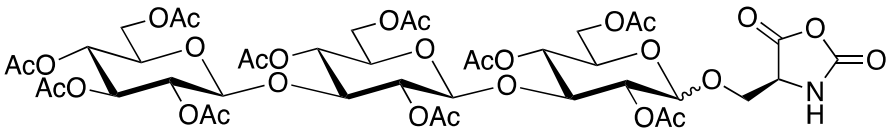

2.2g (1:4 α:β ratio)

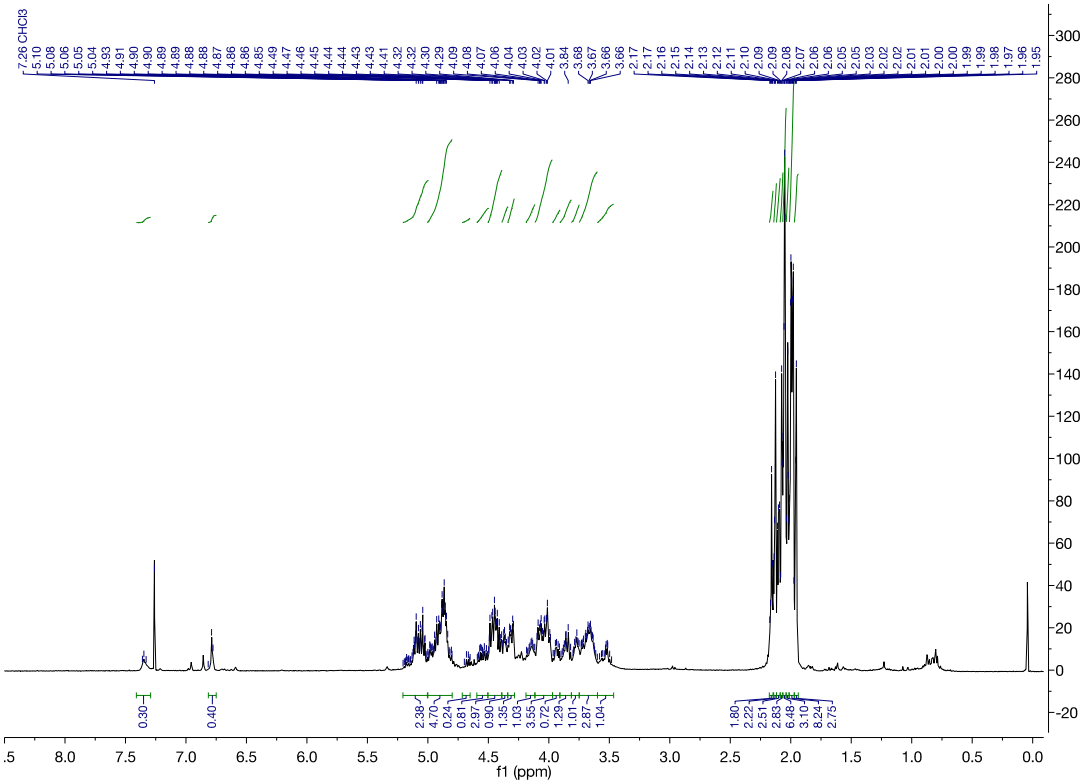

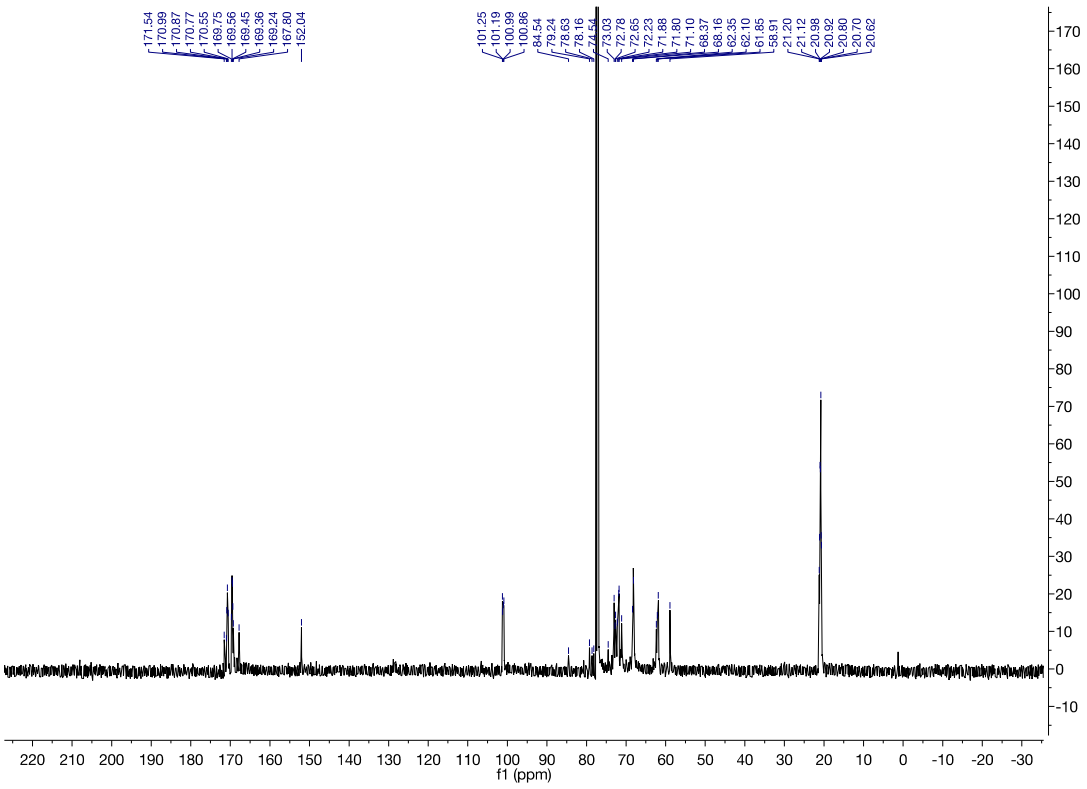
171.54
170.99
170.87
170.77
170.55
169.75
169.56
169.45
169.36
169.24
167.80
152.04
101.25
101.19
100.99
100.86
84.54
79.24
78.63
78.16
74.54
73.03
72.78
72.65
72.23
71.88
71.80
71.10
68.37
68.16
62.35
62.10
61.85
58.91
21.20
21.12
20.98
20.92
20.60
20.70
20.62
f1 (ppm)

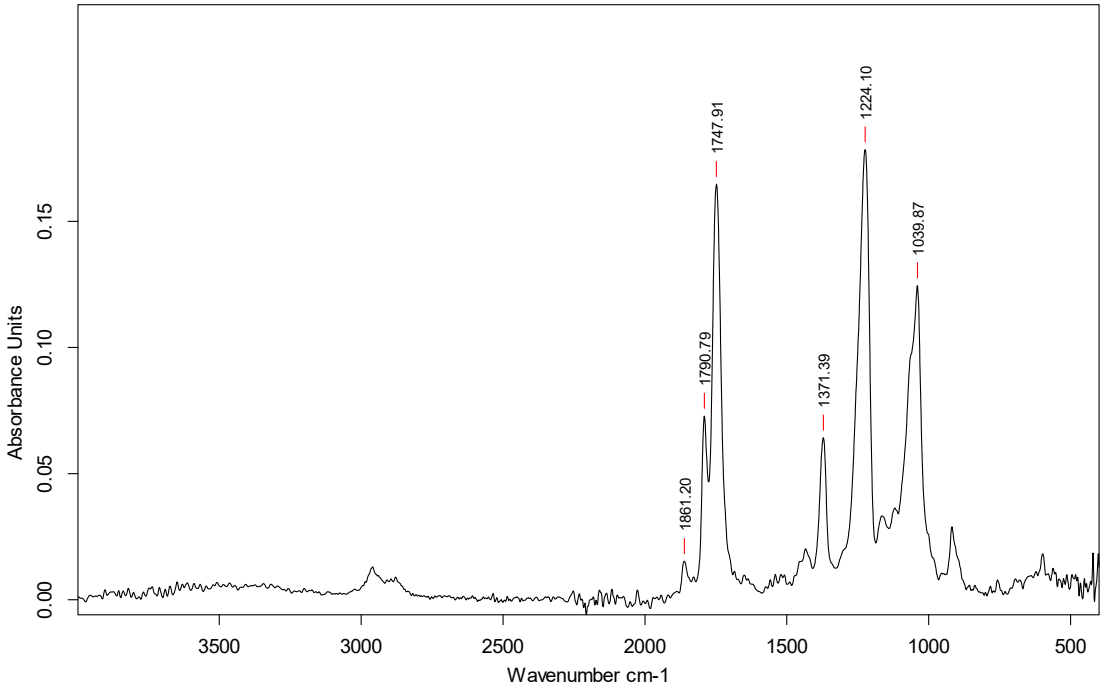
1861.20
1790.79
1747.91
1371.39
1224.10
1039.87
Absorbance Units
Wavenumber cm-1

Representative glycopolypeptide spectra

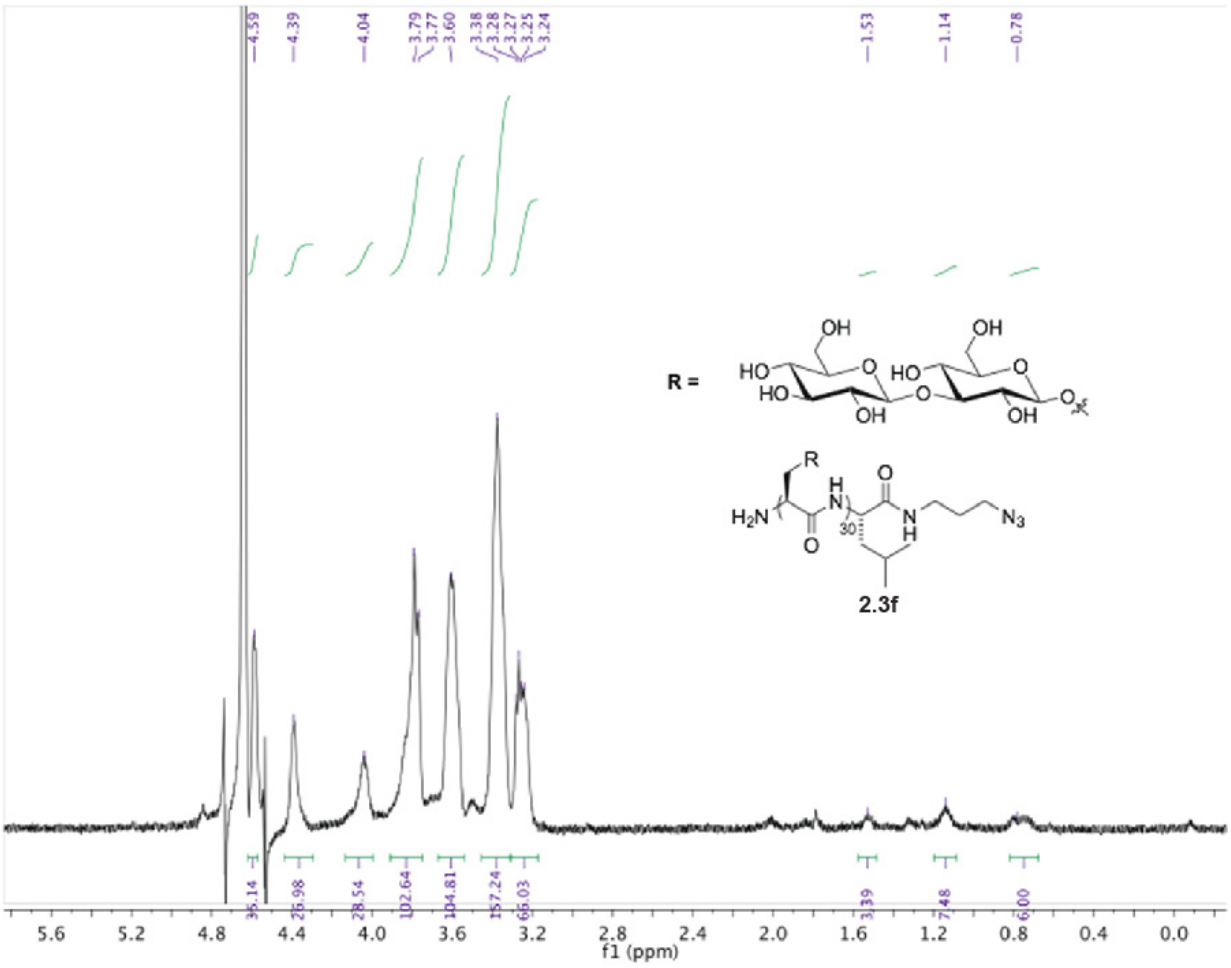

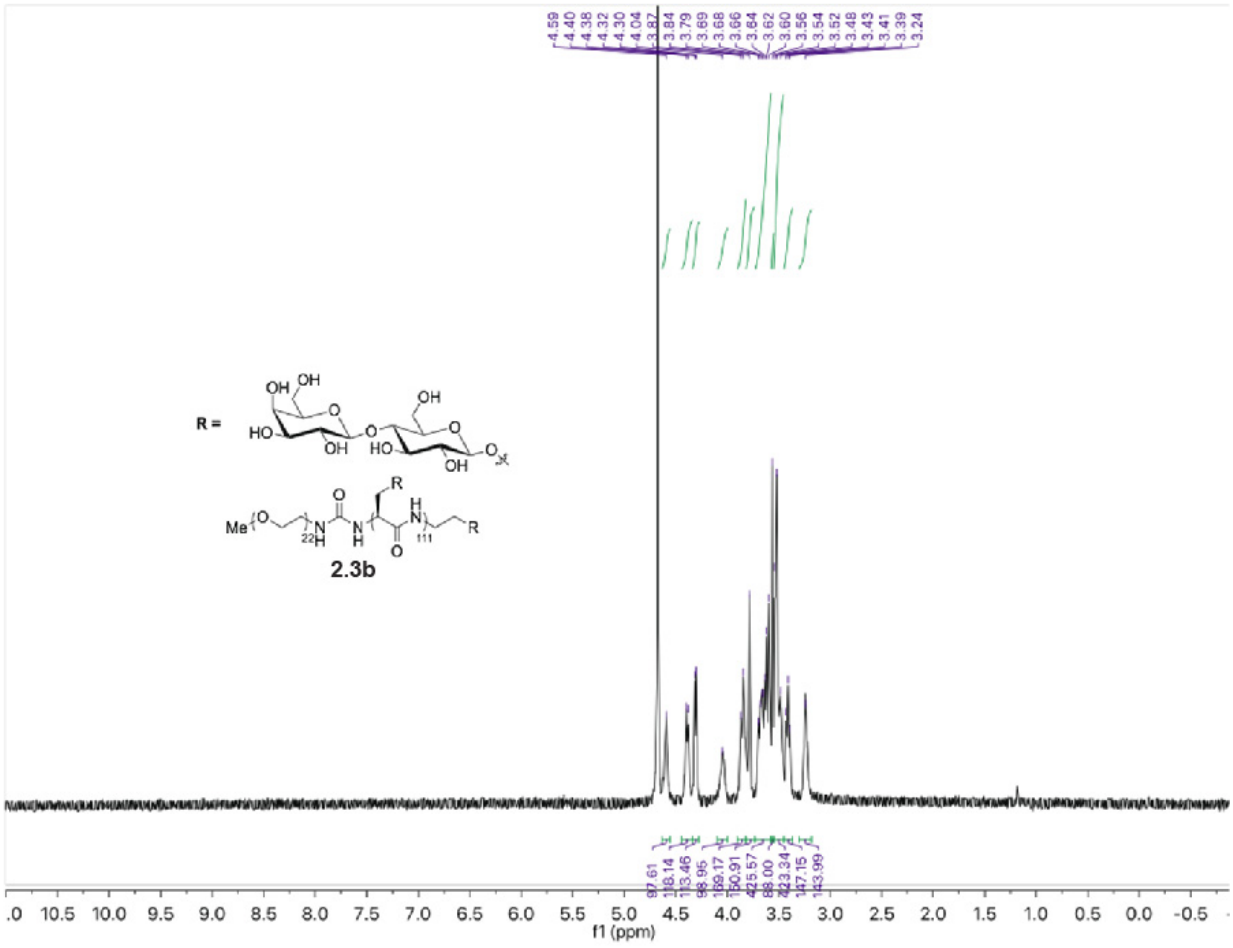
4.59
4.40
4.38
4.32
4.30
4.04
3.87
3.84
3.79
3.69
3.68
3.66
3.64
3.62
3.60
3.56
3.54
3.52
3.48
3.43
3.41
3.39
3.24
R =
OH
HO
O
x
Me
22
111
2.3b
97.61
118.14
113.46
98.95
169.17
150.91
425.57
88.00
423.34
147.15
143.99
f1 (ppm)

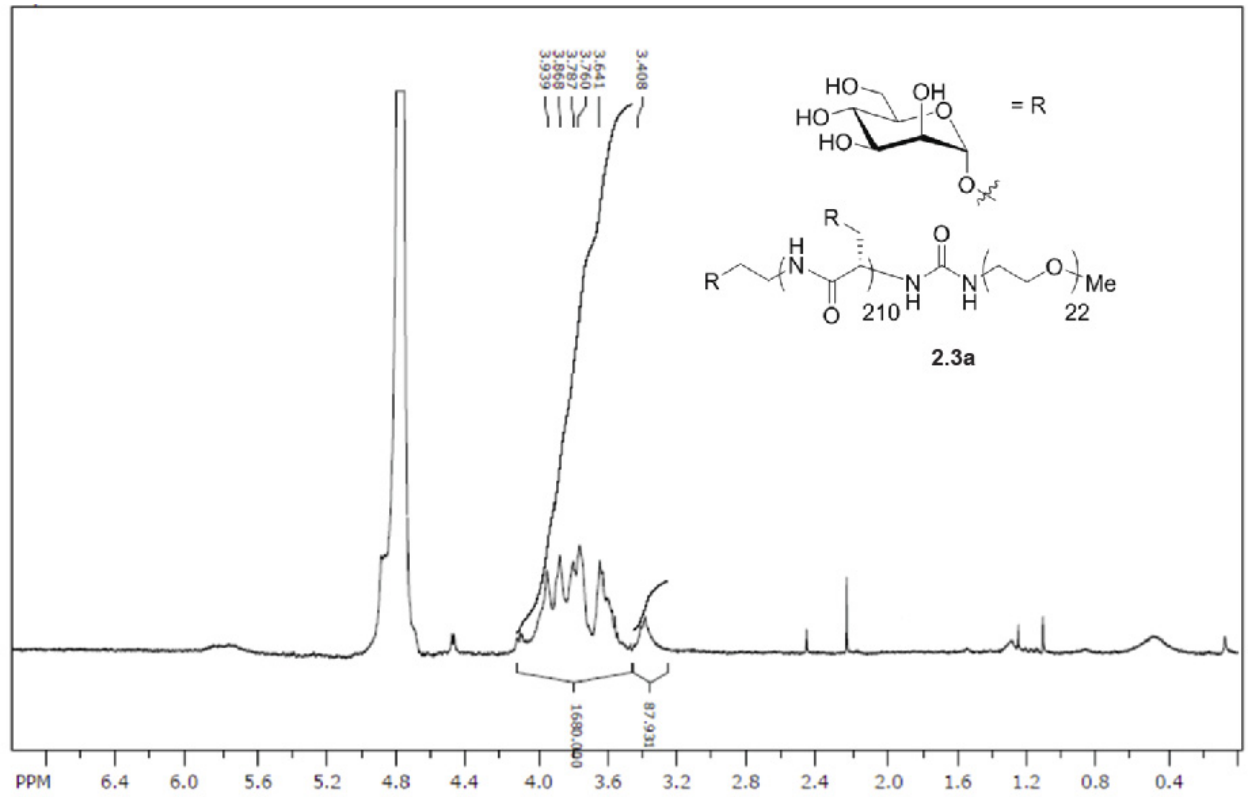
3.939
3.868
3.787
3.760
3.641
3.408
HO
OH
HO
HO
O
= R
R
H
N
O
N
H
O
N
H
O
O
Me
210
22
2.3a
1680.000
87.931
PPM
6.4
6.0
5.6
5.2
4.8
4.4
4.0
3.6
3.2
2.8
2.4
2.0
1.6
1.2
0.8
0.4

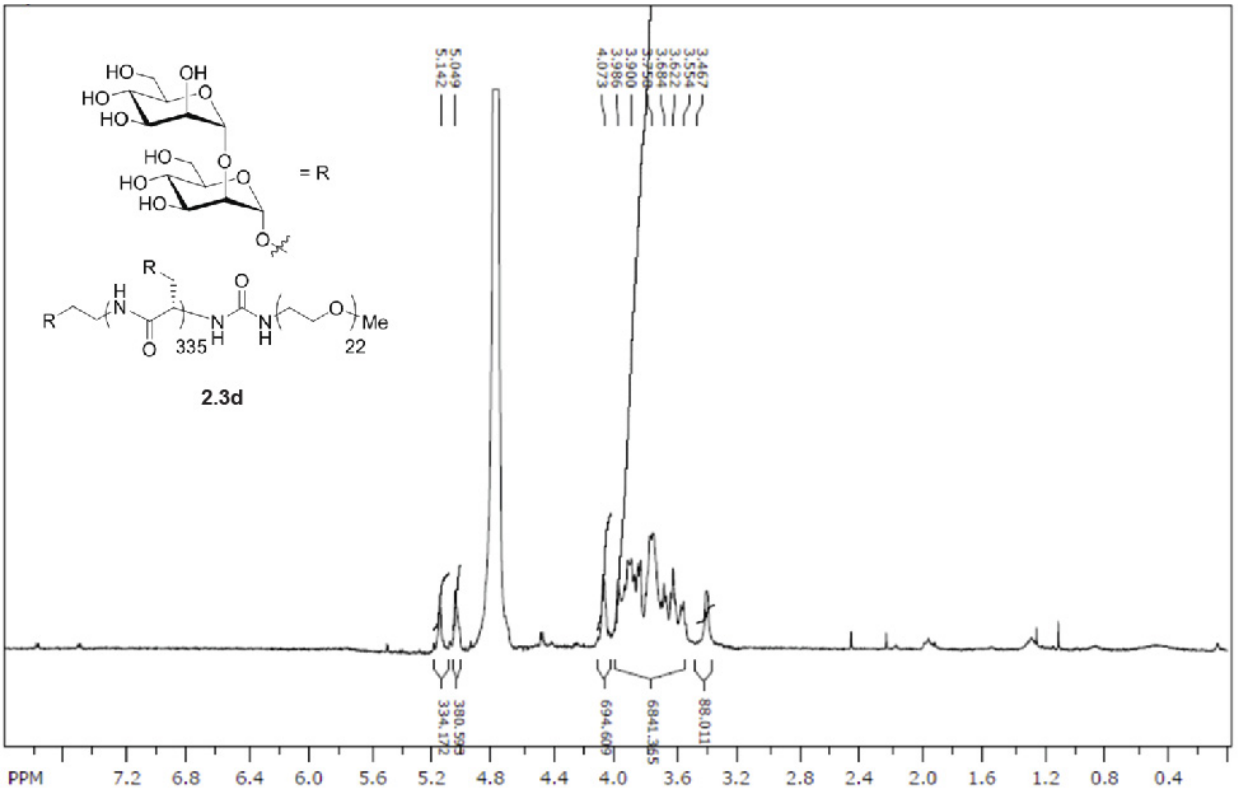
HO
OH
HO
HO
O
HO
HO
HO
O
O
= R
R
H
N
O
N
H
O
N
H
O
O
Me
335
22
2.3d
5.142
5.049
4.073
3.986
3.900
3.467
334.172
380.595
694.609
6841.365
88.011
PPM
7.2
6.8
6.4
6.0
5.6
5.2
4.8
4.4
4.0
3.6
3.2
2.8
2.4
2.0
1.6
1.2
0.8
0.4

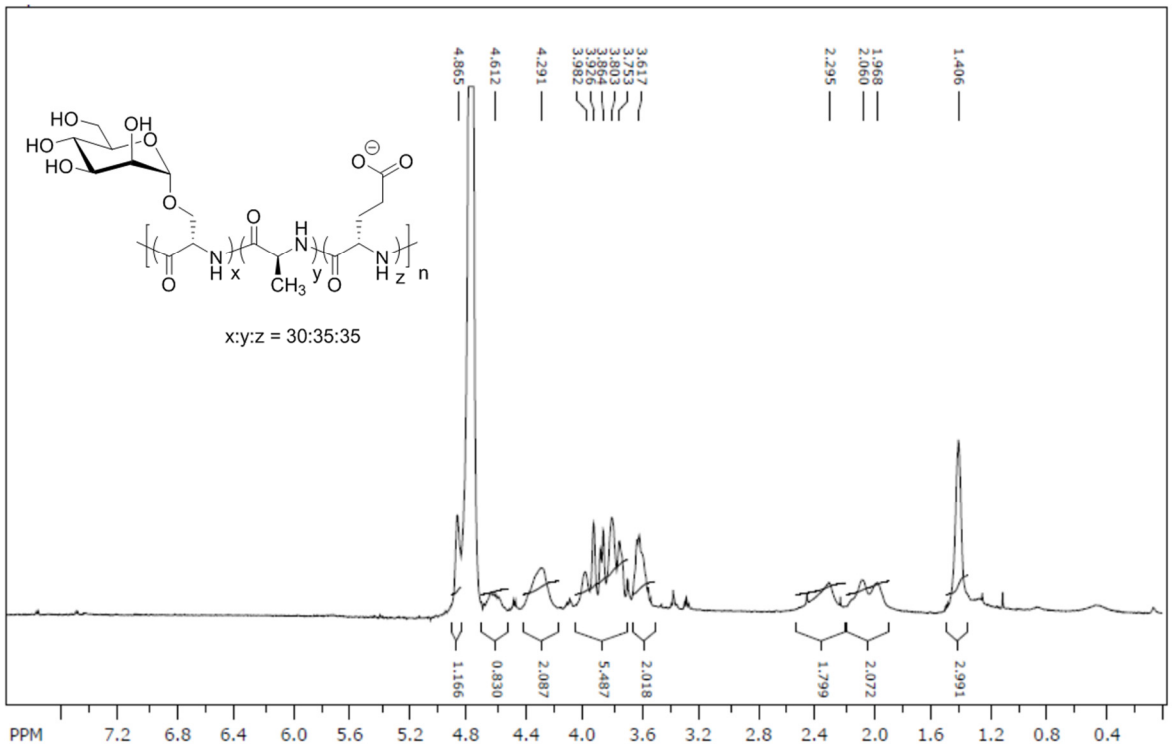
4.865
4.612
4.291
3.982
3.926
3.864
3.803
3.753
3.617
2.295
2.060
1.968
1.406
1.166
0.830
2.087
5.487
2.018
1.799
2.072
2.991
PPM
7.2 6.8 6.4 6.0 5.6 5.2 4.8 4.4 4.0 3.6 3.2 2.8 2.4 2.0 1.6 1.2 0.8 0.4
x:y:z = 30:35:35

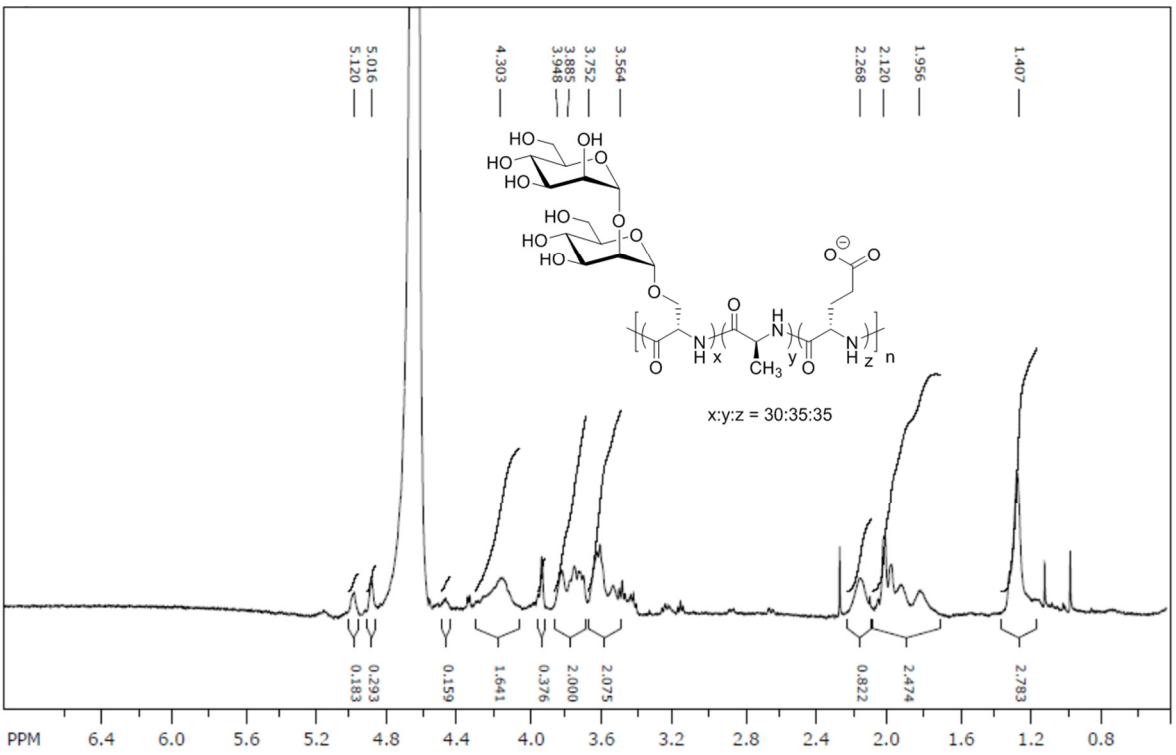
5.120
5.016
4.303
3.948
3.885
3.752
3.564
2.268
2.120
1.956
1.407
0.183
0.293
0.159
1.641
0.376
2.000
2.075
0.822
2.474
2.783
PPM
6.4 6.0 5.6 5.2 4.8 4.4 4.0 3.6 3.2 2.8 2.4 2.0 1.6 1.2 0.8
x:y:z = 30:35:35

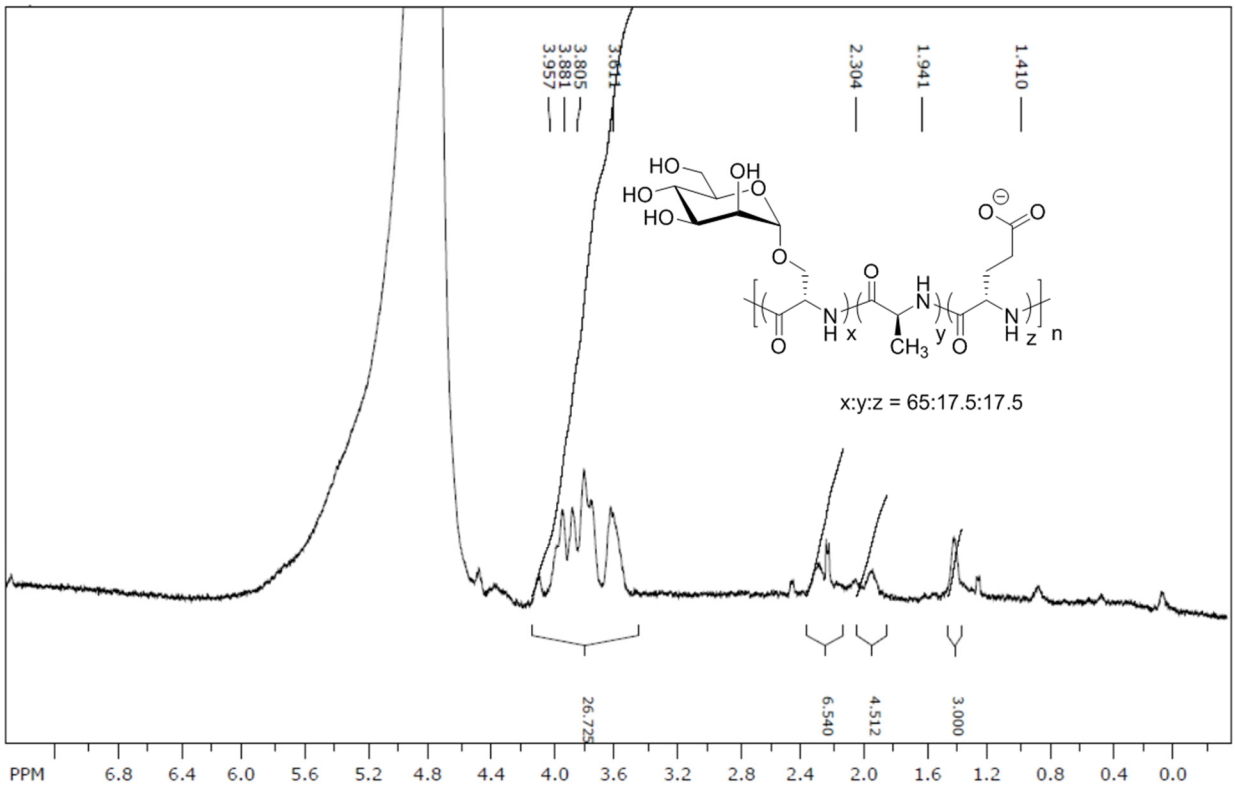
3.957
3.881
3.805
3.611
2.304
1.941
1.410
x:y:z = 65:17.5:17.5
26.725
6.540
4.512
3.000
PPM
6.8 6.4 6.0 5.6 5.2 4.8 4.4 4.0 3.6 3.2 2.8 2.4 2.0 1.6 1.2 0.8 0.4 0.0

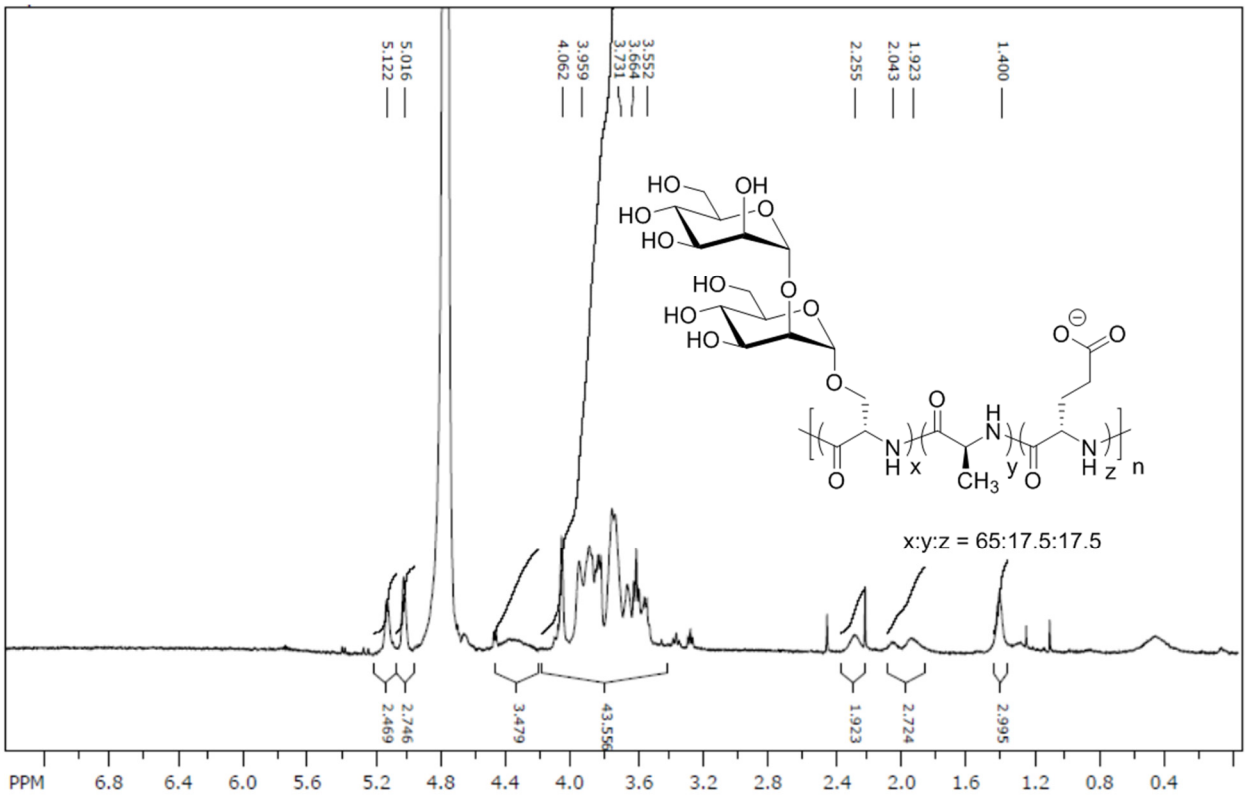
5.122
5.016
4.062
3.959
3.731
3.664
3.552
2.255
2.043
1.923
1.400
x:y:z = 65:17.5:17.5
2.469
2.746
3.479
43.556
1.923
2.724
2.995
PPM
6.8 6.4 6.0 5.6 5.2 4.8 4.4 4.0 3.6 3.2 2.8 2.4 2.0 1.6 1.2 0.8 0.4

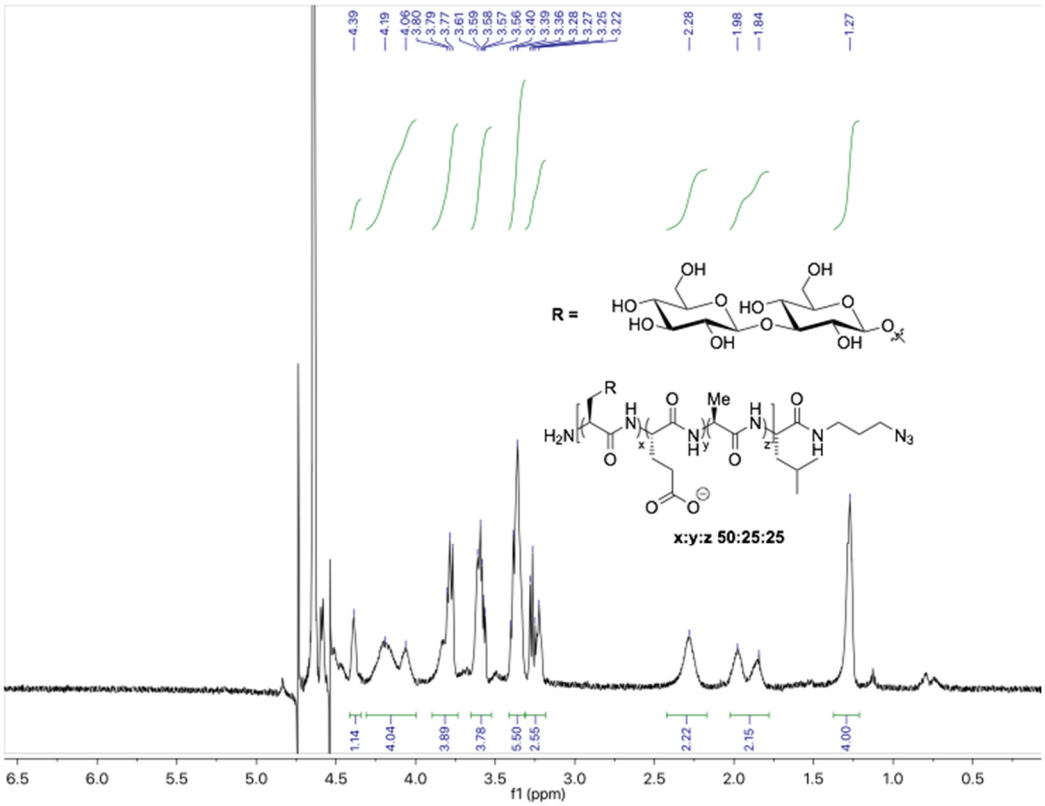
4.39
4.19
4.06
3.80
3.79
3.77
3.61
3.59
3.58
3.57
3.56
3.40
3.39
3.36
3.28
3.27
3.25
3.22
2.28
1.98
1.84
1.27
R =
x:y:z 50:25:25
1.14
4.04
3.89
3.78
5.50
2.55
2.22
2.15
4.00
f1 (ppm)

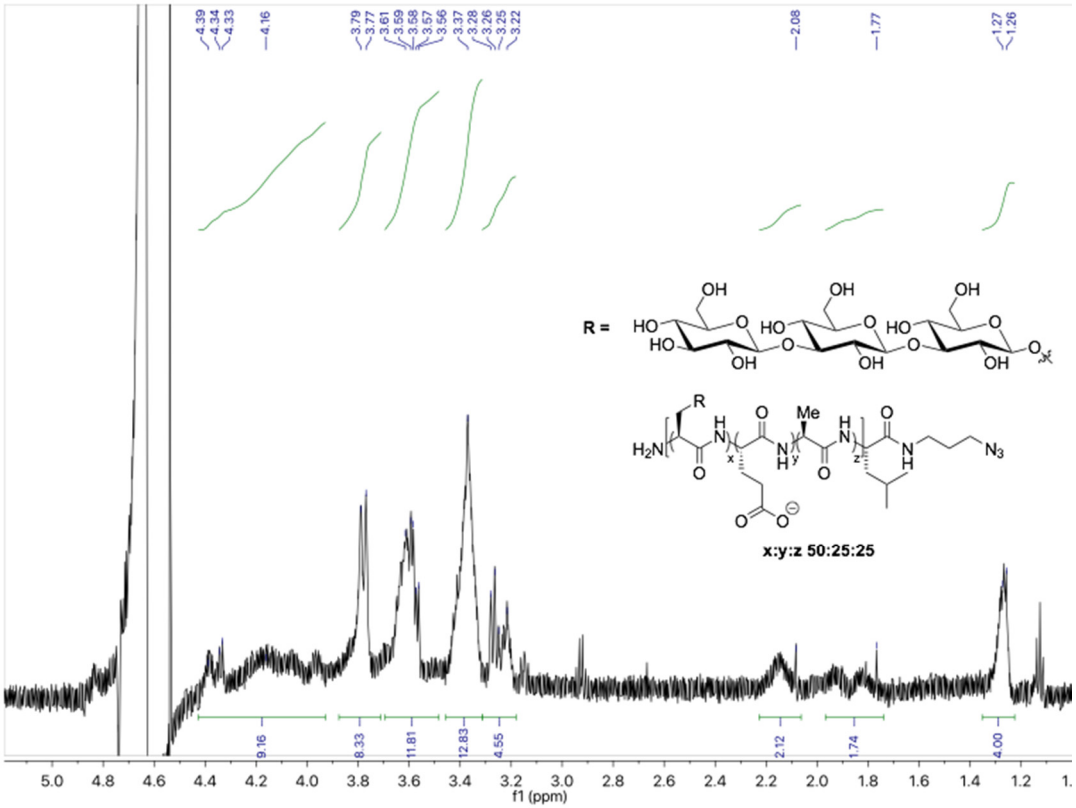
4.39
4.34
4.33
4.16
3.79
3.77
3.61
3.59
3.58
3.57
3.56
3.37
3.28
3.26
3.25
3.22
2.08
1.77
1.27
1.26
R =
x:y:z 50:25:25
9.16
8.33
11.81
12.83
4.55
2.12
1.74
4.00
f1 (ppm)

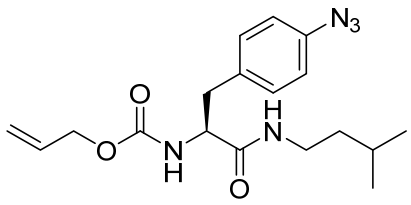

5.5

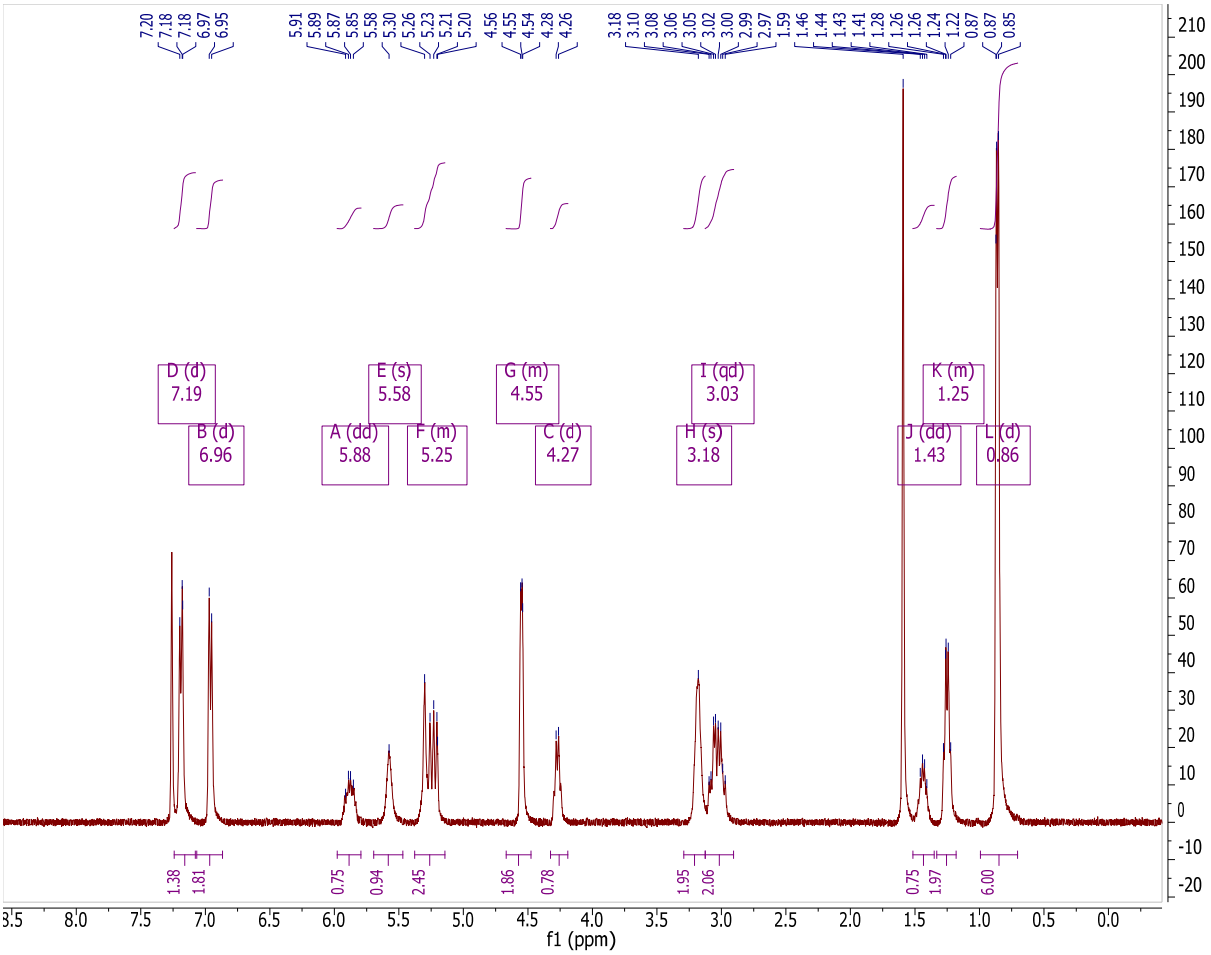
7.20
7.18
7.18
6.97
6.95
5.91
5.89
5.87
5.85
5.58
5.30
5.26
5.23
5.21
5.20
4.56
4.55
4.54
4.28
4.26
3.18
3.10
3.08
3.06
3.05
3.02
3.00
2.99
2.97
1.59
1.46
1.44
1.43
1.41
1.28
1.26
1.26
1.24
1.22
0.87
0.85
D (d) 7.19
E (s) 5.58
G (m) 4.55
I (qd) 3.03
K (m) 1.25
B (d) 6.96
A (dd) 5.88
F (m) 5.25
C (d) 4.27
H (s) 3.18
J (dd) 1.43
L (d) 0.86
1.38
1.81
0.75
0.94
2.45
1.86
0.78
1.95
2.06
0.75
1.97
6.00
f1 (ppm)

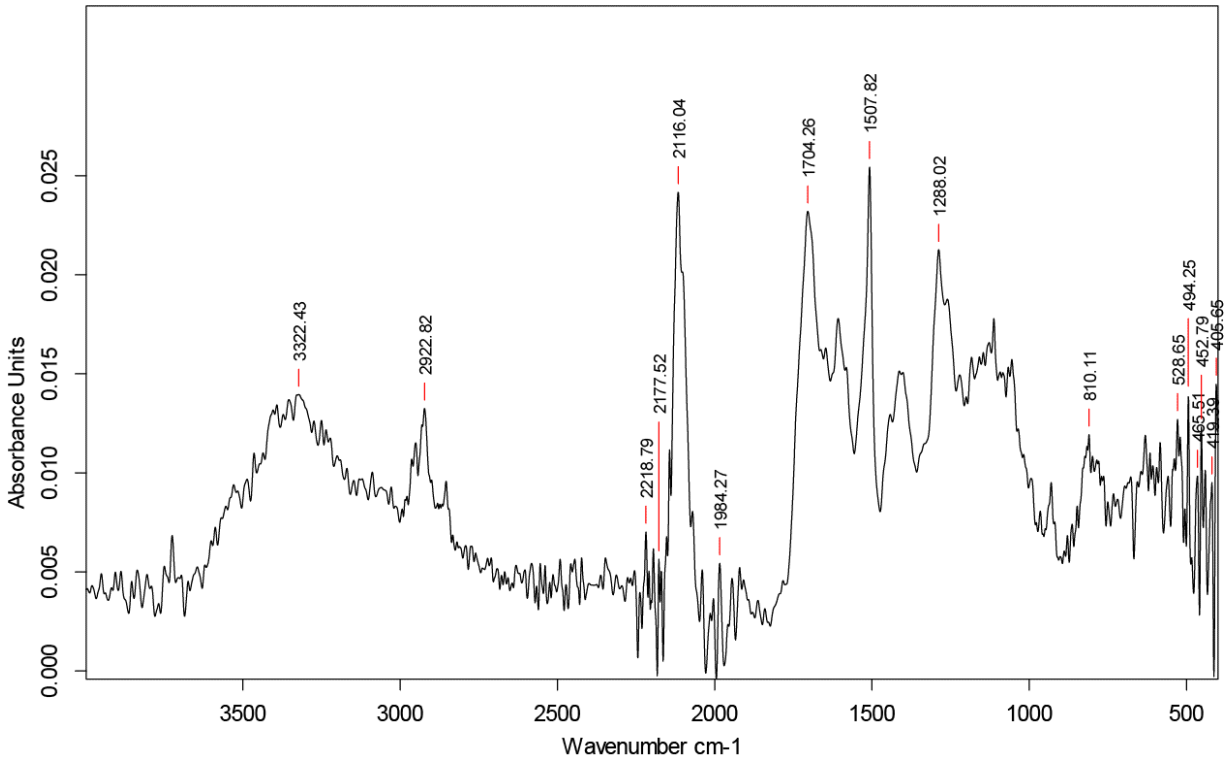
Absorbance Units
0.000
0.005
0.010
0.015
0.020
0.025
3500
3000
2500
2000
1500
1000
500
Wavenumber cm-1
3322.43
2922.82
2218.79
2177.52
2116.04
1984.27
1704.26
1507.82
1288.02
810.11
528.65
494.25
465.51
452.79
406.66

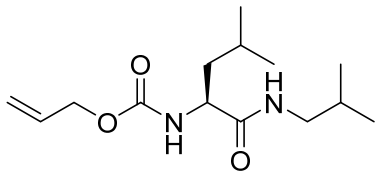

5.7

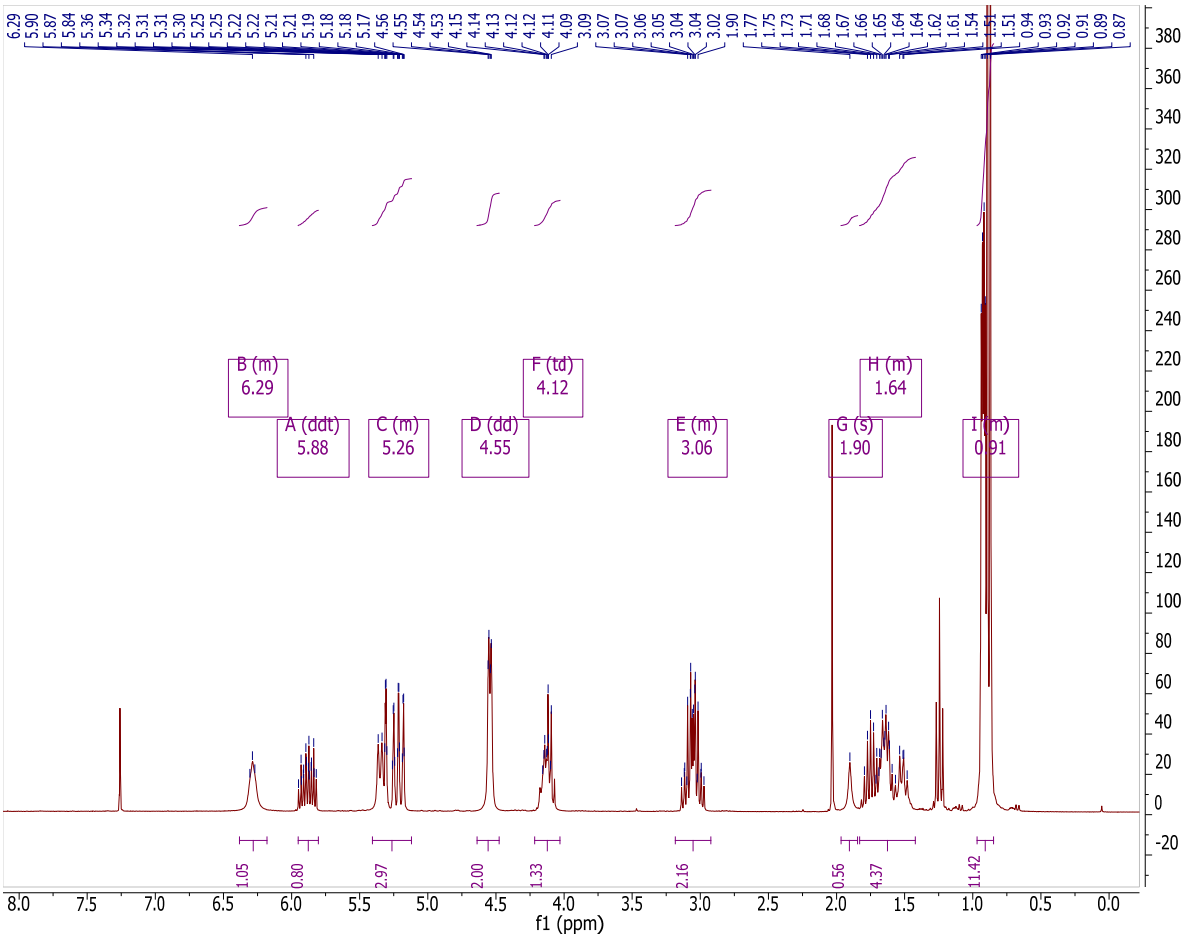
B (m)
6.29
A (ddt)
5.88
C (m)
5.26
D (dd)
4.55
F (td)
4.12
E (m)
3.06
H (m)
1.64
G (s)
1.90
I (m)
0.91
1.05
0.80
2.97
2.00
1.33
2.16
0.56
4.37
11.42
f1 (ppm)

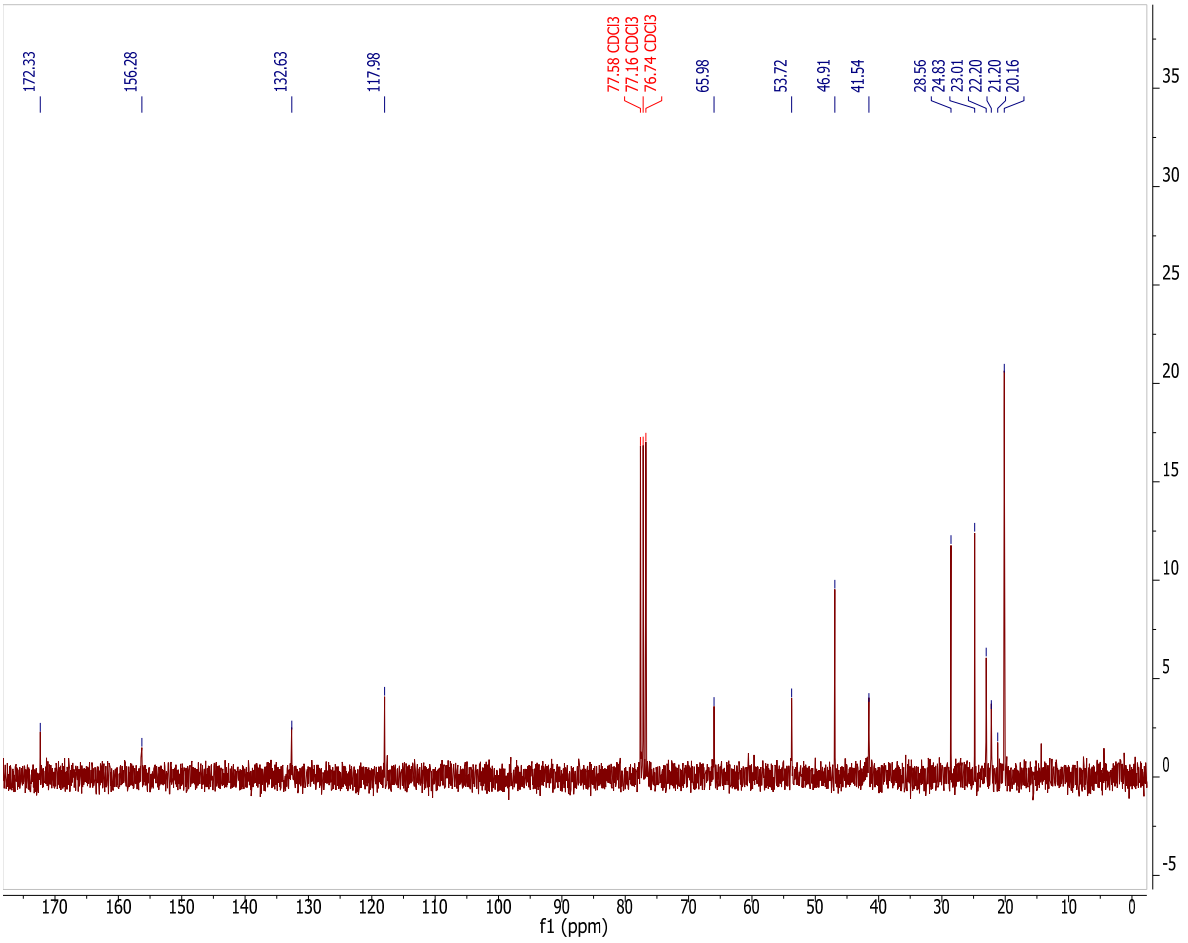
172.33
156.28
132.63
117.98
77.58 CDCl3
77.16 CDCl3
76.74 CDCl3
65.98
53.72
46.91
41.54
28.56
24.83
23.01
22.20
21.20
20.16
f1 (ppm)

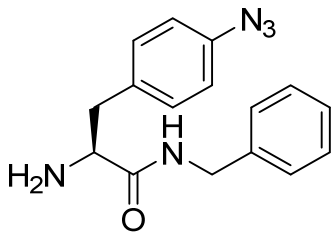
N3
H
N
H2N
O

5.13

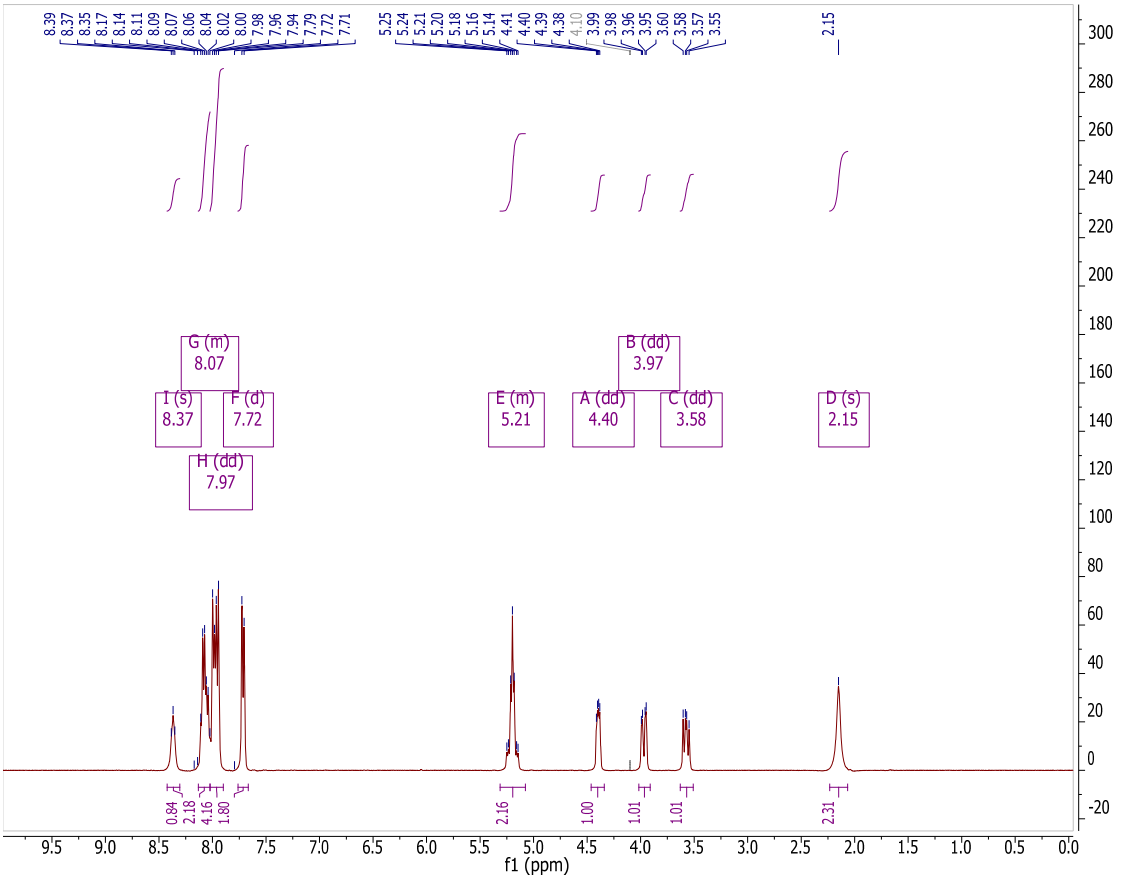
8.39
8.37
8.35
8.17
8.14
8.11
8.09
8.07
8.06
8.04
8.02
8.00
7.98
7.96
7.94
7.79
7.72
7.71
5.25
5.24
5.21
5.20
5.18
5.16
5.14
4.41
4.40
4.39
4.38
4.10
3.99
3.98
3.96
3.95
3.60
3.58
3.57
3.55
2.15
G (m) 8.07
B (dd) 3.97
I (s) 8.37
F (d) 7.72
E (m) 5.21
A (dd) 4.40
C (dd) 3.58
D (s) 2.15
H (dd) 7.97
0.84
2.18
4.16
1.80
2.16
1.00
1.01
1.01
2.31
f1 (ppm)

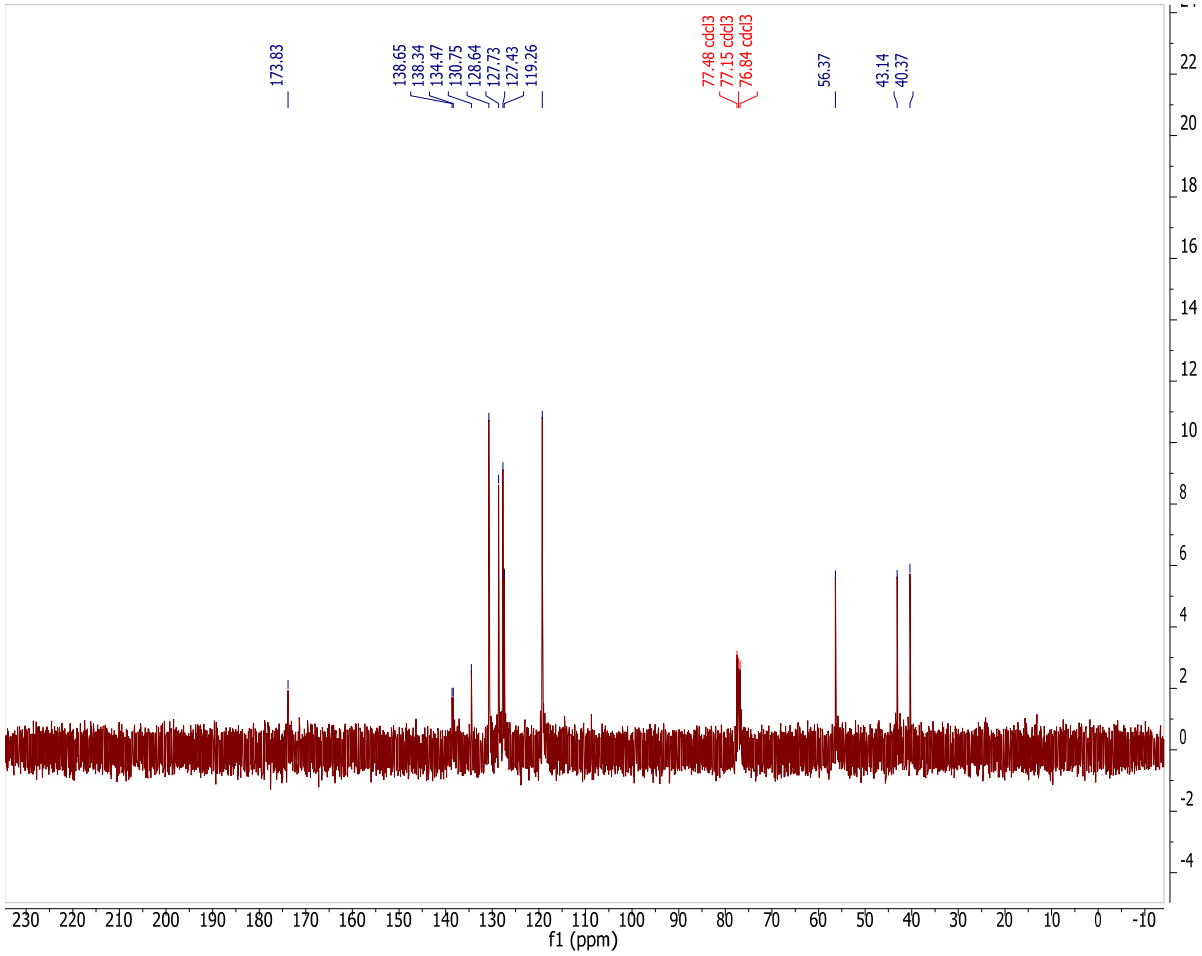
173.83
138.65
138.34
134.47
130.75
128.64
127.73
127.43
119.26
77.48 cdcl3
77.15 cdcl3
76.84 cdcl3
56.37
43.14
40.37
f1 (ppm)

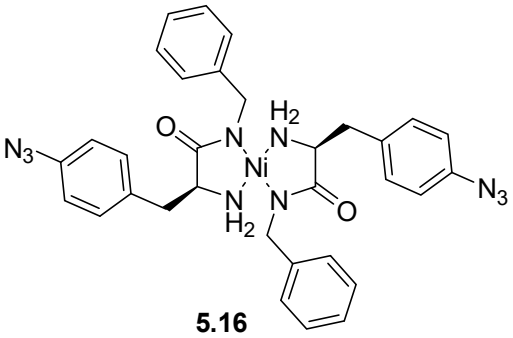
N3
O
N
Ni
N
H2
N
H2
N
O
N3

5.16

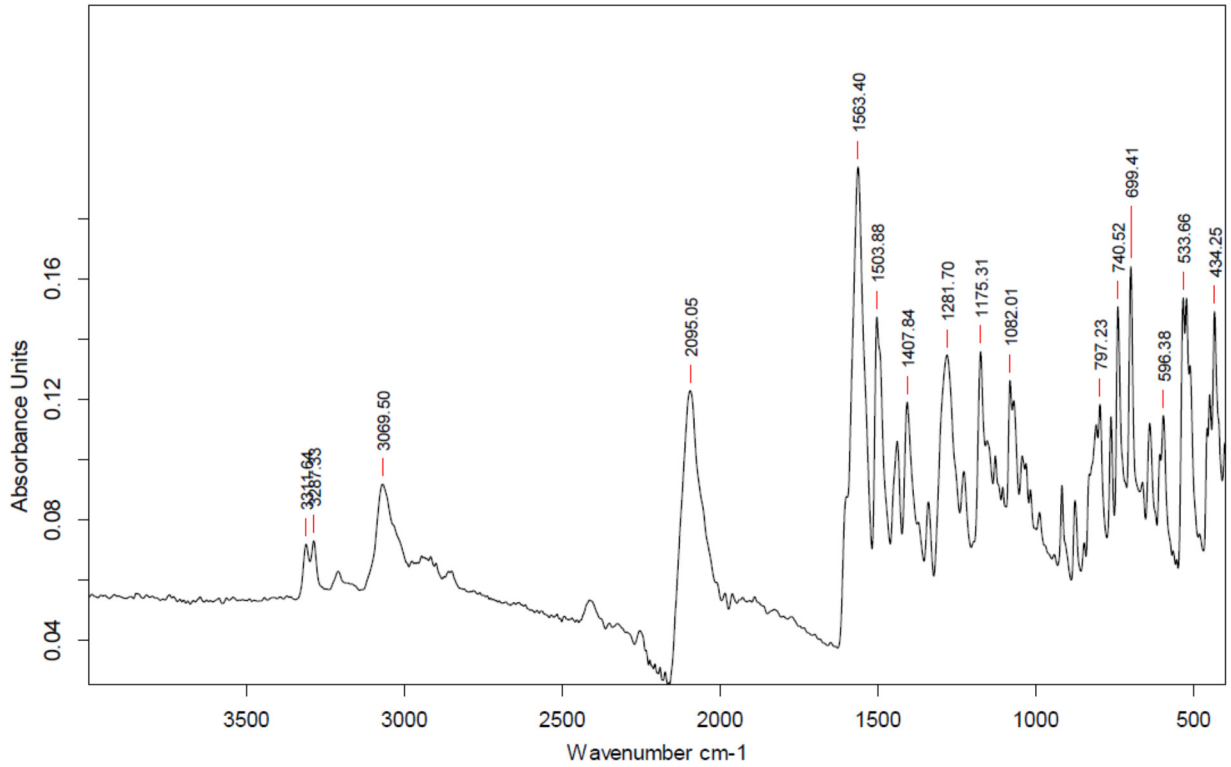
Absorbance Units
0.04
0.08
0.12
0.16
3311.64
3287.33
3069.50
2095.05
1563.40
1503.88
1407.84
1281.70
1175.31
1082.01
797.23
740.52
699.41
596.38
533.66
434.25
3500
3000
2500
2000
1500
1000
500
Wavenumber cm-1

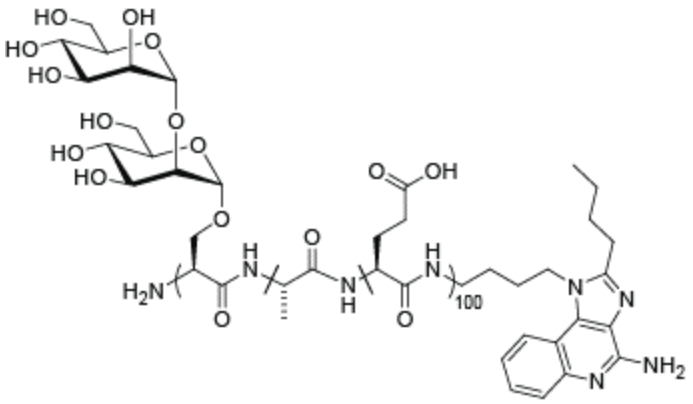

65:17.5:17.5 Ser(Man2):Ala:Glu

5.18

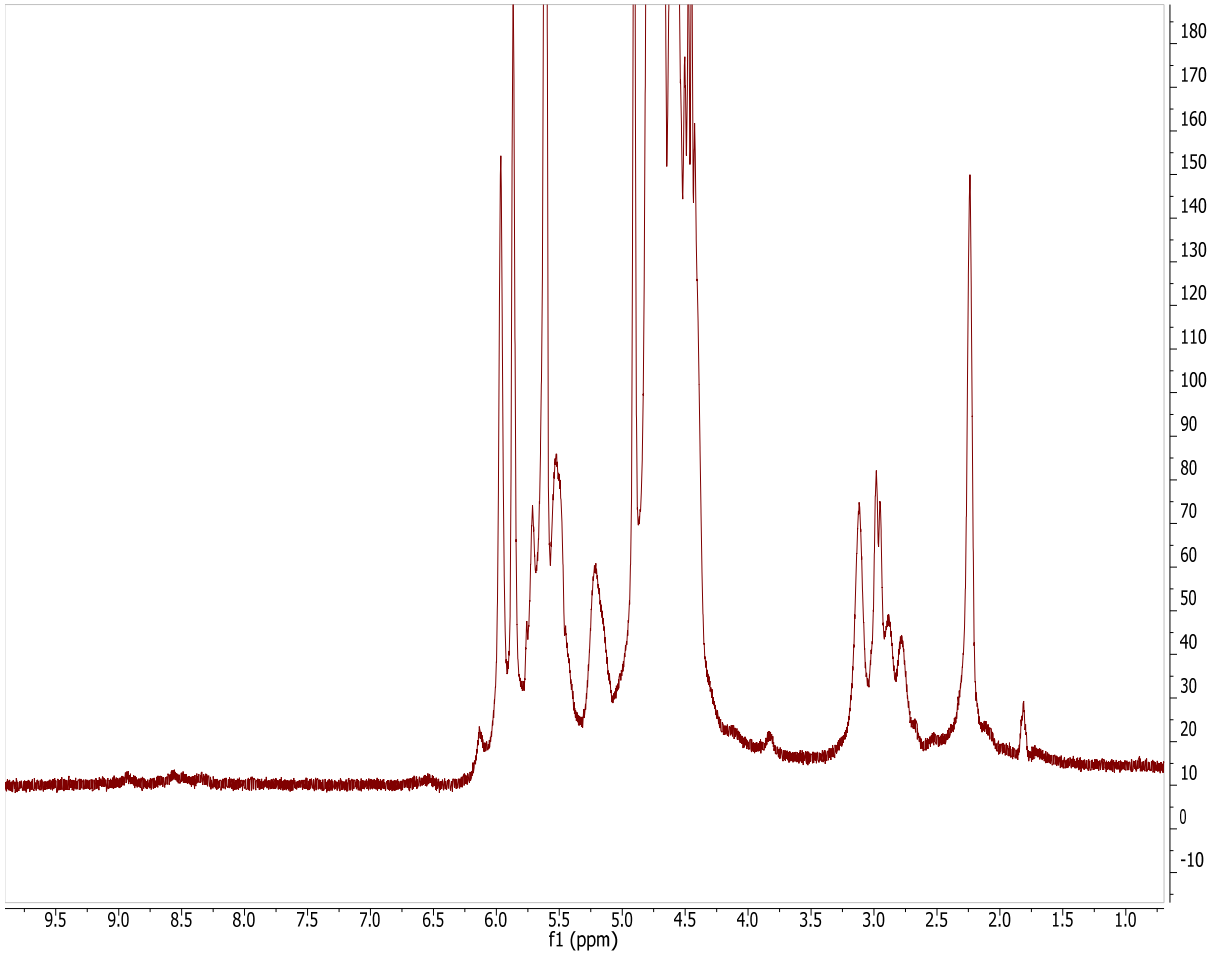

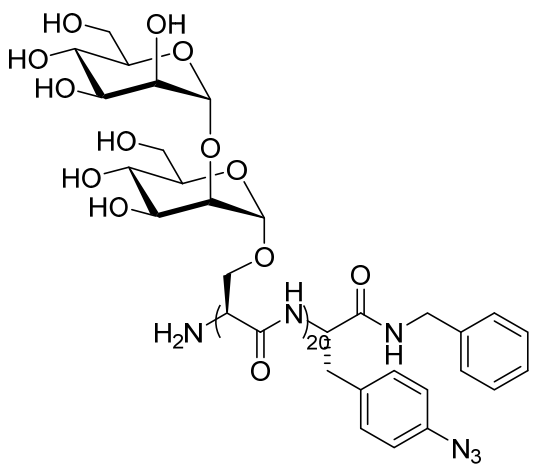
HO
OH
HO
HO
O
HO
O
HO
O
HO
O
H
N
O
H2N
O
20
N
H
N3

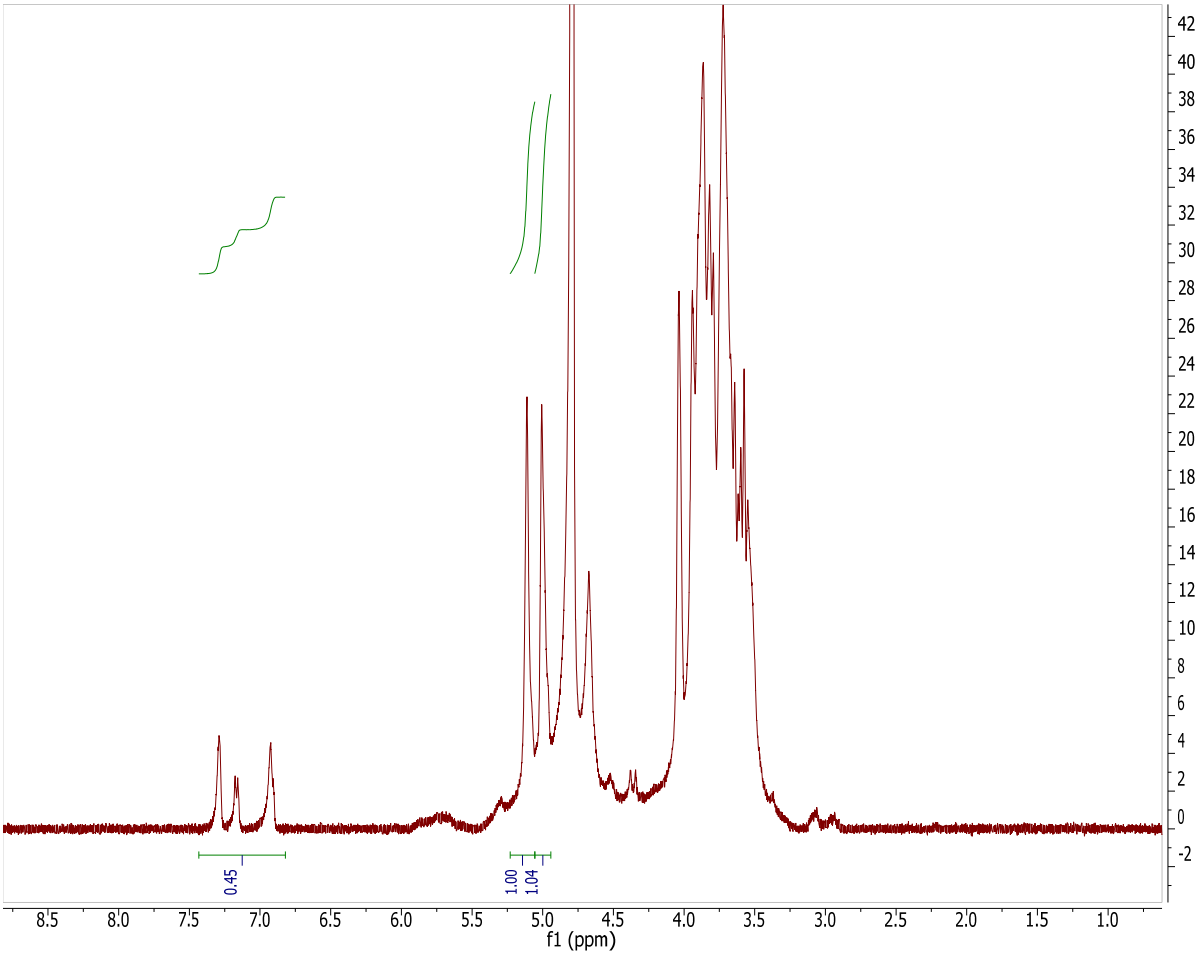
0.45
1.00
1.04
f1 (ppm)

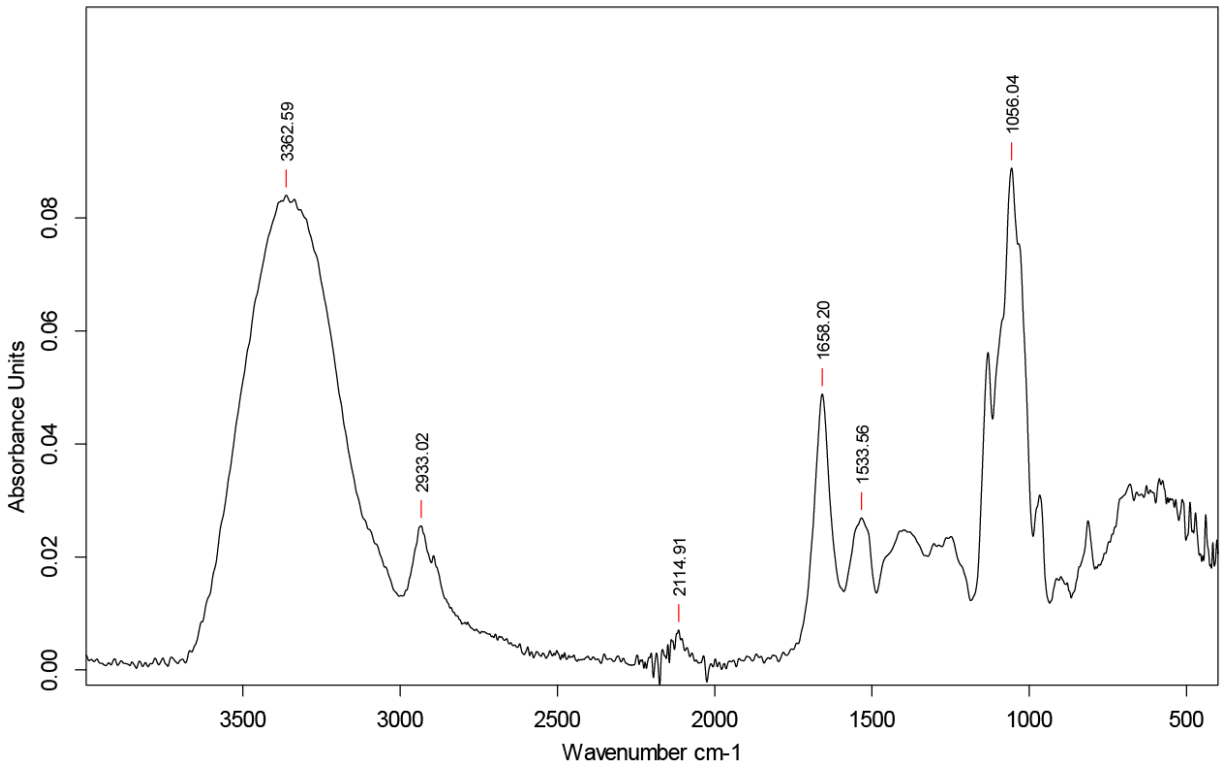
3362.59
2933.02
2114.91
1658.20
1533.56
1056.04
Absorbance Units
0.00
0.02
0.04
0.06
0.08
3500
3000
2500
2000
1500
1000
500
Wavenumber cm-1

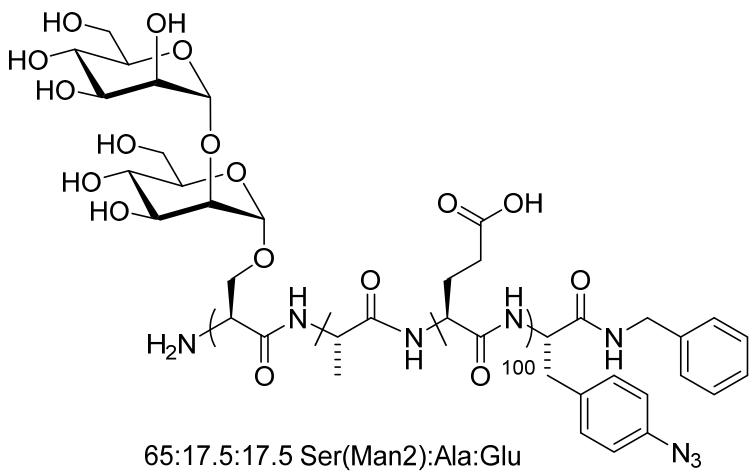

65:17.5:17.5 Ser(Man2):Ala:Glu

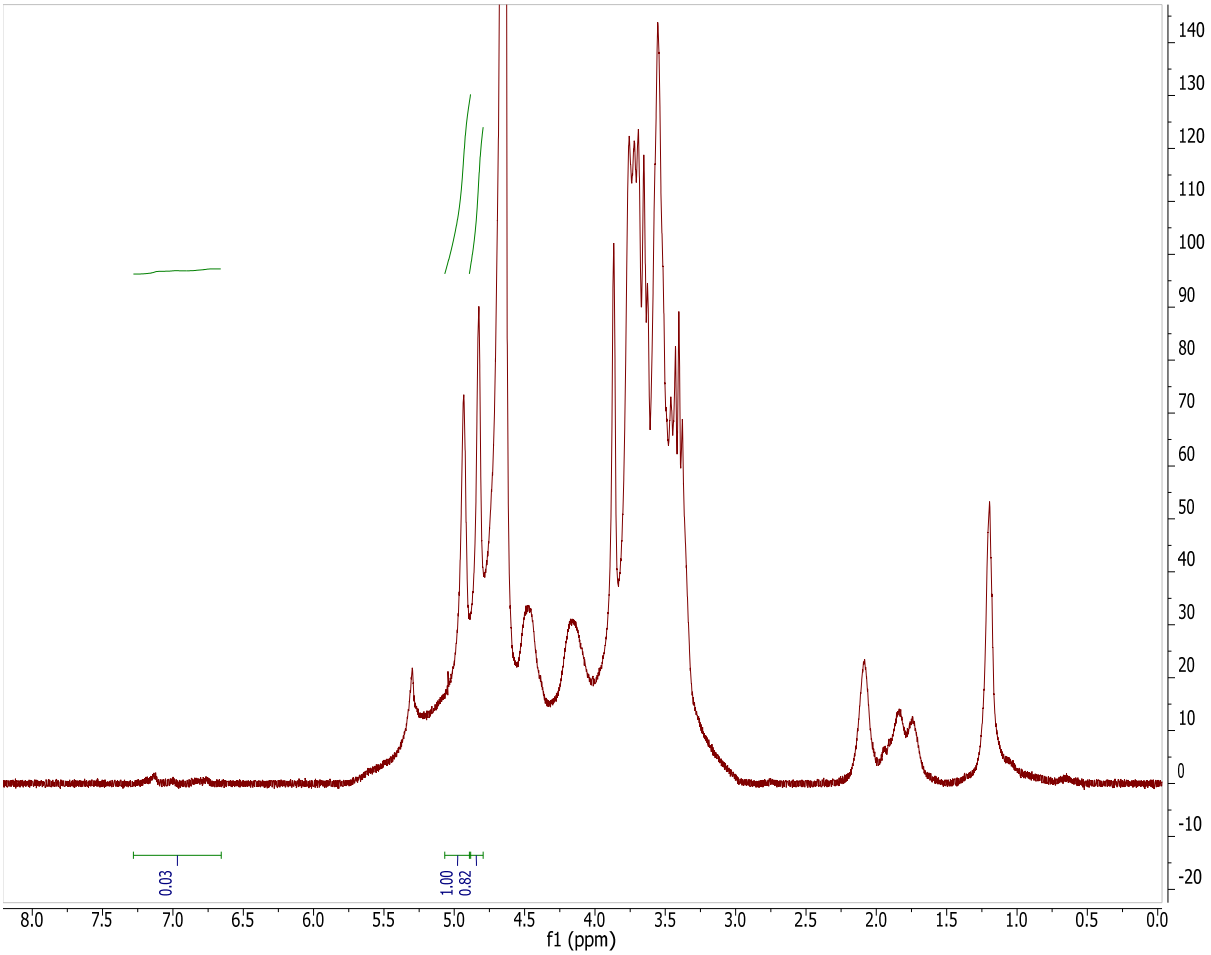

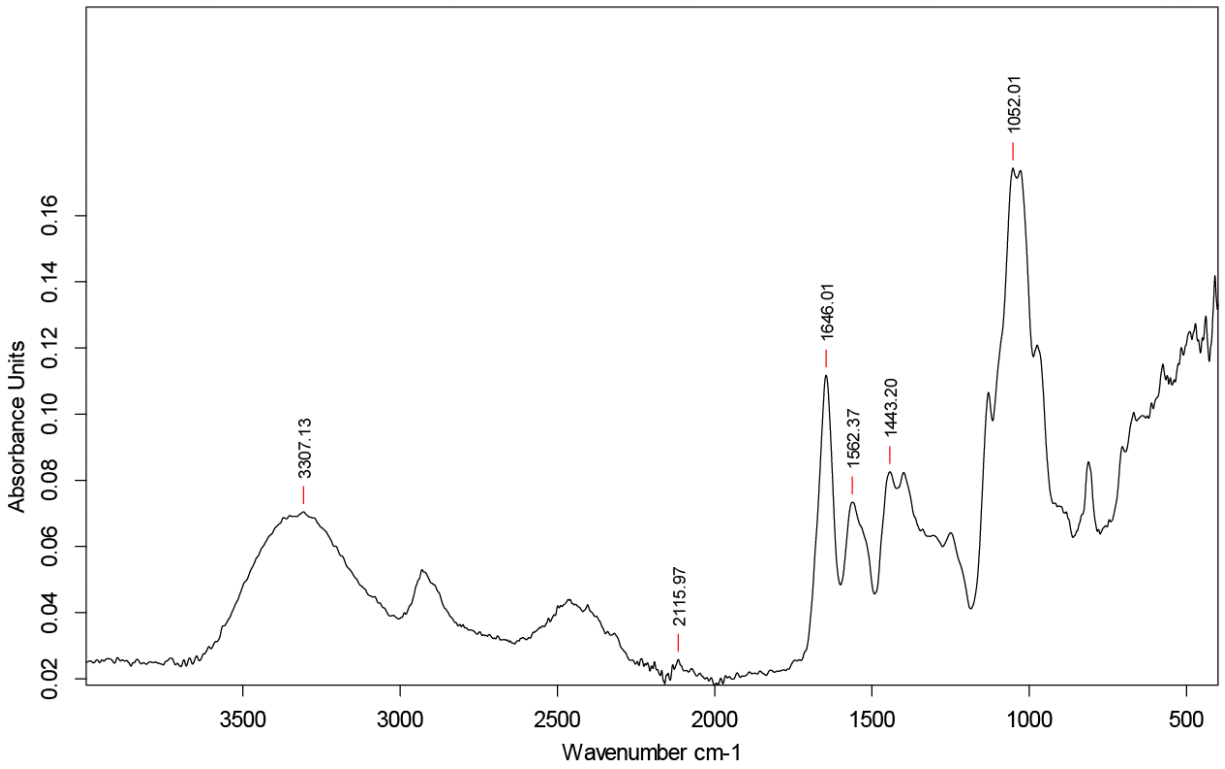
Absorbance Units
0.02
0.04
0.06
0.08
0.10
0.12
0.14
0.16
3307.13
2115.97
1646.01
1562.37
1443.20
1052.01
3500
3000
2500
2000
1500
1000
500
Wavenumber cm-1